

# Inaugural-Dissertation

zur Erlangung der Doktorwürde

der

Fakultät für Physik

der

Universität Bielefeld

vorgelegt von

Diplom-Chemiker Mike Heilemann

aus Leipzig

24.05.2005



# Design of Single-Molecule Optical Devices: Unidirectional Photonic Wires and Digital Photoswitches

Gutachter: Prof. Dr. Markus Sauer  
Priv. Doz. Dr. Andreas Hütten

Hiermit erkläre ich an Eides statt, dass ich die vorliegende Arbeit selbstständig und ohne unerlaubte Hilfsmittel durchgeführt habe.

Bielefeld, 24. Mai 2005

---

Mike Heilemann

## Summary

Molecular photonics is a new emerging field of research around the premise that it is possible to develop optical devices using single molecules as building blocks. Currently used waveguides, applied for example in telecommunication, rely on the classical physics of bulk materials: Maxwell's equations allow propagating modes in the far field, and the wavelength of light imposes a fundamental lower limit on device size. However, nature has evolved several examples of photonic nanostructures to guide light over much smaller length scales for "light harvesting" in plants and photosynthetic bacteria. This fundamentally quantum mechanical solution is most often based on near-field dipole-dipole interactions, i.e. fluorescence resonance energy transfer (FRET). As a consequence, light-harvesting complexes, one of nature's supreme examples of nanoscale engineering, have inspired researchers to engineer molecular optical devices, such as molecular photoswitches or molecular photonic wires. A molecular photonic wire is distinguished from a molecular electronic wire by supporting excited-state energy transfer rather than electron- (or hole-) transfer processes and could find application in, for example, optical computing as short-range interconnects in dense optical circuits. The excited state resulting from light absorption by one chromophore migrates among an array of chromophores, ultimately reaching a fluorescence dye to output an optical signal. In 1994, Lindsey and co-workers realized the first molecular photonic wire based on conjugated porphyrin arrays. However, strong coupling in porphyrin arrays has the disadvantage of forming so-called energy sinks due to different local interactions of the chromophores. As a further prerequisite, molecular photonic wires have to operate at the single molecule level and because such complex molecular systems are expected to exhibit a high degree of heterogeneity they have to be characterised at an individual basis as well.

In this work an alternative access to molecular photonic wires was elaborated. This approach was based on (i) the use of conventional, single molecule compatible chromophores, (ii) an energy cascade as the driving force for the excited-state energy to ensure unidirectionality, and (iii) an arrangement of chromophores such that strong electronic interactions promoting fluorescence quenching are prevented.

In the course of this work, the following challenges had to be met: (i) selection of suitable chromophores, (ii) development of a chemistry to obtain a regular arrangement of chromophores which allows for efficient energy transfer but prevents alterations of photophysical properties resulting in quenching, (iii) development of a single molecule set-up which allows investigation of the performance of individual photonic wires, (iv) elaboration of optimal conditions for the investigation and functioning of individual photonic wires and (v) development of a molecular optical switching unit.

The main requirement the chromophores have to fulfil is their compatibility with single molecule spectroscopy. This affects in particular their photostability, their photophysics and possible ways to improve their performance by optimising conditions. Therefore, more than 20 chromophores of different classes (i.e. rhodamines, oxazines and carbocyanines) were investigated under various conditions. Strikingly, chromophores belonging to the same class showed comparable behaviour with respect to their reactions to different conditions, such as oxygen concentration or reducing and oxidizing agents. For example, oxazine derivatives showed longest survival times and minimal photophysics such as blinking under ambient conditions in buffer. Rhodamines' photostability, on the other hand could be increased by more than tenfold upon addition of reducing agents such as  $\beta$ -mercaptoethanol (MEA), while strong blinking due to long triplet states or charge-separated states was observed upon oxygen removal. Carbocyanines required both, removal of oxygen to increase photostability plus addition of MEA, which here acts as triplet quencher and reduces blinking. This comparative study showed that a photonic wire should be constructed from only one class of chromophores as no conditions could be found satisfying the requirement of all classes. As rhodamines offer the broadest spectral range of chromophores, they were most frequently used in the photonic wires developed.

To achieve a very regular arrangement of chromophores, DNA was used as rigid scaffold. The well-developed labelling and post-labelling strategies of DNA were exploited to introduce a variety of different chromophores in a modular conception. It was shown that best results could be obtained when dye-labelled oligonucleotides were hybridised against a long DNA-strand already carrying a primary donor chromophore and a biotin for specific immobilization. The distance between subsequent chromophores was adjusted to 3.4 nm, i.e. 10 bases, which ensured

efficient FRET and prevented direct orbital interaction. Photonic wires were synthesised carrying up to 5 chromophores and covering a spectral range from 488 nm to 750 nm. In ensemble experiments the maximum overall transfer efficiency was determined to be 21%. However, as indicated by steady state and time-resolved measurements, a broad heterogeneity within the samples was suspected. To disentangle the complexity of the photophysics of so-built photonic wires, a novel fluorescence microscope, single molecule sensitive on four spectrally separated detectors, was developed. The confocal set-up was operated with multiple laser excitation wavelengths and offered the possibility for time-resolved fluorescence experiments, two-colour applications, and polarization-modulated excitation.

For the first time, a quadruple jump of energy transfer along a single photonic wire containing five chromophores and adsorbed on a glass surface was demonstrated with an overall transfer efficiency of ~90%. Confirmation that the energy is transferred stepwise comes from prolonged excitation of single molecules, which results in sequential photobleaching and a shift in the emission from the red back towards the blue. Furthermore, collective transitions of whole photonic wire molecules into nonfluorescent dark states were observed. It was demonstrated that fluorescence spectra from a large number of single photonic wire molecules resembled the ensemble spectrum of the sample.

To increase the homogeneity of photonic wires and better control the photostability, the molecules were anchored on a protein surface by biotin/streptavidin binding in an aqueous environment. Best stability and long observation times of single constructs were attained by using four rhodamines. Here, energy transfer efficiencies of up to ~90% were observed. Photonic wires with five fluorophores in aqueous solution used carbocyanine and carbopyronine derivatives as the final emitting unit, since no long-wavelength absorbing and emitting rhodamines are available for conjugation chemistry. Fluorescence lifetime information revealed further aspects of energy transfer, and complemented spectral data in order to identify fluorophores involved in particular energy transfer steps. Leakages in energy transfer, created by photodestruction of a fluorophore inside the chain, were revealed. Polarization modulation of the excitation light in combination with fluorescence lifetime gave insight into the rotational mobility of the fluorophore serving as input unit, i.e. Rhodamine Green. Three subpopulations, differing in quantum yield, fluorescence lifetime, and degree of rotational freedom, were found.

To further improve the performance of DNA-based photonic wires, a method of subsequent hybridisation of oligonucleotides to an immobilized single-stranded DNA was developed. This highly-efficient process was traced at the single-molecule level and yielded up to 90% of a desired target DNA within minutes. By this technique, (i) sample heterogeneities from ensemble hybridisation were reduced to a minimum and (ii) hindered hybridisation was observed for one hybridisation step, requiring longer incubation times. This observation can be attributed to a less favourable conformation or secondary structures of oligonucleotides, and explains relatively low ensemble energy transfer efficiencies measured in photonic wires with five fluorophores. A fraction of ~30% of all molecules showed energy transfer efficiencies with ~70%, in agreement with experiments carried out on dry glass substrates. Furthermore, single-molecule hybridisation represents a striking tool for a stepwise construction of complex geometrical arrangements to overcome kinetic hindrances.

After the accomplishment of the photonic wire, a further goal was the development of a molecular photoswitch. Hitherto, only one demonstration of chemically synthesized photoswitching of single molecules at room temperature had been reported. In the context of this work, it was shown that commercially available unmodified carbocyanine dyes such as Cy5 and Alexa647 could be used as efficient reversible single-molecule optical switch, whose fluorescent state after apparent photobleaching can be restored at room temperature upon irradiation in the range of 488 – 532 nm. In oxygen-free environment and in the presence of 100 mM  $\beta$ -mercaptoethanol (MEA) as triplet quencher, more than 20 switching cycles could be achieved for single Cy5 molecules with a reliability of >90%. To further characterize the photophysical properties of the reversible switchable state, an energy transfer donor, TMR, in proximity of Cy5 was used to report on the “off” states of the acceptor Cy5. Examination of the single pair FRET (sp-FRET) with high time resolution revealed the existence of three intermediates prior to fluorescence restoration. In addition to the importance of such single-molecule photoswitches e.g. for optical data storage, the results presented in this work imply limitations for the use of carbocyanine dyes in sp-FRET experiments.

# Table of Contents

<b>SUMMARY</b> .....	<b>I</b>
<b>TABLE OF CONTENTS</b> .....	<b>V</b>
<b>1. INTRODUCTION</b> .....	<b>1</b>
<b>2. THEORY</b> .....	<b>11</b>
<b>2.1. Fluorescence Microscopy</b> .....	<b>11</b>
2.1.1. Basic Principles of Fluorescence .....	12
2.1.2. Molecular Interactions Influencing Fluorescence .....	25
2.1.3. The Role of Oxygen .....	33
2.1.4. Fluorescent Probes .....	36
<b>2.2. Single-Molecule Spectroscopy</b> .....	<b>44</b>
2.2.1. Confocal Microscopy .....	45
2.2.2. Confocal Microscopy at the Single-Molecule Level .....	50
2.2.3. Single-Molecule Intensity Fluctuations .....	51
2.2.4. Single-Molecule FRET (smFRET) .....	57
<b>3. MATERIALS AND METHODS</b> .....	<b>61</b>
<b>3.1. Spectrally-Resolved Fluorescence Lifetime Microscopy</b> .....	<b>61</b>
3.1.1. Time-Resolved Fluorescence Microscopy .....	71
3.1.2. Time-Correlated Measurements at the MicroTime 100 Set-up .....	78
3.1.3. Two-Colour Excitation .....	80
<b>3.2. Ensemble Spectroscopic Instrumentation</b> .....	<b>81</b>
3.2.1. Steady-State Measurements .....	81
3.2.2. Time-Resolved Spectroscopy .....	82
<b>3.3. Biological and Chemical Methods</b> .....	<b>84</b>
3.3.1. Conjugation Chemistry .....	84
3.3.2. Surface Preparation Techniques .....	87

---

3.3.3. Influencing the Chemical Environment of Fluorophores.....	89
<b>4. RESULTS AND DISCUSSION.....</b>	<b>93</b>
<b>4.1. Photophysical Properties of Fluorescent Dyes .....</b>	<b>93</b>
4.1.1. Three Classes of Dyes: Carbocyanines, Rhodamines and Oxazines .....	94
4.1.2. Cy5 at the Single-Molecule Level.....	100
4.1.3. MR121 at the Single-Molecule Level.....	104
4.1.4. ATTO647 at the Single-Molecule Level.....	108
4.1.5. Rhodamine Green at the Single-Molecule Level.....	112
4.1.6. Rhodamines in smFRET-Pairs at the Single-Molecule Level.....	119
<b>4.2. Design of a Unidirectional Photonic Wire .....</b>	<b>124</b>
4.2.1. Configuration of Photonic Wires Based on 60bp DNA.....	126
4.2.2. Estimating Energy Transfer Efficiencies in Photonic Wires from Ensemble Steady-State Measurements.....	129
4.2.3. Time-Resolved Ensemble Spectroscopy of Photonic Wires .....	138
<b>4.3. Studying Photonic Wires with Single-Molecule Spectroscopy .....</b>	<b>145</b>
4.3.1. Spectrally Resolving Single Photons on Four Detector Channels.....	146
4.3.2. Photonic Wires Adsorbed on Dry Glass Substrate.....	148
4.3.3. Photonic Wires Immobilized in Aqueous Solution .....	154
4.3.4. Building-Up Single Photonic Wire Molecules on a Surface .....	159
4.3.5. Time-Resolved Single-Molecule Spectroscopy of Photonic Wires.....	162
4.3.6. Polarized Excitation of the Input Unit Rhodamine Green .....	169
<b>4.4. Carbocyanine Dyes as Optical Single-Molecule Switch.....</b>	<b>172</b>
4.4.1. Switching of Single Cy5 Molecules Immobilized in Solution.....	173
4.4.2. Mechanistic Studies on Cy5-Photoswitch .....	175
4.4.3. Optical Switching of Cyanine Dyes in Ensemble Experiments.....	181
<b>5. CONCLUSION AND OUTLOOK.....</b>	<b>183</b>
<b>5.1. DNA Based Photonic Wires .....</b>	<b>183</b>
<b>5.2. Single-Molecule Photoswitch: A Mechanistic View.....</b>	<b>189</b>

<b>6. REFERENCES .....</b>	<b>195</b>
<b>7. PUBLICATION LIST .....</b>	<b>211</b>
<b>7.1. Publications in Scientific Journals .....</b>	<b>211</b>
<b>7.2. Conference Presentations .....</b>	<b>212</b>
<b>8. ABBREVIATIONS.....</b>	<b>213</b>
<b>9. ACKNOWLEDGEMENTS .....</b>	<b>215</b>



# 1. Introduction

Nanometer scale optical architectures are of great interest as photonic and electronic devices with potential applications in dense optical circuits, optical data storage and materials chemistry [Yablonovitch, 2001; Vukusic and Sambles, 2003; Hu and Schulten, 1997]. Two prominent examples of optically addressable nanostructures which were the subject of this work represent molecular photonic wires and optical switches.

While classical optical waveguides rely on propagating modes in the far field, nanometer-sized molecular photonic devices guide light via near-field interactions of molecules in close proximity. In other words, molecular photonic wires transfer light via electronic excitation transfer (EET). On the level of nanometer-sized molecular devices, the transport of excitation energy is advantageous because it circumvents the connection problem present in electric wires, i.e. the bottleneck that occurs when trying to connect molecular devices with macroscopic ones. In the case of a molecular photonic wire, excited state energy is induced into an input unit by means of light, transported through transmission elements and finally emitted at another wavelength and location by an output unit (see figure 1-1). Otherwise, the energy can be used for an electron-transfer reaction, i.e. the conversion of excited-state energy into an electric charge with the possibility for subsequent chemical reactions.

Long before the design and construction of efficient photonic wires with molecular

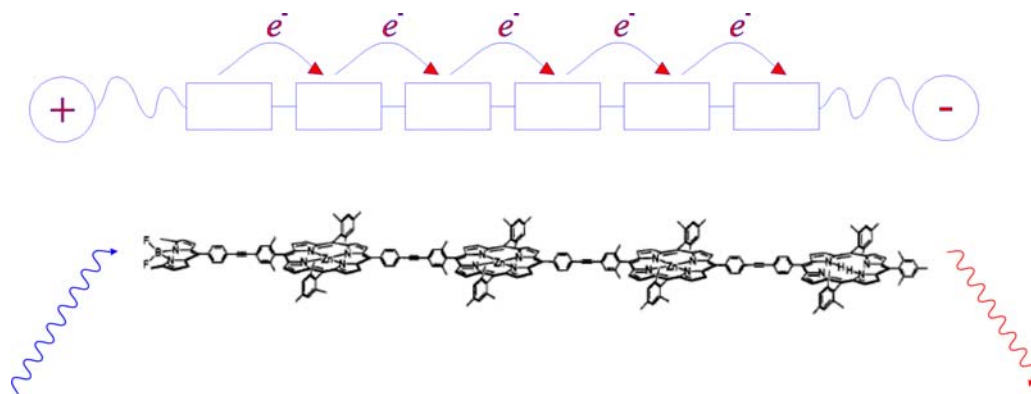


**Figure 1-1: Working principle of an electronic wire compared to a photonic wire.**

dimensions were subject in research, nature had already evolved several examples of photonic nanostructures to guide light from the light-harvesting complexes to the reaction centre as the initial steps of photosynthesis [Deisenhofer et al., 1984; Glazer, 1989; Hu and Schulten, 1997; Glazer, 1989] (illustrated in figure 1-2). After absorption of a photon by a pigment-protein complex has occurred, the excitation energy is conveyed from one light-harvesting chromophore to another in a series of radiationless transfers, which end at a special pair of chlorophyll molecules within the transmembrane reaction centre complex. Often, hundred to thousands of pigment molecules are associated with one reaction centre, and the energy transfer from the absorbing pigment to the reaction centre can comprise up to hundreds of energy-transfer steps.

Intensive experimental and theoretical efforts have been ventured to understand the energy-transport mechanisms in such natural light-harvesting complexes. In particular, the large energy-transfer efficiency achieved by these antenna complexes has stimulated the synthesis of various artificial multichromophoric systems to mimic natural photosynthetic light harvesting systems. Most approaches to artificial systems synthesised arrays of covalently linked chromophores with a specific design to ensure large collection efficiencies and fast and efficient energy migration. Like the natural antenna, most of these systems are based on porphyrin pigments [Wagner

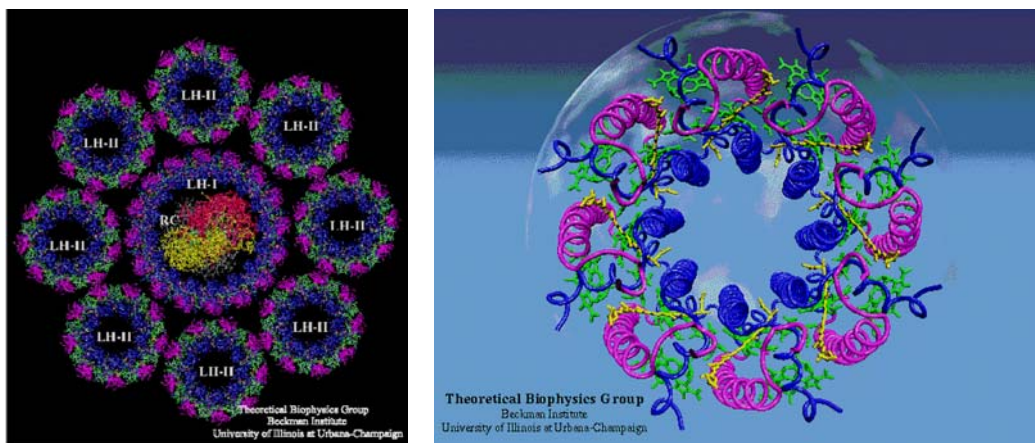


**Figure 1-2: Arrangement of a light harvesting complex in the photosynthetic reaction centre of bacteria (left; subunits LH-I and LH-II, reaction centre RC). LH-II complexes (right side) are responsible for energy transfer to LH-I and serve as antenna complexes. (images are courtesy of the Theoretical Biophysics Group, University of Illinois, Urbana-Champaign).**

and Lindsey, 1994; Seth et al., 1996]. Lindsey and co-workers first demonstrated in 1994 that a wire composed of a boron-dipyrrin (BDPY) input unit, three zinc porphyrins and a free-base porphyrin (Fb) joined via diarylethyne linkers shows predominately emission from Fb after excitation of BDPY at 488 nm. The end-to-end energy-transfer efficiency in the wire was estimated to be 76%.

However, a conceptual difference between light-harvesting complexes and photonic wires has to be pointed out: the former usually exhibit dendritelike structures with the goal being to rapidly and efficiently transfer energy to a reaction centre, and to operate the reaction centre at full capacity. Light-harvesting antennae are exemplary of efficient energy transfer. On the other hand, they are not optimised to transport excited-state energy unidirectionally over long distances.

The key parameters for the design of an artificial EET system are the selection of suitable fluorophores and the precise control of their interactions. Nature uses both parameters to optimise the absorption efficiency and the energy flow from the harvesting complexes to the reaction centre. The pigments used exhibit an energy cascade, which directs the energy towards the lower energy sites and thereby towards the reaction centre. The arrangements of pigments is such that the energy is quickly and efficiently transferred between chromophores without losing energy by alternative pathways, such as internal conversion or energy transfer processes. It is interesting to note that, in order to fulfil this task, not a single energy transfer mechanism is employed, but depending on the species and location in the energy transfer cascade, different mechanisms are realized.

Firstly, chromophore interactions have to be divided into two regimes depending on the extent of their electronic interaction: i) In some cases, the chromophores are arranged so closely that their wave functions mix strongly to produce new, delocalised states (exciton states) as, for example, in the B850 ring of LH2 or in chlorosomes [van Oijen et al., 1999; Psencik et al., 2003]. The presence of excitonic states with different energies leads to substantial changes in the absorption spectrum of the “supermolecule” compared to that of the composite of the individual chromophores (figure 1-3 b). In this strong coupling regime, the interaction energy is much larger than the vibrational energy, so that numerous energy transfers can take place during a single vibration. Under these conditions, electronic excitation becomes a “communal” phenomenon, and intramolecular vibrations are uncoupled from

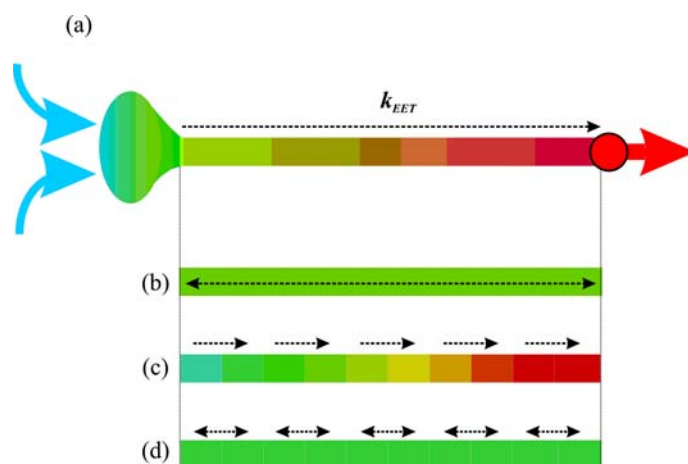


**Figure 1-3: (a) Schematic working principle of a photonic wire: light is collected by a funnel-like input unit and transferred via EET to an output unit. Interactions of fluorophores can be divided into: (b) In the strong coupling limit (coherent EET), donor and acceptor electronic states mix strongly, which results in delocalisation of the excitation energy ideally over the whole molecule. In the weak coupling limit, fast nuclear relaxation localises the initial excitation on the chromophores prior to stepwise EET via a cascade of chromophores (c) or via energy hopping (d).**

electronic excitation, with far-reaching changes in the shape of the absorption band.

ii) In most cases, however, the chromophores are spaced further apart and show weak electronic interaction. Here, energy transfer is governed by Coulombic interactions, and the absorption spectrum constitutes the sum of the individual components. In this weak coupling regime, fast nuclear relaxation localises the initial excitation prior to EET. Accordingly, EET can be well-described within the framework of the FÖRSTER theory [Förster, 1948]. Coulombic interactions can occur either between a donor-acceptor pair with distinct absorption and fluorescence spectra (figure 1-3 c), or between identical chromophores, if they exhibit sufficient energetic overlap for this process (figure 1-3 d). This so-called homotransfer or energy hopping represents a key mechanism for energy transport in some light-harvesting complexes. The challenge in constructing a photonic wire that is optimised for long-range energy transfer is the compromise between providing directionality by introducing an energy cascade and minimising energy loss by exploiting energy hopping as energy-transfer mechanism.

As an extension to mere energy transfer over longer distances in artificial molecular photonic wires, it is of great interest to control the energy flow, i.e. by applying a switching unit. Over the past few years, molecular switches of different types have

been intensively researched, in the quest for molecular electronic devices. Some switching systems operate by a conformational change in the molecule, induced by either an electric field [Donhauser et al., 2001], a STM (scanning tunneling microscope) tip [Moresco et al., 2001], an electrochemical reaction [Bissell et al., 1994] or light [Giordano et al., 2002]. Alternatively, molecular switches can be operated nonconformationally by redox reactions [Gittins et al., 2000] or a chemical binding event [Kasibhatla et al., 2003]. Very recently, it was demonstrated that the fluorescence of individual dye-labelled DNA molecules can be reversibly switched from green to red and vice versa upon application of an electric field [White et al., 2004]. In the present work, the focus was set onto a combined chemical and light-induced manipulation of intermediate states of single fluorescent molecules.

It is the complexity of the described systems - independent of the energy-transfer mechanism employed - which determines the need for new analytical techniques for the characterisation of bottom-up nanotechnological devices, such as photonic wires and photoswitches. Single-molecule fluorescence spectroscopy (SMFS) is a technique that provides detailed information required for the analysis of static heterogeneity [Kapanidis et al., 2005]. In addition, SMFS also enables to probe the quality of the device. Molecular photonic wires and photoswitches have to operate at the single-molecule level and, hence, they have to be characterised at this individual level as well.

Optical single-molecule detection was first realized in the year 1976 with the detection of single antibodies labelled with 80 to 100 fluorophores [Hirschfeld, 1976]. Thirteen years later, two groups independently demonstrated the detection of a single fluorescent molecule at cryogenic temperature in a solid host matrix [Moerner and Kador, 1989; Orrit and Bernard, 1990]. A short time later fluorescence emission from single molecules could be detected at room-temperature [Shera et al., 1990]. An important step towards better sensitivity in SMFS was made in 1992 by combining this technique with the principle of confocal microscopy [Rigler et al., 1992]. In the following years, a dramatic increase of research efforts towards new techniques based around SMFS were observed.

Nowadays, confocal SMFS is a well-established technique, which is elaborated in a number of reviews [Nie and Zare, 1997; Moerner and Orrit, 1999; Ambrose et al., 1999; Boehmer and Enderlein, 2003; Moerner and Fromm, 2003; Tinnefeld and

Sauer, 2005; Neuweiler and Sauer, 2005]. Applications of this technique touch various fields of research, comprising physical, chemical and biological sciences [Weiss, 1999; Bustamante, 2000; Weiss, 2000]. The strength of this technique lies in the ability to detect single fluorophores both in solution and adsorbed onto a surface. Averaging of molecular properties observed in ensemble experiments is circumvented, and subpopulations or molecular processes otherwise not accessible can be investigated using SMFS.

As an important rule underlying the observation of single molecules, the *ergodic principle* concludes that the sum of many single-molecule events, integrated over a long period of time, should reflect the results from an ensemble measurement. In other words, the result of an average measurement is also obtained from a single molecule, observed for a long time. The principle is portrayed in figure 1-4: if a single fluorophore is observed, a distinct wavelength of each emitted photon can be recorded. All photons emitted by this molecule can be summed up and represent the emission spectrum of an ensemble of fluorophores.

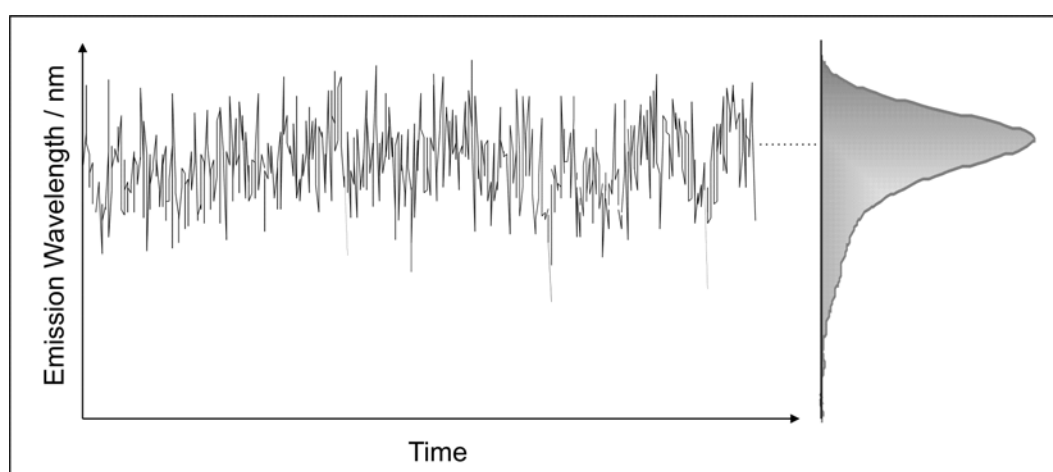


**Figure 1-4: Representation of the ergodic principle: the emission wavelength of fluorescence photons from one single fluorophore observed for a long time (left side) reflects the averaged emission spectrum of an ensemble of fluorophores (right side).**

Due to a very small excitation volume in confocal microscopy, SMFS in solution can be used for very sensitive detection of fluorescent probes down to concentrations of  $10^{-12}$  M, which also opens applications in diagnostic research [Neuweiler et al., 2002]. Adsorbed onto a surface, the fluorescence response of a single fluorophore and its



**Figure 1-5: Confocal fluorescence image of fluorophores anchored on a protein surface (10  $\mu\text{m}$  x 10  $\mu\text{m}$ ). Fluorescence signatures of single molecules exhibit “blinking” and “bleaching”.**

interactions with the nearest environment can serve as a probe for the nanoscopic environment [Macklin et al., 1996].

The main technique for single-molecule detection applied in this work is spectrally-resolved fluorescence lifetime imaging microscopy (SFLIM) [Tinnefeld et al., 2001]. A confocal line scanning microscope was equipped with four spectrally separated detectors and various excitation sources. The method goes beyond the mere detection of fluorescence photons and provides additional information, such as fluorescence lifetime and emission wavelength. Together with the modulation of the polarization of an excitation light source, the method provides a powerful tool for the investigation of multichromophoric compounds. Fluorescence signatures derived from single fluorophores anchored on a protein surface are portrayed in figure 1-5. The scan image shows two typically observed properties of single fluorophores, which are intermittencies in fluorescence emission (often termed “blinking”) due to reversible transitions into dark-states of different nature and irreversible photodestruction (“photobleaching”).

To be able to investigate the performance of complex nanomolecular constructs at the single-molecule level, the device has to fulfil certain conditions in terms of photostability and fluorescence quantum yield. Fluorophores must be selected carefully, and conditions for high photostability have to be found for a set of fluorophores to realize multichromophoric compounds. Combined with a modular approach, the construction of complex devices is simplified. This underscores the strength of the DNA-based conception, which enables the free choice of fluorophores and manifold arrangements and combinations of fluorophores.

Recent developments in nanotechnology and optoelectronics have focused research attention onto the possibility to use single fluorescent molecules as molecular photonic switches and optical data storage elements [Gittins et al., 2000; Dickson et al., 1997; Irie et al., 2002]. To store one bit per molecule by its fluorescence intensity in a reversible fashion, single molecules have to be switched digitally in a controlled manner by external stimuli. Usually, changes in fluorescence intensity from single molecules are attributed to quenching, stochastic intersystem crossing events to triplet states, or spectral diffusion due to fluctuations in the local environment of the chromophores. In cases where such fluctuations can be controlled, highly reproducible switching can be achieved, as was shown for light-induced frequency jumps in liquid helium temperature experiments [Basché and Moerner, 1992]. The green fluorescent protein (GFP) and some derivatives constitute the first room temperature all-optical examples of chromophores that can be reversibly switched between different nonfluorescent and fluorescent states at the single-molecule level [Dickson et al. 1997; Peterman et al., 1999; Jung et al., 2005, Chirico et al., 2004]. These natural photoactivatable chromophores are particularly interesting for precise photolabelling and tracking of proteins in living cells [Chudakov et al., 2004].

More recently, the first room temperature single-molecule photoswitch based on optical switching of the transfer efficiency in a fluorescence resonance energy transfer (FRET) pair was demonstrated [Irie et al., 2002; Fukaminato et al., 2004]. In a two-color experiment, a donor chromophore (bis(phenylethynyl)anthracene) connected to a switchable quenching unit (a diarylethene derivative) could be switched on and off by 488- and 325-nm light, respectively. UV light was used to activate the quencher (energy transfer acceptor), while 488-nm light was used for deactivation of the quenching unit and probing of the fluorescence of the donor chromophore. The use of identical wavelengths (488 nm) for probing and switching was possible because the deactivation (isomerisation) is about 1000 times less efficient than the activation of the quenching unit. Thus, probing and isomerisation can be controlled by changing the excitation light intensity.

On the other hand, single-molecule fluorescence experiments have revealed several expected and unexpected photophysical phenomena of the carbocyanine dye Cy5 such as cis-trans isomerisation, off states additional to triplet formation, and complex photobleaching pathways including nonfluorescent intermediates that still absorb light in the visible range [Ha 1999; Tinnefeld 2001; Tinnefeld 2003; Ha 2003; Widengren

and Schwille 2000]. These facts raise hope that a controlled microenvironment might stabilize intermediate states and open the way for reversible transitions, recovering the fluorescent state of the fluorophore.

This thesis presents the design and spectroscopic investigation of photonic nanostructures such as unidirectional molecular photonic wires and optical switches. Methods involved to scrutinise the working principle of these optical elements include ensemble spectroscopic and single-molecule fluorescence techniques. In the frame of this work, a confocal line scanning microscope with four detector channels and various excitation sources for laser-induced fluorescence was built. The set-up allowed time- and spectrally-resolved detection of single fluorescence photons and modulation of the polarization of the excitation light. The sum of information obtained from each detected photon qualified the single-molecule set-up for spectroscopic studies on complex multichromophoric systems.

The main focus was on photophysical studies of unidirectional molecular photonic wires and digital photoswitches. The synthetic strategy to design photonic wire structures involved DNA as a rigid scaffold and molecular building block system. Light energy was injected into an input unit, transported along a multichromophoric arrangement of fluorophores via dipole-dipole energy transfer, and emitted by a final unit. Suitable fluorophores were attached chemically to single oligonucleotides, and hybridisation allowed the construction of different arrangements of fluorophores. Strategies towards reduced heterogeneity, improved photostability and controlled photophysics were elaborated. Furthermore, stabilizing conditions for the chemical class of rhodamine derivatives were investigated and optimised.

A second focus was set onto the development of another photonic device, i.e. an optical switching unit constituted of a fluorophore. An optical photoswitch was realized on the basis of commercially available carbocyanine dyes, e.g. Cy5 (Roche, USA) and Alexa647 (Molecular Probes, USA). An understanding of the complex pathway of photobleaching, exhibiting many intermediate states which can selectively be manipulated, allowed the microenvironment of individual carbocyanines to be arranged in a way that enabled the optical generation of reversible transitions into a dark state. By optical manipulation with two different excitation wavelengths, highly reversible “switching” of fluorescence could be demonstrated.



## 2. Theory

### 2.1. *Fluorescence Microscopy*

In the last decades, a trend towards working interdisciplinary between the classical fields of science has led to the emergence of new principal techniques. One widely used technique is fluorescence microscopy, which has developed into a method widely used in many different fields of research.

Fluorescence was first observed by SIR GEORGE G. STOKES in the middle of the nineteenth century. He made the observation that the mineral fluor spar showed blue light emission when illuminated with ultraviolet light, and coined the word "fluorescence". Stokes observed that fluorescence exhibits longer wavelengths than the excitation light, a phenomenon that has become known as the STOKES-shift.

Nowadays, fluorescence microscopy has developed into a widely applied tool in many fields of research ranging from molecular biology and biochemistry to chemistry and physics [Lakowicz, 1999]. Any system that is fluorescent or can be modified in a way that it becomes fluorescent is suitable for fluorescence microscopy. Therefore, the technique profits enormously from a large number of fluorescent probes, e.g. organic chromophores, nanocrystals or quantum dots, metallic clusters and fusion proteins. It allows the investigation of processes on a large both temporal and spatial scale, ranging from nanoseconds to seconds, and nanometers to micrometers. The spectrum of uses includes colocalization of biological substrates in cell compartments using widefield mercury lamp excitation, to single-molecule sensitive high-precision colocalization with few nanometer accuracy by spectrally resolved fluorescence lifetime microscopy (SFLIM) [Heilemann et al., 2002]. Beyond basic fluorescence information, a large number of additional parameters, e.g. spectral characteristics, polarization or coincidence, allow a high level of description in an observed system [Heinlein et al., 2005].

Fluorescence microscopy is the main technique used in this work. The basic principle of fluorescence, the spontaneous emission of a photon upon electronic excitation of a molecule via light absorption, shall therefore be described in detail in the following paragraphs.

### 2.1.1. BASIC PRINCIPLES OF FLUORESCENCE

#### Absorption

The interaction between an electromagnetic wave with matter, i.e. atoms or molecules, is based on resonant coupling of an incoming light wave inducing oscillations in a second system [Atkins, 1995]. Depending on the energy of the electromagnetic wave and the nature of the coupled system, the excitation of rotational, vibrational or electronic states may be induced. For any process of interaction between light and matter, the frequency condition of NILS BOHR represents the link between light frequency  $\nu$  and transition energy  $\Delta E$ ,

$$h\nu = \Delta E = E_0 - E_1 \quad ( 2-1 )$$

where  $h$  is PLANCK's constant. If the resonance condition is satisfied and the energy of the incoming light is suitable to excite an atom or molecule from a lower energy level  $E_0$  to a higher energy level  $E_1$ , the strength of an interaction between an electron and the electric field  $\mathbf{E}$  is related directly to the ability of the electron to "follow" the light wave and to the magnitude of the maximal charge separation effected by this interaction. The magnitude of development of charge separation as one proceeds from a ground state, represented by the wave function  $\Psi_0$ , to an excited state, represented by the wave function  $\Psi_1$ , is related to the transition dipole moment  $\vec{\mu}_{0 \rightarrow 1}$ ,

$$\vec{\mu}_{0 \rightarrow 1} = \int \Psi_1^* \hat{\mu} \Psi_0 \quad ( 2-2 )$$

where  $\hat{\mu}$  is the operator of the electric dipole moment [Atkins, 1995]. As a fundamental requirement for absorption and emission, the value of  $\vec{\mu}_{0 \rightarrow 1}$  must be finite. Described with other words, a transition can interact much better with the electric field if the charge rearrangement has an explicit dipole character.

The transition of a molecule from a lower energy state to a higher energy state is explained by oscillations between the electromagnetic field and the frequency of a transition. This process is described as induced absorption and depends on the

energy density of the electromagnetic field,  $\rho$ . The transition probability  $w$ , which describes the change of the probability to find a molecule in an excited state,  $\frac{dP}{dt}$ , has been described by EINSTEIN to be

$$w = \frac{dP}{dt} = B\rho \quad ( 2-3 )$$

In this equation,  $B$  is the EINSTEIN coefficient for induced absorption,

$$B = \frac{|\bar{\mu}_{0 \rightarrow 1}|^2}{6\varepsilon_0 \hbar^2} \quad ( 2-4 )$$

showing a square dependency on the value of  $\bar{\mu}_{0 \rightarrow 1}$  ( $\varepsilon_0$  is the dielectric constant in the vacuum). EINSTEIN could show that the coefficient for induced emission, a process important for generation of laser light, equals the coefficient for induced absorption.

For any further description, we must now differentiate between an isolated atom, or a molecule consisting of several atoms. In the first case, only electronic transitions are possible, and the degrees of freedom for motion are limited to translation of the atom. As a result, electronic transitions in atoms are discrete, or, in other words, atomic spectra are line spectra. Depending on the type of atom and the shell the excited electron originated from, excitation energies lie in a range of less than 1 eV up to hundreds of eV. Transitions in the visible light region are typically in the range of 1 to 4 eV and are usually attributed to valence band electrons.

In the case of a molecule, e.g. an aromatic compound, a certain number of degrees of freedom for both vibrational and rotational transitions exist, additional to electronic transitions. At a first point, this means that an excitation will not occur purely of electronic, vibrational or rotational nature only, but as a mixture out of all. Reflecting the energy gap between the states themselves, they are energetically separated by a factor of 100. If using wavenumbers to express the energetic difference, a common habitude in spectroscopy, characteristic values of around  $10 \text{ cm}^{-1}$  for rotational, around  $1000 \text{ cm}^{-1}$  for vibrational and around  $100\,000 \text{ cm}^{-1}$  (which equals a few eV) for electronic transitions can be given. The important point here is that any light induced transition of a molecule, following the absorption of a photon with appropriate energy, leads to a mixed excitation of different nature. Different to atoms,

these transitions are broader due to the mixing of different states, leading to broader band spectra for molecules in general.

Furthermore, we have to distinguish between the observation of absorption and emission of molecules. A *chromophore* is defined with respect to a molecule's absorption properties, whereas a *lumophore* describes a molecule exhibiting light emission. If emission is caused by fluorescence, the term *fluorophore* is used.

In the following general considerations for molecules, rotational levels are excluded for clarity, and only electronic and vibrational transitions are taken into account. In this context, a simultaneous transition of a mixed nature of both vibrational and electronic kind is often termed *vibronic*.

Light absorption is a process which can be regarded as instantaneous, and transitions occur at a time scale of  $10^{-15}$  s. Since the mass of an electron is at least three orders of magnitude lower than the mass of the nuclei, the transition time is too short for any significant displacement of nuclei. As a consequence, all electronic transitions in the energy-distance plot are vertical, which is described by the FRANCK-CONDON principle [Condon 1928] (figure 2-1). In more detail, this means that an electronic transition out of the lowest vibrational state of the ground state  $S_0$  of the molecule, which is

mainly populated at room temperature conditions, will take place into a higher vibrational level of the first electronic excited state. Upon this excitation, the molecules rapidly relax to the lowest vibrational energy of the first excited electronic state,  $S_1$ , a process referred to as vibrational relaxation. Spontaneous emission of a fluorescence photon with a similar time scale as light absorption follows the FRANCK-CONDON principle, which goes hand in hand with a vertical transition from the lowest vibrational level of  $S_1$  to a higher vibrational energy in  $S_0$ . As a result, if a particular

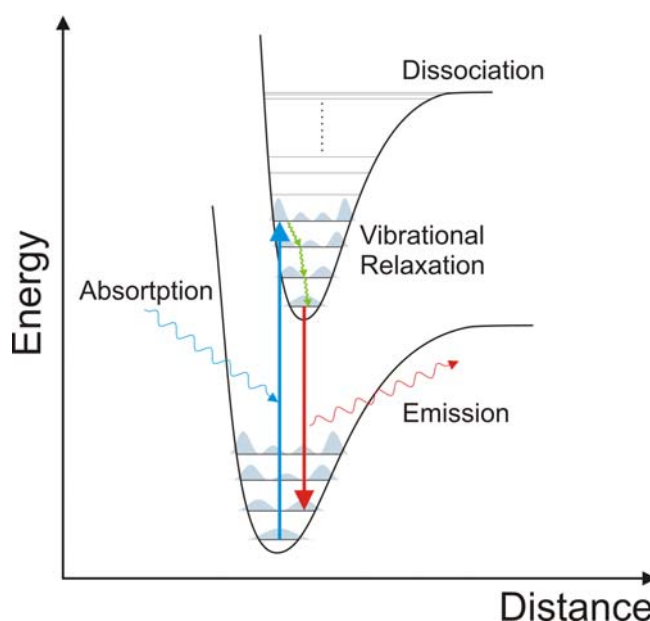


**Figure 2-1: FRANCK-CONDON-principle: Excitation of electronic transitions is fast with respect to nuclei movement, which leads to horizontal transitions into excited vibrational states.**

transition probability, also known as FRANCK-CONDON factor, between the first and second vibrational level is largest in absorption, the reciprocal transition is also most probable in emission. This fact explains the mirror image rule of fluorescence, which shall be discussed later.

A more detailed view of all possible processes in an energetic scheme of a molecule can be given using the JABLONSKI diagram, and a typical example is shown in figure 2-2. Here, the singlet ground, first and second electronic states are depicted by  $S_0$ ,  $S_1$  and  $S_2$  and so on. Triplet states of the molecule are depicted  $T_1$ ,  $T_2$  and  $T_n$ . At each electronic level, numerous vibrational and rotational levels exist, where a molecule can exist for a certain time. To simplify the scheme, only vibrational levels are included.

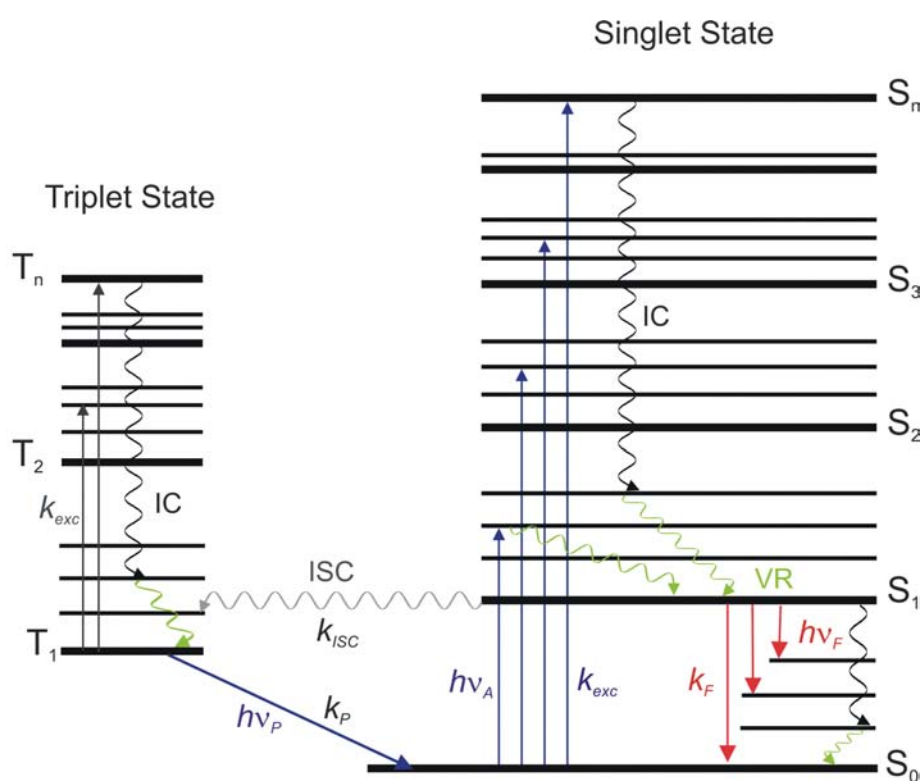


**Figure 2-2: JABLONSKI-diagram, showing a simplified scheme of energetic levels for organic chromophores (rotational states are neglected). ISC: intersystem crossing, VR: vibrational relaxation, IC: internal conversion.**

Depending on the transition probabilities of a given chromophore, the interaction of an electron with the electric field may excite a molecule out of the ground state  $S_0$  to any vibrational excited state of a higher electronic singlet state  $S_n$ . In a next step, molecules usually relax to the higher vibrational state of  $S_1$  by internal conversion on

a sub-picosecond timescale, followed by vibrational relaxation, occurring in  $\sim 10^{-12}$  s. The energy is hereby dissipated as heat via collisions with neighbouring molecules. Compared to the natural lifetime of the first excited state  $S_1$  being around  $10^{-8}$ - $10^{-9}$  s, all internal conversion processes are usually complete before emission of a fluorescence photon.

From the first excited state  $S_1$ , several radiative and non-radiative pathways of depopulation are now possible for a molecule to return to the ground state  $S_0$ , which are either directly or indirectly. The one leading to fluorescence is the radiative depopulation of  $S_1$  by spontaneous emission of a photon. According to the FRANCK-CONDON principle, this process is described by a vertical transition to a higher excited vibrational level of the ground state  $S_0$ , followed by vibrational relaxation again, and hereby reaching thermal equilibrium.

The non-radiative depopulation process of  $S_1$  is coined internal conversion (IC), which can be described as a close approach between the energy landscapes of both  $S_1$  and  $S_0$ , allowing electrons to “tunnel” between them. As a result, the molecule will be found in a highly excited vibrational level of the ground state, which is deactivated by vibrational relaxation.

A molecule in the  $S_1$  state can also undergo a spin conversion to the first triplet state,  $T_1$ . Since this transition is not spin allowed, these events are rare, and kinetic rates strongly depend on the nature of a chromophore and the transition probability. From this triplet state  $T_1$ , similar processes as already discussed for the first excited singlet state  $S_1$  are now possible, including absorption to  $T_n$ , vibrational relaxation and emission of a photon, which is now termed phosphorescence. Due to the spin forbidden transition, this takes place on a much longer timescale, from microseconds up to many seconds.

Triplet states play an important role in photophysical behaviour of organic chromophores and can be manipulated, either by increasing the intersystem crossing rate  $k_{ISC}$  using the heavy atom effect [Kasha, 1952], or depopulating triplets by using triplet quenching molecules [Widengren and Schwille, 2000]. The importance of selectively manipulating excited states in general lies in the fact that photophysical reactions, for example optically induced transitions of chromophores, have several possible pathways, e.g. higher excited singlet states, triplet states or isomerised

states. To elucidate the correct mechanism, certain pathways have to be controlled selectively.

An overview of timescales of all transitions mentioned in the JABLONSKI diagram is given in table 2-1.

Transition	Description	Rate	Time (s)
$S_0 \rightarrow S_1 \dots S_n$	Absorption (Excitation)	$k_{exc}$	$10^{-15}$
$S_n \rightarrow S_1$	Internal Conversion	$k_{IC}$	$10^{-14} - 10^{-10}$
$S_1 \rightarrow S_1$	Vibrational Relaxation	$k_{VR}$	$10^{-12} - 10^{-10}$
$S_1 \rightarrow S_0$	Fluorescence	$k_F$	$10^{-9} - 10^{-7}$
$S_1 \rightarrow T_1$	Intersystem Crossing	$k_{ISC}$	$10^{-10} - 10^{-8}$
$S_1 \rightarrow S_0$	Non-radiative Relaxation Quenching	$k_{nq}$	$10^{-7} - 10^{-6}$
$T_1 \rightarrow S_0$	Phosphorescence	$k_P$	$10^{-3} - 100$
$T_1 \rightarrow S_0$	Non-radiative Relaxation Quenching	$k_{nq,T}$	$10^{-3} - 100$

**Table 2-1: Overview of possible depopulation pathways of the first excited singlet state.**

## Emission

The emission of a fluorescence photon is a spontaneous process based on an electronic transition of a vibrational ground state of a higher excited singlet state, to a higher vibrational energy level of the electronic ground state of a molecule. According to the KASHA rule, this process usually originates from the first excited state,  $S_1$ , to a vibrational excited level of the ground state,  $S_0$ . Though excitation of an electron to higher singlet states is possible if the energy of incoming light is appropriate, there is fast relaxation from those higher excited singlet to the first excited singlet,  $S_1$ . An exception to this rule is observed in some molecules, e.g. azulene and its derivatives, which fluoresces from its  $S_2$  state [Viswath and Kasha, 1956]. The reason for the observation of  $S_2 \rightarrow S_0$  fluorescence in azulene is the relatively large  $S_2 - S_1$  energy

gap, which slows down the normally very rapid rate of internal conversion from  $S_2$  to  $S_1$  by decreasing the FRANCK-CONDON factor for radiationless transitions [Turro, 1991].

Although absorption of light resulting in electronic excitation is a completely general experimental observation, emission of light is not. Most saturated organic molecules and polyenes do not display efficient emission. However, if the process of fluorescence is observed to an observable extent, the photons emitted contain information that describe interactions of a fluorophore with its environment. The emission wavelength, i.e. the energetic component, reflects changes in the polarity of the medium surrounding a fluorophore. Fluorescence lifetime, the kinetic component of emitted photons, together with the quantum yield depend critically on competing processes which reduce the average time of population of a first excited state. In this context, resonance energy transfer or dynamic quenching processes due to photoinduced electron transfer have to be mentioned. Finally, polarization and anisotropy measurements, which exploit the similar timescale of rotation from a molecule and fluorescence, allow a description of the rotational mobility of a fluorophore and give information about the larger molecular system the fluorophore is attached to.

## **Spectrum**

A fluorescence emission spectrum is usually the mirrored image of an absorption spectrum. The reason for this behaviour lies in similar probabilities of electronic transitions into excited vibrational levels, i.e. absorption, and their reciprocal transitions, that is fluorescence. This can be easily understood if recalling the fact that electronic excitation is a very fast process that does not greatly alter nuclear geometry. Additionally, the spacing of the vibrational levels both in the ground state and the excited state are comparable. The resembling vibrational structures of the ground and excited state are the origin for the similarity of both absorption and emission spectrum. Exceptions to the mirror rule can occur if the geometry of the electronic excited state is clearly different, or, excimer or exciplex structures are formed.

Generally, a fluorescence emission spectrum does not show a dependency on the excitation wavelength for most fluorescent probes. Any excitation to higher electronic or vibrational states leads to fast relaxation to  $S_1$ , described by KASHA's rule.

### Fluorescence Lifetime and Quantum Yield

Both fluorescence lifetime, the kinetic component of fluorescence, and fluorescence quantum yield as a measure of brightness of fluorophores, are important characteristics of fluorescent probes. These parameters depend strongly on the chemical structure and the environment of a fluorescent probe. It is of high importance to choose fluorophores with the appropriate lifetime and quantum yield for a particular experiment, e.g. high quantum yield and long fluorescence lifetime for energy transfer experiments.

The fluorescence quantum yield  $\Phi_f$  is the ratio of photons emitted through fluorescence to photons absorbed, and hereby represents a measure of the efficiency of the emission process. It is described by two types of depopulation rates of the excited state  $S_1$ , which is the radiative rate  $k_r$  and the nonradiative rate  $k_{nr}$ , according to the following equation:

$$\Phi_f = \frac{k_r}{k_r + k_{nr}} \quad ( 2-5 )$$

Quantum yields close to unity suggest that the predominant pathway of depopulation of the excited state is fluorescence photon emission. In other words, the depopulation of  $S_1$  is mostly via radiative pathways. Nonradiative transitions as relaxation or internal conversion play, in this case, a minor role.

The determination of the absolute fluorescence quantum yield for a fluorophore is experimentally difficult to realize. A commonly applied method is "thermal blooming", measuring the change in refractive index of a solvent due to a temperature increase caused by thermal relaxation of excited molecules. More often, values for fluorescence quantum yields are determined with respect to a fluorophore with nearly 100% quantum yield, e.g. Rhodamine6G or Rhodamine 101. Basically, quantum yields can be determined with respect to any fluorescent probe with the absolute quantum yield known.

The average time a molecule stays in its excited state  $S_1$ , which may be referred to the kinetic information of fluorescence emission, is described by its fluorescence lifetime  $\tau_{fl}$ ,

$$\tau_{fl} = \frac{1}{k_r + k_{nr}} \quad ( 2-6 )$$

In contrast to the intrinsic or natural lifetime  $\tau_n$ , which is the lifetime of the fluorophore in the absence of any nonradiative process, its fluorescence lifetime  $\tau_{fl}$  can be observed by optical techniques like time-resolved fluorescence measurements. As shown in the JABLONSKI-diagram in figure 2-2, fluorescence is only one of several possible pathways that can result from the first excited state  $S_1$ . As a result, the observed fluorescence lifetime contains information about both radiative and nonradiative processes.

The radiative depopulation process of fluorescence is fully spontaneous and is described by first order kinetics. Similar to a radioactive decay, the temporal distribution of fluorescence photon emission,  $I(t)$ , is described by a single exponential function,

$$I(t) = I_0 \exp\left(-\frac{t}{\tau_{fl}}\right) \quad ( 2-7 )$$

If more than one depopulation process exhibiting fluorescence is, which is the case in heterogeneous samples or samples with more than one fluorophore, the temporal change of fluorescence intensity is described by

$$I(t) = \sum_i \alpha_i \exp\left(-\frac{t}{\tau_{i,fl}}\right) \quad ( 2-8 )$$

By applying time-resolved techniques, it is possible to quantify the relative contribution,  $\alpha_i$ , of the  $i$ -th component and determine its characteristic fluorescence lifetime,  $\tau_{i,fl}$ .

As a more general view, fluorescence spectroscopy can be classified into two types of measurements, steady-state and time-resolved. Steady-state measurements are characterized by constant illumination and observation of a sample and are the most common method of fluorescence experiments. Because of the nanosecond timescale of fluorescence, most experiments are done under steady-state conditions. Time-

resolved measurements are used to obtain kinetic information about fluorescence emission, and require complex and expensive instrumentation like a pulsed light source, fast electronics and sensitive detection elements. Regarding the light source used, a narrow pulse width with respect to the fluorescence decay time is required, which explains the common use of fast light emitting diodes (LED) or even better, laser diodes.

Fluorescence lifetime has a characteristic value for each fluorophore and strongly depends on any condition or environmental effect that may affect any of the rate constants involved in depopulation processes of the excited state  $S_1$ . It therefore widens the field of application of basic fluorescence spectroscopy and microscopy. Prominent examples that should be mentioned here are energy transfer rates determined by measuring decreased fluorescence lifetime as well as quenching of fluorescence taking place if a suitable fluorophore is in close proximity to quenching molecules, e.g. tryptophan or guanosine [Marmé et al., 2003].

### Measurement of Fluorescence Lifetimes

In principle, there are two widely used methods for the measurement of fluorescence lifetimes, the pulse method and the phase modulation method. In this work, the pulse method, i.e. time-correlated single-photon counting, has been preferred due to its sensitivity and ability to deal with low photon count rates. It has been the method of choice for time-resolved experiments in both ensemble and single-molecule measurements.

The underlying principle of TCSPC can be described as periodical

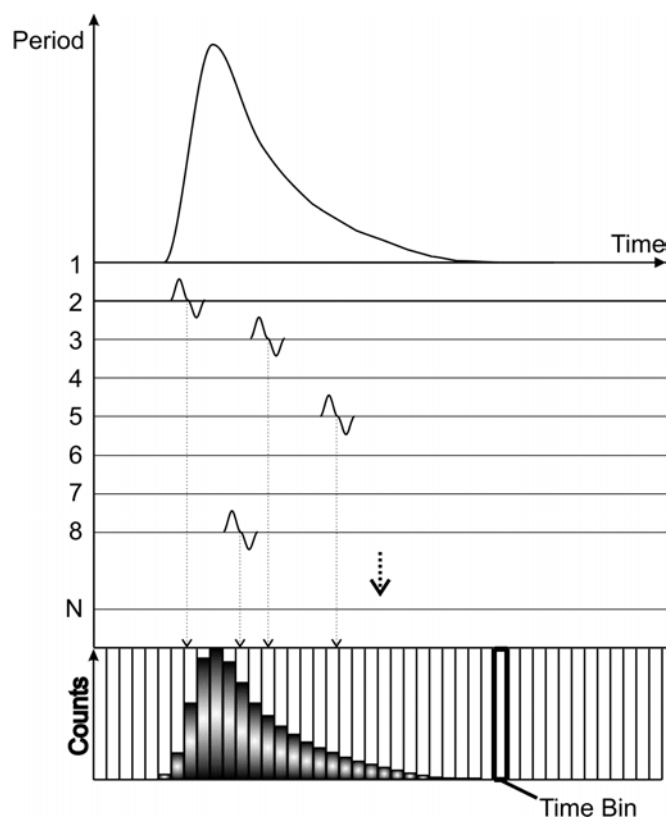


Figure 2-3: TCSPC measurement principle.

detection of photons referred to a pulse signal. Especially in experiments with low photon detection probability, i.e. a probability much smaller than one of detecting a photon during one pulse cycle, several photons arriving in one period can be neglected, and the principle shown in figure 2-3 can be used. There are many signal periods without photons, other signal periods contain one photon pulse. Periods with more than one photon are very rare. When a photon is detected, the time of the corresponding detector pulse is measured. The events are collected in memory by adding a '1' in a memory location with an address proportional to the detection time, representing a time bin. After many photon detection events, the histogram of the arrival times representing the fluorescence decay is obtained. The main advantage of this method lies in the fact that the accuracy of the time measurement is not limited by the width of the detector pulse. Thus, the time resolution is much better than with the same detector used in front of an oscilloscope or another linear signal acquisition device. Furthermore, all detected photons contribute to the result of the measurement. To prevent any detection signal from a previous excitation pulse in a measurement period, the distance between two succeeding pulses is usually chosen to be around five times the fluorescence lifetime of a measured decay. Furthermore, the photon detection probability should not exceed a value of around 5%, to prevent "pile-up" effects shortening the fluorescence lifetime decay. Pile-up effects occur if occasionally, more than one photon arrives in one detection period, and since only the first photon contributes to the histogram, photons are piled up at shorter times, leading to the appearance of shorter fluorescence lifetimes.

In many fluorescence experiments involving laser as excitation light source, the laser pulse width itself is of a comparable order of magnitude as the fluorescence lifetime. Especially excitation pulses from semiconductor lasers show a full width half maximum (FWHM) in a range of a few hundred picoseconds. As a consequence, the observed fluorescence decay  $R(t)$  obtained by the method described is represented as a convolution of the excitation pulse  $L(t)$  with the impulse response of a sample that would be obtained by applying an infinitesimal small  $\delta$  pulse,  $F(t)$ ,

$$R(t) = L(t) \otimes F(t) = \int_0^t L(\tau)F(t-\tau)d\tau \quad ( 2-9 )$$

The inverse process of deconvolution is mathematically difficult, but many different approaches to circumvent this time consuming algorithm have been developed. Two

prominent methods are used in most experiments, allowing the extraction of exact fluorescence decay information from the observed signal.

For most measurements, the simple least square (LS) approach is sufficient. This method is based on finding a set of fluorescence decays,  $\alpha_i \exp(-t/\tau_i)$ , and comparing the calculated signal,  $R_c(t)$ , which is obtained after convolution with the excitation pulse, with the measured signal,  $R(t)$ . The parameters  $\alpha_i$  and  $\tau_i$  are varied iteratively, and the quality of the result is estimated using  $\chi^2$ ,

$$\chi^2 = \sum_{i=1}^n \omega_i (R(t) - R_c(t))^2 \quad (2-10)$$

where  $\omega_i$  is a statistical weighting factor for individual errors in each value of  $R(t)$ .

If photon counts are low, as is the case in single-molecule measurements, an alternative method appears to be more suitable, called the maximum likelihood estimator (MLE). In particular for monoexponential decays, which is normally the case if a single molecule is observed and no competing interactions on the same timescale occur, the MLE offers a fast method to obtain reliable data with low error component [Enderlein et al., 1997]. The underlying function is described as

$$1 + (e^{T/\tau} - 1)^{-1} - m(e^{mT/\tau} - 1)^{-1} = N^{-1} \sum_{i=1}^m iN_i \quad (2-11)$$

where  $T$  is the width of each channel,  $m$  the number of utilized time channels,  $N$  the number of photon counts taken into account, and  $N_i$  the number of photon counts in time channel  $i$ . The left-hand side of equation 2-11 is not dependent upon the data and is a function only of  $\tau$ , while the right-hand side is determined from the experimental data. The lifetime can be abstracted from the data by the use of an reiterative technique such as NEWTON's algorithm which was applied in this work to determine the fluorescence lifetimes from single molecules.

### Fluorescence Anisotropy

If fluorescent molecules are excited by polarized light, preferentially molecules with an absorption dipole aligned parallel to the electric field vector  $\mathbf{E}$  will absorb the incoming light. As a result, selective excitation of fluorophores leads to partially polarized fluorescence emission. The transition moments for both absorption and

---

emission have fixed orientations within a fluorophore, and the relative angle between these moments determines the maximum measured anisotropy. The fluorescence anisotropy  $r$  and polarization  $P$  are defined by

$$r = \frac{I_{vv} - I_{vh}}{I_{vv} + 2I_{vh}} \quad ( 2-12 )$$

$$P = \frac{I_{vv} - I_{vh}}{I_{vv} + I_{vh}} \quad ( 2-13 )$$

where  $I_{vv}$  and  $I_{vh}$  are fluorescence intensities after vertical (v) excitation measured in the vertical and the horizontal (h) emission polarization.

If observing fluorophores freely diffusing in an isotropic solution of low viscosity, the anisotropy will mostly be close to zero. The reason for this is rotational diffusion of the molecules. With a typical rotation time around 100 ps, the orientation of the fluorophores in the excited state is then randomised, and fluorescence emission does not show any polarized component.

If the rotation time is larger than the time spent in an excited state, as is often the case for fluorophores conjugated to large biomolecules with high molecular masses, anisotropy measurements provide information about size and shape of these biomolecules. Furthermore, fluorescence anisotropy can be applied to study protein-protein interactions or interactions between proteins and nucleic acids [Lakowicz, 1999]. As a solution-based methodology, it offers a true equilibrium measure, allowing to evaluate changes in solution conditions as salt concentration, pH, and temperature [LeTilly and Royer, 1993].

Combining polarized excitation and detection with a pulsed light source, this method can be expanded to time-resolved anisotropy measurements. A time-resolved anisotropy decay is obtained and can be approximated by an exponential function, yielding the rotation time of a fluorescent molecule. Since rotation times of small molecules are in the order of 100 ps, a narrow excitation pulse and deconvolution methods are even more important than for time-resolved fluorescence measurements.

### 2.1.2. MOLECULAR INTERACTIONS INFLUENCING FLUORESCENCE

If two molecules are in close proximity, interactions of different nature depopulating the excited state without photon emission of the donor molecule may occur. These processes, varying in their distance dependence characteristics and sensitivity, are of strong interest for energy transfer studies, especially for the design and characterization of multichromophoric systems.

These molecular interactions which influence fluorescence properties of molecules can be used for the temporal observation of intermolecular distance changes below 10 nm. Any spatial or conformational change of intermolecular distance between two interacting molecules over a large timescale from nanoseconds to seconds is accessible, and these mechanisms are exploited in many fluorescence spectroscopic applications [Neuweiler and Sauer, 2004].

Molecular interactions that cause quenching of fluorescence can be divided into four basic principal mechanism, listed in table 2-2.

Energy Transfer	$F_D^* + F_A$	$\rightarrow$	$F_D + F_A^*$
Electron Transfer	$F^* + Q$	$\rightarrow$	$F^{+/-} + Q^{-/+}$
Proton Transfer	$F^* + QH$	$\rightarrow$	$FH^+ + Q^-$
Exciplex/Excimer-Formation	$F^* + M$	$\rightarrow$	$(FM)^*$

**Table 2-2: Overview of quenching processes depopulating the first excited state of an excited molecule  $F^*$ , relevant in fluorescence spectroscopy.**

Energy transfer processes can be divided into two different mechanisms. On the one hand, there is weak coupling and non-coherent interaction, which is the case in fluorescence resonance energy transfer (FRET), and takes place in a range of 2 to 10 nm interchromophoric distance. The mechanism of FRET is based on Coulombic interactions of two or more chromophores, which has been theoretically derived from classical electrodynamics [Förster, 1948] and the model of dipole-dipole coupling. The second mechanism, i.e. electron exchange energy transfer (EEET), requires

closer proximity of the molecules in order to allow orbital interactions and is characterized by electron exchange from a donor to an acceptor molecule.

Fluorescence resonance energy transfer (FRET) plays a major role in many of the chromophoric systems investigated in this work. Single molecular photonic wires of different nature have been constructed using DNA as a rigid backbone molecule, which opens the possibility to place numerous fluorophores in well defined positions relative to each other and thus enables resonant dipole-dipole coupling between the chromophores. Furthermore, the principle of FRET can be used to probe nonfluorescent dark states of acceptor molecules, that still can be in resonance with a donor molecule. This allows for photophysical and mechanistic studies of fluorophores, and was used to investigate the photoinduced conversion of carbocyanine dyes.

Electron transfer processes, often referred to as photoinduced electron transfer (PET), are part of the complex mechanism of photosynthesis, by converting light energy into chemical energy. This mechanism involves an interaction of a fluorophore with electron donating or accepting molecules, and results in quenching of fluorescence through the generation of radical states. In contrast to FRET, a collision between molecules is required. Though, electron transfer occurs only on shorter distances, and the method allows the monitoring of smaller spatial changes, which has been successfully applied in folding studies of peptides, proteins, DNA or RNA biomolecules [Neuweiler and Sauer, 2004].

Photoinduced electron transfer, which results in the formation of either radical cation or anion of a chromophore and hereby substantially changes its fluorescence properties, is a redox active process which has been exploited in studies of chromophores of different nature [Speiser, 1996]. By changing the redox properties of the surrounding microenvironment of a molecule and choosing the appropriate redox partner molecule, a longer observation time and stable fluorescence emission of single chromophores could be achieved. Additionally, the process of switching cyanine dyes in aqueous solution requires the presence of electron donating molecules in millimolar concentration, which strengthens the mechanistic interpretation that radical states of the fluorophore are involved.

The reversible protonation or deprotonation of a fluorescent probe can also cause quenching of fluorescence. The protonation of the chromophoric centre of a protein

was recently shown to be the origin of the switching behaviour of fluorescence observed in the fusion proteins green fluorescent protein (GFP) and yellow fluorescent protein (YFP) [Kennis et. al, 2004; McAnaney et al., 2005].

Due to their importance in this work, both FRET and PET merit a more detailed description.

## Fluorescence Resonance Energy Transfer (FRET)

Energy transfer interactions based on through space dipole-dipole coupling, often referred to as weak coupling or non-coherent coupling, are the heart of FÖRSTER'S theory of fluorescence resonance energy transfer (FRET) [Förster, 1948]. In a simple mechanistic view, an initially excited donor molecule transfers its excited

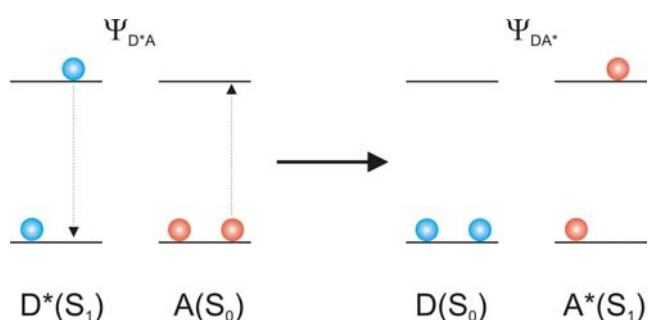


**Figure 2-4: Schematic representation of the Förster transfer mechanism, FRET.**

energy radiationless to an acceptor molecule via the electrodynamic coupling of both molecules. This process, which in the case of commonly used organic chromophores occurs at distances between 2 and around 10 nm, is depicted in figure 2-4. A large number of reviews from many fields of different application of the FÖRSTER mechanism have already been published [Clegg, 1992; Clegg, 1995; Yang and Millar, 1997; Selvin, 2000; Jares-Erijman and Jovin, 2003], showing the impact of resonant energy transfer.

The donor molecule in the weak coupling limit usually emits at a shorter wavelength, and the emission spectrum of the donor overlaps with the absorption spectrum of the acceptor

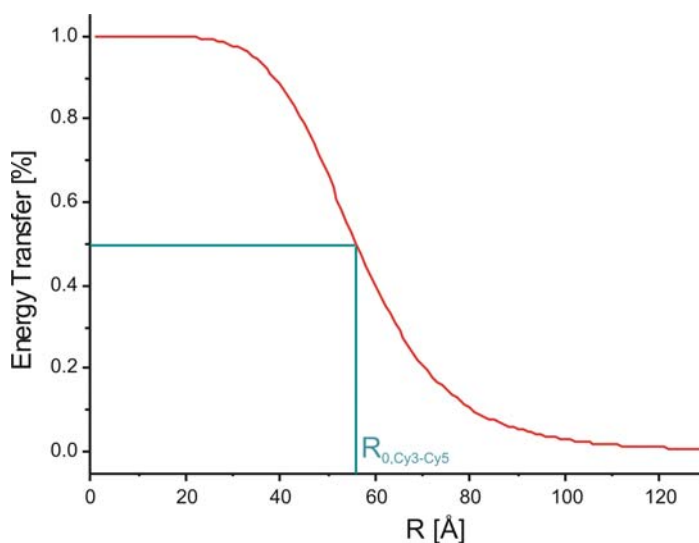


**Figure 2-5: Distance dependency of FRET. The blue line emphasizes 50% transfer efficiency for a FRET pair of Cy3 and Cy5 (Förster radius,  $R_0 = 5.6$  nm).**

molecule. In his work, FÖRSTER could derive a theoretical model for resonance energy transfer, and could show that the rate of energy transfer,  $k_T$ , depends on the inverse 6<sup>th</sup> power of the interchromophoric distance,  $r$ , (see figure 2-5), via

$$k_T(r) = \frac{1}{\tau_D} \left( \frac{R_0}{r} \right)^6 \quad (2-14)$$

$R_0$  is a characteristic value for a given set of chromophores, often called FÖRSTER radius, and can be determined from the following equation,

$$R_0^6 = \frac{9000(\ln 10)\kappa^2 Q_D}{128\pi^5 N n^4} \int_0^\infty F_D(\lambda) \varepsilon_A(\lambda) \lambda^4 d\lambda \quad (2-15)$$

Here,  $Q_D$  is the quantum yield of the donor molecule,  $n$  is the refractive index,  $N$  is AVOGADRO's constant, and the integral expression describes the spectral overlap of the fluorescence of a donor molecule,  $F_D$ , and the extinction of an acceptor molecule,  $\varepsilon_A$ , with respect to the wavelength,  $\lambda$ . This spectral overlap integral has a crucial impact on transfer efficiency, explained by energetic overlap of the donor emission spectrum and the acceptor absorption spectrum.

Of the experimental factors necessary for an energy transfer distance estimate, the hardest to determine is  $\kappa^2$ , the "orientation" factor:

$$\kappa^2 = (\cos \theta_T - 3 \cos \theta_D \cos \theta_A)^2 \quad (2-16)$$

Depending on the orientation of dipoles to each other and their mobility on the timescale of energy transfer, this value may adapt values from 0 to 4 (figure 2-6).

In general, the actual value of  $\kappa^2$  is not experimentally measurable. The simplest approximation is to assume that both donor and acceptor transition dipoles are undergoing motion that randomises orientations much faster than the donor is decaying to its ground state. The randomisation must be due to each probe sampling all orientations, not due to static distribution probes. Assuming oriental randomisation of both fluorophores, the dynamically averaged isotropic limit holds, and unhindered and independent rotation of both dipoles yields a value of  $\kappa^2 = 2/3$  [Dale et al., 1979; Torgerson and Morales, 1984]. Methods to verify the assumption of a freely rotating fluorophore include anisotropy measurements or modulated excitation.

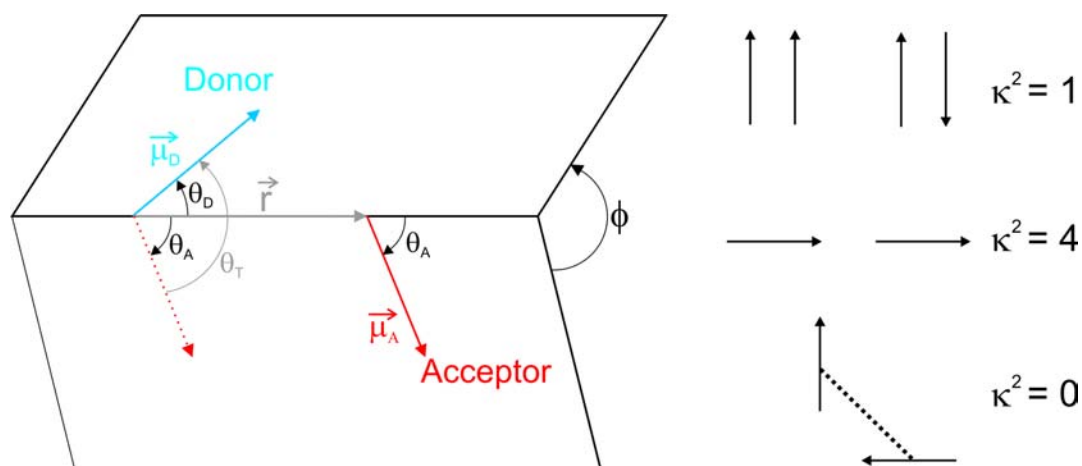


Figure 2-6: Dependence of the orientation factor  $\kappa^2$  on the directions of the emission dipole of the donor and the absorption dipole of the acceptor.

Typical  $R_0$  values for a number of fluorophores that were also used to build photonic wire molecules in the experimental section of this work, together with their quantum yields and spectral properties, are listed in table 2-3.

	$\lambda_{\text{abs}}/\text{nm}$	$\lambda_{\text{em}}/\text{nm}$	$\varepsilon/l \text{ mol}^{-1} \text{ cm}^{-1}$ ( $\times 10^5$ )	$\Phi_{\varepsilon}$	$R_0/\text{\AA}$
<i>RhodGreen</i>	508	534	0.74	0.9	65.0
<i>TMR</i>	560	582	0.95	0.9	71.7
<i>ATTO590</i>	603	625	1.20	0.8	72.3
<i>LCR</i>	622	638	1.20	0.8	74.5
<i>ATTO680</i>	689	703	1.25	0.3	

Table 2-3: Spectroscopic parameters and  $R_0$ -values of some chromophores used for the construction of DNA-based photonic wires.

The efficiency of energy transfer,  $E$ , which is the fraction of photons absorbed by the donor and transferred to the acceptor, is given by

$$E = \frac{k_T}{\tau_D^{-1} + k_T} \quad (2-17)$$

As a result, the efficiency  $E$  is the ratio of the transfer rate to the total decay rate of the donor molecule, and is easily rearranged using equation 2-14 to

$$E = \frac{R_0^6}{r^6 + R_0^6} \quad ( 2-18 )$$

In practice, fluorescence energy transfer efficiency is typically determined in two different ways [Clegg 1992]. One possible method is to determine the relative fluorescence intensity of the donor both in the absence and presence of the acceptor,  $F_D$  and  $F_{AD}$ . Similarly, fluorescence lifetime values under the same conditions,  $\tau_D$  and  $\tau_{AD}$  respectively, can be used to determine  $E$ :

$$E = 1 - \frac{F_{DA}}{F_D} \quad ( 2-19 )$$

$$E = 1 - \frac{\tau_{DA}}{\tau_D} \quad ( 2-20 )$$

Both equations 2-19 and 2-20 are only applicable for a pair of chromophores with fixed distance and a homogeneous sample. If fluorescence lifetimes are used to determine  $E$  and no single exponential decay is observed, it is important to use average lifetimes, given by the sum of the  $\alpha_i \tau_i$  products, where  $\alpha_i$  describes the relative fraction of a component  $i$ .

The distance dependency of FRET and the range of 2 – 10 nm typical for this type of energy transfer suggests its use as a spectroscopic ruler [Stryer and Haugland, 1984; Dietrich et al., 2002]. In most experiments, it is more common to use relative distance changes, hereby selecting the range from  $0.5R_0$  to  $1.5R_0$ . In this range, the important slope of  $E$  with respect to the distance can be exploited. As an example for larger distances: assuming a distance of  $r=2R_0$  yields to a relative energy transfer rate decreased to 1.56%. Nevertheless, using short and rigid molecular scale molecules like DNA or polyprolines, FRET is sometimes used to determine absolute distances and subpopulations [Schuler et al., 2005].

### Electron Exchange Energy Transfer

In the case of electron exchange energy transfer, much shorter distances between molecules are needed. The mechanism involves an electron exchange step between the lowest unoccupied molecular orbital (LUMO) of an acceptor A and the semi occupied molecular orbital (SOMO) of a donor D, depicted in

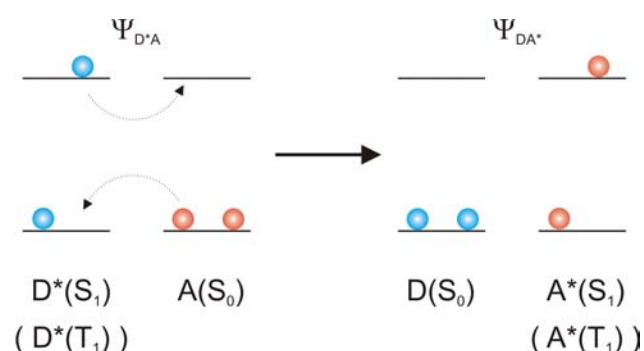


**Figure 2-7: Schematic representation of electron exchange mechanism.**

figure 2-7. Theoretical work was first carried out by DEXTER [Dexter, 1953] who proposed an exponential distance dependency for the rate of electron exchange energy transfer,  $k_{EEET}$ ,

$$k_{EEET} = KJ e^{(-2R_{DA}/L)} \quad (2-21)$$

In the proposed model,  $k_{EEET}$  depends on the spectral overlap integral,  $J$ , of donor and acceptor, which is normalized to the extinction coefficient of the acceptor A and thereby independent on the acceptor's absorption characteristics, which is in contrast to the mechanistic model presented for FRET (see equation 2-15). Further,  $K$  represents a specific constant for a specific orbital interaction,  $R_{DA}$  is the distance between donor and acceptor and  $L$  is the sum of the VAN DER WAALS radii of both molecules.

### Photoinduced Electron Transfer (PET)

Light-induced transfer of an electron occurs due to changes in the redox properties of excited molecules. In those cases, molecules are more potent electron donors or acceptors. If a quencher molecule is present a redox reaction will take place. Like any electrochemical reaction based on electron transfer, this is only possible if free energy is won, which can be estimated from the electrochemical potentials of the participating molecules.

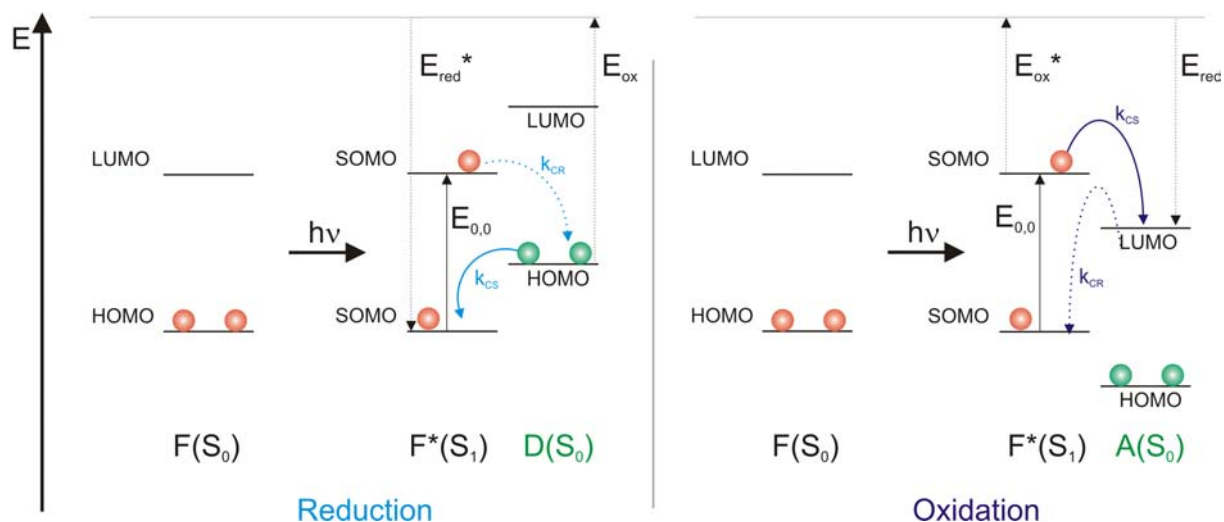


**Figure 2-8: Simplified schematic presentation of photoinduced electron transfer, left: reduction of fluorescent molecule in its excited state  $F^*$  by an electron donor  $D$ , right: oxidation by an electron acceptor  $A$ .  $k_{CS}$  and  $k_{CR}$  denote the rate of charge separation and recombination, respectively.**

After excitation of a donor molecule by light, one electron from the highest occupied molecular orbital (HOMO) is transferred to an energetically higher semi occupied molecular orbital (SOMO). Depending on the redox potential of the excited molecule and a second molecule around, two reaction pathways are possible. In the first, which represents the oxidation of the first molecule, the electron from the SOMO is transferred into the lowest unoccupied molecular orbital (LUMO) of an acceptor molecule,  $A$ , forming a radical cation. In the reduction path, an electron from the HOMO of a donor molecule,  $D$ , is transferred into the lower SOMO of the excited fluorescent molecule, generating a radical anion and inhibiting fluorescence (figure 2-8).

Whether an electron transfer is feasible depends on the change of the free energy of the charge separation process,  $\Delta G_{CS}^0$ , which can be estimated by the oxidation and reduction potentials,  $E_{ox}$  and  $E_{red}$ , the transition energy  $E_{0,0}$  and the COULOMB potential of the charge separated state,  $\Delta G_{Coul}^0$ ,

$$\Delta G_{CS}^0 = E_{ox} - E_{red} - E_{0,0} + \Delta G_{Coul}^0 \quad (2-22)$$

If fluorescence quenching experiments are carried out in the same solvent used for the determination of the redox potentials, solvation energies of the radical ion pair

can be neglected and the free reaction enthalpy can be calculated using the classical REHM-WELLER equation [Rehm 1969]:

$$\Delta G_{Coul}^0 = \frac{-e^2}{\epsilon_s R_C} \quad ( 2-23 )$$

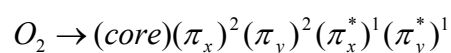
This equation describes the distance dependency of the coulombic term  $R_C$  in PET to be  $\sim 1/R_C$ , including the solvent dielectric constant,  $\epsilon_s$ .

### 2.1.3. THE ROLE OF OXYGEN

Molecular oxygen is an important participant in photochemical processes because of its high chemical energy content, its unique reactivity characteristics and its low lying excited states. In many reaction systems, the ubiquitous presence of molecular oxygen influences the photophysics of fluorophores. At single molecule concentrations, the concentration of oxygen becomes important as the probability of a collision with a fluorophore increases. The result of such a collision depends on the energy of photophysical states involved in the reaction, and subsequent reactions, e.g. photobleaching due to epoxide formation, are possible.

#### Molecular Description

In its ground state, oxygen appears as a biradical, and can be described by the following electron configuration:



where  $\pi_x$  and  $\pi_y$  denote binding  $\pi$ -orbitals filled each with two paired electrons, and  $\pi_x^*$  and  $\pi_y^*$  are unbinding  $\pi$ -orbitals filled each with one electron that have parallel spin orientation to each other, presenting a triplet ground state. Considering the orbital occupancies of the unbinding  $\pi$ -orbitals filled with two electrons, four possible occupancies are possible. Besides the triplet ground state, three possible excited states with singlet character can be constructed. The electron orbital occupancy corresponding to all four states, together with energy levels and spectroscopic annotations, are shown in figure 2-9.

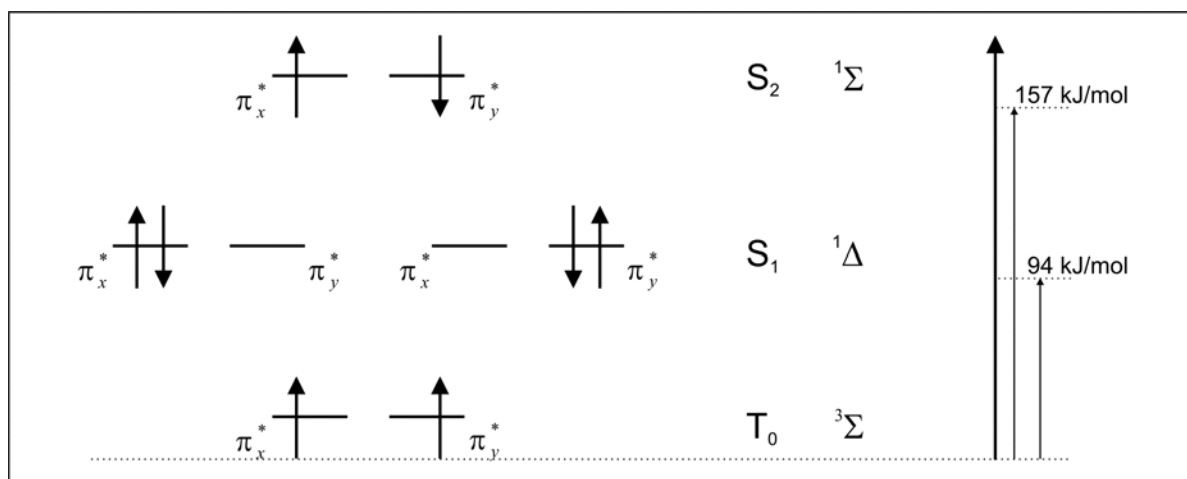


**Figure 2-9: A qualitative description of the three lowest electronic orbital configurations and states of molecular oxygen.**

The pure radiative lifetimes of the singlet states  $^1\Delta$  and  $^1\Sigma$  are relatively long,  $2.7 \times 10^3$  s and 7.1 s, respectively [Badger et al., 1965], but are usually not observed under laboratory conditions because of efficient deactivation due to chemical or collisional quenching. In solution, the lifetime of  $^1\Delta$  depends strongly on the chemical surroundings, and longest values of around 1  $\mu$ s are obtained in solvents considered to be chemically inert. The lifetime in water is around 2  $\mu$ s, and around 30  $\mu$ s are observed in acetonitrile [Merkel and Kearns, 1972]. The lifetime of the higher energetic  $^1\Sigma$  is not known and assumed to be too short-lived for any further reaction.

### Generation of singlet state oxygen $^1O_2$

In its triplet ground state, molecular oxygen can react with a photosensitizer molecule, which is commonly a strong absorbing dye, producing singlet oxygen in the  $^1\Delta$  state, following the scheme:



The mechanism underlying equation 2-25 represents a triplet-triplet annihilation which results in an energy transfer to yield singlet oxygen. It is generally assumed that an electron exchange energy transfer mechanism operates in the triplet-photosensitized formation of singlet oxygen [Turro, 1991]. Based on the theoretical work of DEXTER [Dexter, 1953], electron exchange energy transfer is characterized by

a collision of both molecules, and hereby enabling direct interaction of the orbitals involved. The process of triplet-triplet annihilation and energy transfer following the FÖRSTER mechanism is not allowed, since the spin orientation of the acceptor molecule is necessarily changed [Förster, 1948].

Photochemical mechanisms for generating singlet oxygen are radical-like in nature, since the key interactions involve diradicaloid structures. The thermal generation of singlet oxygen usually involves two electron (zwitterionic) processes. A synthetically used path to generate singlet oxygen is the decomposition of ozonides, e.g. phosphite ozonides or endoperoxides [Turro, 1991].

### Quenching of Excited Singlet and Triplet States by Molecular Oxygen

Ground state molecular oxygen is a general and efficient quencher of the  $S_1$  and  $T_1$  states of organic molecules. The mechanism of quenching can be either physical or chemical in nature. The most common chemical quenching mechanisms are diradicaloid electron transfer and addition:



Physical quenching mechanisms include exciplex formation and energy transfer. In general, the quenching of  $S_1$  of aromatic hydrocarbons occurs close to the diffusional rate. Quenching of  $T_1$  occurs within an order of magnitude of the diffusional rate, but is consistently slower.

An organic fluorophore therefore can interact with molecular ground state oxygen from its  $S_1$  or  $T_1$  state, depending on the energy of the SOMO in its photoactivated state. By removing oxygen, it is possible to find out the more important reaction pathway. Certainly, this depends on the chemical structure of a fluorophore and has to be explored for each molecule separately.

### 2.1.4. FLUORESCENT PROBES

Whether or not efficient emission of a molecule is observed is determined by the radiative rate constant  $k_r$ , the fluorescence quantum yield  $\Phi_f$  and the excited state lifetime  $\tau_n$ . These parameters are closely related to the chemical structure of a molecule on the one hand, and sensitive to experimental conditions on the other hand. As an overview, a number of different classes of fluorophores used in fluorescence microscopy are presented in the following section.

#### Organic Fluorophores

The group of synthetically designed organic fluorophores is the most widely used in fluorescence spectroscopy. A large number of fluorophores with wavelengths from around 350 nm to 800 nm are commercially available, and may be modified chemically to allow further conjugation reactions to other molecules of interest, e.g. proteins, nucleic acids and others.

Organic chromophores exist in many basic structures. Most commonly used and known are cyanines (e.g. Cy5, Amersham Biosciences), rhodamines (e.g. Rhodamine Green) and oxazines (e.g. MR121, AttoTec-GmbH), representing the main classes of dyes used in this work. The chemical structures of one chromophore of each type is shown

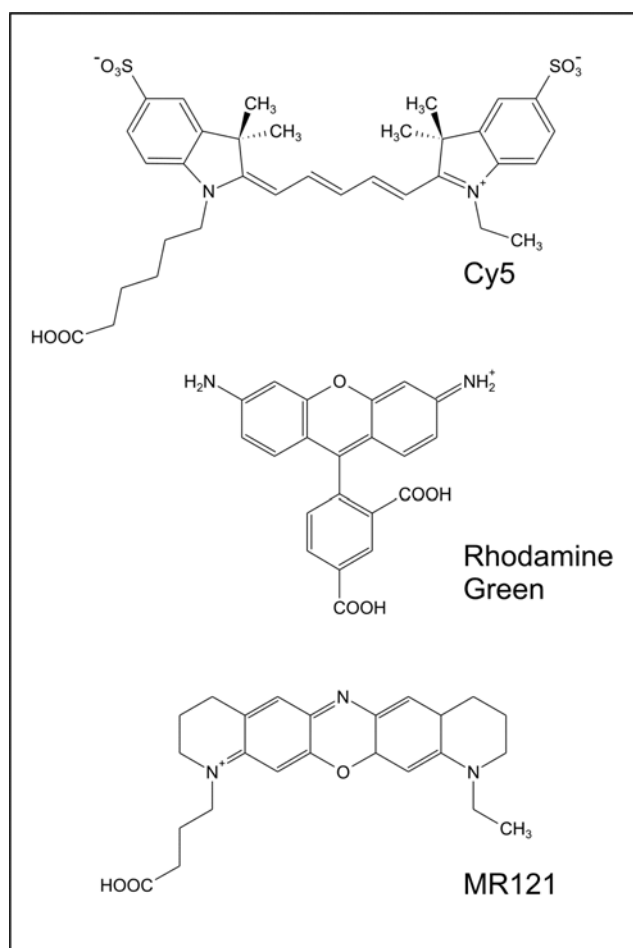


**Figure 2-10: Structure of three dyes representing main classes of chromophores: Carbocyanine Cy5, rhodamine derivative Rhodamine Green and oxazine dye MR121.**

in figure 2-10. Since they are all chemically distinct and show largely different photophysical properties, an important part of this work was dedicated to intensive studies of organic chromophores under different conditions, e.g. pH-value, redox potential and solvent.

Absorption and emission of an organic chromophore can easily be described by using a simple quantum mechanical approach of a particle-in-a-box. In this principle, only the possible path of electron delocalisation is taken into account. This example shall be briefly discussed with respect to cyanine dyes, Cy3 and Cy5, illustrated in figure 2-11. In each of these dyes the polymethine chain forms a conjugated chain extending from the nitrogen atom on one end of the molecule to the nitrogen atom on

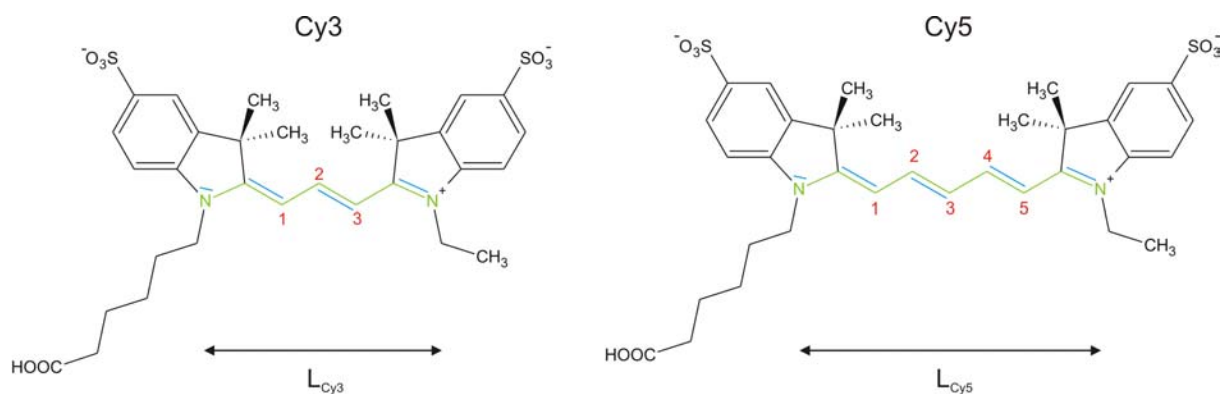


**Figure 2-11:** The principle of a particle-in-a-box applied to cyanine dyes, Cy3 (left) and Cy5 (right). The polymethine chain (green) connecting both indole moieties represents the box where  $\pi$  electrons (blue) are delocalised.

the opposite side of the molecule. These nitrogen atoms are assumed to be the walls of a one-dimensional box of length  $L$ . Assuming that the electrons do not interact, the potential energy along the chain is essentially zero and sharply rises to infinity at the ends of the chain. With this approximation, the length of the box is  $kb$ , where  $k$  is the number of bonds along the polymethine chain and  $b$  is 139 pm, the carbon-carbon bond length in benzene. The energy levels of this particle-in-a-box system are given by

$$E_n = \frac{n^2 h^2}{8m_e L^2} \quad (2-28)$$

where  $n$  is the quantum number,  $m_e$  is the electron mass, and  $h$  is PLANCK'S constant. The number of  $\pi$  electrons and the length of the polymethine chain in each dye are related to the number of double bonds between the nitrogen atoms. Each carbon

atom in the chain donates one  $\pi$  electron and the two nitrogen atoms donate a total of 3 electrons to form a mobile cloud of electrons along the conjugated chain (above and below the plane of the chain). The PAULI exclusion principle allows no more than two electrons in each energy level. For molecules with an even number of  $\pi$  electrons,  $N$ , the ground state will have  $N/2$  filled energy levels. Electronic transitions can occur from filled to unfilled levels when light of the appropriate energy is absorbed. The lowest transition energy will be that of an electron jumping from the highest occupied molecular orbital (HOMO), where  $n_{\text{HOMO}} = N/2$ , to the lowest unoccupied molecular orbital (LUMO) with  $n_{\text{LUMO}} = (N/2 + 1)$ . This is the transition observed in absorption spectra of the dyes. The energy change upon excitation of one electron is given by:

$$\Delta E = \frac{h^2(n_{\text{LUMO}} - n_{\text{HOMO}})}{8m_e L^2} = \frac{h^2(N+1)}{8m_e L^2} \quad (2-29)$$

The wavelength of the transition is

$$\lambda = \frac{8m_e c L^2}{h(N+1)} \quad (2-30)$$

where  $c$  is the speed of light.

Applying these theoretical assumptions to the polymethine dyes Cy3 and Cy5 in figure 2-11, we obtain an approximation of the absorption wavelength of Cy3 and Cy5, summarized in table 2-4:

	<b>Cy3</b>	<b>Cy5</b>
Number of $\pi$ electrons involved	8	10
Box length $L$	1.11 nm	1.39 nm
Calculated absorption wavelength	453 nm	579 nm
Measured absorption wavelength	550 nm	649 nm

**Table 2-4: Comparison of calculated and measured absorption wavelengths of Cy3 and Cy5.**

Although a difference of 70 nm and 97 nm in absolute values is obtained, this calculation allows a rough estimation of absorption wavelengths and is a good example to understand the basics of chromophore structure. It has to be mentioned

that a modification of the box length  $L$  was made according to the assumption of KUHN who suggested adding one extra bond length at each side of the polymethine chain [Kuhn 1959]. This procedure balances out the non-vertical potential jump occurring at the nitrogen atom site. If we assume a perfect box and no interaction between electrons, the expected box length for Cy5 and Cy3 using this simple model would be 1.39 nm and 1.11 nm, respectively. Extended to Cy7, an infrared cyanine dye with similar structure but one additional methine bridge, the difference of calculated and experimentally derived values decreases. The calculated absorption maximum is at 706 nm, whereas 743 nm are measured. This shows the critical influence of the box length, which is the weak point of this simple model.

In a more general view, organic chromophores show the expected broad absorption and fluorescence spectra as expected from theoretical considerations, involving mixed transitions of electronic and vibrational type (often termed *vibronic*). Figure 2-12 shows the absorption and emission spectrum of a previously presented and commonly used fluorophore, the cyanine dye Cy5.

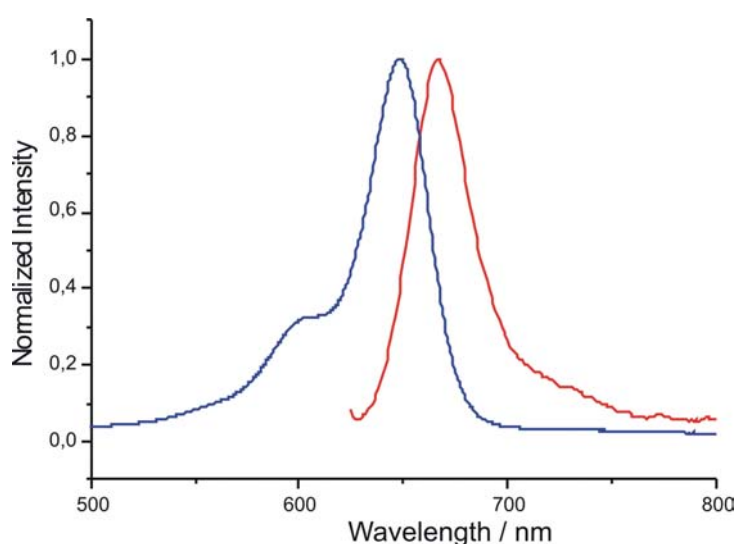


**Figure 2-12: Absorption and fluorescence emission spectrum of the organic chromophore Cy5, conjugated to a short 20bp DNA strand.**

Whether a fluorophore is suitable for fluorescence microscopy experiments depends on its photostability. This is, in other words, a measure for the number of excitation cycles a molecule undergoes, before it is irreversibly destroyed, i.e. photobleached. This results in a limited number of photons emitted by a fluorophore. Photobleaching of a dye can be characterized by the quantum yield of photobleaching  $\Phi_{PB}$ , which is defined as

$$\Phi_{PB} = \frac{N_{PB}}{N_{abs}} \quad ( 2-31 )$$

where  $N_{abs}$  is the number of photons absorbed, and  $N_{PB}$  is the number of molecules photobleached [Eggeling et al., 1998]. Prominent examples for poor photostability are

coumarin dyes and carbocyanines, whereas rhodamines and oxazines are more photostable. One possible pathway for photobleaching is the interaction between molecular oxygen and a fluorophore [Christ et al., 2001] (discussed in detail in section 2.1.3). Other pathways of photobleaching originate from higher excited singlet or triplet states. An increasing antibonding character of these states leads to destabilized and more reactive molecules and favours photodestructive reactions.

One focal point in this work was dedicated to investigate the influence of a change in the microscopic environment of a fluorophore on its photostability. Here, a change in pH, redox potential, solvent or oxygen concentration has to be mentioned. Finally, the aim was to find specific stabilizing conditions for different types of fluorophores which then allow to build complex multichromophoric systems, e.g. photonic wires, and make single-molecule measurements possible. The accuracy of the observation of single multichromophoric systems depends critically on the number of detected photons, so stabilized and “heterogenized” systems are desirable. Longer observation times can be achieved, and a better accuracy of interpretations can be obtained.

Besides being influenced directly via the local environment, a single fluorophore can sometimes be manipulated externally by physical means, e.g. light. As an example, an interesting result obtained during this work is the laser-induced reactivation of a fluorophore in a temporal dark-state by a second wavelength of excitation light, performed with cyanine dyes, namely Cy5 and Alexa647 (Molecular Probes, USA). Attached to DNA and exposed to a reductive environment, these molecules show a reversible switching behaviour between an “on”- and an “off”-state which can be generated using two different laser wavelengths, one near the absorption maximum of the chromophore, and a second with 150 nm shorter wavelength.

## Quantum Dots

A new class of fluorescent probes which have in recent years become commercially available are colloidal quantum dots, which are nanometer-sized crystalline structures of semiconductor materials (figure 2-13). Today, quantum dots spanning the whole visible spectrum are available, the surface can be functionalised with biomolecules or chemical groups activated for conjugation reactions, and they are used in many different areas of research today [Alivisatos, 2004; Michalet et al., 2005].

If a semiconductor quantum dot, e.g. with cadmium selenide (CdSe) as core material, is excited with light, charge is separated compared to the ground state, and an excitonic state or “exciton” is created. This process results in the transfer of an electron being located mostly on selenium atoms to cadmium atoms, which corresponds to a transition of an electron from the valence band to the conduction band of the semiconductor. By

doing this, the electron leaves behind a positive charge or a hole, and creates a negative charge in a new location. Fluorescence emission of quantum dots is described as the recombination of this electron-hole pair, or exciton. The wavelength of light emission depends solely on the size of the quantum dot, following the model of a particle-in-a-box previously described for organic fluorophores. Therefore, the smaller the radius, the shorter fluorescence emission occurs.

Usually, fluorescence lifetimes of quantum dots are in the range of 10 to 100 ns. As another interesting property, a unique broad band excitation spectrum allows simultaneous excitation of different quantum dots emitting at different wavelengths, which has been exploited for colocalization studies [Lacoste et al., 2000; Michalet et al., 2001]. Furthermore, photobleaching is a rare event, and so they allow collection of a much higher number of photons than any other fluorescent probe. Nowadays, the use of quantum dots in biology has been demonstrated *in-vivo* [Smith et al.,

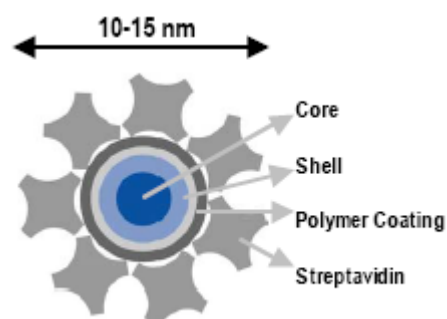


**Figure 2-13: Structure of a Quantum Dot.**

2004], but the applications are still limited, which is mainly due to deficiencies in conjugation chemistry and to the size.

### Metallic Nanoparticles

Besides quantum dots, which represent a huge class of well described and confined nanocrystal structures exhibiting fluorescence, many metallic structures have also been found to be fluorescent. Prominent examples here are size-tunable  $\text{Ag}_n\text{O}$ -clusters or  $\text{Au}_n$ -clusters [Zheng et al., 2003]. Silver oxide clusters are less suited for conjugation chemistry than gold clusters that can easily be conjugated

to sulphhydryl groups, but the use of either of these in a similar way like organic chromophores or quantum dots is currently not in sight.

Fluorescence spectra of recently discovered and brightly fluorescent gold dots  $\text{Au}_8$  are shown in figure 2-14. Synthesized in a polymer matrix, they exhibit an absorption maximum at 375 nm and a fluorescence maximum around 460 nm. A monoexponential fluorescence lifetime of 7.4 ns was determined.

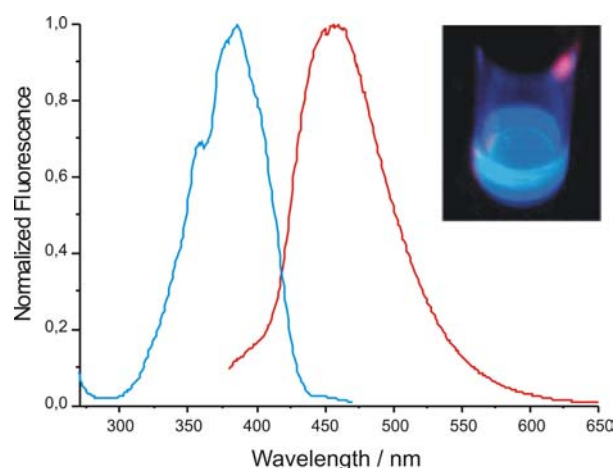


**Figure 2-14: Fluorescence excitation and emission spectrum of  $\text{Au}_8$  clusters.**

## Fusion Proteins

Another class of fluorescent molecules, derived directly from nature, is represented by a number of fusion proteins, containing a chromophoric unit embedded into a protein's tertiary structure. The first fluorescent protein which had been discovered was the green fluorescent protein (GFP) from *aequorea jellyfish* [Shimomura et al., 1962]. A three dimensional view of this 27 kDa protein is depicted in figure 2-15. It can be described as a  $\beta$ -barrel structure embedding the chromophoric unit in the inner of the protein. The chromophoric unit in the protein is spontaneously formed by three amino acids, i.e. glycine, tyrosine and threonine (or serine), and totally shielded from the surrounding environment by a cylindrical can of the protein backbone.

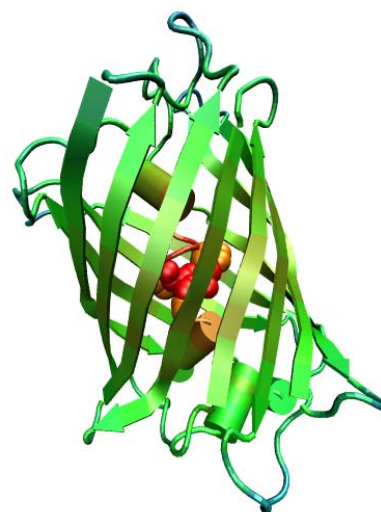


**Figure 2-15: Green fluorescent protein (GFP) from jellyfish.**

In the last decades, GFP and similar fluorescent proteins have been widely used in fluorescence microscopy (a comprehensive review is given in [Tsien, 1998]). The major advantage of fusion proteins is the ability to express the target protein directly fused to the desired fluorescent protein by “melting” the genetic information of both. In most cases, the functionality of the modified protein is hereby conserved. This simplifies the use of fusion proteins in biological assays, especially *in-vivo*, since labelling techniques or invasive treatment of organisms are not necessary.

Since the discovery of GFP, many mutants of this protein have been derived, but also other natural fluorescent proteins from other organisms have been discovered. A short overview of a small number of representative proteins is given in table 2-5 [Shimomura, 1979; Baird et al., 2000; Tsien, 1998].

Protein	Organism	$\lambda_{exc}$	$\lambda_{em}$
Green Fluorescent Protein, GFP	Aequorea jellyfish	480 nm	509 nm
DsRed	Discosoma	558 nm	583 nm
Yellow Fluorescent Protein, YFP	Mutant of GFP	514 nm	527 nm
Cyan Fluorescent Protein, CFP	Mutant of GFP	402 nm	468 nm

**Table 2-5: Overview of a number of fusion proteins exhibiting fluorescence.**

Both GFP/dsRED and YFP/CFP represent FRET pairs commonly used in biological experiments [Chan et al., 2001; Kluge et al., 2004]. Extended to two-photon FRET imaging microscopy, this technique can provide details of specific protein molecule interactions in living cells [Chen and Periasamy, 2004]. Very recently, three-chromophore FRET using the three fusion proteins CFP, YFP and RFP was used to investigate multi-protein interactions in living cells [Galperin et al., 2004].

An interesting property of the chromophoric unit of fusion proteins which was first discovered in 1997 for GFP and is related to one important topic in this work is on/off blinking and switching behaviour [Dickson et al., 1997]. After preparing a dark state of a single GFP unit by irradiation with 488 nm over 90 s, fluorescence could be recovered by irradiation with 405 nm for about 5 min. This procedure could be repeated several times. Similar optical switching behaviour was found for CFP [Chudakov et al., 2004] and YFP [McAnaney et al., 2005]. The mechanism of reversible photoswitching was found to go hand in hand with proton transfer at the central chromophoric unit of the fusion protein [Stoner-Ma et al., 2005].

## 2.2. Single-Molecule Spectroscopy

First realized in 1989 by MOERNER and KADOR at low temperature [Moerner and Kador, 1989], optical single-molecule spectroscopy (SMS) based on detection of fluorescent photons of single fluorophores at room temperature has found many applications [Weiss, 1999]. Nowadays, laser-induced fluorescence detection is used for various ultrasensitive analytical techniques in chemistry, biology and medicine by probing reagents that are either autofluorescent or tagged with a fluorescent dye [Eigen and Rigler, 1994; Goodwin and Ambrose, 1996]. In contrast to the averaging

process inherent to ensemble measurements, the observation of single molecules reveals subpopulations with different nanoenvironment.

In this work, single-molecule fluorescence measurements were performed on the basis of a confocal microscope. Experiments were carried out both in solution and on dry surfaces. State-of-the-art instrumentation and software allowing for single-photon analysis using photon-histogram techniques and autocorrelation, together with fluorescence lifetime and spectral information were exploited for the characterization of single fluorophores or multichromophoric systems. Together with single-pair FRET (spFRET) and multistep single-pair FRET (multi-spFRET), these principles shall be discussed in the following section.

### **2.2.1. CONFOCAL MICROSCOPY**

The basic principle of confocal microscopy was first established by MINSKY in the 1950s (and patented in 1957) [Minsky, 1957]. This technique offers several advantages over conventional widefield optical microscopy, including the ability to control depth of field, reduction of background originating above or below the focal plane, and the capability to collect serial optical sections from thick specimens. The key principle of the confocal approach is the use of spatial filtering techniques to eliminate out-of-focus light.

In 1992, RIGLER and co-workers first used confocal microscopy to detect single molecules [Rigler and Mets, 1992; Rigler et al., 1993]. By reducing the focal volume of excitation and applying the confocal principle, background is reduced considerably such that the technique has evolved to the most common one used in single molecule spectroscopy in the last decade.

### **Resolution Limit in Microscopy**

In the middle of the 19<sup>th</sup> century, it was the work of ERNST KARL ABBÉ that led to the emergence of microscopic techniques. By developing the first achromatic microscope objective and making microscopy available to many fields of science, he founded modern light microscopy.

To generate an image in microscopy, a parallel light beam from an excitation source must be diffracted by a sample. Together with an objective lens, the resolution limit of

the microscope is defined. If we assume the observation of an periodic grating with a spacing  $d_{min}$  that can just be resolved, the resolution obtained is given by

$$d_{min} = \frac{\lambda}{n \sin \alpha} = \frac{\lambda}{NA} \quad ( 2-32 )$$

where  $n$  is the refractive index of the medium,  $\alpha$  is the opening angle of the objective,  $NA$  is the objective's numerical aperture, and  $\lambda$  is the wavelength of the diffracted light.

A complementary method for defining the limit of resolution was presented by HELMHOLTZ and uses point objects instead of line gratings. The image of an infinitively small luminous object point, i.e. a point source like a single fluorescent molecule, is itself not infinitively small, but is a circular AIRY diffraction image with a bright disk in the centre and progressively weaker concentric bright and dark rings. The intensity profile of the AIRY-disk is described by

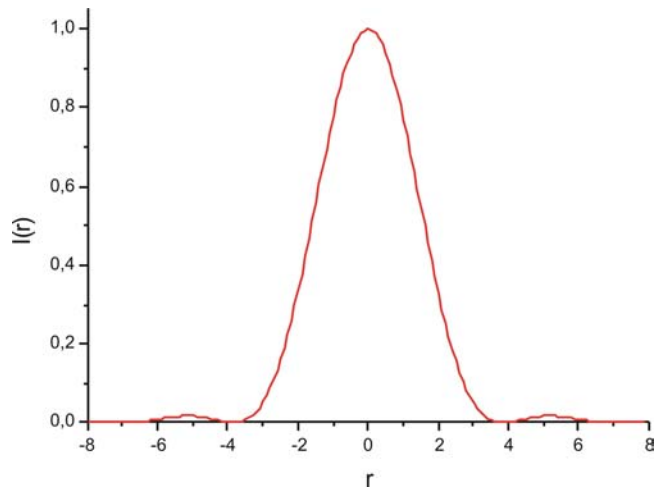


**Figure 2-16: Intensity distribution described by the AIRY function.**

$$I(r) \propto \left( \frac{J_1(r)}{r} \right)^2 \quad ( 2-33 )$$

where  $J_1(r)$  is a BESSEL function of the first order and the first kind. This intensity distribution is also called the AIRY pattern, shown in figure 2-16, and represents the lateral intensity distribution of the point spread function (PSF) of a microscope in optical units.

The radius of the first dark ring around the central disk of the AIRY diffraction image,  $r_{Airy}$ , which equals the distance of the first minimum to the principal of the intensity function, depends on  $\lambda$  and  $NA$  of the objective:

$$r_{Airy} = 0.61 \frac{\lambda}{NA} \quad ( 2-34 )$$

If there exist two equally bright points in the same image plane, they are said to be resolved if their distance  $d$  to each other is larger or equal to the radius of the AIRY disk. This is called the RAYLEIGH criterion and relies on the assumption that two point sources radiate monochromatically and incoherently (whereas the approach of ABBÉ assumes coherent excitation). The intensity between both point sources drops of to 76% of the maximum intensity [Born and Wolf, 2002].

The axial resolution, i.e. the resolution along the optical axis of the microscope or  $z$ -axis, is defined using the three-dimensional diffraction image of a point source that is formed near the focal plane. The distance from the centre of a three-dimensional diffraction pattern to the first axial minimum is given by

$$z_{\min} = \frac{2n\lambda}{(NA)^2} \quad ( 2-35 )$$

where  $n$  is the refractive index of the object medium.  $z_{\min}$  corresponds to the distance a microscope objective has to be raised in order to focus the first intensity minimum observed along the microscope axis of a three-dimensional intensity pattern instead of the central maximum. Comparable to the lateral resolution image,  $z_{\min}$  is a measure of the axial resolution of the microscope optics. In contrast to the lateral resolution, the axial resolution decreases with the square of the numerical aperture of the objective,  $NA$ .

These considerations for resolution assume that the object is viewed in conventional wide-field (WF) microscopy. In the case of confocal microscopy, where the field of view becomes extremely small, the resolution can in fact be greater than in wide-field techniques. This phenomenon is the issue of the following paragraph..

### **The Confocal Principle**

The optical path of an epi-illuminated confocal laser scanning microscope is characterized by an identical focus used both for excitation and for detection [Pawley, 1995]. A scheme of the optical path is shown in figure 2-17. Parallel light emitted by the laser system (excitation source) enters into the rear aperture of a microscope objective via a dichroic mirror, which is used to separate excitation light from fluorescence emission of the sample. The fluorescence signal (red in figure 2-17) of the sample now passes back through the dichroic mirror and, by passage through a

second lens, is focused as a second focal point onto the detector pinhole aperture. Finally, the signal is recorded by a detecting device, e.g. a photomultiplier or an avalanche photodiode. Not that if light does not come from the focal plane of detection (blue lines in figure 2-17), it will not pass the pinhole aperture and though not reach the detector.

As a result, the field of view in confocal microscopy becomes extremely small, and only fluorescent and light scattering objects in the axial and lateral resolution are viewed.

Compared to the classical resolution limit achieved by applying the RAYLEIGH criterion (or more precisely, by applying the criterion of 76% sum intensity between two point-like objects), an increase for both lateral and axial resolution by a factor of 1.41 is achieved in confocal microscopy,

$$r_{lateral} = 0.40 \frac{\lambda}{NA} \quad (2-36)$$

$$r_{axial} = 1.41 \frac{n\lambda}{NA^2} \quad (2-37)$$

The factor of 1.41 is derived from the square of the AIRY intensity distributions (see eq. 2-33) in confocal microscopy caused by a focussed excitation light source.

In this work, a high numerical aperture oil immersion objective with  $NA = 1.45$  (100x, Zeiss, Jena, Germany) was used for most experiments. A calculation of resolution considering as example two common emission wavelengths of 530 nm and 670 nm (as used in this work), one obtains a maximum lateral resolution of about 150 nm and

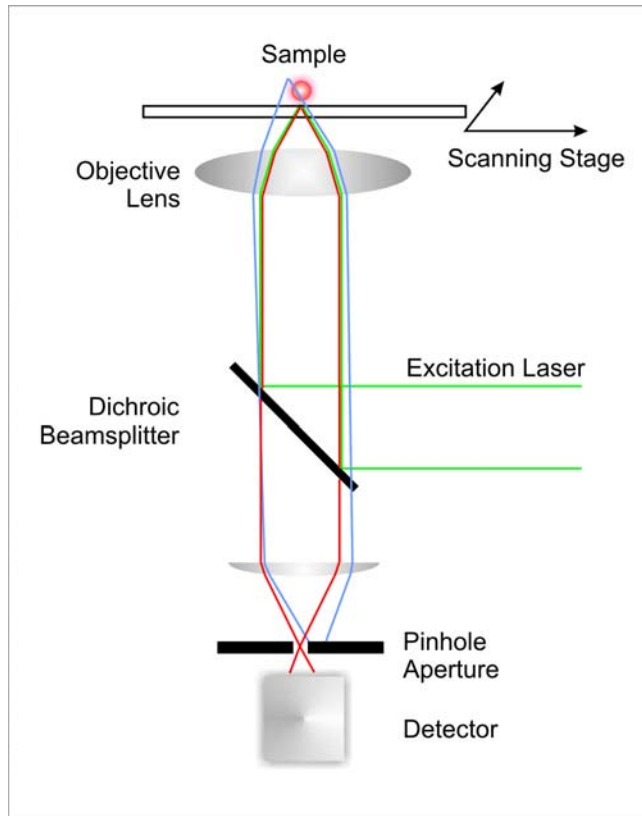


**Figure 2-17: Optical path of an epi-illuminated confocal microscope. The excitation light (green) is reflected by a dichroic mirror, whereas fluorescence (red) is let through. Out of focus light (blue) does not reach the detector.**

185 nm, and an axial resolution of about 525 nm and 665 nm (immersion oil refractive index  $n = 1.52$  at room temperature).

The major advantage of this technique over non-confocal detection is that only light coming directly from the focal plane will be detected, light above and below this plane does not reach the detector. This allows confocal scanning microscopy by scanning an object in all three spatial dimensions,  $x, y$  and  $z$ , and hereby creating a true three dimensional image. Due to the optical sectioning realized by applying small diameter laser foci, stray light is minimized, resulting in clearer images with higher resolution.

### Pinhole Aperture

The primary reason a pinhole is used in the detection path of a confocal microscope is to reduce the amount of stray light or, generally spoken, light originating from out-of-focus objects. The size of a pinhole is hereby related to the size of the AIRY function, representing the point spread function of a small light emitting object.

The FWHM of the AIRY function for a microscope objective with  $NA = 1.45$  and a magnification of  $M = 100$ , together with an emission wavelength,  $\lambda$ , has a size of 55  $\mu\text{m}$ , calculated from the position of the first minimum,

$$r = \frac{3.77M\lambda}{2NA\pi} \quad ( 2-38 )$$

To achieve the best possible resolution, the size of the pinhole is chosen to 50 to 60% of the FWHM of the AIRY disk, which would suggest a diameter of 28 to 32  $\mu\text{m}$ . Since increasing the resolution goes hand in hand with a reduction in collected photons, a pinhole in single-molecule research commonly has a diameter beginning with 50  $\mu\text{m}$ , and, at low signal to noise ratios, even 100  $\mu\text{m}$  or larger. A second factor to be taken into account is the fact that the pinhole position in the detection path, situated in the image plane of the microscope, is critical and any misalignment leads to severe loss of photons and reduced resolution, since out-of-focus light is projected onto the detectors. Especially in experiments requiring detection of a wide range of different wavelengths, achromatic behaviour of any component of the microscopic system makes the resolution dependent on the wavelength of light detected. Therefore, a 100  $\mu\text{m}$  pinhole which compromises both resolution and low photon statistics was used in most experiments presented in this work.

### 2.2.2. CONFOCAL MICROSCOPY AT THE SINGLE-MOLECULE LEVEL

To achieve the optical detection of a single chromophore, the advantages of confocal microscopy have been applied, and the microscopic system has been modified to realize a high detection sensitivity in order to be able to collect single photons emitted from single chromophores.

#### Single-Molecule Event

The detection of a single molecule can theoretically be achieved by stepwise dilution of a solution until the concentration of molecules in a certain time bin is around one per detection volume. Assuming a typical excitation and detection volume of a few femtoliter in confocal microscopy, this is achieved with concentrations below  $10^{-8}$  M. Since typical diffusion times of molecules through the laser focus are in the range of hundreds of microseconds, a probability to detect one molecule per second is observed for concentrations of  $\sim 10^{-11}$  M.

Similar, the dilution criterion can be applied to measurements on dry surfaces, or molecules immobilized at a surface, surrounded by a liquid environment. Generally, a density of about 1 molecule per  $\mu\text{m}^2$  is well suited to most point spread functions and allows undisturbed detection of photons originating from one single fluorophore. As opposed to diffusion-controlled experiments in solution, the observation of single molecule fluorescence trajectories reveals some typical effects which are commonly attributed to the presence of a single chromophore, e.g.

- Fluorescence intermittency (“blinking”) due to reversible transition into a dark state
- Irreversible photobleaching due to photo-induced reaction of the chromophore
- The correlation between emitted photons exhibits the signature of antibunching [Harnbury-Brown and Twiss, 1956]
- Polarized excitation exhibits the presence of a well defined absorption and emission dipole.

Most of the arguments mentioned above provide evidence for singleness. Unfortunately, some fluorophores have very unique optical properties that can interfere with the proposed criteria. One-step photobleaching, discrete intensity fluctuations and spectral jumps have also been observed in multi-chromophoric systems such as light harvesting complexes [Bopp et al., 1997; van Oijen et al., 2000], conjugated polymers [Vanden Bout et al., 1997; Yip et al., 1998; Huser et al., 2000] or polyphenylene dendrimers [Hofkens et al., 2000]. B-Phycoerythrin, a protein playing an essential role in light harvesting processes of cyanobacteria, have actually been found to be comprised of several fluorophores, which act effectively as one quantum emitter [Wu et al., 1996]. Spherical quantum dots, for example, have two degenerated emission dipoles [Empedocles et al., 1999] making it more complicated to prove singleness by polarization measurements.

Typical single-molecule signatures of fluorophores immobilized onto a protein surface under aqueous conditions are shown in figure 2-18.

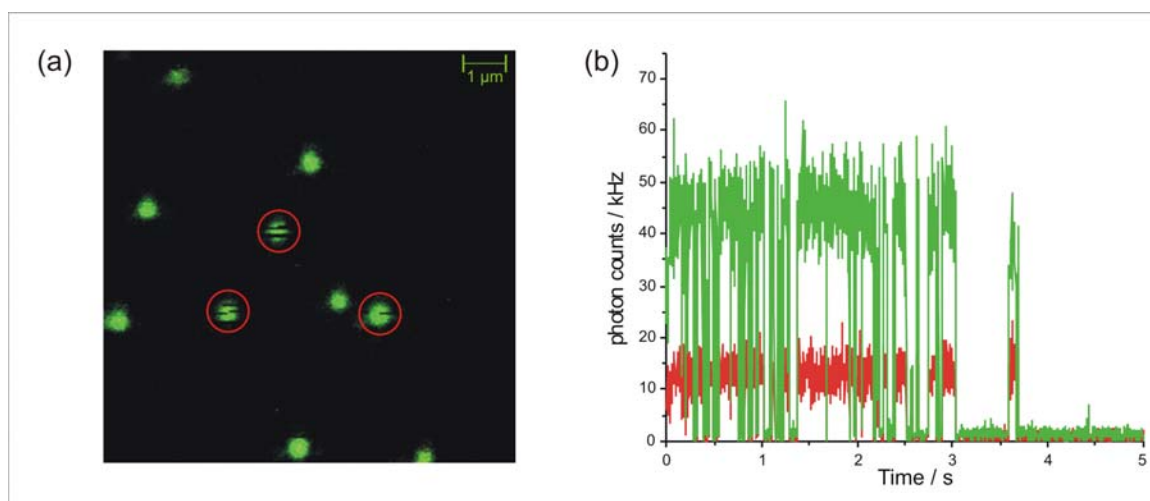


**Figure 2-18: Typical single molecule fluorescence signatures, (a) immobilized at protein surface under aqueous conditions, (b) fluorescence trajectory recorded from one single fluorophore, both exhibiting blinking and bleaching of single fluorophores. (Atto647 conjugated to a double strand 60bp DNA, anchored to surface by biotin linker, PBS).**

### 2.2.3. SINGLE-MOLECULE INTENSITY FLUCTUATIONS

One commonly observed source of single-molecule intensity fluctuations involves discrete intensity jumps from an “on” (high) to an “off” (background) intensity level. This effect, which is usually denoted by the term “blinking”, is due to quantum jumps

of the single molecule to long-lived nonemissive “dark” states. A common source of blinking in organic fluorophores involves intersystem crossing to a long-lived triplet dark state. Other well-known sources for intensity fluctuations are cis-trans-isomerizations [Widengren and Schwille, 2000], spectral jumps or the formation of radical states [Yip et al., 1998].

Detailed analysis of single-molecule intensity fluctuations can provide insight into the underlying excited-state dynamics and help in the classification of photophysical processes. Two common methods that were used in this work are intensity duration histograms and autocorrelation analysis of single-molecule fluorescence fluctuations. Both methods are presented in the following.

### Duration Histograms

Especially if fluorescence count rates of single molecules are high and fluctuations between a fluorescent and a nonfluorescent state have a digital character with two

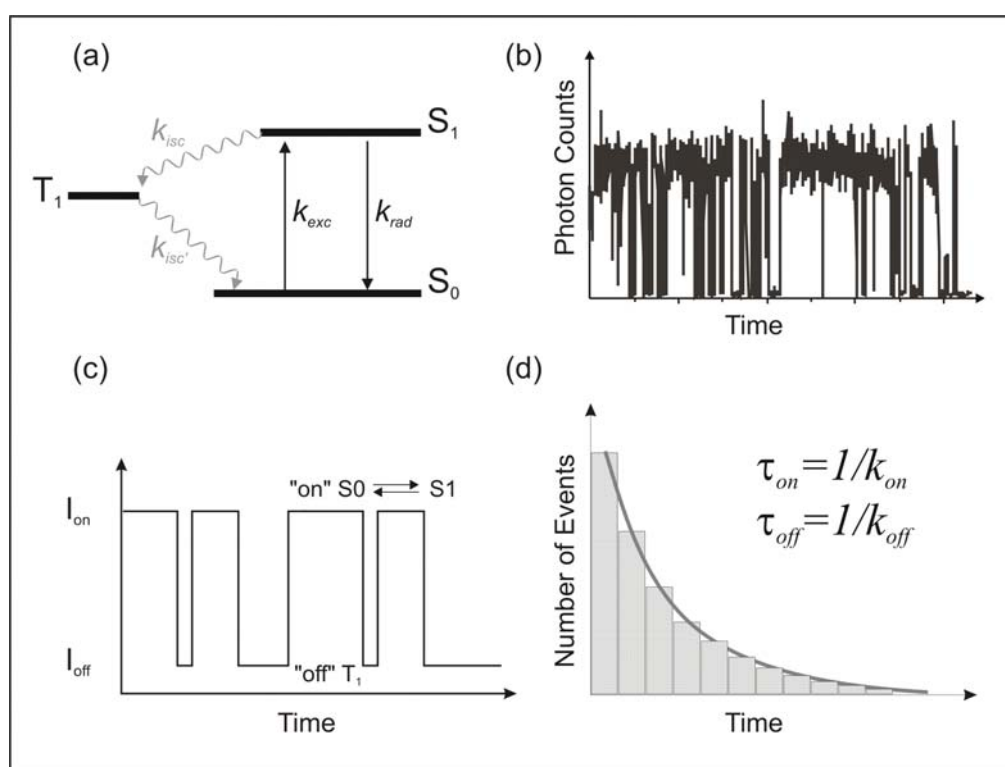


**Figure 2-19. Procedure of deriving kinetic information about a single emitter using the duration histogram method. Assuming a simple three-state model, (a), with a long-lived nonfluorescent triplet state appearing in fluorescence emission, (b). “on” and “off” periods describe transitions between energetic levels, (c), and are summed in a histogram, (d). Characteristic times and rates are extracted from histograms by approximation with exponential functions.**

well-defined intensity levels, duration histograms allow to obtain kinetic information down to around hundreds of microseconds [Yip et al., 1998]. Briefly described, the fluorescence emission is classified into “on” and “off” periods. The “lifetime” of these periods is then summed up in histograms. The bin width used to histogram these “on” and “off” states should be the lowest possible time resolution which allows to differentiate between the emission levels unambiguously. Duration histograms obtained with this procedure can now be approximated by exponential functions, yielding characteristic transition times,  $\tau_{on}$  and  $\tau_{off}$ , and transfer rates  $k_{on}$  and  $k_{off}$ , respectively. A summary of this procedure is presented in figure 2-19.

The kinetic parameters necessary to completely describe intensity fluctuations due to triplet blinking within this model are  $\tau_{on}$ , the average lifetime of the kinetic “on” state, during which the molecule is cycling between  $S_0$  and  $S_1$ ,  $\tau_{off}$ , the average lifetime of the dark state, and  $I_{on}$ , the single molecule fluorescence intensity during the “on” cycle. Together with the expression for the excitation rate  $k_{exc}$ ,

$$k_{exc} = I_{exc} \sigma(\lambda) \gamma \quad (2-39)$$

where  $I_{exc}$  is the excitation power,  $\sigma(\lambda)$  is the absorption cross section of a molecule and  $\gamma$  a correction factor, the following relationships of these quantities are obtained:

$$\tau_{on} = (k_{exc} \phi_{isc})^{-1} \quad (2-40)$$

$$\tau_{off} = \tau_{T1} = (k_{isc'})^{-1} \quad (2-41)$$

$$I_{on} = k_{exc} \phi_{fl} E_{det} \quad (2-42)$$

Here,  $\phi_{fl}$  and  $\phi_{isc}$  are the quantum yields of fluorescence and the triplet state transition,  $E_{det}$  is the overall detection efficiency, and  $\tau_{T1}$  is the spontaneous lifetime of the lowest energy triplet state  $T_1$ , which in turn is the inverse of the rate constant  $k_{isc'}$ . It has to be mentioned that this is only the case if there are no higher triplet states involved as an additional photoinduced channel [English et al., 2000].

### Autocorrelation Function

If count rates are lower or a higher time resolution is desired, the second order autocorrelation function is the method of choice. Since no discrete and

---

distinguishable levels of intensity are required, a much lower time binning than in duration histograms is possible, thus enabling the measurement of fluctuations between molecular states occurring on a much shorter timescale.

Mathematically, the normalized second order autocorrelation function is defined as

$$g^{(2)}(t') = \frac{\langle I(t)I(t+t') \rangle}{\langle I(t) \rangle^2} \quad (2-43)$$

where  $I(t)$  is the observed fluorescence intensity. The intensity is shifted by a parameter  $t'$  and integrated and normalized over the measurement period.

The physical meaning of the autocorrelation as defined above is that it is proportional to the probability to detect a photon at time  $t'$  if there was a detection event at time zero. This probability is composed of two basically different terms: The two photons detected at time zero and at time  $t'$  can originate from uncorrelated background or from different fluorescing molecules and therefore do not have any physical correlation (provided there is no interaction of the different fluorescing molecules). These events will contribute to a constant offset of  $g^{(2)}(t')$  that is completely independent on  $t'$ . Alternatively, the two photons originate from one and the same molecule and are therefore physically correlated, leading to a time dependent component of  $g^{(2)}(t')$ . Thus, the temporal behaviour of the autocorrelation function is solely determined by the correlated contributions of individual molecules. In many experiments more than one process is involved, and sophisticated analysing techniques of the obtained autocorrelation data allow to extract information on each fluctuation originating from a different process [Enderlein et al., 2004]. Quantitative information is available from amplitude data characterizing a fraction of molecules fluctuating between two particular states.

Often applied to measurements in solution, this technique with its numerous modifications is summarized under fluorescence correlation spectroscopy (FCS) [Widengren and Rigler, 1998; Haustein and Schwille, 2003]. The autocorrelation function allows determination of the mobility or diffusion characteristics of molecules and hereby gives information about the particular mass of fluorophores or larger biomolecules which are labelled with fluorophores. Furthermore, kinetic data on additional transitions between other states, e.g. intersystem crossing, *cis-trans*

isomerizations or general fluorescence quenching pathways, can be derived using this technique. A basic mathematical description is given by

$$g_{(2)}(t) = \frac{1}{N} \left( 1 + \frac{t}{\tau_{diff}} \right)^{-1} \left( 1 + A e^{-t/\tau_{exp}} \right) \quad ( 2-44 )$$

where  $N$  is the average number of molecules in the laser focus,  $\tau_{diff}$  is the diffusion time and  $\tau_{exp}$  is the time constant of a transition with an amplitude  $A$  that can be described by exponential kinetics.

The advantage of FCS is the relative simplicity of the analysis. Its drawback is that it works only within a very limited concentration range: If the concentration of fluorescing molecules becomes too large (typically  $> 10^{-8}$  M), the contribution from correlated photons from individual molecules, scaling with the number  $N$  of molecules within the detection volume, becomes small compared with the contribution by uncorrelated photons from different molecules, scaling with  $N^2$  [Enderlein et al., 2004]. Another limiting factor in FCS measurements is that kinetic data cannot be obtained beyond the diffusion time, i.e. the average time a molecule stays in the detection volume, preventing measurements longer than a few milliseconds. Furthermore, an overlay of diffusion events with other events of similar timescale makes data analysis complicated.

The autocorrelation function, if applied to single-molecule fluorescence traces of fluorophores immobilized on surface, is independent of the diffusion term and removes the limited time window inherent to solution experiments. As a result, this allows the analysis of fluorescence fluctuations on a much larger time scale, only limited by the total measurement time, i.e. until a fluorophore is finally photobleached. The remaining photophysical processes usually exhibit first order kinetics and can be described by a sum of exponential functions of all  $i$  processes,

$$g^{(2)}(t) = 1 + \sum_i A_i \exp\left( -\frac{t}{\tau_{i,char}} \right) \quad ( 2-45 )$$

where  $\tau_{i,char}$  denotes the characteristic time constant, and  $A_i$  the amplitude of the  $i$ -th component. An autocorrelation function calculated for a solution measurement compared to an autocorrelation calculated for a surface-immobilized molecule is presented in figure 2-20. The figure demonstrates that transitions into longlived dark

states with a typical time constant larger than the diffusion time are not accessible by solution measurements.

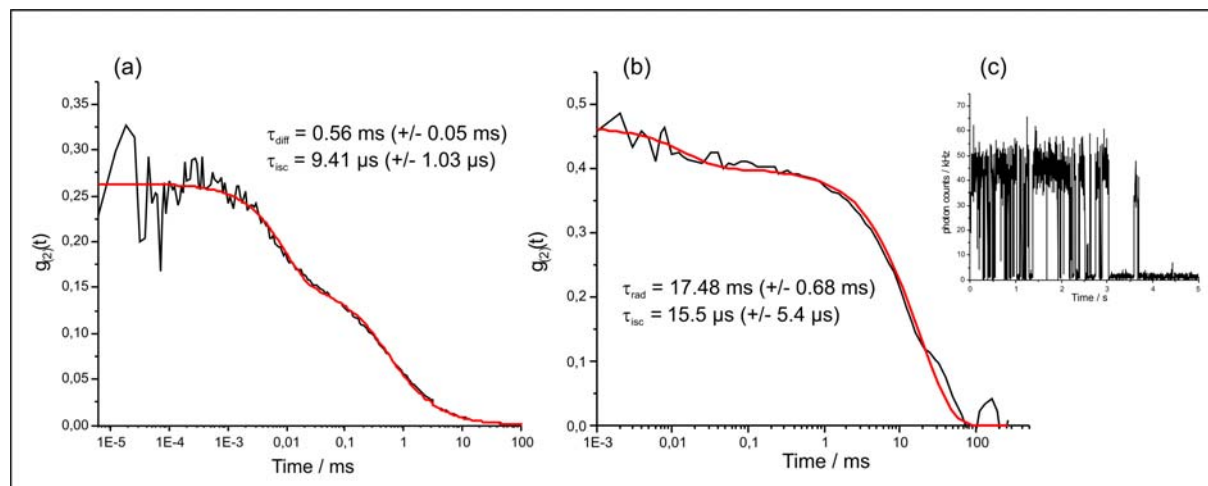


**Figure 2-20: (a) Autocorrelation of diffusing Atto488 molecules in a laser focus (excitation power of 1 mW) with a diffusion time of 0.56 ms and an exponential time of 9.41  $\mu$ s. (b) autocorrelation of Atto647-DNA immobilized on protein surface, exhibiting two exponential time constants of 17.48 ms and 15.5  $\mu$ s, respectively, obtained from the fluorescence trace shown in (c). The longer time component, attributed to the formation of a radical state, is not accessible in solution measurements.**

As a result,  $g^{(2)}(t)$  can be used as a method to directly determine the lifetime of “off” and “on” states and their corresponding amplitudes from fluorescence intensity trajectories only. Under the assumptions that the autocorrelation is only examined at times that are large compared to the fluorescence lifetime of the molecule and that the integration times are smaller than the average on- and off-times,  $\tau_{char}$  of the  $i$ -th component can be expressed as [Weston et al., 1998; Bernard et al., 1993]:

$$\frac{1}{\tau_{char}} = \frac{1}{\tau_{off}} + \frac{1}{\tau_{on}} = k_{off} + k_{on} \quad (2-46)$$

$$A \cong \frac{\tau_{off}}{\tau_{on}} = \frac{k_{on}}{k_{off}} \quad (2-47)$$

Similarly to duration histograms, on- and off-times for transitions into nonfluorescent states can be determined in this way.

In this work, both approaches to derive kinetic data from the photon signature of single emitters were used and complement each other. If molecules are immobilized under aqueous conditions using a molecular anchor, the direct influence of chemical

changes on certain types of chromophores can be investigated quantitatively. It hereby becomes feasible to observe the effect induced by changing pH or redox properties, removing oxygen or adding triplet quenching substances.

#### 2.2.4. SINGLE-MOLECULE FRET (smFRET)

Fluorescence resonance energy transfer, first discovered by FÖRSTER in the late 1940s, was used as a powerful tool to characterize interactions between fluorophores, possibly attached to a larger molecule or more complex systems of interest [Clegg, 1992]. In 1996, resonance energy transfer between a single donor and acceptor chromophore was first realized by WEISS and co-workers, coined single pair FRET (spFRET) or single molecule FRET (smFRET) [Ha et al., 1996]. As a model system, they used two dyes, tetramethylrhodamine (TMR) and Texas Red, attached to the 5'-ends of two complementary single stranded oligonucleotides with an interchromophoric distance of 3.4 nm and 6.8 nm. After hybridisation of the DNA sample, they obtained energy transfer efficiencies at the single molecule level of 85% and 53%, respectively, which is in good agreement with ensemble data of the same samples. An example of a fluorescence intensity trace of a single FRET system with Rhodamine Green and TMR, spaced by 3.4 nm, is shown in figure 2-21.

In contrast to ensemble FRET measurements, the efficiency of energy transfer is determined in a slightly different way, which is caused by the digital event of bleaching of either the donor or the acceptor molecule. In the case of acceptor bleaching, the efficiency  $E$  can be determined by

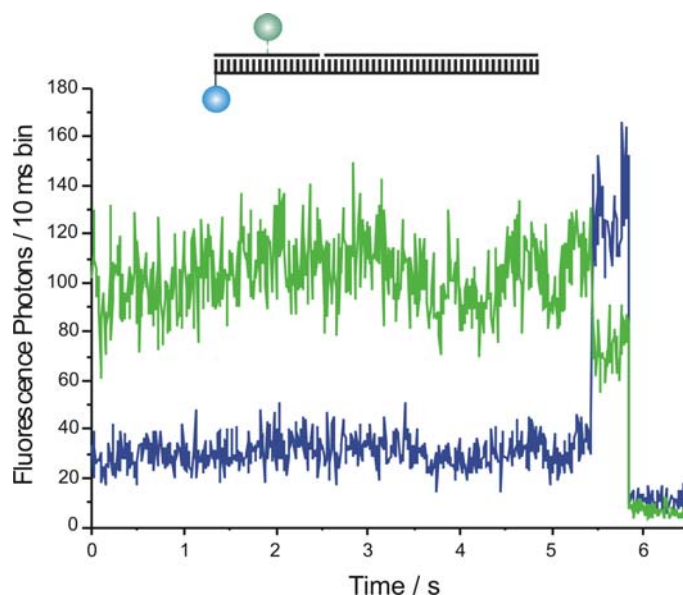


**Figure 2-21: Fluorescence intensity versus time in a smFRET system of Rhodamine Green and TMR, spaced by around 3.4 nm, recorded on two spectrally separated detector channels.**

$$E = \frac{I_D - I_{DA}}{I_D - \alpha I_{DA}} \quad ( 2-48 )$$

Here,  $I_{DA}$  and  $I_D$  represent the donor fluorescence intensity before and after photobleaching of the acceptor, respectively. The correction factor  $\alpha$  ( $< 1$ ) is necessary because a photobleached acceptor may still absorb light. If  $\alpha$  is zero, this formula is equivalent to the conventional FRET equation (equation 2-19). Applying equation 2-48 to figure 2-21 and the tolerable assumption that the donor fluorophore does only emit on the blue channel, a FRET efficiency of 82% is determined.

If the donor molecule photobleaches first, the efficiency of energy transfer is

$$E = \left( 1 + \frac{I_{DA} \phi_A}{I_{AD} \phi_D} \right)^{-1} \quad ( 2-49 )$$

where  $\phi_A$  and  $\phi_B$  represent the quantum yield of the single donor and acceptor.

In the following years, smFRET has become a common tool to investigate single molecule dynamics on a large range of timescales and a huge variety of systems [Deniz et al., 1999; Ha, 2001]. This can particularly be observed in biological research, including stepwise rotation of an ATPase [Diez et al., 2004], protein structure and dynamics [Wang and Geva, 2005], or fluctuations between open and closed states of single nucleosomes [Tomschik et al., 2005]. Furthermore, smFRET experiments are not limited to organic chromophores. Recently, the activation of the Ras protein has been studied using YFP as a donor for smFRET [Murakoshi et al., 2004]. Quantum dots begin to be used as well. [Hohng and Ha, 2005] Due to the unique excitation spectrum of quantum dots, they may only be used as a donor molecule, transferring energy to an organic chromophore or a fusion protein.

As a further development of FRET with two molecules involved, several approaches to more-step FRET in ensemble measurements have been made in the past years [Liu and Lu, 2002; Ohya et al., 2003]. At the single-molecule level, first results in triple chromophore FRET have also been published recently [Hohng et al., 2004]. As an extension to both spFRET and multistep FRET in ensemble studies, the aim of this work was to realize a multistep FRET system and investigate this system at the single-molecule level. In these experiments, it is advantageous to work with a number of "orthogonal" properties of chromophores, since spectrally resolved fluorescence information is not an unambiguous mean to differentiate energy transfer

steps. Pulsed excitation, different fluorescence spectra and fluorescence lifetime, together with modulation of the polarization of excitation light are additional parameters important to reveal single energy transfer steps. This is facilitated further by stepwise building up of a multichromophoric system at the single molecule level, which enables the observation of each energy transfer step separately.



### 3. Materials and Methods

#### 3.1. Spectrally-Resolved Fluorescence Lifetime Microscopy

The main set-up built during the course of this work is a confocal line scanning fluorescence microscope with laser light excitation. This set-up allows capture of spectral and temporal information on single photons, detected from single fluorophores. Depending on experimental requirements, the set-up has been modified or extended, e.g. for time-correlated measurements at different laser wavelengths or with polarized excitation. As it presents a central element in this work, it will be discussed in detail in the following section.

A simplified scheme of the fundamental set-up for fluorescence imaging microscopy with single-molecule detection efficiency is portrayed in figure 3-1.

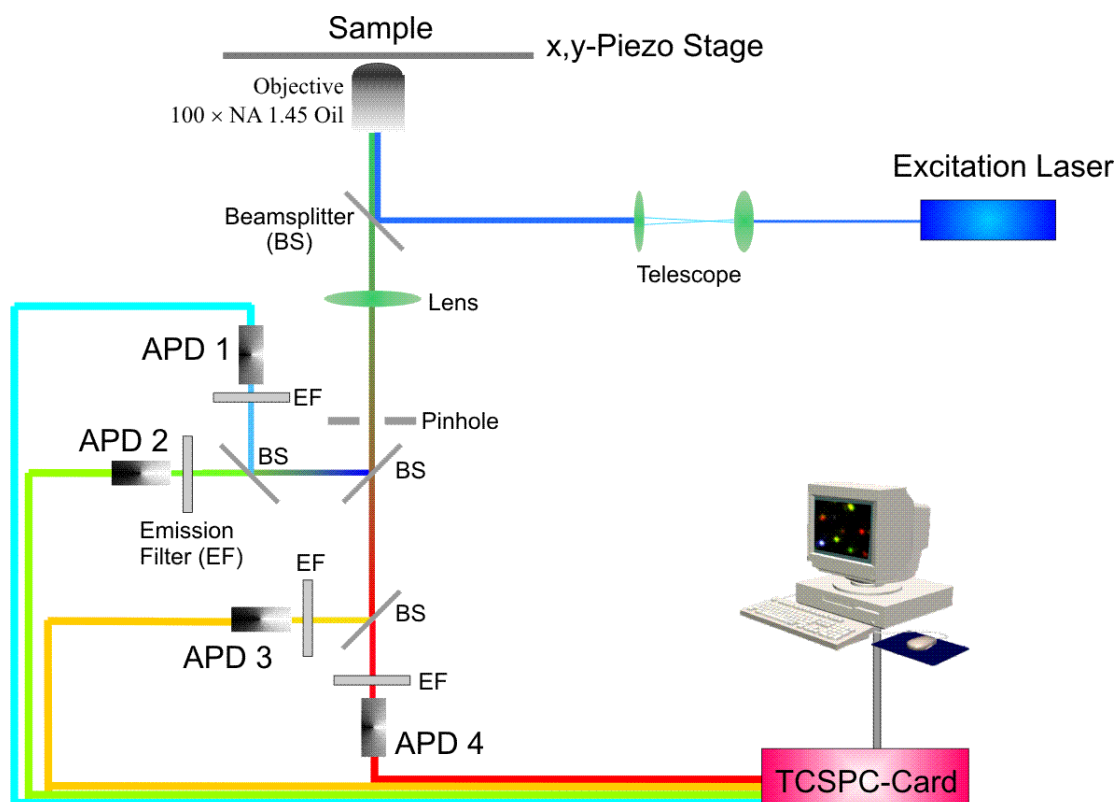


Figure 3-1: Principal set-up for spectrally-resolved fluorescence lifetime microscopy. BS: beamsplitter, EF: emission filter, APD: avalanche photodiode.

Before going into details of a number of important elements of the set-up, a brief summary about the working principle will be given in the following passage.

The core unit of the set-up consists of an inverted microscope (Axiovert 200M, Zeiss, Germany) equipped with an x,y,z-piezo stage (PI-509, Physik Instrumente, Germany) controlled via analog output computer cards (PCI-6713, National Instruments, USA). The scanning range of the stage is 100  $\mu\text{m}$  in x and y direction and 20  $\mu\text{m}$  in z direction, and the stage is directly connected to the microscope. A number of different laser light sources, both continuous wave and pulsed, with wavelengths from 440 nm to 635 nm were used as excitation light source. If necessary, especially if using broad band emitting diode lasers as light source, a narrow excitation filter in front of the laser output was used. The laser beam was extended using a telescope and coupled into the backport of the microscope, where it was directed into the microscope objective (100x oil immersion PlanFluar, NA = 1.45, Zeiss, Germany). The light beam was focused onto the sample and fluorescence light was collected by the same objective, but separated in the detection path of the set-up using a dichroic beamsplitter, which allows separating fluorescence light from shorter wavelength excitation light. The parallel light beam was first focused onto a pinhole. To spectrally resolve the incoming photons in the detection arm, three different dichroic beamsplitters with appropriate cut-off wavelength were used. Finally, emitted photons were focused onto the active area of four separate avalanche photodiodes (APD; AQR-14 and AQR-16, PerkinElmer, USA). Photon arrival generates an electric signal which is then processed by a time-correlated single-photon counting device (SPC-630, Becker&Hickl, Berlin, Germany), which allows both continuous mode operations and time-correlated measurements. If working in the time-correlated mode, the synchronization signal of a pulsed laser source supplies the reference for the SPC-630 device and allows obtaining fluorescence lifetime information. Together with the spectral information, this method is referred to as spectrally resolved fluorescence lifetime imaging microscopy (SFLIM) [Herten et al., 2000].

In the set-up presented here, the confocal detection path has been realized applying the so-called  $2f$  principle. According to the lens equation for a lens with a focal length  $f$ ,

$$\frac{1}{f} = \frac{1}{g} + \frac{1}{b} \quad ( 3-1 )$$

where  $g$  and  $b$  denote the object and the image length, respectively, both object size and image size remain unchanged for  $g = b = 2f$ .

The whole set-up is synchronized by LabView (National Instruments, Austin, USA) based software, allowing the piezo scan stage to be controlled on the one side and attributing photon information obtained by the photon counting device to the appropriate x,y-position on the sample.

The basic set-up presented in figure 3-1 has been extended by several components, according to experimental requirements. Simultaneous excitation with two different laser light sources were applied for dual colour measurements. Modulation of linearly polarized laser light by an electrooptical modulator (EOM; Linos, Germany) allowed for rotational dynamic studies of fluorophores conjugated to biomolecules. A charge coupled device (CCD) camera (Cascade, Roper Scientific, USA) connected to the sideport of the microscope equipped with a spectrograph was used for single molecule spectra and alignment purposes.

## Microscope

Most experiments in this work were performed on the Axiovert 200M inverted microscope (Zeiss, Jena, Germany). This fully motorized microscope (see figure 3-2) is equipped with a backport, sideport, frontport and baseport, which facilitates the construction of a multifunctional set-up. The collimated laser beam enters the microscope via the backport and is reflected by a dichroic mirror into the objective. Additionally, a mercury lamp is connected to the backport through a lense system, and a software controlled flippable mirror allows changing between excitation sources. Emission light collected by the objective passes the dichroic mirror followed by a convex lens, and can now be detected on either of the remaining ports. A simultaneous detection of 50% on both sideport and baseport is also feasible.

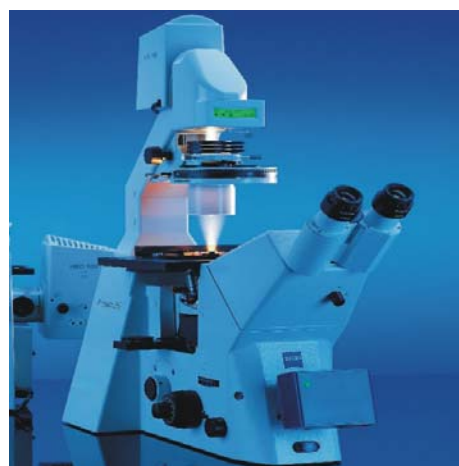


**Figure 3-2: Axiovert 200M, Zeiss, Germany.**

The detection pathway connected to the baseport of the microscope is realized by applying a modified confocal scheme using two lenses, one inside the microscope ( $f = 160$  mm) and one in the detection arm ( $f = 300$  mm). Spectral discrimination of the emission light is achieved by using up to four avalanche photodiodes (APD) and appropriate dichroic beamsplitters and filters.

### Excitation Sources

Single-molecule fluorescence experiments were performed using laser light as excitation source, exhibiting highly collimated and monochromatic light. Depending on experimental needs, different types of lasers were used, that can be classified into continuous wave and pulsed laser. An overview of both groups, together with characteristic wavelengths and repetition rates, is given in table 3-1.

<b>Name</b>	<b>Type</b>	<b>Wavelength (nm)</b>	<b>Power (mW)</b>	<b>Repetition Rate (MHz)</b>
95 SHG-6W Lexel Laser Inc., USA	Argon-Ion Laser	514.5 496.5 488.0 476.5 457.9	200 30 100 10 10	cw “ “ “ “
LHYP-0201 Research Electro Optics, USA	Helium-Neon Laser	594	2.0	cw
Polytec, Germany	Helium-Neon Laser	632.8	2.0	cw
Tsunami Spectra Physics, USA	Ti:sapphire Laser	740-935	650-1350	80.4 MHz (80.77 MHz at 976 nm)
Mira 900 Coherent, USA	Ti:sapphire Laser	680-980 (980-1050)	200-1400	76.8 MHz (at 976 nm)
LDH-P-C-440 Picoquant, Germany	Diode Laser	440	1 (at 40 MHz)	5 – 40 MHz
LDH-635 Picoquant, Germany	Diode Laser	635	3.5 (at 80 MHz)	5 – 80 MHz

**Table 3-1: Summary of laser systems used as excitation sources (see text for details).**

Due to low photostability of many fluorescent dyes absorbing in the blue and green spectral region, most experiments had to be carried out using continuous wave excitation to avoid excitation of higher excited states and thus further destabilization of the fluorophores. For these experiments, the continuous wave operating argon ion laser served as excitation source, mainly operating at 488 and 514 nm. The laser provided linear polarized light with narrow emission and <1.5 mm beam diameter. For longer wavelengths that cannot be obtained from the argon ion laser, two continuous wave helium neon lasers with 594 and 633 nm were used.

Time-resolved measurements reveal information about fluorescence kinetics and depopulation processes of the excited state due to energy transfer or interactions with the microscopic surroundings of fluorophores. Experiments were realized with a number of different pulsed excitation lasers and are the subject of a following section.

### **Scanning Stage**

As scanning stage, a three-dimensional closed-loop piezo scanner P-517.3CL (Physikinstrumente, Göttingen, Germany) in combination with a three-channel amplifier E503.00 (Physikinstrumente, Germany) and a capacitive sensor controlling unit E509.C3A (Physikinstrumente, Germany) was used. The range of the scanning device is 100  $\mu\text{m}$  x 100  $\mu\text{m}$  x 20  $\mu\text{m}$ , controlled by a voltage ramp of 1 V /  $\mu\text{m}$ . To address the scanning device, custom-made software (LabView Version 7.0, National Instruments, USA) together with an analogue output PC-card (PCI-6713, National Instruments, USA) was used, and allowed synchronized stage movement with data acquisition of the fluorescence detectors.

### **Detector**

Single-photon detection was realized using up to four avalanche photodiodes (APD; sometimes referred to as single photon avalanche diode, SPAD; AQR-14 and AQR-16, PerkinElmer, USA).

An APD is a solid-state, semiconductor based device that converts photons into electrons in a different way than an ordinary photodiode. In ordinary photodiodes, the photon/electron ratio is one to one. In APDs, however, photon-generated electrons can excite additional electrons creating an avalanche effect and resulting in an

internal gain that can be adjusted with the bias voltage, e.g. 1 to 1000 V. The resulting signal is proportional to the light's intensity. The active area of APDs from the AQR-1x-series has a diameter of about 180  $\mu\text{m}$ . They are thermoelectrically cooled and have a dark count rate of < 100 counts per seconds (cps) (AQR-14) and <25 cps (AQR-16), respectively. The dead time between two subsequent photon arrival events lies in the range of around 300 ns. The photon arrival time itself is measured from the rise of the electric signal, generated by the APD, and can be measured with a temporal resolution of 300 ps, an important factor contributing to the instrument response function (IRF).

Besides avalanche photodiodes, other detector devices commonly in use for single-molecule fluorescence microscopy are photomultiplier tubes (PMT) and charge coupled device (CCD) cameras. The advantage of a PMT over an APD is a low dark count rate (typically around 5 Hz) and a shorter dead time of around 10 ns. On the other hand, a PMT suffers from poor quantum efficiency of around 20%. The detection efficiency of an APD reaches its maximum at 700 nm with over 70%, and the range of detection with more than 50% efficiency lies between 500 and 850 nm (see figure 3-3). Best quantum efficiencies for photon detection are offered by CCD devices, realizing more than 90 % in modern cameras. With frame rates in the kHz regime, parallel image processing and straightforward alignment, CCD devices are used more and more in many fluorescence microscopy applications.

Compared to a CCD device, an APD works on a considerably faster timescale, since a CCD can not avoid readout and capacity charging times. Lifetime measurements cannot be realized photon by photon, but require summing up over longer timescales. Thus, dynamic changes in fluorescence lifetime at short timescales cannot be observed.

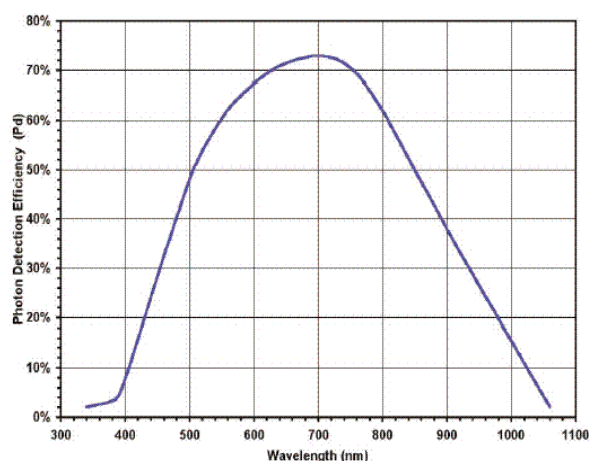


**Figure 3-3: Photon detection probability for an APD of the AQR-1x series.**

As a result, an APD represents the detector of choice for sensitive single molecule experiments in a spectral range of 500 to 800 nm. A moderately high quantum yield

together with a short temporal resolution and acceptable dark count rate is a well suited compromise, and APDs have been used as detectors in all set-ups.

### Filters and Dichroics

The information of a photon detection event can be refined by spectral discrimination, which results in a valuable increase of information. Therefore, many experimental set-ups operate with more than one detector and spectral resolution was achieved by the use of dichroic beamsplitters and appropriate excitation and emission filters (Omega Filters, Brattleboro, USA).

In the excitation path, a combination of a narrow band excitation filter and a dichroic beamsplitter were used. An excitation filter can be set aside if the excitation laser is characterized by narrow emission at exactly one wavelength, and no fundamental wavelengths or other sources of light emission appear. This is particularly the case if fundamental wavelengths of atom or gas lasers, e.g. continuous wave argon ion lasers, are used. The following table 3-2 shows commonly used combinations of excitation filters and beamsplitters

<i>Excitation Wavelength</i>	<i>Excitation Filter</i>	<i>Dichroic Beamsplitter</i>
440 nm	445 DF 20	465 DRLP
488 nm	480 DF 40*	500 DRLP
635 nm	633 DF 9	647 DRLP
635 nm and 488 nm	633 DF 9**	Dual Band 635/488

**Table 3-2: Combinations of dichroic beamsplitters and excitation filters used in fluorescence microscope set-ups with laser excitation; (\*) excitation filter is only necessary if frequency-doubled titan sapphire laser are used, removing fundamental wavelength of infrared light; (\*\*) excitation filter was used for the red laser diode only.**

Experiments with an excitation wavelength of 488 nm required a combination of dichroic beamsplitter (500 DCLP) and long pass emission filter (500 ALP). The transmission curves of both components are shown in figure 3-4 (left side). The reason therefore lies in the property of band pass filters which were chosen for longer wavelength detection channels and exhibited a small fraction of transmission at the

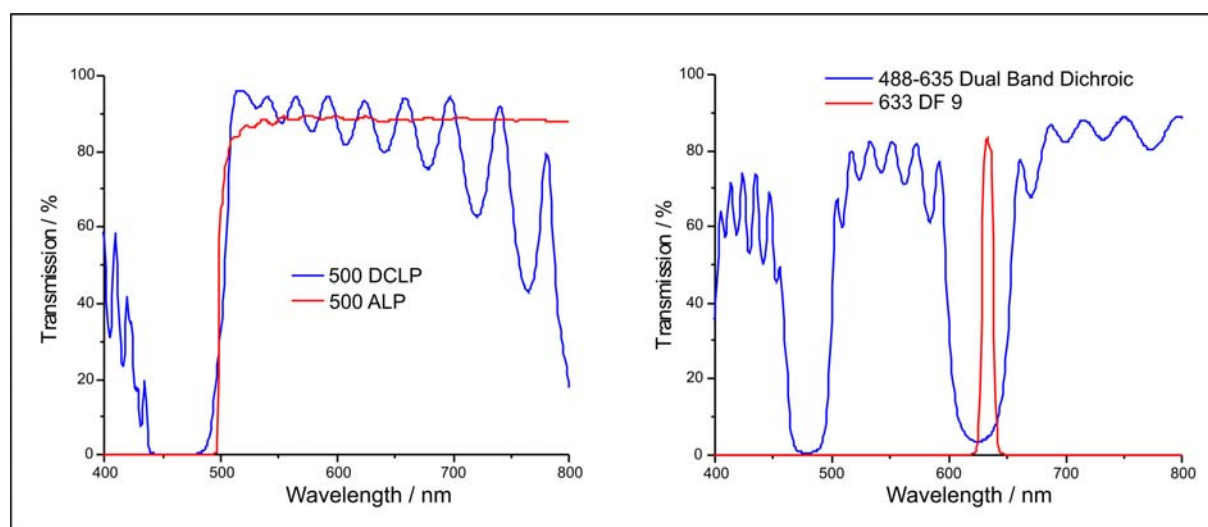


**Figure 3-4: Transmission curves of excitation beamsplitter and long pass filter in experiments with 488 nm excitation (left) and dual wavelength excitation beamsplitter with excitation filter for a 635 nm laser diode (right) and high reflectivity at 488 nm.**

excitation wavelength of 488 nm. Additional background signals on the detectors can thus successfully be avoided by using a long pass filter before spectrally separating emitted light onto the detectors. Experiments with dual-wavelength excitation were carried out using a dual wavelength beamsplitter exhibiting high reflection at 488 nm and 635 nm. A narrow band excitation filter (633 DF 9) has been used to spectrally select laser diode emission (see figure 3-4, right side).

Spectrally resolved information on fluorescence photons has been realized by using a set of dichroic beamsplitters and filters in the emission path of the set-up. Configurations for two different excitation wavelengths are listed in table 3-3.

<i>Excitation Wavelength</i>	<i>Dichroic Beamsplitter</i>	<i>Emission Filter</i>
635 nm	680 DRLP	665 DF 60, 675 DF 50
		700 DF 75
488 nm	560 DRLP 600 DCLP 680 DRLP	525 DF 45
		580 DF 60
		645 DF 75, HQ 542 LP
		700 DF 75

**Table 3-3: Beamsplitter and filters used in the emission pathway for 635 nm and 488 nm excitation.**

As an example configuration, transmission spectra for a set-up with 488 nm excitation and four detector channels are shown in figure 3-5. In the lower part of figure 3-5, the resulting spectral range for detection of each APD is depicted.

It is clearly visible that dichroic beamsplitters, e.g. the one shown at the left side in figure 3-4, do unfortunately not exhibit constant transmission over a long range of

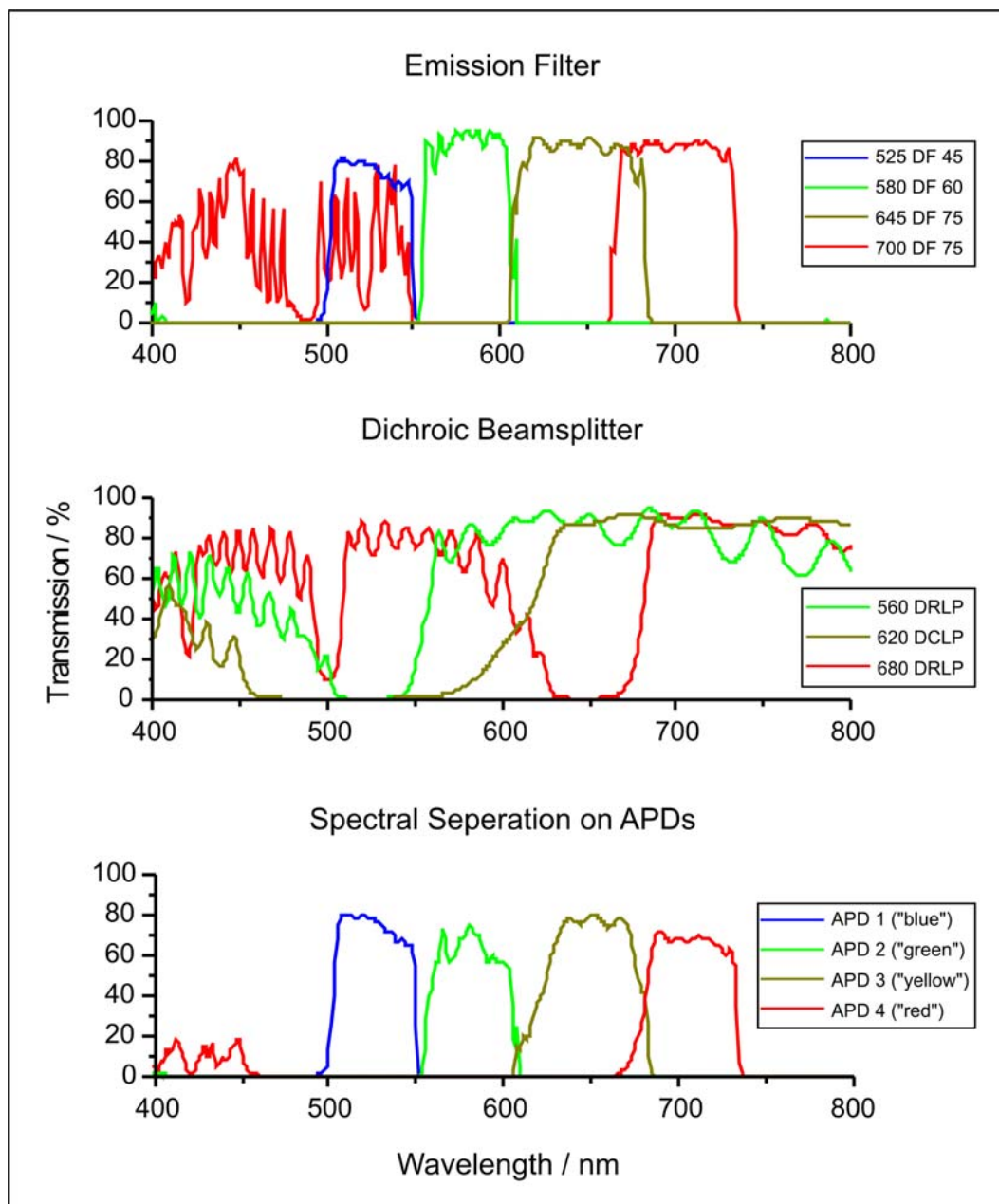


**Figure 3-5: Example of a configuration of beamsplitters and filters used with 488 nm excitation and four detector channels. Transmission spectra of filters (top) and dichroic beamsplitters (middle) are shown. The resulting spectral separation (bottom) has been calculated for each detector, ranging from 500 nm to 740 nm.**

wavelengths. Especially in experiments with a large spectral detection range, one has to be aware of a decreasing transmission of the excitation beamsplitter occurring at higher wavelengths, which have an important impact on spectral information. The influence onto the detection pattern of the previously described four detector set-up with 488 nm excitation is shown in figure 3-6. Additionally, the quantum yield for an APD was considered, and total collection efficiencies are depicted by filled areas in the graph. It is remarkable that the total detection efficiency is now reduced to an average value of 30% of photons emitted.

Furthermore, some beamsplitters exhibit strong polarization dependency, depending on the fabrication type. As a result, the rising edge in the transmission spectrum can shift up to 20 nm, according to the polarization properties of incoming light. It is therefore advantageous to use dichroic reflectors (titled DRLP), characterized by a steep transition slope and low polarization dependence, if available for a desired wavelength. Dichroic filters (DCLP) on the other hand

provide wide regions of both transmission and reflection, but exhibit a high degree of polarization along with a somewhat shallow transition slope.

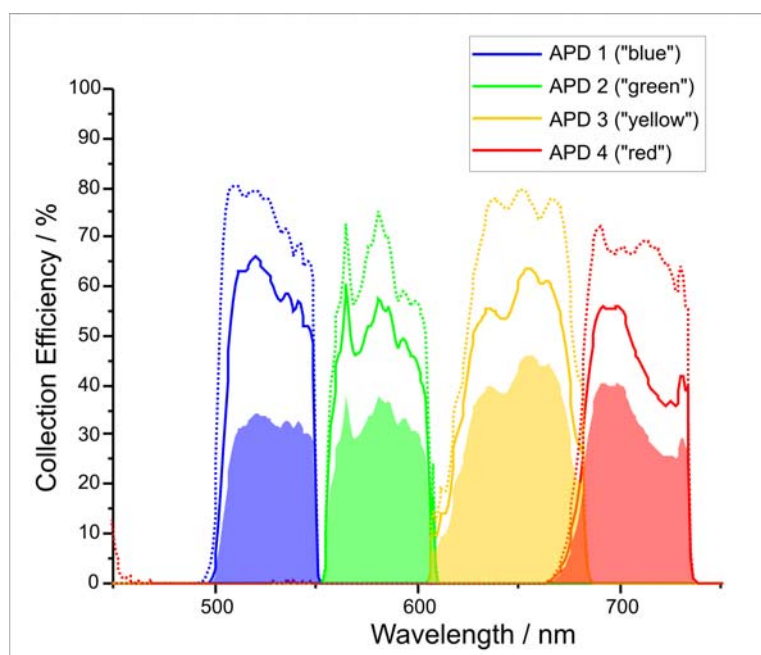


**Figure 3-6: Comparison of detection patterns (dotted curves) of a four detector set-up and corrected patterns (full curves) by considering an excitation beamsplitter (500 DRLP) and long pass emission filter (500 ALP). Filled areas below take into account the detection efficiency of APDs and yield total detection patterns.**

### 3.1.1. TIME-RESOLVED FLUORESCENCE MICROSCOPY

As a further extension to the basic set-up described above, time-correlated measurements with four channel spectral separation were performed, using pulsed excitation sources and a time-correlated single-photon counting (TCSPC) PC-plug-in card (SPC-630, Becker&Hickl, Germany). Thus, excited state information in a nanosecond timescale with minimum channel size of  $\sim 3$  ps could be realised, and allowed a further characterization of complex multichromophoric systems. The basic changes in the set-up together with the working principle of the SPC-630 and the characterization of the instrument is discussed in the following section.

#### Time-Correlated Single-Photon Counting (TCSPC) Using SPC-630

The computer based assignment of photons, both spectrally and temporal, was carried out using a PC-plug-in card for time-correlated single-photon counting, SPC-630 (Becker&Hickl, Berlin, Germany). Since this card represents the heart of data acquisition, it shall be discussed in more detail. The basic structure is shown schematically in figure 3-7.

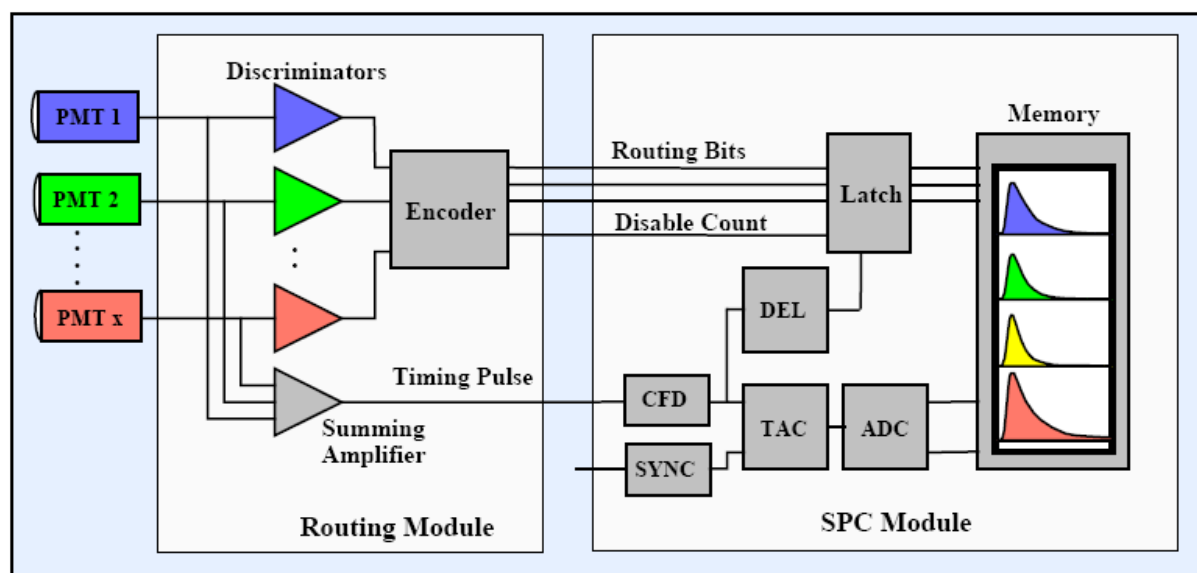


Figure 3-7: Schematic representation of the multichannel measurement principle, composed of a router unit and the PC-plug-in card SPC-630 for single-molecule photon counting.

Briefly, photons detected by several single-photon counting devices, e.g. APDs or PMTs, are spectrally encoded by attributing a routing bit to the temporal information, done by the routing module. Together with a constant-fraction discriminator (CFD) signal, responsible for an exact output pulse independent of the pulse height from the detector, the routing signal is transferred to the SPC-630. Besides several other functions, the CFD allows the reduction environmental noise or small background pulses (particularly “after-pulses”, which are common if working with APDs) by applying a threshold to incoming pulses from the detector.

The synchronization signal (SYNC) that is derived from the pulses of the light source is essentially important as a trigger signal for the SPC-630 card, since the microscopic times, i.e. fluorescent lifetime information, are calculated with respect to the SYNC pulses. Comparably to the CFD discrimination capabilities, electronic after-pulses from photodiodes or delay units can be corrected by adjusting SYNC properties.

In the next step, the time-to-amplitude converter (TAC) is used to determine the exact temporal position of a photon arrival signal with respect to the SYNC signal, resulting in the microscopic time of a photon. Since the probability of detecting a photon is considerably lower than detecting a SYNC signal, the TAC is usually processed in the “reversed start-stop” mode, which avoids many cycles without photon detection. In other words, after the arrival of a start signal generated by a photon on a detector, the temporal position towards the next SYNC signal is measured. To do so, the TAC generates a linear voltage ramp until the stop signal, provided by the SYNC, is detected. Depending on adjustable TAC parameters, an output voltage that depends linearly on the microscopic time is generated.

In a next step, the analogue digital converter (ADC) converts the analogue signal into a memory address, MEM, by resolving it into 4096 time channels. In this step, a maximum time resolution of ~3 ps can be achieved.

The SPC-630 module can be operated in continuous flow or in the first-in-first-out (FIFO) mode. Processed in the continuous-flow mode, photon histograms are recorded on board using two available memory banks and hereby preventing read-out gaps during the measurement. This mode is strictly hardware based and thus provides an extremely accurate recording sequence. Alternatively, a FIFO structure of the memory of the card can be used. In this mode, the measurement does not

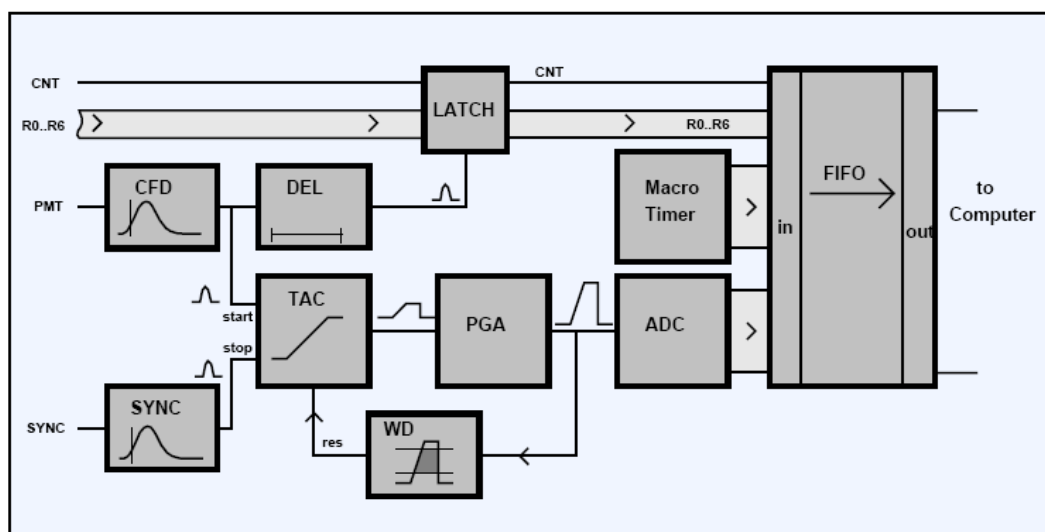


Figure 3-8: SPC-630 card working in the FIFO-mode.

deliver a histogram but a continuous stream of information about the individual photons. The principle is shown in figure 3-8.

Additionally to the signal created by the ADC, a macro timer delivers the macroscopic time since the beginning of the measurement. The resolution of the macro timer of the SPC-630 is 50 ns. By this, each photon is encoded by the routing information, a microscopic time and a macroscopic time, together with some control flags to process overflow, invalid photons or other events. These data are bundled into one FIFO unit, which, depending on the time resolution chosen, has a size of either 32 or 48 bits. Software can continuously read out the FIFO buffer after a certain number of photon arrival events, and time resolved information on fluorescence data is now available, photon by photon.

The fundamental advantage of this method is that each photon is fully described by its FIFO package. Hence, a powerful and multidimensional data analysis becomes possible, from fluorescence intensity time traces including spectral information, fluorescence lifetime and coincidence of photons. Additionally, photons can be histogrammed or correlated, which allows the identification of kinetic information on both a microscopic and a macroscopic timescale.

If the set-up is operated in a multichannel mode and separate microscopic times for each channel are of interest, the response from each detector channel is not necessarily in the same time window and has to be synchronized. This is caused by

unequal detection pathway lengths of different channels by variable cable lengths that connect the detectors' signal with the routing unit. To circumvent the loss of photons and assure the accuracy in such measurements, one channel is chosen as a reference signal. Further detector channels are overlaid in time using three delay units with 1 ps time resolution (DG535, Stanford Research Instruments, USA)

### **Pulsed Laser Excitation**

If particularly fluorescence kinetics and not photostability of fluorophores were of interest, different pulsed laser systems were used as excitation source. Due to increased photostability of fluorescent dyes in the far red, these dyes are available for excitation with a pulsed source, namely a diode laser with a centre wavelength of 635 nm (LDH-635, Picoquant, Berlin, Germany) and a pulse width between 100 and 300 ps, depending on the laser output power. A picosecond pulsed diode laser driver (PDL-800-B, Picoquant, Berlin, Germany) was used for pulsing the laser diode with a base frequency of 80 MHz, which could be adjusted dividing by constant factors of 2, 4, 8 or 16. Since the emission profile of diode lasers is usually broader and sometimes slightly shifted in maximum intensity, a narrow band excitation filter was used (e.g. 639DF9, Omega Optics, USA) to further narrow down the excitation wavelength.

Pulsed excitation at shorter wavelengths was realized with three different laser systems, mainly distinguished by the operating wavelength, pulse width and repetition rate. A peltier cooled laser diode with 440 nm centre wavelength (LHD-P-C-440, Picoquant, Berlin, Germany) and a pulse width ranging from 90 to 300 ps was used in the lower spectral range, but is only suited for excitation of poorly stable coumarine dyes. To access the excitation of rhodamine dyes which are generally preferred to coumarines in single molecule experiments, and to allow comparable conditions to continuous wave excitation using the 488 nm line of an argon ion laser, two different frequency doubled titan sapphire lasers were used. Pulsed light with a centre wavelength between 480 nm and 490 nm was provided, exhibiting a pulse width of 150 fs (MIRA 900, Coherent, USA) and 130 fs (Tsunami, Spectra Physics, USA), respectively. Due to extremely short pulses and hence high pulse energy densities of femtosecond titan sapphire systems, the frequency doubled Tsunami laser was coupled into a single mode optical fiber (3.2  $\mu\text{m}$  core; S405-Custom,

Nufern, USA) of 50 m length. The broadening of the pulse by dispersion in the fiber could be estimated by

$$\Delta\tau_{out} = \Delta\tau_{in} \sqrt{1 + \left[ \frac{4 \ln 2}{(\Delta\tau_{in})^2} \beta_2 L \right]^2} \quad ( 3-2 )$$

where  $\Delta\tau_{in}$  represents the input pulse width,  $\Delta\tau_{out}$  the output pulse width,  $L$  is the length of the fibre, and  $\beta_2$  is the group velocity dispersion (GVD) of the fibre material, depending on the wavelength. With  $\beta_2 = 70 \text{ ps}^2 \text{ km}^{-1}$  and  $\Delta\tau_{in} = 130 \text{ fs}$ , a pulse width of around  $\Delta\tau_{out} = 100 \text{ ps}$  is obtained. To verify this result experimentally, a fast photodetector (Antel Optronics, USA) with a spectral range of 300 to 1100 nm and a FWHM pulse width of  $< 65 \text{ ps}$ , together with a fast sampling oscilloscope (Tectronix 7904, Oregon, USA) with a time constant of 25 ps have been used. The oscilloscope response is shown in figure 3-9 (left side) and shows a broadening of around 160 ps for the FWHM of the observed pulse, which exhibits a tailing of up to 500 ps. This is comparably to the theoretically obtained result, if one takes into account that the measured pulse is convoluted with the detector and oscilloscope characteristics. The spectral distribution of the frequency doubled laser wavelength was determined to be 5 nm (figure 3-9, right side).

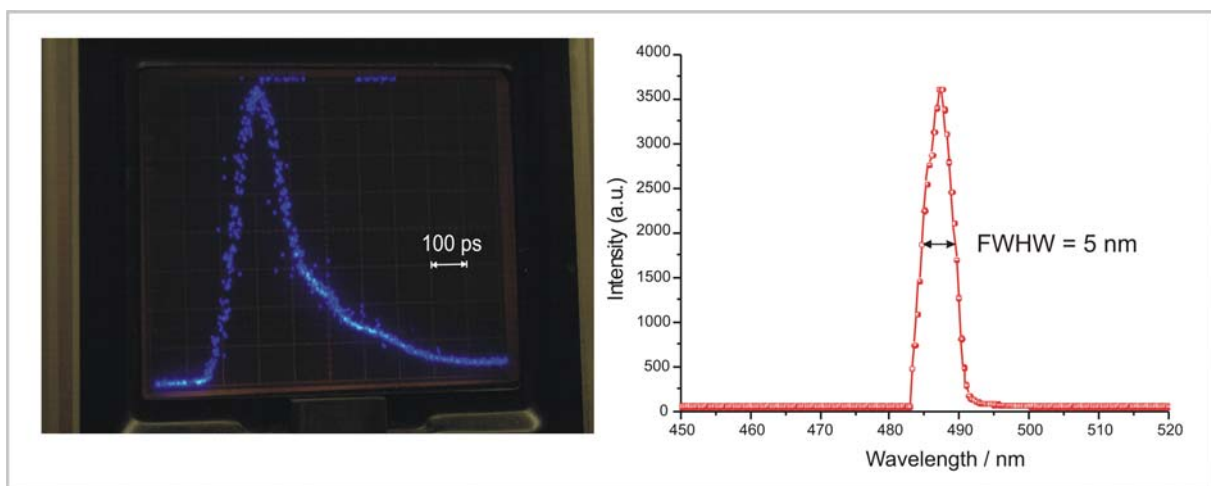


**Figure 3-9:** left: response function of a Tsunami laser pulse after 50 m single mode fibre, measured with a fast oscilloscope, pulse width of 160 ps (one grid represents 100 ps); right: spectrum of the same laser centred at 487 nm, and a FWHM of 5 nm.

## Instrument Response Function

The instrument response function (IRF) of a set-up which is operated with pulsed excitation represents the bottleneck for the accessible time resolution. Typically in the same order of magnitude as fluorescence kinetics from organic chromophores, the accuracy of data analysis depends strongly on the width of the IRF.

Theoretically, an IRF is described by the convolution of all steps influencing the pulse width, both from the excitation path and the emission path. Here to mention are the pulse width of the laser source as well as the time resolution of the detector elements and the TCSPC plug-in cards. Some of the components of an IRF can be measured independently, as shown for the pulse width of the Tsunami laser previously. Others depend strongly on experimental conditions, as the time resolution of an APD correlates with the fraction of the active area which is used to detect photons. Assuming a laser pulse width of 160 ps, a temporal response of 200 ps for the PC plug-in card and 300 ps as best response of an APD, the theoretically best value for an IRF can be estimated to be around 350 ps, using the following estimation:

$$FWHM_{IRF} = \sqrt{\sum_i (FWHM_i)^2} \quad ( 3-3 )$$

where  $FWHM_i$  represent the full width half mean of the IRF of the single components, yielding the total IRF, denoted  $FWHM_{IRF}$ .

The total IRF for each detector channel of the Tsunami set-up described in this section has been previously determined to have a FWHM of between 1.0 and 1.2 ns, shown in figure 3-10. Main reasons for this significant broadening of the IRFs are derived from bandwidth of the SYNC signal of the laser, provided by an internal

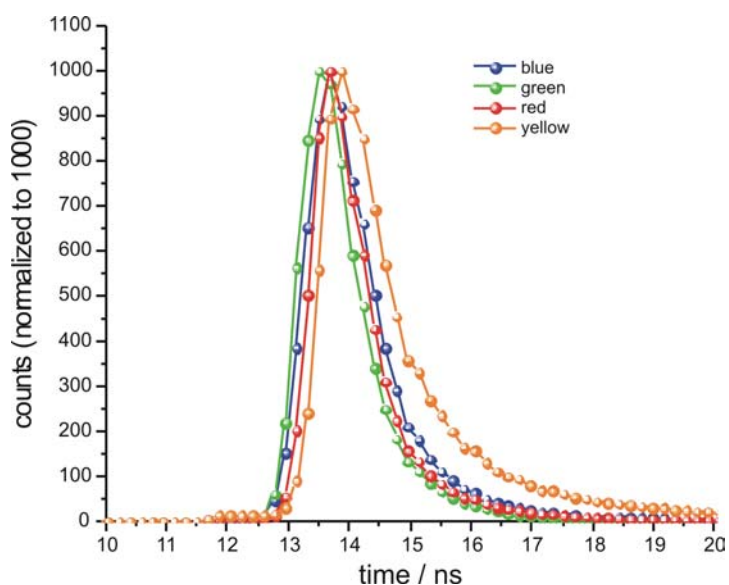


**Figure 3-10: Instrument response functions measured for each detector of the Tsunami set-up, exhibiting a FWHM between 1.0 ns and 1.2 ns.**

photodiode, as well as each individual APD, whose resolution function depends on the effectively used fraction of the active area. This is particularly important if a  $2f$  detection path is used, which is often poorly sensitive in the  $z$ -direction and produces considerably larger images on the detector.

Instrument response functions of around 1 ns are a limit to time resolution, and fluorescence decays of around 0.5 ns are the shortest which can be observed. In experiments with efficient depopulation of a fluorophore's  $S_1$  state by e.g. energy transfer or quenching, fluorescence decays of this magnitude are generally observed. Therefore, deconvolution of fluorescence decays of each channel with the corresponding IRF have been applied, which allow a theoretical time resolution of around  $1/20$  of the FWHM of the IRF, i.e. 50 to 60 ps.

To substantially improve the time resolution, a modified detection scheme with parallel optical paths to all detectors, finally focussing onto a small fraction of the active detector area with a lens of short focal length, can be applied. Experiments on a set-up designed with this detection principle have been carried out using the MicroTime 100 system (PicoQuant, Berlin, Germany). A brief description is given in the following section.

### 3.1.2. TIME-CORRELATED MEASUREMENTS AT THE MicroTime 100 SET-UP

Additional to the set-up mentioned above, time correlated measurements were performed on the MicroTime100 set-up (Picoquant, Berlin, Germany) containing four APDs and a 470 nm laser diode as excitation source, pulsed with 40 MHz. The schematic principle is shown in figure 3-11, and a more detailed description is the subject of this paragraph.

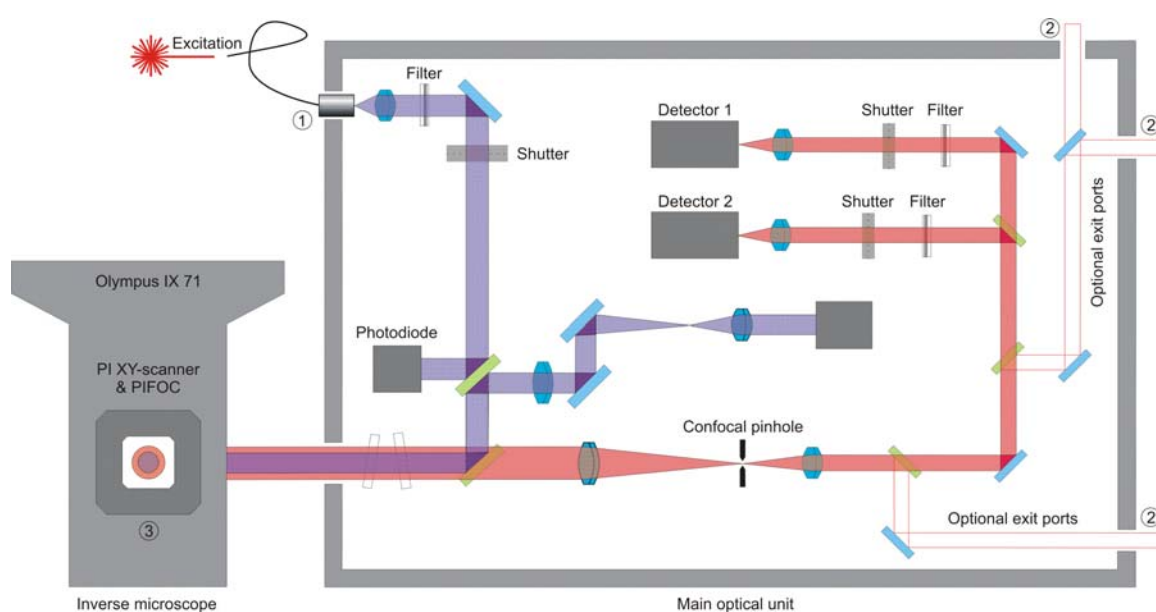


**Figure 3-11: Schematic view of the Microtime100 set-up (Picoquant, Berlin, Germany). A modified set-up with four detector channels was used in this work.**

The MicroTime100 set-up uses an IX71 (Olympus, USA) inverted microscope and a similar x,y piezo stage to the one previously described. The excitation laser is coupled into a fibre, enters the optical part of the set-up and is directed into the sideport of the microscope via a dichroic mirror. Fluorescence light passes through the same sideport, transmits the dichroic mirror and is spectrally resolved onto four detector channels using the same dichroic beamsplitters and filters in the detection path as described for the basic set-up.

The most striking difference is located in the detection pathway of the optical part of the set-up. In earlier described set-ups, light leaves the microscope already focused by a lens positioned directly after the excitation dichroic beamsplitter, is then projected onto a pinhole and finally on the active area of a detector. In this particular

set-up, parallel light leaves the microscope, and the confocal pinhole is placed between two lenses of a telescope. Subsequently, the light beam is parallel again until reaching the desired detector, which allows the length of the detection path to be independent and gives more freedom in designing a detection path. Furthermore, all optical elements like filters or beamsplitters do not affect the quality of the image and can be exchanged easily. A lens with a short focal length, which can be adjusted in all three dimensions, is finally used to focus light onto the detector. Easy adjustment of the detectors is achieved, and using a small area in the centre of the active area has been experimentally proven to have a positive effect onto the FWHM of the instrument response function.

Similar to the SPC-630 card used in previously described set-ups, the MicroTime 100 is processed by a TimeHarp 200 PC-plugin card. The operation mode is similar, although titled time-tagged time-resolved (TTTR), with a time resolution of <40 ps.

Again of particular interest to estimate the quality of the nanosecond time resolution, the total IRF of this set-up was determined for all four detector channels independently. The graphical representation is shown in figure 3-12. The FWHM of the IRF of all channels was determined to be around 0.7 ns each, which is around 0.3 ns shorter than for the Tsunami set-up described above.

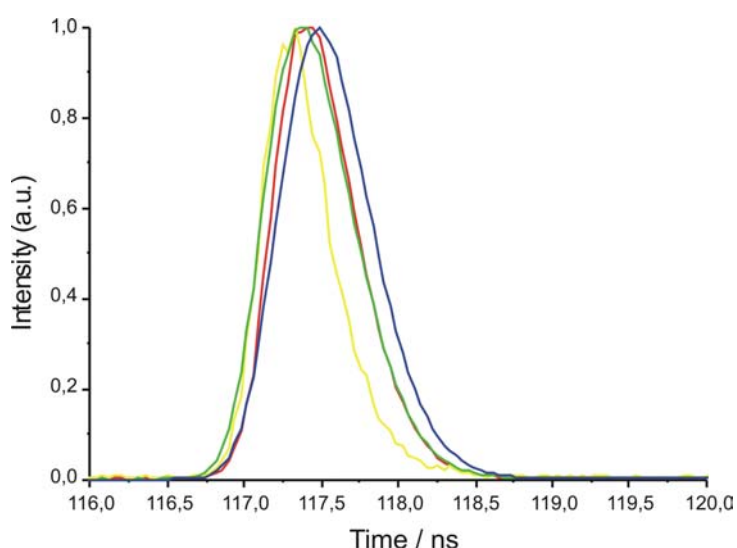


**Figure 3-12: Total IRF measured for all four detector channels of the MicroTime 100 set-up independently.**

### 3.1.3. TWO-COLOUR EXCITATION

In experiments aiming to probe a single chromophore with two different wavelengths, two laser beams were overlaid using a dichroic beamsplitter before entering the backport of the microscope. A schematic representation of two-colour excitation is presented in figure 3-13. First, both lasers, exhibiting different beam diameters, were extended using a telescope, and two beams with identical diameter were obtained. By using a dichroic beamsplitter (658 DRLP, Omega Optics, USA) which shows high reflectivity for 635 nm and sufficient transmission around 488 nm, the laser beams were overlaid.

To assure the best possible overlay of the excitation volumes of both foci, one telescope was equipped with an adjustment along the optical axis. Using a CCD device and the electronic movement of the objective provided by the microscope, the focal volumes could hereby be overlaid with an accuracy of more than 0.5  $\mu\text{m}$  along the optical axis.

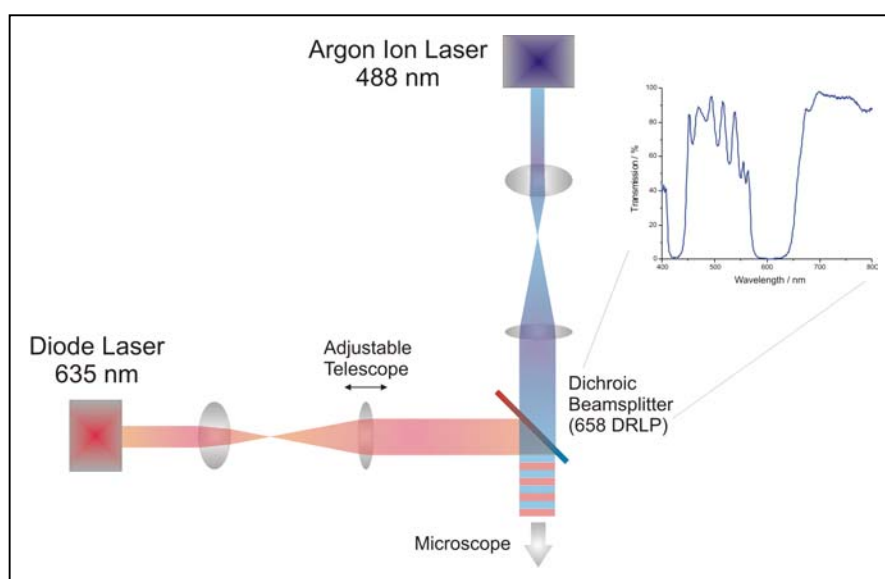


**Figure 3-13: Schematic principle of two-colour excitation. A dichroic beamsplitter (658 DRLP, Omega Filters, USA) reflecting light at 635 nm and transmitting light in the region of 500 nm was used to overlay different laser beams.**

### **3.2. Ensemble Spectroscopic Instrumentation**

Ensemble spectroscopic measurements can be divided into steady-state and time-resolved measurements. Although suffering from averaging of subpopulations and poorer sensitivity, ensemble methods are indispensable for characterization purposes of fluorophores and modified biomolecules. These standard techniques served to characterise complex multichromophoric constructs which further are investigated in single-molecule experiments. A short overview is given in the following passages.

#### **3.2.1. STEADY-STATE MEASUREMENTS**

##### **Absorption Spectroscopy**

Absorption measurements were performed on two UV/VIS spectrometers, a Lambda 25 spectrometer from Perkin Elmer (USA) and a Cary 500 spectrometer from Varian (Darmstadt, Germany). Samples were measured in silica precision cuvettes (suprasil) from Hellma (Mülheim, Germany). Depending on experimental conditions, both semi-micro cuvettes with a path-length of 10 mm and micro cuvettes with a path-length of 3 mm were used.

To avoid intermolecular interactions in absorption measurements and fluorescence emission re-absorption effects, the concentration of samples did not exceed  $10^{-6}$  M. In this case, the LAMBERT-BEER law is valid,

$$A = \log \frac{I_0}{I(\lambda)} = \varepsilon(\lambda)cd \quad ( 3-4 )$$

where  $A$  is the absorption defined as the decadic logarithm of the fraction of the reference intensity,  $I_0$ , and the measured intensity,  $I(\lambda)$ . If the absorption is below a value of around 1, linearity to the concentration,  $c$ , of the sample is observed, normalized by the path-length of the sample,  $d$ , and the wavelength dependant extinction coefficient,  $\varepsilon(\lambda)$ .

## Fluorescence Spectroscopy

Fluorescence spectra were obtained using a Cary Eclipse spectrometer from Varian (Darmstadt, Germany). Besides fluorescence intensity measurements, the instrument offers the possibility to obtain dynamic fluorescence measurements at different emission wavelengths simultaneously. Furthermore, polarized excitation and detection is possible, enabling anisotropy measurements. A temperature control unit based on a thermoelectric peltier device allows measurements of thermal profiles between 4 and 90 °C.

Briefly, the spectrometer uses a xenon flash lamp technology providing an excitation range between 290 to 1100 nm. A photomultiplier tube (PMT) is used as detector, and sample concentrations down to  $10^{-9}$  M can be measured.

### 3.2.2. TIME-RESOLVED SPECTROSCOPY

Ensemble fluorescence lifetime measurements were carried out using the technique of time-correlated single photon counting (TCSPC) with an IBH spectrometer (model 5000MC; Glasgow, Scotland). As excitation sources, various pulsed light emitting diodes (LED) with a central wavelength of 450 nm, 495 nm and 590 nm and a pulse width of around 500 ps were used. For excitation at 635 nm, a laser diode with a pulse width of around 50 ps was used. The repetition rate is set to 1 MHz. Photon detection is realized by a photomultiplier tube (PMT), sensitive for single-photon detection. For the purpose of time-resolved anisotropy measurements, both excitation and emission polarization could be modified.

Lifetime histograms were taken by collecting a fixed number of photons in the maximum channel, e.g. 2000 to 5000 photons, depending on the sample concentration. Up to 4096 time channels with a minimum bin width of 12 ps were used. A fluorescence decay of a DNA bound fluorophore upon excitation with 450 nm is shown in figure 3-14, together with the pulse profile of the excitation source, i.e. the lamp profile or “prompt” signal.

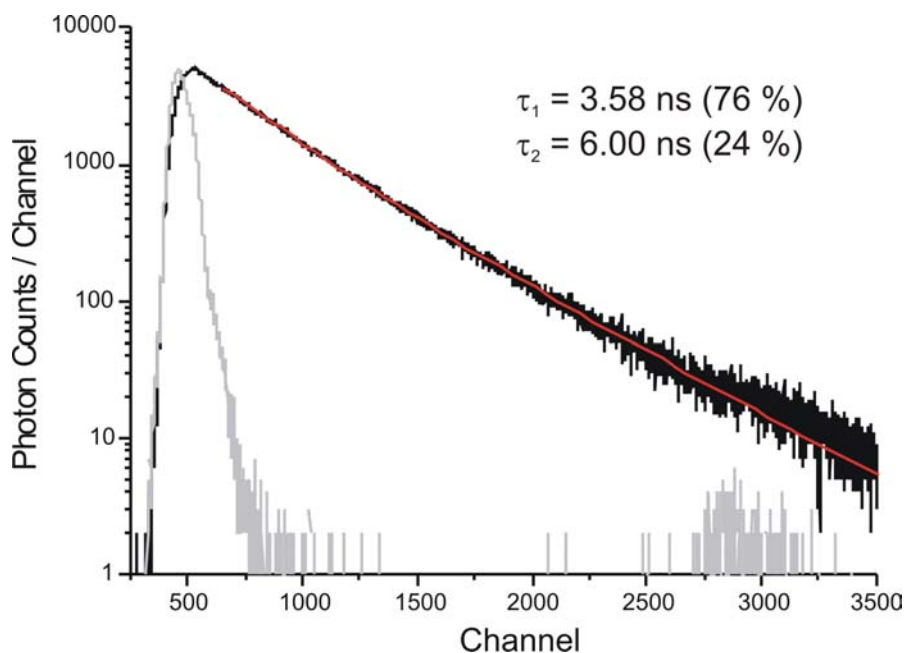


**Figure 3-14: Fluorescence decay of Alexa430 conjugated to the 5'-end of a 60 base pair double stranded DNA, obtained by excitation with 450 nm LED (pulse of LED in gray). Fluorescence lifetimes were calculated after deconvolution and applying a biexponential fit.**

As the excitation pulse is not infinitesimal short, a convolution method was used to obtain exact fluorescence lifetimes of multi-exponential decays with up to four components. The mathematical routine was part of the spectrometer's software package "Data Station 2000". Briefly, a set of start parameters is defined, followed by the calculation of a fluorescence decay by a deconvolution and fitting procedure. With the software provided, the decay in figure 3-14 was fitted to two components of 3.58 and 6.00 ns. An estimation of the quality of a fit is given by a normalized  $\chi^2$  value calculated by the software. As a rule of thumb,  $\chi^2$  values better than 1.20 give a confidence level of 90% for the calculated fit, and best fits are obtained with  $\chi^2$  values around 1. The bi-exponential fit in figure 3-14 has a  $\chi^2$  value of 1.08.

As an extension to fluorescence lifetime measurements at only one detection wavelength, the spectral dependence of a fluorescence decay is accessible by time-resolved emission spectroscopy (TRES). This is of particular interest if a depopulation process of  $S_1$  of a fluorophore is influenced by the presence of a second fluorophore within short distance, which is the case in fluorescence resonance energy transfer experiments. If multichromophoric systems are subject to

investigation, time resolved fluorescence measurements can help to unravel the efficiency of single transfer steps, additionally to spectral intensity changes.

### 3.3. Biological and Chemical Methods

#### 3.3.1. CONJUGATION CHEMISTRY

A broad spectrum of reactive organic fluorophores are commercially available. Two main classes of chemical modification are used frequently, which are amine-reactive dyes containing a succinimidyl ester (NHS ester) group, and thiol-reactive dyes containing a maleimide ester group. The underlying chemical reactions are depicted in figure 3-15.

In short, a nucleophilic substitution at the carboxylic ester group (case A in figure 3-15) initiates the conjugation of an amine-reactive fluorophore ( $R_1$ ) with  $R_2$ , the molecule of interest, e.g. an amino modified DNA. The reaction is driven by the formation of an energetically stable N-succinimide. A thiol-reactive probe undergoes a nucleophilic addition of a thiol-containing molecule (e.g. cysteine residues from proteins) at the double bond of the maleimide (case B in figure 3-15). The

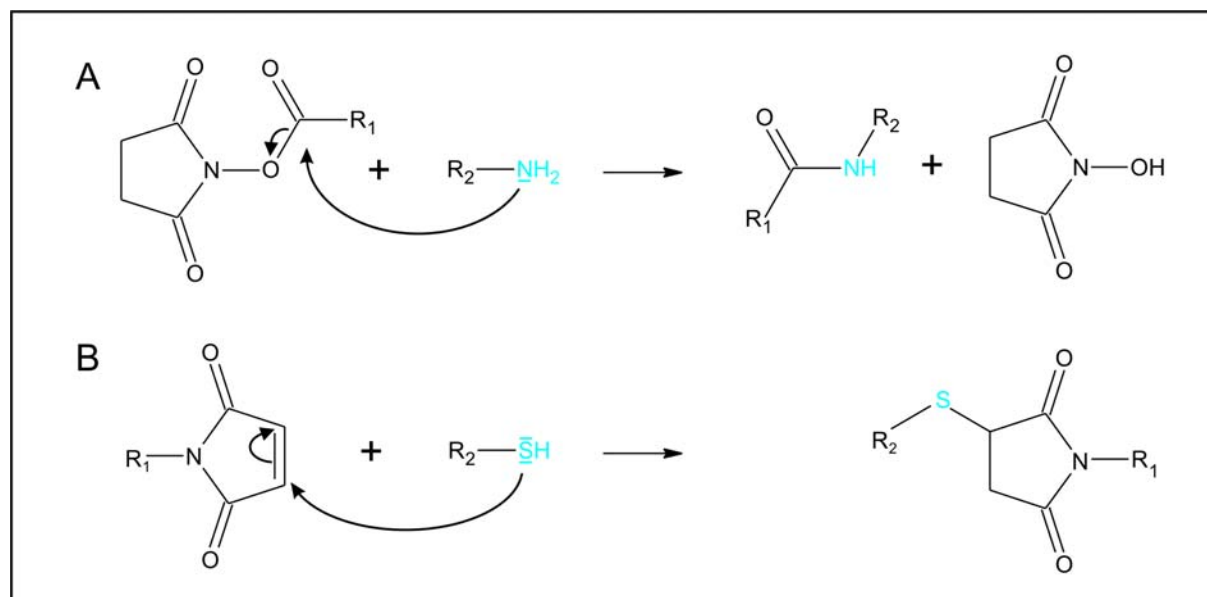


**Figure 3-15: Chemical reaction scheme for labelling biomolecules. (A) succinimidyl ester of fluorophores are conjugated to amino functionalised molecules, (B) maleimide ester are conjugated to thiol groups.**

nucleophilic substitution of NHS esters is catalysed by slightly alkaline conditions, whereas maleimide esters react in neutral environment.

If the molecule of interest has to be labelled with two different fluorescent probes at well-defined sites, both strategies are applied and the selectivity of each reaction type results in a doubly labelled molecule.

Amino modified oligonucleotides (purchased from IBA GmbH, Göttingen, Germany) were the molecular basis for many samples generated in this work. A large number of fluorescent probes from different companies, summarised in table 3-4, were conjugated to oligonucleotides of different length.

<b>Company</b>	<b>Fluorophores</b>
AttoTec GmbH, Siegen, Germany	Atto590, Atto620, Atto647 and others
Amersham Biosciences, NJ, USA	Cy3, Cy3.5, Cy5, Cy5.5
Molecular Probes, Eugene, USA	Alexa488, RhodamineGreen and others
Sigma Aldrich, St. Louis, USA	HIDC
Denovo Biolabels, Münster, Germany	Oyster 656 and others

**Table 3-4: List of manufacturers of different types of chromophores, used in this work.**

Activated fluorophores are provided as dry powder and are only poorly stable in water. Therefore, the dyes are usually diluted in DMF, and aliquots are stored at – 20 °C.

### **Dye-Labeling and Purification of DNA Oligonucleotides**

Using post-labelling techniques together with hybridisation, synthetic oligonucleotides offer a strong basis to construct multichromophoric compounds with defined structure. Many modifications of oligonucleotides, including amino modification or biotin tags as molecular anchor, are available and make DNA to a well suited candidate as a molecular building block system. By using several independently labelled single stranded oligonucleotides, various combinations of a final arrangement are possible.

In the frame of this work, oligonucleotides of different length between 20 and 60 bases, modified with amino groups and biotin as anchor molecule were used. Post labelling and a multi-step purification by gel-filtration and high performance liquid chromatography (HPLC; 1100 series, Agilent, USA) ensured purity of samples. Labelling of single strand oligonucleotides with NHS-esters of various fluorophores was realized using the following protocol:

10 nmol	Oligonucleotide (solution, ca. $10^{-4}$ M)
40 $\mu$ l	Phosphate buffered saline (PBS; Sigma-Aldrich))
10 $\mu$ l	100 mM carbonate/bicarbonate buffer, pH=9
30 nmol	Dye, diluted in DMF (Fluka)

After shaking for 1 – 2 h of, the sample was loaded onto a gel filtration column (NAP-10, Amersham Biosciences, USA), previously conditioned with PBS. This purification step allows a first separation step of DNA and excess dye by size exclusion. Molecules with a molecular mass below  $\sim 1500$  g/mol are retarded, while larger molecules pass through the column without hindrance. Further purification was realized by HPLC, using a reversed phase C-18 column and a 20-minute gradient between two solvents A and B with following compositions:

Solvent A (aqueous)	0.1 M Triethylammonium acetate (TEAA) in water
Solvent B (organic)	0.1 M TEAA in 75% acetonitrile, 25% water

To remove solvents used in the HPLC purification step, the obtained solution of dye-labelled DNA was in vacuum. If the fluorescent dyes used are not stable at alkaline conditions, another gel filtration step had to be applied to replace the solvent mixture by PBS or water. Otherwise, the pH during this step reaches strongly alkaline values due to up-concentration of TEAA.

### **Hybridisation of Single Strand Oligonucleotides**

Concentrations of dye-modified oligonucleotides were derived from steady state absorption spectroscopy as described previously. Since the extinction coefficient of a fluorophore might be slightly changed if attached to an oligonucleotide, the sample concentration was calculated using the absorption of both the fluorophore at its maximum and the DNA itself, absorbing at 260 nm.

Purified and dye-labelled single-strand oligonucleotide fragments could now be mixed, and thermal hybridisation was realized using a programmable thermo controller (PTC 100, MJ Research, USA). To surely exceed the melting temperature of DNA (which can be estimated to be around 70 °C), the samples were heated shortly to 95 °C, cooled down to 65 °C in a minute, and slowly cooled down to room temperature for about one hour.

### **3.3.2. SURFACE PREPARATION TECHNIQUES**

To observe single fluorophores for a longer period of time, i.e. until photobleaching, they have to be immobilized on a surface. This can generally be realized by different techniques, either in dry or liquid environment. Throughout this work, two different approaches to prepare samples with immobilized fluorophores were used: molecules adsorbed on dry glass surfaces or dispersed into polymer films on the one hand, and molecules attached to a protein surface using an anchor strategy on the other hand.

#### **Dry Glass Surface**

Cover slides (Roth, Karlsruhe, Germany) with a thickness of ~170 µm were used to adsorb dye molecules. Before use, cover slides were treated with a 0.5% solution of hydrofluoric acid in water. Afterwards, a solution of 0.1% of 3-aminopropyl-triethoxysilane (APS; Sigma-Aldrich) in methanol was added and washed off with water after five minutes incubation. The surface treatment results in a slight adsorption of negatively charged DNA molecules onto a positively charged surface. Samples for single molecule experiments were prepared by incubating the cover

slides with a  $10^{-10}$  M solution of DNA-dye-conjugates for several minutes. After a washing step with water, samples were dried under nitrogen flow. This treatment avoids contamination with impurities and yields the desired areal density for single molecule experiments on a surface, which is around 1 molecule per square micrometer.

Polyvinyl-alcohol (PVA, Sigma-Aldrich) as a polymeric host matrix was used to prepare samples of fluorophores in an oxygen-free environment. The polymer was dissolved in water at a concentration of 1% (w/v) by stirring and heating in a water bath. Fluorophores were embedded in the polymer solution and coated onto a cover slide surface using a spin coater, rotating the sample with 2500 rounds per minute. Hereby, the solvent was removed and a homogeneous polymer matrix was obtained.

### Immobilizing Molecules Under Aqueous Conditions

To allow the observation of biomolecules in a homogeneous environment, measurements under aqueous conditions are the method of choice. A further advantage lies in the possibility to change the chemical environment rapidly, and hereby investigate the direct influence on a the photophysical behaviour of fluorophores. In this work, a protein based anchoring technique which exploits the binding of biotin molecules with the protein streptavidin was used [Anzai et al., 1995; Dohnta et al., 1997].

To prepare the protein surface, cover slides with eight chambers (LabTek, Nunc,

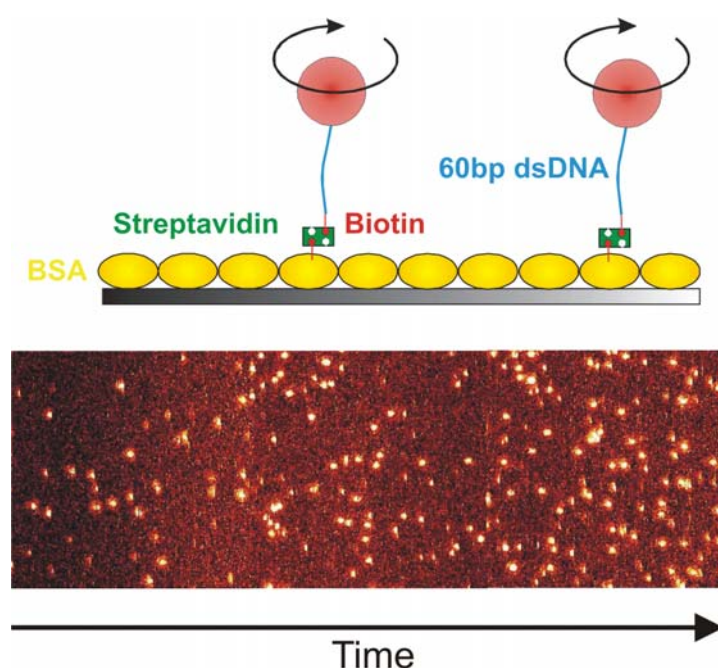


**Figure 3-16.** Immobilization of fluorophores using the binding protein streptavidin. A surface coated with BSA and BSA-biotin is treated with streptavidin. Fluorophores attached to oligonucleotides containing biotin as anchor bind to streptavidin. The lower part shows an increasing number with time, immobilized at the surface and tracked online.

Karlsruhe, Germany) glued to a glass slide were used. The surface was shortly treated with 0.5% hydrofluoric acid solution (less than one minute), washed with water, and incubated for several hours with a solution of 5 mg/ml of bovine albumine serum (BSA, Sigma Aldrich, USA) and 1 mg/ml of biotinylated BSA (ca. 13 mole biotin / mole BSA; Sigma Aldrich) in PBS. Prior to measurements, the BSA solution was washed off the chambers several times with PBS. Subsequently, the surface was incubated with a solution of 0.1 mg/ml streptavidin (recombinant, assuring efficient binding of at least two biotin molecules per streptavidin molecule; Roche, USA) for a couple of minutes. After application of washing steps, surfaces were ready for use.

On the scanning stage of the microscope, the surface was loaded with a sample, which was usually a fluorophore attached to an oligonucleotide having a biotin linker at one of its ends. A few microlitres with a concentration around  $10^{-9}$  M were added, and the “loading” of the surface was tracked online. After a few minutes, the desired density of molecules at the surface was reached. To remove remaining sample molecules in the solution, the chamber was washed a several times with PBS. Figure 3-16 portrays this immobilization method and shows the increase of fluorophores attached to the surface with time.

Using this technique, fluorophores attached to oligonucleotides rotate freely in solution, which can be proved by rotating the polarization of the excitation source. Furthermore, single stranded oligonucleotides anchored to the surface are accessible for hybridisation, if a complementary DNA strand with slightly higher concentration is added into the chamber. Altogether, this technique allows for higher flexibility in single-molecule experiments, and opens many possible ways of experimental modifications.

### **3.3.3. INFLUENCING THE CHEMICAL ENVIRONMENT OF FLUOROPHORES**

The photophysical properties of fluorophores strongly depend on the environmental conditions. The heterogeneity of photophysical parameters can be reduced if a homogeneous microenvironment is realized. In other words, the distributions of parameters as fluorescence lifetime and emission wavelength are broader if fluorophores are adsorbed to a glass surface, compared to molecules immobilized under liquid conditions using the anchor strategy. This can be explained by a

randomly oriented adsorption of fluorophores and the lack of mobility on a glass surface, resulting in different conformations and “nano-environments” for each molecule, which alters fluorescence properties. Anchoring fluorophores in liquid environment circumvents these effects and additionally offers the possibility to change the chemical microenvironment easily. Especially the oxygen concentration and redox properties of the surrounding solvent have been found to be important for photophysical properties of organic fluorophores. The strategy to influence these parameters is outlined in the following section.

### Oxygen Removal

Efficient removal of oxygen was realized using an enzymatic approach [Funatsu et al., 1995]. A solution of oxygen consuming enzymes, i.e. glucose oxidase and catalase, was added to the solvent covering the fluorophores attached to the protein surface. The following protocol was used to prepare 1 ml of enzyme stock solution (20x):

- 1 mg Glucose oxidase (Sigma-Aldrich)
- 0.5 ml Tris buffer (Roth, Germany), 25 mM KCl
- 2  $\mu$ l Catalase 30 mg/ml (Sigma-Aldrich)
- 4  $\mu$ l 1 M Dithiothreitol (DTT, mol. biology grade; Sigma-Aldrich) in PBS
- 0.5 ml Glycerol (GC-grade, Sigma-Aldrich)

Fractions of 50  $\mu$ l were stored at  $-20^{\circ}\text{C}$ . Prior to use, one fraction was diluted in 1 ml of a 0.1 g/ml glucose (Sigma-Aldrich) solution in PBS. About 500  $\mu$ l of this mixture were transferred into a LabTek chamber. To reduce oxygen exchange with the surrounding air, a “Press-To-Seal” silicone plastic (Molecular Probes, USA) was used, covering the chamber.

In a first step, glucose oxidase requires glucose as substrate and consumes oxygen to oxidize the substrate forming hydrogen peroxide. In a second step, catalase reduces hydrogen peroxide to water.

Enzymatic removal of oxygen is an efficient technique and decreases the concentration of oxygen with a comparable efficiency to other methods, e.g. replacing of oxygen by nitrogen flow or embedding molecules into PVA polymer matrices. As a nice advantage, these proteins only slightly increase the background intensity and make their application in single-molecule experiments possible.

### Redox properties

Populations of the radical state of fluorophores can be manipulated by changing the redox properties of the solvent. Fluorophores are either quenched by an electron transfer reaction, or recover fluorescence if they are currently in a nonfluorescent radical state. Furthermore, molecular switches exhibiting fluorescence states depending on the redox environment have been demonstrated [Yan et al., 2005]. An overview of chemicals which generate reducing or oxidising conditions is given in table 3-5.

<b><i>Reducing reagent</i></b>	<b><i>Supplier</i></b>
$\beta$ -mercaptoethanol (BME)	Fluka
2-Mercaptoethylamine (MEA)	Fluka
L-cysteine	Fluka
Tetrachlorobenzoquinone (TCBQ)	Sigma-Aldrich
L-tryptophane	Fluka
Guanosine monophosphate (dGMP)	Sigma-Aldrich
<b><i>Oxidising reagent</i></b>	<b><i>Supplier</i></b>
NaCNBH <sub>3</sub>	Sigma-Aldrich
Ascorbic acid	VWR Prolabo
Hydrogen peroxide (H <sub>2</sub> O <sub>2</sub> , 30%)	Fluka

**Table 3-5: Summary of reducing and oxidising reagents used to manipulate single fluorophores in liquid environment.**

Both tryptophane and dGMP interact with some fluorophores by transferring an electron via the mechanism of PET [Sauer 2003; Neuweiler et al., 2002;]. This process of oxidation leads to static or dynamic quenching of fluorescence and can be exploited for mechanistic studies of small distance changes or binding studies. A prominent fluorophore which exhibits strong interaction with tryptophane by ground-state complex formation is MR121 [Doose et al., 2005].

One widely used group of reducing chemicals contains a thiol group. These reagents have an appropriate energetic potential which leads to electron transfer to some classes of fluorophores, e.g. rhodamines. As a further property, these reagents exhibit significant quenching of energetically appropriate triplet states of fluorophores [Widengren and Schwille, 2000]. In addition, a reductive environment is a necessary prerequisite for carbocyanine switching studies presented later in this work [Heilemann et al., 2005; Bates et al., 2005].

## 4. Results and Discussion

### 4.1. Photophysical Properties of Fluorescent Dyes

To realize functional multichromophoric systems and to allow stable observation of single systems under well-defined conditions over an extended period of time, a number of considerations has to be made. First, different classes of fluorescent dyes have to be explored under various conditions. Single-molecule experiments were carried out both on dry glass substrates and under aqueous conditions. A comparison of both environments should elucidate the influence of inhomogeneous broadening on fluorescence properties of chromophores. Dyes of different chemical classes were subject of a systematic investigation in this first part of this work. By reducing photodestruction caused by laser induced irreversible reactions of the chromophore and preventing all types of chemical destruction, a maximum of fluorescent photons can be obtained.

Fluorophores suitable for single molecule experiments have to fulfil a number of requirements. They must show a high quantum yield, high photostability to allow the detection of as many photons as possible before irreversible photobleaching, and low rates of parallel depopulation pathways of the first single state  $S_1$ , i.e. low triplet quantum yield and poor tendency to form radical states.

Furthermore, possible interactions with other molecules which influence the photophysical behaviour become more and more interesting. The study and prevention of possible photophysical pathways can result in a better stability. As a prominent example, it has been shown that carbocyanine dyes which exhibit energetically favourable interactions with molecular oxygen and hereby depopulating the triplet state, can be stabilized by removing oxygen and adding millimolar concentrations of a triplet quencher [Funatsu et al., 1995; Ha et al., 2002]. This method is applicable to a large number of carbocyanine dyes, spanning an important part of the visible spectrum. Today, this class of dyes is widely used in single pair FRET experiments, and oxygen-free environments allow studies of hundreds of seconds without photobleaching events [Hohng et al., 2004; Rasnik et al., 2005].

#### 4.1.1. THREE CLASSES OF DYES: CARBOCYANINES, RHODAMINES AND OXAZINES

A number of different classes of synthetic organic fluorophores are commercially available. They can be further classified by their solubility in solvents, absorption and emission wavelength, fluorescence lifetime and fluorescence quantum yield. The choice of a particular type of chromophore first depends on the desired wavelength for an experimental application. Rhodamine dyes span the visible spectrum from an absorption wavelength of ~500 nm to ~800 nm. Unfortunately, rhodamine derivatives with a functional group for conjugation chemistry are only available up to 650 nm. As an alternative for the red part of the visible spectrum, a class of fluorophores which is derived from the chemical structure of rhodamines and exhibits longer absorption and emission wavelengths is available with carborhodamines. Structurally, they are generated by replacing the central oxygen-atom by a methylen group. It will be demonstrated in the following section that they exhibit similar properties, which justifies to adjoin carborhodamines to the class of classical rhodamine dyes. Other classes of fluorophores which can be used for conjugation chemistry are oxazines (>600 nm, the spectral shift in absorption and emission is caused by the nitrogen atom), carbocyanines (~500 to ~700 nm) and coumarins (mostly below ~550 nm).

It is generally approved that fluorescent dyes in the visible spectral region are more stable, although exhibiting lower quantum yields. Especially under pulsed excitation conditions at the single molecule level, stability is dramatically increased compared to short-wavelength fluorophores. This can be explained by the high energy density in short pulses, which leads to an increase of the probability for two-photon processes. After two-photon absorption, transitions into higher excited states  $S_n$  and  $T_n$  can occur and hence lead to destabilized electronic configurations in molecules, i.e. increasing the number of antibinding contributions to molecular orbitals [Eggeling et al, 1998; Eggeling et al., 2005]. In these configurations, photodestruction by light of short wavelength is more favourable than by light of longer wavelength, e.g. by photoinduced chemical reactions and generation of a radical ion/electron pair ( $M^+ e^-$ ).

Besides the advantage of higher photostability observed for chromophores absorbing in the red spectral region, a lower quantum yield of fluorescence is generally observed, a result of the increasing influence of nonradiative processes if

the energetic gap between HOMO and LUMO becomes smaller. The main process observed is internal conversion from the lowest vibrational level of  $S_1$  to a high vibrational level of  $S_0$ , followed by rapid relaxation to the vibrational ground state of  $S_0$ . This process is generally attributed to hydrogen stretching vibrations and mainly expected from hydrogen atoms attached directly to the chromophore [Drexhage 1973].

For further examination, three fluorescent dyes from three different classes were chosen, all absorbing in the red spectral region and available for conjugation chemistry. Most of them have derivatives over a broad spectral range which makes them interesting candidates as fluorophores in photonic wires exhibiting an energy transfer cascade. Molecular structures, spectral properties, fluorescence lifetime and quantum yields are summarized in figure 4-1.

All three fluorophores are structurally symmetric and only exhibit a small change in the dipole moment upon excitation from the ground state to the first excited state. The first fluorophore, Cy5, belongs to the class of symmetric carbocyanines. The chemical structure contains a polymethine-bridge which connects two indole moieties. Carbocyanine dyes are generally characterized by high extinction coefficients, short fluorescence lifetimes and relatively low quantum yield  $<0.30$  (this is observed if the polymethine backbone is flexible; higher quantum yields are observed if the structure is rigid, e.g. for Cy3B with a value of 0.65, which is explained by the influence of structural mobility on nonradiative processes [Drexhage 1973]). Two other fluorophores chosen are the oxazine dye MR121 and the carborhodamine dye ATTO647. Both exhibit lower extinction coefficients and hence reduced probability for excitation. Fluorescence lifetimes are considerably longer, and a high quantum yield of 0.65 is observed for ATTO647.

### **Time-Resolved Ensemble Spectroscopy**

Time-resolved measurements of the three representative dyes mentioned above were performed using a 635 nm laser diode and a TCSPC based fluorescence lifetime spectrometer. Dye concentration was chosen to  $10^{-6}$  M to exclude interchromophoric interactions or pile-up effects. Since fluorescence properties substantially depend on the polarity of the solvent, fluorescence lifetimes of fluorophores were measured in different solvents: phosphate buffered saline (PBS)



Experimental results of time-resolved ensemble fluorescence measurements are listed in table 4-1.

	<b>Solvent</b>	$\tau_1$	$\tau_2$	$\chi^2$
<b>Cy5</b>	PBS	0.39 ns (53%)	0.91 ns (47%)	1.04
	PBS:CH <sub>3</sub> CN 1:1	0.47 ns (48%)	1.17 ns (52%)	1.05
	CH <sub>3</sub> CN	0.41 ns (39%)	1.06 ns (61%)	0.93
<b>ATTO647</b>	PBS	0.92 ns (18%)	3.38 ns (82%)	1.13
	PBS:CH <sub>3</sub> CN 1:1	1.26 ns (23%)	3.90 ns (77%)	1.11
	CH <sub>3</sub> CN	1.76 ns (25%)	4.50 ns (75%)	1.17
<b>MR121</b>	PBS	0.45 ns (10%)	1.79 ns (90%)	0.96
	PBS:CH <sub>3</sub> CN 1:1	0.73 ns (11%)	2.73 ns (89%)	1.00
	CH <sub>3</sub> CN	1.64 ns (27%)	4.23 ns (73%)	1.09

**Table 4-1: Fluorescence lifetime data derived from time-resolved measurements of the fluorophores Cy5, ATTO647 and MR121 in solvents of different polarity. Lifetime data was obtained after applying a biexponential fit, yielding  $\tau_1$  and  $\tau_2$  (amplitudes in brackets), and a  $\chi^2$ -value as a measure of goodness for the fit.**

Best fit results on experimental data of fluorescence lifetime were obtained if a biexponential model was applied. Experiments were carried out with dye samples obtained directly by the supplier without any further purification. This is likely the main reason for the inhomogeneity observed in fluorescence lifetimes: one species of a fluorophore in a homogeneous solvent and constant measurement conditions should be characterized by one fluorescence lifetime only. Largest inhomogeneities were observed for the carbocyanine dye Cy5. Nevertheless, the dependency of the fluorescence lifetime on solvent polarity can be derived from the data shown in table 4-1: the carbocyanine exhibits the smallest changes, and fluorescence lifetime can be regarded as constant in the range of polarities from the solvents used. The carborhodamine dye ATTO647 shows an increase of 33%, and the strongest change is observed for the dye MR121, which more than doubles its fluorescence lifetime in acetonitrile, compared to aqueous surroundings [Buschmann et al., 2003]. This effect

is explained by interactions with the O-H-vibration of water, leading to fast depopulation of the first excited state and is not observed in D<sub>2</sub>O [Sauer 1995].

If fluorophores are observed in solvents with higher viscosity or bound to biomolecules, fluorescence lifetimes are influenced as well. Increasing viscosity leads to longer reorganization times of solvent molecules surrounding a fluorophore, hereby affecting the depopulation of the first excited state. In water, reorientation dynamics of less than 100 ps are observed. Fluorophores bound to biomolecules are subject to an increased viscosity in the “nano-environment”, yielding similar effects as in solvents with higher viscosity [Lakowicz, 1995]. A further aspect observed for many fluorophores leading to an increase in nonradiative depopulation of the excited state lies in interactions with biomolecules, e.g. quenching by nucleobases or amino acid residues of a protein. Studies of rhodamines attached to oligonucleotides revealed three different states with different fluorescent lifetimes for tetramethylrhodamine (TMR) [Eggeling et al., 1998b]: the freely rotating dye exhibits a lifetime of 2.2 ns (which is similar to the fluorescence lifetime of the free dye), the dye closely bound to nucleobases (except guanosine) shows a broad distribution around 3.5 ns as a result of a more immobile molecule, and a third lifetime of 0.8 ns together with a strongly decreased quantum yield is observed if interactions with guanosine residues occur due to electron transfer from guanosine to the dye [Knemeyer et al., 2000].

In the following passages, single-molecule experiments with these fluorophores using the confocal set-up developed in the course of this work (see 3.1) will be discussed. To circumvent the inhomogeneities and broadening of fluorescence properties known from experiments with fluorophores adsorbed randomly on a glass substrate [Weston et al., 1998] experiments were carried out in liquid environment. Single-molecule measurements were realized by conjugating the fluorophores to the 5'-end of a double-stranded 60 base pairs DNA with a biotin anchor on its 3'-end. As described in the experimental section (see 3.3.2), such fluorophore-DNA-conjugates can be immobilized onto a protein-surface and measured in liquid environment [Anzai et al., 1995; Piestert et al., 2003]. The preparation technique allowed the elaboration of the influence on two main effects onto the photophysical behaviour of fluorophores, i.e. the presence of oxygen and the presence of electron-donating substances. Oxygen was removed enzymatically from the buffer solution [Funatsu et al., 1995]. To

prepare a reductive environment, a solution of 100 mM mercaptoethylamine (MEA) in PBS was used (described in section 3.3.3).

Experiments in the following section were made in the following chemical environments:

PBS only (used as reference)

PBS with 100 mM MEA, i.e. reductive environment

PBS with oxygen removed enzymatically

PBS with 100 mM MEA and oxygen removed.

Single dye molecules were excited with a helium-neon laser with a centre wavelength of 632.8 nm. Fluorescence was recorded on two spectrally separated detectors by using a beamsplitter with a cutting edge at 680 nm (680DRLP; Omega Filters, USA) and two bandpass filters (675DF50, 700DF75; Omega Filters, USA). Fluorescence scan images were generally recorded with a spatial resolution of 50 nm per pixel and an integration time of 2 ms per pixel. To derive kinetic information from photon statistics of single molecule fluorescence trajectories, both autocorrelation and duration histogram analysis were carried out (these methods are described in 2.2.3) by using custom-written software (LabView 7, National Instruments, USA). Time resolution of autocorrelation analysis was set to 1  $\mu$ s (this time resolution was chosen due to practical reasons; the limit is set by the time resolution of the macroscopic time of FIFO data, i.e. 50 ns, but leads to a dramatic increase in calculation time and only poor additional information in single-molecule experiments, as the total number of photons detected is limited). Duration histograms were only used when fluorescence fluctuations were accessible by this method, i.e. a clear distinction between “on” and “off” states was possible. Fluorescence trajectories were binned in 10 ms intervals (if not stated otherwise).

#### 4.1.2. CY5 AT THE SINGLE-MOLECULE LEVEL

The carbocyanine dye Cy5 is the red representative of a series of symmetric polymethine dyes with indole moieties. Particularly in single-molecule experiments, this class of fluorophores has been used for many applications, from mere fluorescence detection if bound to biomolecules over FRET-based experiments to complex trichromophoric assays [Yildiz et al., 2003; Diez et al., 2004; Hohng et al., 2004]. Another aspect intensively investigated for Cy5 are complex photophysical reactions, such as isomerisation from a fluorescent *trans*-configuration to a nonfluorescent *cis*-configuration together with intersystem crossing into triplet-states were investigated [Widengren and Schwille, 2000]. It was observed that the isomerisation process can lead to delayed fluorescence involving a thermal-induced backisomerisation out of the *cis*-triplet state, occurring in the timescale of phosphorescence [Huang et al., 2005]. The photophysical pathway towards irreversible photodestruction was found to be composed of several steps with different dependencies on excitation intensity or the presence of oxygen [Ha and Xu, 2003; Füreder-Kitzmüller et al., 2005]. Very recently, it could be demonstrated that Cy5 fluorophores in solution could be reactivated to fluorescence emission out of a nonfluorescent dark-state by an electric field [White et al., 2004]. Even more recently, new studies and part of the present work demonstrated that all-optical switching of Cy5 molecules by applying a second laser wavelength is possible and can be repeated up to 100 times [Heilemann et al., 2005; Bates et al., 2005]. In this section, fluorescence fluctuations of individual Cy5 molecules bound to DNA and observed in different aqueous environment will be the focus. Fluctuations are analysed by using the autocorrelation function and duration histograms. Optical switching of single carbocyanine molecules will be discussed in more detail in a section later.

Fluorescence scan images, trajectories and autocorrelation curves of individual Cy5-molecules recorded in different chemical environments are presented in figure 4-2 (Cy5 in PBS with 100 mM MEA is omitted at this point, since no influence on fluorescence properties is observed). The scan image (A) recorded in PBS reflects the poor photostability of carbocyanine dyes generally observed. From 14 molecules observed in the area of  $5 \times 5 \mu\text{m}^2$ , 8 molecules are photobleached during scanning

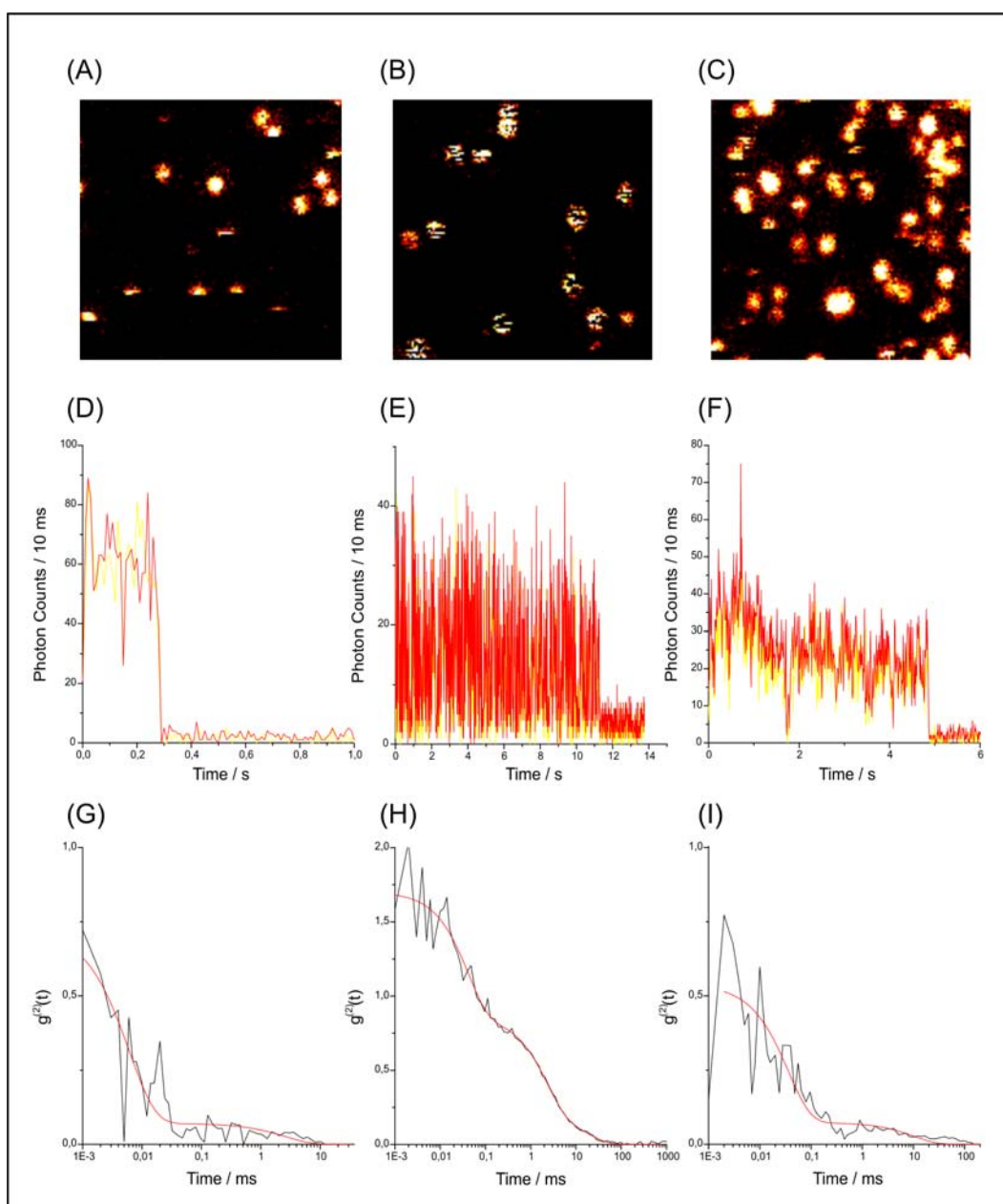


**Figure 4-2:** Fluorescence scan images of Cy5 in (A) PBS, (B) PBS with oxygen removed and (C) PBS/MEA with oxygen removed (50 nm pixel, integration time / pixel = 2 ms, 2 kW/cm<sup>2</sup>, intensity scale 10-40 counts / 2 ms). In similar environment, fluorescence trajectories (D)-(F) were recorded and autocorrelation functions of trajectories were calculated, (G)-(I).

the image, representing a fraction of more than the half the molecules under moderate excitation conditions (2 kW/cm<sup>2</sup>). Upon removal of oxygen from the solution, long “off”-periods appear in image (B). These “off”-states are generally attributed to triplet-states which are efficiently quenched in the presence of molecular-oxygen [Veerman et al., 1999, Tinnefeld et al., 2001] or charge separated states formed via the triplet state [Zondervan et al., 2003]. Although exhibiting severe intensity fluctuations, fluorescence spots of molecules show significantly less

photobleaching than observed for experiments made in PBS. Fluorescence blinking of Cy5 molecules is strongly reduced in PBS/MEA, portrayed in scan image (C). In the case of carbocyanines, MEA acts as efficient triplet quencher in the absence of oxygen [Widengren and Schwille, 2000]. Compared to the scan image recorded in PBS, a considerably lower number of fluorescence spots exhibits photobleaching.

Fluorescence trajectories (D)-(E) in figure 4-2 demonstrate the influence of the chemical environment on fluorescence intensity pattern. In PBS, photobleaching is a rapidly occurring event, and mainly short trajectories are observed. A mean value of 3400 photons was determined from 22 individual Cy5 molecules in PBS. Oxygen removal leads to “off” periods on the millisecond timescale, which again are reduced dramatically by adding MEA. Both environments lead to drastically longer observation times: a mean number of 85000 photons (oxygen-free PBS) and 45000 (PBS/MEA) was determined from 39 and 14 individual trajectories, respectively.

Fluorescence trajectories were further analysed by correlating fluorescence fluctuations, yielding autocorrelation functions (G)-(I) (grey curves). Results of multi-exponential fits (red curves) are listed in table 4-3.

	$\tau_{1,on} / \text{ms}$	$\tau_{1,off} / \text{ms}$	$\tau_{2,on} / \text{ms}$	$\tau_{2,off} / \text{ms}$	$\tau_{3,on} / \text{ms}$	$\tau_{3,off} / \text{ms}$
<i>PBS</i>	0.015	0.010	40	2.8	-	-
<i>PBS, oxygen removed</i>	0.090	0.076	14	2.7	120	23
<i>PBS 100 mM MEA oxygen removed</i>	0.115	0.053	150	11	-	-

**Table 4-3: Correlation times derived from approximation of autocorrelation curves by exponential fit.**

For Cy5 in PBS, two correlation times are observed. According to results published in literature, the shorter contribution is attributed to *cis-trans* isomerisation of the polymethine backbone, and the longer contribution to intersystem crossing to the triplet state [Tinnefeld et al., 2001; Widengren and Schwille, 2000; Heilemann et al., 2005]. In oxygen-free environment, two longer contributions to the correlation function appear and are more dominant than in the presence of oxygen. Here, the absence of oxygen leads to the observation of longer triplet states now expanding to

milliseconds. If MEA is added to the solution, correlation times observed lack the long contribution observed before, and exhibit two components with a comparable timescale to those observed in PBS.

If oxygen is removed, an increase in nonfluorescent periods is observed which are attributed to longer triplet-states, formerly quenched in the presence of oxygen. As a second effect, the observation time prior to irreversible photodestruction increases. Therefore, it is generally assumed that molecular oxygen – after depopulating the triplet state of the carbocyanine and forming very reactive singlet oxygen – plays an important role in the photobleaching pathway of Cy5 [Ha and Xu, 2003]. This is supported by experiments with MEA as triplet quencher for carbocyanines where shorter characteristic times appear in the autocorrelation.

Interestingly, other reductive agents containing a thiol-moiety induce a similar effect as observed for MEA. Here to mention are  $\beta$ -mercaptoethanol (BME), cystein or dithiothreitol (DTT). In a general view, these reagents have electron-donating properties and create a reductive environment. In the presence of carbocyanines, they demonstrate important triplet depopulation of the fluorophores [Widengren and Schwille, 2000].

Fluctuations in fluorescence intensity observed for the carbocyanine dye Cy5 are in agreement with published data. Furthermore, it could be demonstrated that carbocyanines can be stabilized if molecular oxygen is removed, allowing a 25-fold increase in the total number of photons detected and hereby dramatically longer observation times of single fluorophores. In the following sections, similar chemical environments are applied in experiments with other fluorophores, which belong to the classes of oxazines and rhodamines.

### 4.1.3. MR121 AT THE SINGLE-MOLECULE LEVEL

The fluorescent dye MR121 is the representative chosen out of the structural class of oxazine dyes (available as DYE121, AttoTec, Germany; single-molecule experiments discussed in this section were carried out with a structural very similar dye, ATTO655, which shows nearly identical photophysical properties but is better soluble in aqueous media and more suitable for conjugation to DNA). This class of dyes is frequently used in experiments exploiting PET for small structural changes, since fluorescence emission is efficiently quenched in the presence of tryptophane or guanosine [Neuweiler et al., 2002; Marmé et al., 2003; Doose et al., 2005; Heinlein et al., 2003]. In this context, the focus was set on fluorescence intermittencies of an oxazine dye appearing in different chemical environment (figure 4-3), in comparison to carbocyanines and rhodamines.

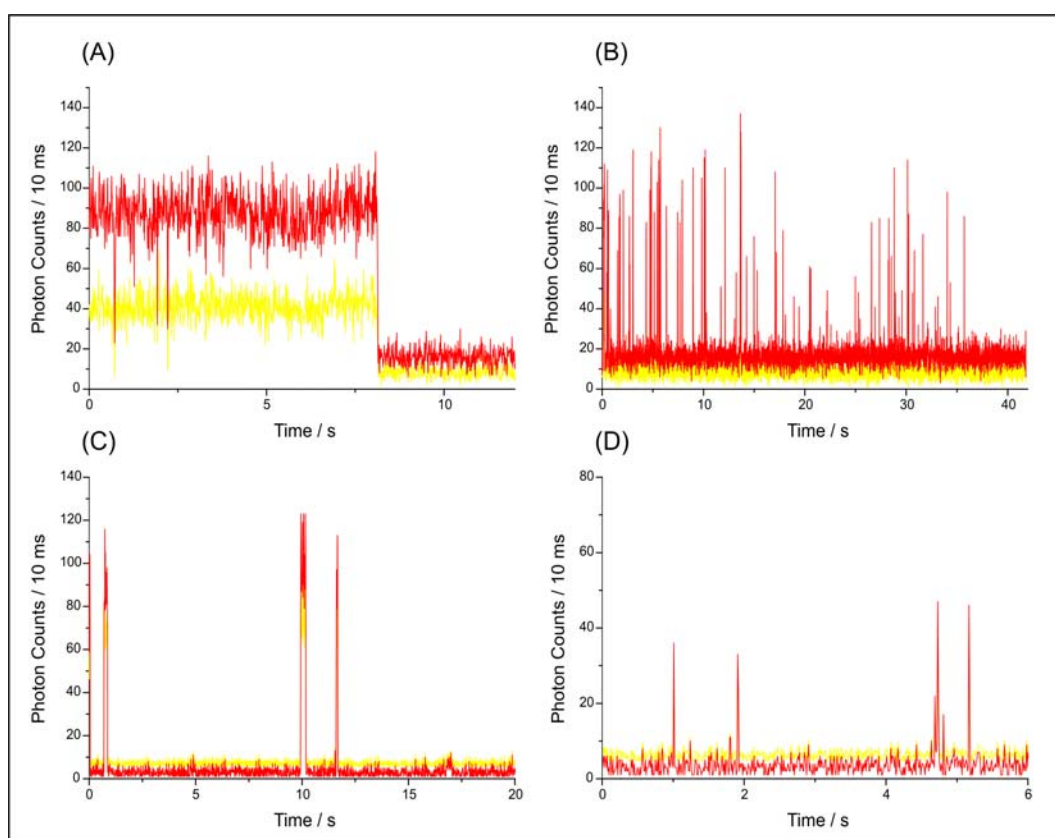


**Figure 4-3: Fluorescence trajectories of ATTO655 bound to DNA in (A) PBS, (B) PBS with 100 mM MEA, (C) oxygen-free PBS and (D) oxygen-free PBS with 100 mM MEA (2 kW/cm<sup>2</sup>, 10 ms binning time).**

Oxazine dyes already exhibit constant and bright fluorescence emission in PBS. At the timescale of 10 ms, almost no fluorescence intermittencies are observed (see trajectory (A) in figure 4-3). This situation changes in reductive environment: fluorescence “spikes” are observed and long intermittencies on timescales of up to hundreds of milliseconds appear (trajectory (B) in figure 4-3). If oxygen is removed, nonfluorescent periods increase in length and “on”-periods get very rare, further reduced in intensity if MEA is added (trajectories (C) and (D) in figure 4-3). As a first result, it is evident that ATTO655 is suited for measurements in PBS only, but is not suitable for experiments in oxygen-free or reductive environment. Scan images shown in figure 4-4 further emphasize that the behaviour exemplified on individual molecules represents indeed a general characteristic of ATTO655 trajectories in the

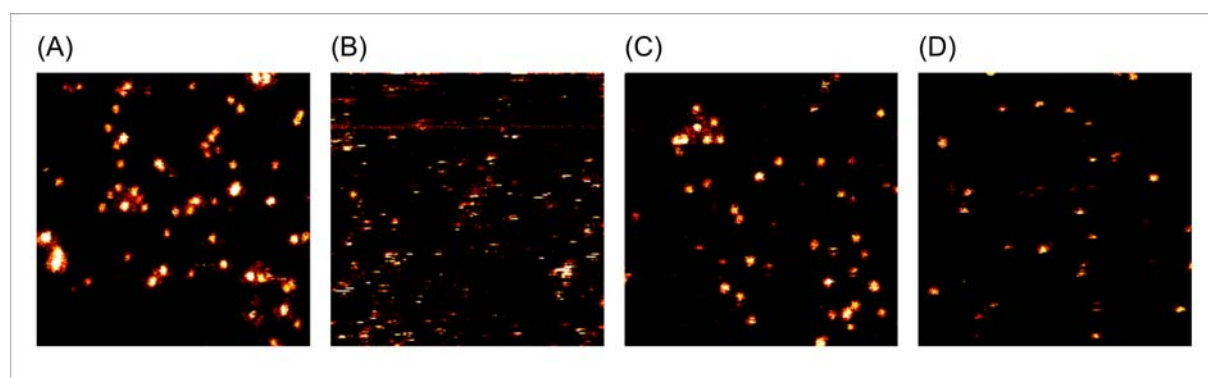


**Figure 4-4:** 10 x 10  $\mu\text{m}^2$  scan images of ATTO655 bound to dsDNA in (A) PBS, (B) PBS with 100 mM MEA, (C) PBS oxygen removed, (D) PBS with oxygen removed and 100 mM MEA (Excitation power 2 kW/cm<sup>2</sup>, 50 nm pixel size and 2 ms integration time / pixel; intensity scale from 15-40 counts / 2ms).

respective environment. The scan images recorded in PBS show brightest fluorescence emission and nearly no fluorescence intermittencies (image (A) in figure 4-4). Pronounced fluctuations are observed in PBS/MEA (image (B)) and reproduce “off”-periods of several milliseconds, according to observations made in fluorescence trajectories. A considerably lower density of molecules due to long “off”-periods is observed if oxygen is removed from the solution (image (C) and (D)).

Autocorrelation curves and exponential fits of fluorescence trajectories in PBS and PBS/MEA are presented in figure 4-5. No significant correlation term down to 1  $\mu\text{s}$  is observed for ATTO655 in PBS. This explains the use of this class of fluorophores for fluctuation analysis in peptides, DNA or RNA molecules, since they do not exhibit any triplet transitions or other transitions into nonfluorescent states [Doose et al., 2005]. If

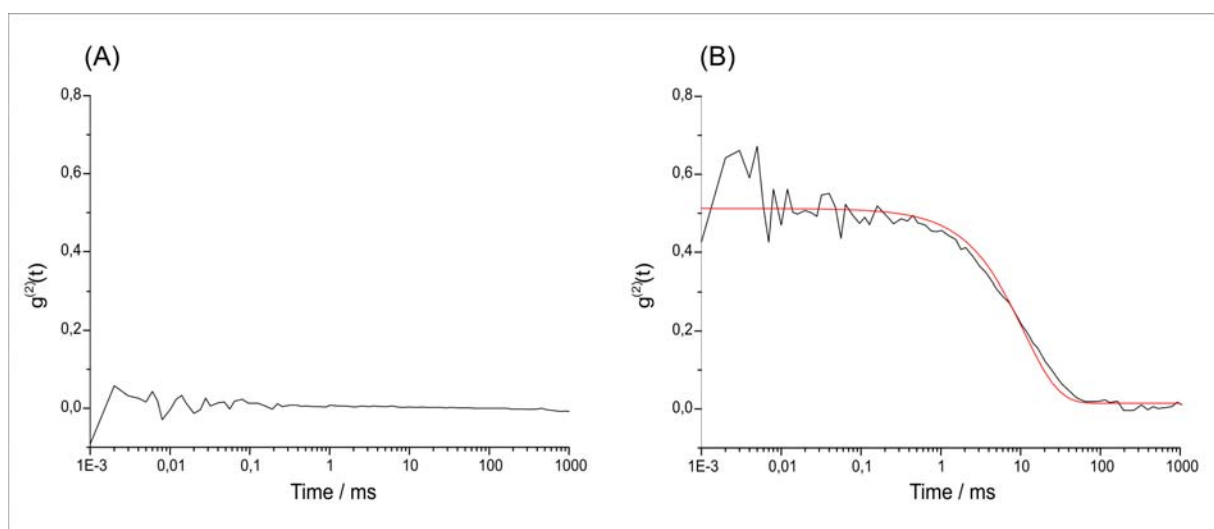


**Figure 4-5: Autocorrelation analysis of fluorescence trajectories from ATTO655 in (A) PBS and (B) PBS with 100 mM MEA (binning width 1  $\mu$ s). The red curve in (B) represents monoexponential approximation of autocorrelation data.**

MEA is added, the autocorrelation function exhibits fluctuations in the timescale of a few milliseconds, and a monoexponential fit function yields an “on”-time of 33.2 ms and an “off”-time of 16.6 ms. The longer “off”-periods which are clearly visible in trajectory (B) of figure 4-3 can not be identified in the autocorrelation function, but can be derived from duration histogram analysis, yielding a value of 315 ms (the “on”-time derived from duration histograms has a value of 30 ms and therefore is identical to the one derived from autocorrelation analysis). The analysis of 49 fluorescence trajectories from individual ATTO655 molecules delivered mean values for fluorescence intermittencies listed in table 4-4, obtained by both autocorrelation and duration histograms.

	$\tau_{\text{on}} / \text{ms}$	$\tau_{\text{off}} / \text{ms}$
<i>Autocorrelation</i>	29 (20)	19 (14)
<i>Duration Histograms</i>	19 (8)	378 (124)

**Table 4-4: Mean values for “on”- and “off”-periods calculated from 49 single ATTO655 fluorophores in PBS/MEA, standard deviations in brackets.**

The results from photon statistics listed in table 4-4 suggest the presence of two “off”-states, a short one with 19 ms and a longer one in the order of 378 ms. Both “off”-times are not observed in the absence of MEA, and are therefore assigned to

electron transfer towards the fluorophore in reductive environment. The broadness of the distributions suggests a certain heterogeneity which influences the back-transition from this dark-state to the ground state or an excited state.

Fluorescence trajectories in the absence of oxygen are more difficult to evaluate. Several characteristic terms on largely different timescales are observed in autocorrelations, and did not allow unambiguous analysis of photon statistics. Fluorescence intermittencies under these experimental conditions are usually ascribed to triplet transitions, but usually exhibit similar signatures for different fluorophores of one kind.

It can be presumed that MEA as reductive agent is acting similar to tryptophane and guanosine, i.e. electron transfer to the fluorophore and hereby creating a radical anion [Doose et al., 2005]. In this state, the fluorophores do not exhibit fluorescence anymore. This radical anion exhibits a certain lifetime which strongly depends on its chemical environment, i.e. the ability of the solvent to stabilize the radical state.

The mechanism observed is best characterized by PET and exploited for short-range changes in conformation of biomolecules [Neuweiler et al., 2002; Marmé et al., 2003]. In the context of this work, the use of oxazine dyes is problematic, because their redox potential easily accesses these fluorophores for electron transfer into a nonfluorescent state.

#### 4.1.4. ATTO647 AT THE SINGLE-MOLECULE LEVEL

The carborhodamine dye ATTO647 is the last dye of the representative choice of chromophores. Structurally, a carborhodamine is closely related to rhodamines: the central oxygen-atom is replaced by a methylen group.

Exemplary fluorescence trajectories in four respective environments are shown in figure 4-6. As visible from fluorescence trajectory (A), the fluorophore exhibits long fluorescence intermittencies in the range of hundreds of milliseconds, not observed for either oxazines or carbocyanines. This typical behaviour for ATTO647 bound to DNA and in aqueous solution is observed for all molecules, but on strongly different timescales. In reductive environment, no fluorescence intermittencies are observed anymore, as shown in trajectory (B). This behaviour resembles the one observed for quantum dots, which do exhibit intensity fluctuations at different timescales which can

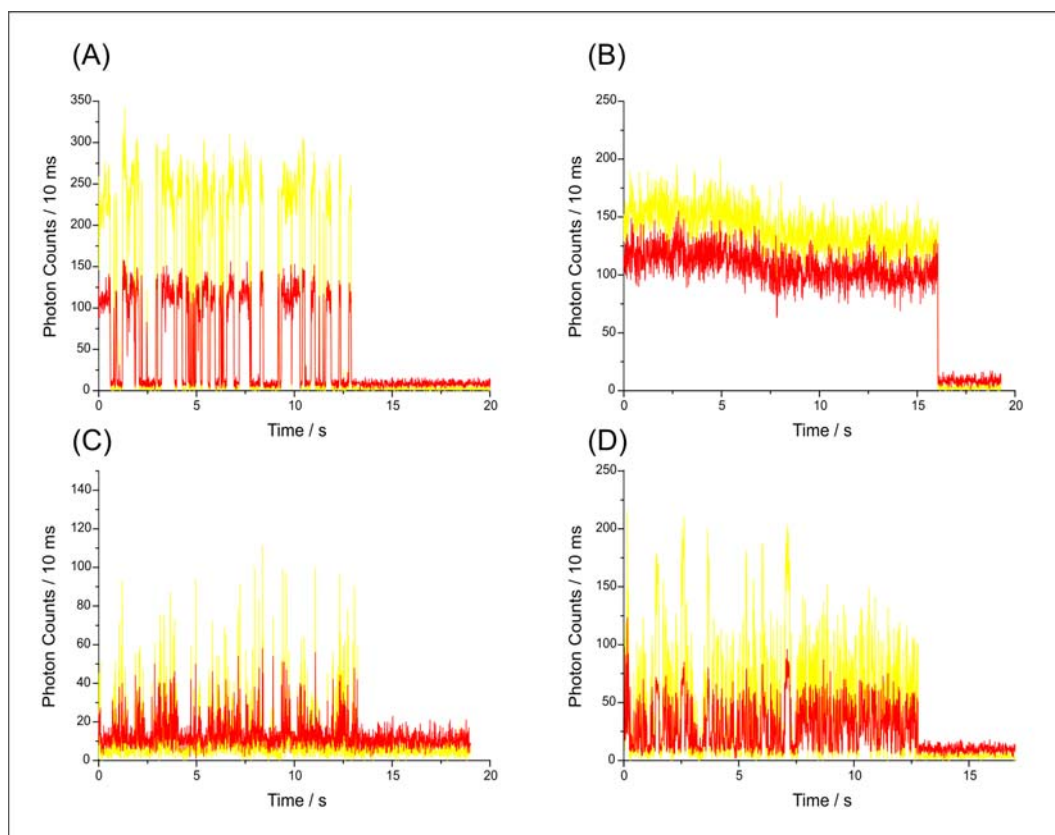


**Figure 4-6: Fluorescence trajectories of ATTO647 bound to DNA in (A) PBS, (B) PBS with 100 mM MEA, (C) oxygen-free PBS and (D) oxygen-free PBS with 100 mM MEA (3 kW/cm<sup>2</sup>, 10 ms binning time).**

be suppressed by electron-donating reagents, e.g. MEA or BME [Hohng and Ha, 2004]. Total photons detected are  $\sim 260000$  in (A) and  $\sim 400000$  in (B). This reflects a tendency to higher photon counts detected from single fluorophores observed for most trajectories: mean values of 163000 and 270000 photons detected were determined from 11 and 22 single-molecule trajectories, respectively. Remarkably, some trajectories reach a total photon detection of nearly  $10^6$  per molecule in reductive environment. The observation time until photodestruction of single ATTO647 molecules under both conditions is very similar. Therefore a comparable number of excitation cycles probably occur, but with the difference that a large number of these cycles do not lead to fluorescence in pure buffer.

Upon oxygen-removal, fluorescence trajectories are characterized by “spikes” of fluorescence emission (part (C) of figure 4-6), comparable to carbocyanine dyes. Contrary to Cy5, these intermittencies are not suppressed by adding MEA (part (D)). To obtain a more qualitative description of fluorescence kinetics observed,

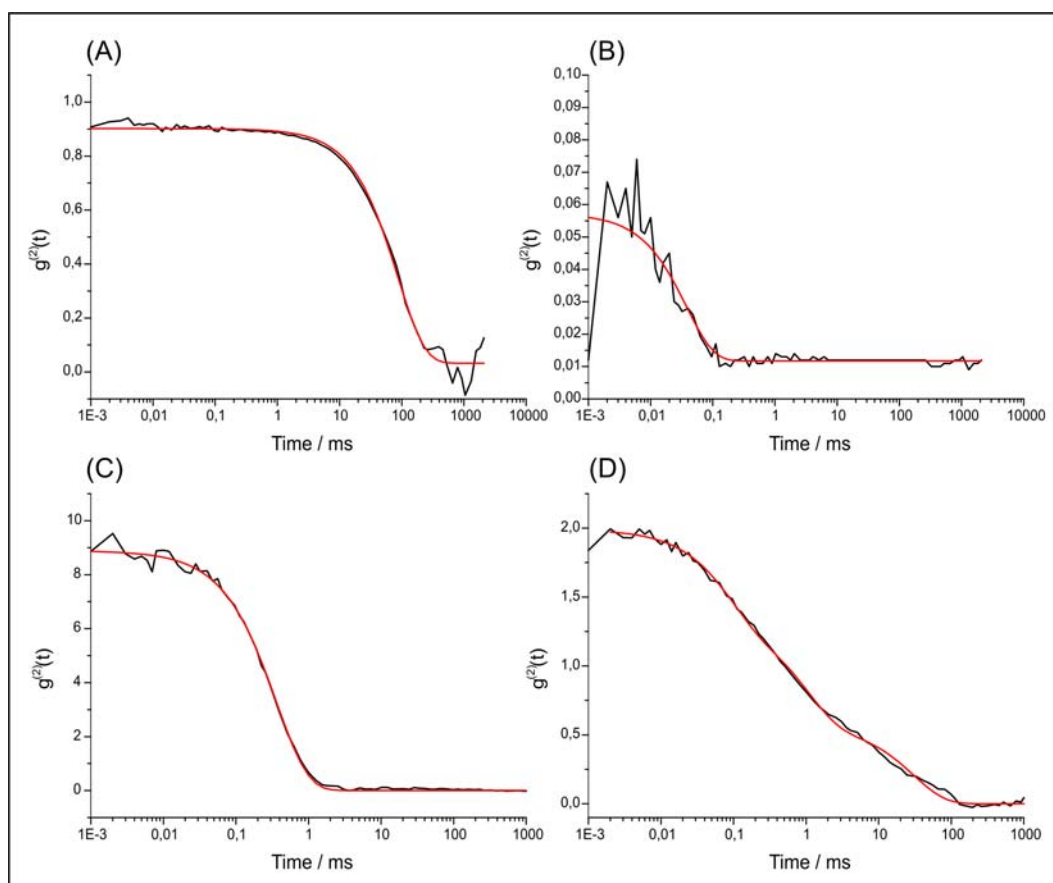


**Figure 4-7: Autocorrelation functions (black) and exponential fit (red) derived for fluorescence trajectories of ATTO647 in (A) PBS, (B) PBS/MEA, (C) oxygen-free PBS and (D) oxygen-free PBS/MEA; mono-exponential fits in (A)-(C) and a three-exponential fit in (D) are shown.**

fluorescence fluctuations were evaluated applying the autocorrelation function. Curves calculated for the fluorescence trajectories presented above are depicted in figure 4-7.

Correlation curves (A)-(C) were approximated by a monoexponential fit function, whereas a three-exponential fit was applied for correlation curve (D). Characteristic times derived from autocorrelation analysis are listed in table 4-6.

	$\tau_{\text{char}} / \text{ms}$	<b>A</b>	$\tau_{\text{on}} / \text{ms}$	$\tau_{\text{off}} / \text{ms}$
<i>PBS</i>	86.7	0.87	186	162
<i>PBS 100 mM MEA</i>	0.038	0.045	0.88	0.04
<i>PBS Oxygen-free</i>	0.36	8.88	0.40	3.56
<i>PBS Oxygen-free 100 mM MEA</i>	0.087	0.68	0.21	0.15
	1.03	0.75	2.4	1.8
	30.3	0.56	84	47

**Table 4-6: Characteristic times for “on” and “off” states observed in ATTO647 fluorescence trajectories, derived from autocorrelation and exponential approximation.**

Fluorescence fluctuations shown in figure 4-7 merit a further discussion. In reductive environment (B), a short time of 40  $\mu\text{s}$  appears which does not in (A). This leaves the question if this component was neglected due to a  $\sim 20$ fold lower amplitude, or if it arose in the presence of MEA. Concerning the second case, this might be explained by reduction of the fluorescent state of ATTO647 to a radical anion (comparable to ATTO655). Another possible interpretation starts with the fact that “off” times observed in PBS and oxygen-free PBS differ strongly, yielding 162 ms and 3.56 ms respectively. This suggests that species of different nature are generating this nonfluorescent state, which are created by the nanoenvironment. In the presence of oxygen (A), the photooxidized species of ATTO647 is observed. In the presence of MEA (B), this species is vanishing, and a short-lived species appears which could represent the reduced state. In the absence of oxygen (C), a shorter time could represent the triplet state of ATTO647. The correlation curve in (D) shows a longer and shorter time in the millisecond range, but fluorescence intermittencies observed

under these conditions seem to exhibit “off”-times on many timescales and cannot be characterized properly. Derived from a number of different correlation curves under equal conditions, different characteristic times were determined, which supports the fact that changes of transition rates with time are observed.

Characteristic “on”- and “off”-times of ATTO647 in PBS lie in the 100 ms-range and can be determined as well from duration histograms. Applying this method for trajectory (A) in figure 4-6, values of 188 ms and 171 ms for the “on”-state and the “off” state are obtained and are in good agreement with values derived from autocorrelation (see table 4-6).

It has to be mentioned that characteristic times for “on” and “off” states vary substantially. Fluorescence trajectories recorded in PBS exhibit a broad distribution for both times, which suggests a great heterogeneity that may arise from interactions with the scaffold molecule, DNA. Values obtained by autocorrelation analysis of 40 fluorescence trajectories are presented in figure 4-8. A mean

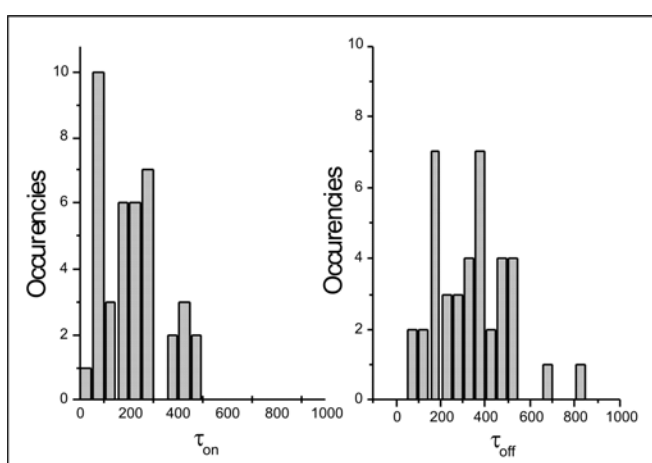


**Figure 4-8: Distribution of “on”- and “off”-times derived from 40 individual fluorescence trajectories of single ATTO647 molecules.**

value of 211 ms is obtained for collected “on” times, and 341 ms for “off”-times (standard deviation of 122 ms and 161 ms respectively). No obvious correlation between “on” and “off” states could be observed. A similar inhomogeneous behaviour for “on”- and “off”-periods is observed for trajectories recorded in other chemical environment.

To summarize, it can be stated that constant fluorescence emission without transitions to intermediate states with nonfluorescent nature are observed in reductive environment, created by 100 mM MEA. Same results were obtained when MEA was replaced by BME, which supports the thesis of a dominating influence of the reductive potential of the SH-group present in both substances. In a more depictive way, the fluorescence intermittencies of ATTO647 bound to DNA can nicely be seen on fluorescence scan images, shown in figure 4-9.

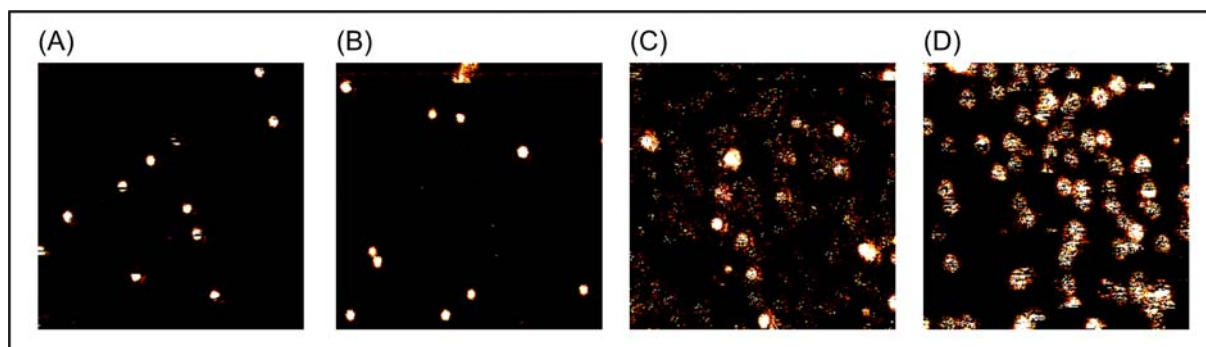


Figure 4-9:  $10 \times 10 \mu\text{m}^2$  scan images of ATTO647 bound to dsDNA in (A) PBS, (B) PBS with 100 mM MEA, (C) PBS oxygen removed, (D) PBS with oxygen removed and 100 mM MEA (Excitation power  $2 \text{ kW/cm}^2$ , 50 nm pixel size and 2 ms integration time / pixel; intensity scale from 20 – 100 counts / 2ms).

#### 4.1.5. RHODAMINE GREEN AT THE SINGLE-MOLECULE LEVEL

Promising results obtained for the carborhodamine dye ATTO647 in the previous sections were subject for further investigation on the class of rhodamine dyes, which is structurally closely related to carborhodamines. They offer the biggest group of fluorophores which is commercially available. In table 4-7, a list of three rhodamine dyes and their spectroscopic properties in water are listed.

	$\lambda_{\text{abs}}$	$\lambda_{\text{em}}$	$\tau_{\text{fl}}$	$\phi_{\text{fl}}$
<i>Rhodamine Green</i>	508	534	3.70	0.9
<i>TMR</i>	560	582	2.20	0.9
<i>ATTO590</i>	603	625	3.70	0.8

Table 4-7: Spectroscopic properties of rhodamine dyes RhG, TMR and ATTO590 bound to dsDNA in water. Fluorescence lifetimes represent the population of fluorophores that freely rotate.

Single-molecule fluorescence studies of rhodamine derivatives are the topic of the following sections. Different to previous experiments, a continuous-wave argon laser operating at 488 nm was used as excitation source. Excitation energies were

~5 kW/cm<sup>2</sup>. Fluorescence was recorded with up to four detector channels using the standard filter set described in materials and methods (see 3.1).

In the first section, single-molecule fluorescence studies of Rhodamine Green are presented. The fluorophore was used as input unit for photonic wire constructs (see 4.2 and 4.3). In the following sections, FRET-pairs constructed exclusively of rhodamine derivatives will be discussed.

### **Single-Molecule Experiments with RhG in PBS and Reductive Environment**

Fluorescence trajectories of single Rhodamine Green molecules are shown in figure 4-10 (A) and (B). Typically, trajectories show a constant emission of fluorescence without fluorescence intermittencies at a timescale of the binning chosen (10 ms). A background fluorescence intensity of below 1 kHz is observed.

Fluorescence trajectories in reductive environment are presented in (C) and (D) of figure 4-10 and show a significantly increased photostability. On the other hand, the count rate is not affected. Trajectories (C) and (D) exhibit a survival time of ~20 s and ~15 s before irreversible photobleaching. As a consequence of the changed chemical environment, higher background intensities are now observed, reaching up to 3 kHz as a sum of both detectors and hereby representing a threefold increase compared to measurements in PBS only. This observation was not made when using red laser excitation.

To quantify the increased number of photons emitted by single Rhodamine Green fluorophores in reductive environment, statistic evaluations of the total number of photons before irreversible photobleaching were carried out. Histograms obtained from ~80 fluorescence trajectories measured in PBS and ~40 trajectories measured in PBS with 100 mM MEA are shown in part (E) of figure 4-10. The blue bars represent the number of emitted photons of fluorophores collected in PBS, showing a distribution at lower photon counts with a mean value of 24000 photons/molecule (this value is comparable to what was found for Rhodamine6G in water, with on average 25000 photons per molecule [Mets and Rigler, 1994]). The red bars represent the number of photons emitted in PBS with MEA, and show a distribution with two distinguishable “populations”: at lower photon counts, the distribution

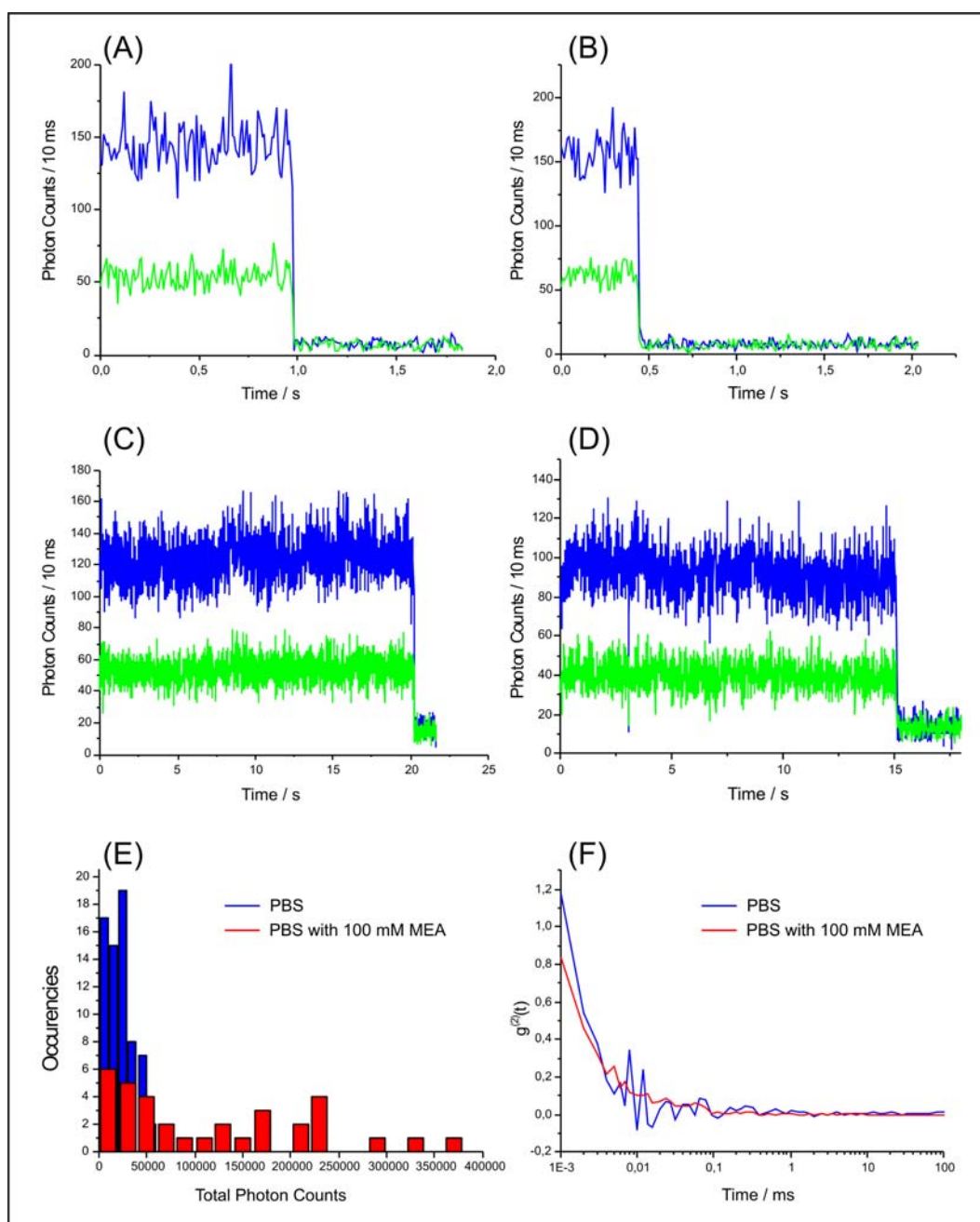


**Figure 4-10: (A) and (B): RhG fluorescence trajectories of single fluorophores recorded in PBS; (C) and (D): fluorescence trajectories recorded in PBS with 100 mM MEA; (E): Total photon counts until photobleaching of single fluorophores occurred (blue bars for RhG in PBS, red with 100 mM MEA added); (F): Autocorrelation functions of single trajectories (1  $\mu$ s binning) do not show significant fluctuations.**

resembles the one derived from measurements in PBS. Additionally, a second distribution around 200000-250000 photons/molecule can be observed.

Strikingly, fluorescence trajectories observed for Rhodamine Green in reductive environment resemble those of the carbhorhodamine ATTO647 (see 4.1.4). For both fluorophores, a similar number of photons can be detected prior to photobleaching.

Different between both fluorophores is the fluorescence signature observed in pure buffer. This could suggest the formation of an oxidized species in both cases, with the difference that the transition towards a possible radical cation is reversible for ATTO647 and irreversible for Rhodamine Green.

To reveal fluorescence intermittencies at a lower timescale as derived from trajectories with a binning of 10 ms, autocorrelation functions with a time resolution of 1  $\mu$ s were calculated, see part (F) in figure 4-10. Due to a better signal-to-noise ratio, autocorrelations were calculated from fluorescence data detected on the blue channel. For both PBS (blue curve) and PBS/MEA (red curve), no significant intensity fluctuation can be observed down to a correlation time of 10  $\mu$ s (which is in agreement with triplet times below 1  $\mu$ s and poor triplet quantum yields observed for rhodamine dyes in water with low excitation energies, [Widengren and Rigler, 1996]). At shorter observation times, a steep rise in the correlation function appears which is sometimes obtained with such low photon statistics and is attributed to afterpulses from the detectors (APD) [Zhao et al., 2003].

### **Experiments in Oxygen-free Environment**

Fluorescence trajectories of Rhodamine Green in PBS with oxygen removed are shown in part (A) of figure 4-11. Here, two interesting differences to fluorescence trajectories observed for carbocyanines do appear: first, the total measurement time is in the same order of magnitude as for measurements in PBS containing oxygen. Contrary to Cy5 in oxygen-free solution, this means that molecular oxygen does not participate dominantly in the photobleaching pathway of Rhodamine Green. On the other hand, fluorescence intermittencies are now observed, and well-distinguishable levels of “on” and “off” appear in single-molecule trajectories. Similar fluctuations are observed in reductive and oxygen-free environment, shown in an exemplary trajectory in part (B) of figure 4-11.

Additionally, a similar effect on fluorescence trajectories is observed as presented in figure 4-10 for Rhodamine Green in PBS/MEA, i.e. a considerably increase in the total lifetime of the fluorophore before irreversible destruction. Total photon counts for both experimental conditions of  $\sim$ 40 molecules are histogrammed in part (E) of figure 4-11. For oxygen-free PBS only (blue bars), a narrow distribution with lower photon counts is observed. A mean value of 9500 counts/molecule is calculated, which

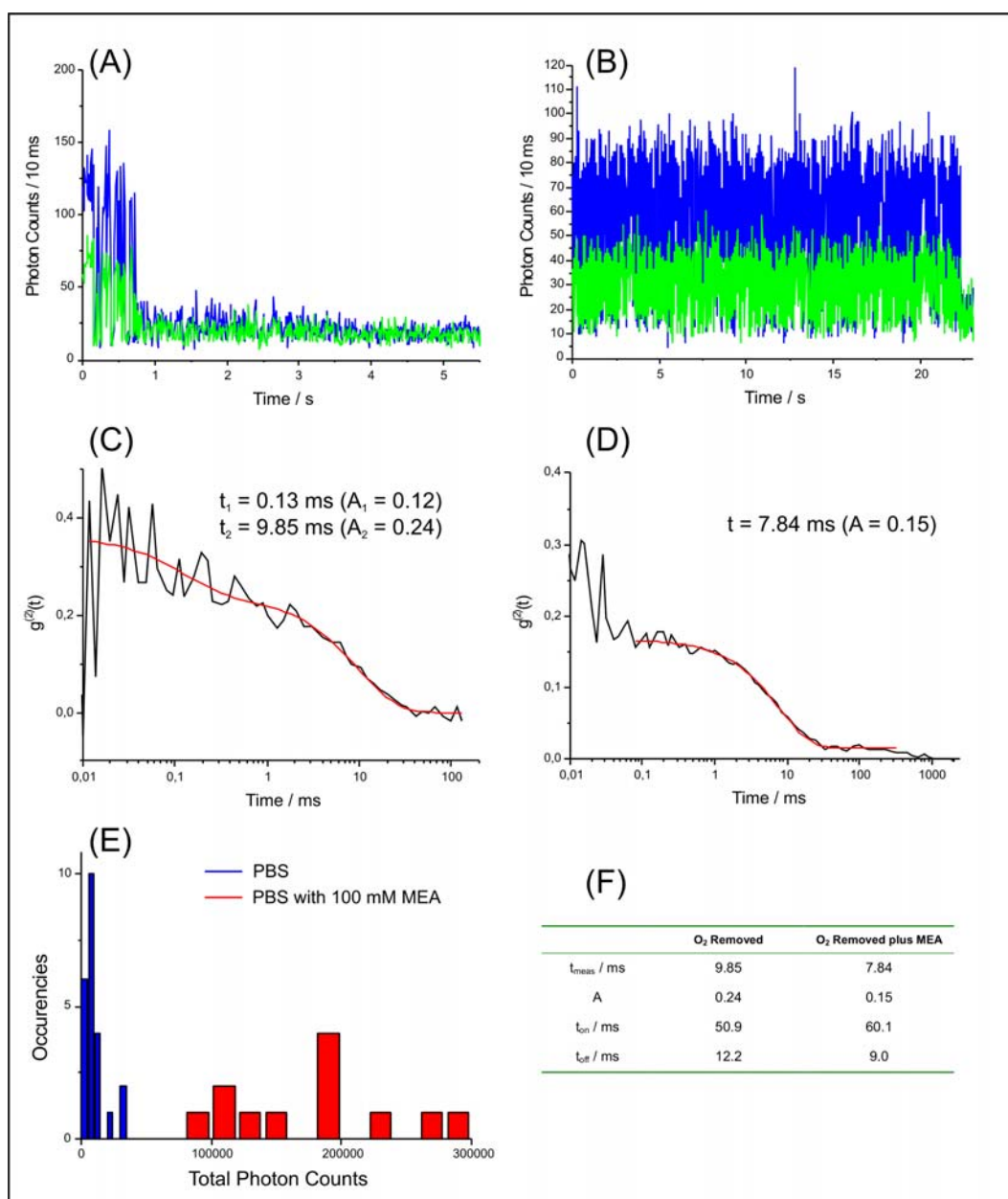


**Figure 4-11: RhG fluorescence trajectories of a single fluorophore recorded in oxygen-free PBS, (B) 100 mM MEA added. Autocorrelation curves of the same fluorophores are shown in oxygen-free PBS (C) and oxygen-free PBS/MEA (D). Statistical data on total photon counts is shown in (E), autocorrelation fit values and “on”- and “off”-times are listed in (F).**

represents less than 40% from total photon counts if oxygen is present. In reductive and oxygen-free solution (red bars), a broad distribution with a mean value of  $\sim 200000$  photons/molecule is determined, which is comparable to the oxygen-containing PBS/MEA measurements.

In addition, fluctuations of single-molecule fluorescence trajectories in oxygen-free solution were analysed by autocorrelation, as shown in part (C) (oxygen-free PBS) and part (D) (oxygen-free PBS/MEA) of figure 4-11. In both environments, correlation

times by applying a mono- or biexponential model can be derived. Low photon counts in oxygen-free environment led to poor statistics in the autocorrelation function, and a reasonable approximation could only be achieved applying a biexponential model. The first time constant is not taken into account due to important interference with afterpulsing characteristics from the APDs. The second correlation time of 9.85 ms is comparable to the one derived from oxygen-free PBS/MEA measurements, 7.84 ms. Both correlation functions lead to similar values for the “on” state and the “off” state (figure 4-11, (F)).

Fluorescence intermittencies of 15 (oxygen-free) and 13 (oxygen-free/MEA) single-molecule trajectories were analysed by applying the autocorrelation function and duration histograms. Mean values for “on” and “off” states derived from these calculations together with standard derivations are presented in table 4-8:

	Autocorrelation Analysis		Duration Histograms	
	$\tau_{\text{on}} / \text{ms}$	$\tau_{\text{off}} / \text{ms}$	$\tau_{\text{on}} / \text{ms}$	$\tau_{\text{off}} / \text{ms}$
<i>O<sub>2</sub>-free</i>	51 (28)	19 (9.0)	36 (12)	40 (15)
<i>O<sub>2</sub>-free/MEA</i>	51 (25)	8.7 (1.3)	56 (16)	20 (2)

**Table 4-8: Photon statistics of “on“- and “off“-states from single Rhodamine Green molecules in oxygen-free PBS in the presence and absence of MEA, derived by autocorrelation or duration histogram analysis.**

Because of relatively low fluorescence count rates observed for single Rhodamine Green trajectories, trajectories had to be binned with 10 ms to sufficiently distinguish “on“- from “off“-states. As a consequence, duration histograms are less suited to derive characteristic times around 10 ms than autocorrelation analysis is. This explains the deviation of the “off“-state lifetime from the value determined by applying autocorrelation analysis. Smaller values for the standard deviations are obtained for oxygen-free/MEA trajectories, which is explained by drastically longer observation times. To summarize, an “off“-state with a lifetime around 19 ms for oxygen-free and 8.7 ms for oxygen-free/MEA environment suggests the presence of a relatively long-lived species which is suppressed if oxygen is present. It can be anticipated that this species is a triplet state of Rhodamine Green, which is effectively quenched by

oxygen and appears to interact slightly with MEA. The quenching of the triplet-state by MEA is substantially smaller than observed for carbocyanines.

As already mentioned in the discussion of the autocorrelation function shown in (D) of figure 4-11, short times appear for oxygen-free/MEA environment, but may suffer from overlap with afterpulsing from APDs. No such short time is observed in experiments in oxygen-containing environment. Autocorrelation analysis with a biexponential model were applied to 12 appropriate fluorescence trajectories which yielded a satisfactory quality of the fit-function. Values obtained for “on”- and “off”-times are

$$\tau_{\text{on}} = 0.17 \text{ ms (0.14 ms) and}$$

$$\tau_{\text{off}} = 0.06 \text{ ms (0.05 ms).}$$

It is difficult to further characterize the nature of this state. Short contributions to the autocorrelation function implicate large errors and distributions are broad. These contributions are only observed if oxygen is removed and no MEA is added, a similar observation was made for carbocyanine derivatives and is attributed to the appearance of long-lived triplet states (see 4.1.2). Low photon statistics and short fluorescence trajectories do not allow any further examination of these states.

#### 4.1.6. RHODAMINES IN SMFRET-PAIRS AT THE SINGLE-MOLECULE LEVEL

Single-molecule FRET (smFRET) is a widely used tool to investigate distance fluctuations at the single-molecule level in the range of 2 to 10 nm [Ha et al., 1996]. Fluorescence intensity of both a donor and an acceptor molecule are monitored and fluctuations in energy transfer derived from the emission spectrum of the FRET-pair are attributed to distance changes in the system under investigation. Therefore, it is desired to use a pair of fluorophores where each component does not exhibit any intrinsic intensity fluctuations, leading to a misinterpretation of experimental data [Ha et al., 1999].

Results obtained for Rhodamine Green and ATTO647 suggest the use of rhodamines in single-molecule FRET-applications. As the last section discussed in detail (see 4.1.5), measurement conditions best suited for this class of chromophores is an oxygen-containing and reductive environment, e.g. 100 mM MEA. In a next step, a double-stranded DNA was constructed with Rhodamine Green at the 5'-end of one single strand and TMR spaced by 10 base pairs at the opposite single strand. In this configuration, the fluorophores are spaced by ~3.4 nm, and the rigid structure of DNA should not reveal structural dynamics. The  $R_0$ -value calculated for this FRET-pair equals 6.5 nm, so high transfer efficiency can be expected. Fluorescence emission was recorded on the three detector channels denoted “blue”, “green” and “yellow” (see section 3.1).

Fluorescence emission of Rhodamine Green is mainly recorded on the blue and green detector. The spectral distribution on different detectors can be described more pictorial by introducing a fractional intensity,  $F$ , defined as the fraction of intensity recorded on the long-wavelength detector divided by the sum of intensities,

$$F_{Det2,Det1} = \frac{I_{Det2}}{I_{Det1} + I_{Det2}} \quad ( 4-1 )$$

Here,  $I_{Det2}$  stands for the photons recorded on the long-wavelength detector, and  $I_{Det1}$  for photons recorded on the short-wavelength detector. For Rhodamine Green only, a fractional intensity of  $F_{green,blue} = 0.30$  is calculated from single-molecule fluorescence trajectories, and fluorescence detection on the “yellow” channel can be

neglected. For the acceptor TMR, practically no emission is observed on the “blue” channel, and a value of  $F_{yellow,green} = 0.42$  was determined (via direct excitation).

Fluorescence trajectories of the sm-FRET-pair RhG-TMR in PBS and PBS/MEA in oxygen-containing environment are shown in figure 4-12. Trajectories recorded in PBS suffer from short measurement times and rapid photodestruction (part (A)), whereas the reductive environment induced by 100 mM MEA leads to longer observation times and a similar increase in photon counts as observed for Rhodamine Green only. Fractional intensity traces and histograms exhibit resembling characteristics: calculated values from photons detected on the “blue” and “green” channel show a distribution with two populations with maximum values of  $F_{green,blue} = 0.36$  and  $0.68$  (PBS, (B) in figure 4-12) and of  $F_{green,blue} = 0.27$  and  $0.70$  (PBS/MEA, (C) in figure 4-12). The first value can be assigned to the part of the traces where Rhodamine Green is emitting predominantly, that is, after photodestruction of the acceptor chromophore TMR. The second value stems from the first section of the fluorescence trajectories exhibiting energy transfer and is a measure of the efficiency of this process. In an ideal case with an energy transfer efficiency approaching 100% and a low fraction of background-to-signal, this value should be close to 1, since the emission spectrum of TMR does not show any significant contribution on the “blue” detector, i.e. below 548 nm. From both trajectories, a value of around 0.70 is derived and denotes efficient energy transfer with dominant emission from TMR. For the fractional intensity calculated from photon detection on the “green” and “yellow” channel, a mean value of  $F_{yellow,green} = 0.37$  (PBS) and  $F_{yellow,green} = 0.35$  was calculated. Due to similar reasons discussed before, this value is slightly lower as expected from ensemble spectral data for TMR, but suggests high energy transfer efficiency.

Both traces show a relatively high efficiency of energy transfer. An absolute value can be derived from the fluorescence emission of Rhodamine Green detected on the “blue” channel. Assuming no relevant contribution from TMR on the “blue” channel and a constant value of  $F_{green,blue}$  for Rhodamine Green, the intensities recorded on this detector during the presence of the acceptor and after the photodestruction of the acceptor can be used for calculation of transfer efficiencies. Values obtained are 0.86 (PBS) and 0.75 (PBS/MEA), which confirms the highly efficient transfer of excited state energy expected in this construct. Interestingly, neither of the trajectories exhibits fluctuations in energy transfer. Trajectory (D) in figure 4-12

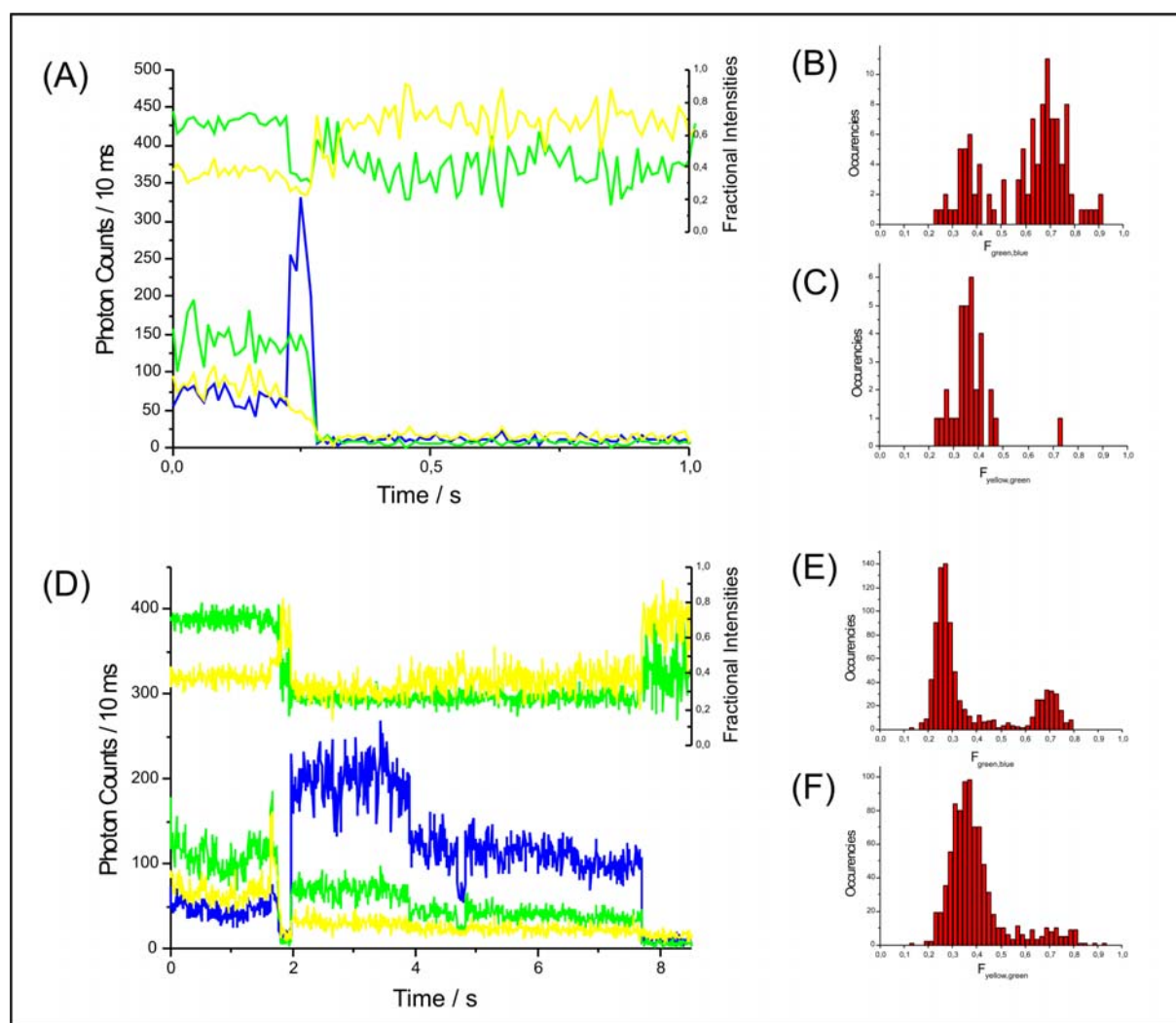


**Figure 4-12: (A): Spectrally-resolved single-molecule trajectory of the FRET-pair RhG-(N)<sub>10</sub>-TMR measured in PBS, with fractional intensities  $F_{\text{green,blue}}$  (green) and  $F_{\text{yellow,green}}$  (yellow), histogrammed in (B) and (C). Longer observation times are observed in PBS/MEA (D) with similar spectral distribution, (E) and (F).**

shows another photophysical phenomenon, which is a collective “off” state of both donor and acceptor, which could be the result of a radical state of RhG or TMR.

As a logical consequence, one might now think of adding more fluorescent dyes and further extend the system. This was realized by “adding” two more fluorophores, ATTO590 and ATTO647, with identical spacing of 10 base pairs or 3.4 nm. Fluorescence trajectories recorded in the presence of 100 mM MEA are shown in figure 4-13.

Trajectories (A) and (B) show spectrally resolved fluorescence intensity emitted by a construct of three fluorophores: RhG, TMR and ATTO590. A fourth fluorophore was added in trajectories (C) and (D), i.e. ATTO647. A fourth detector channel was also

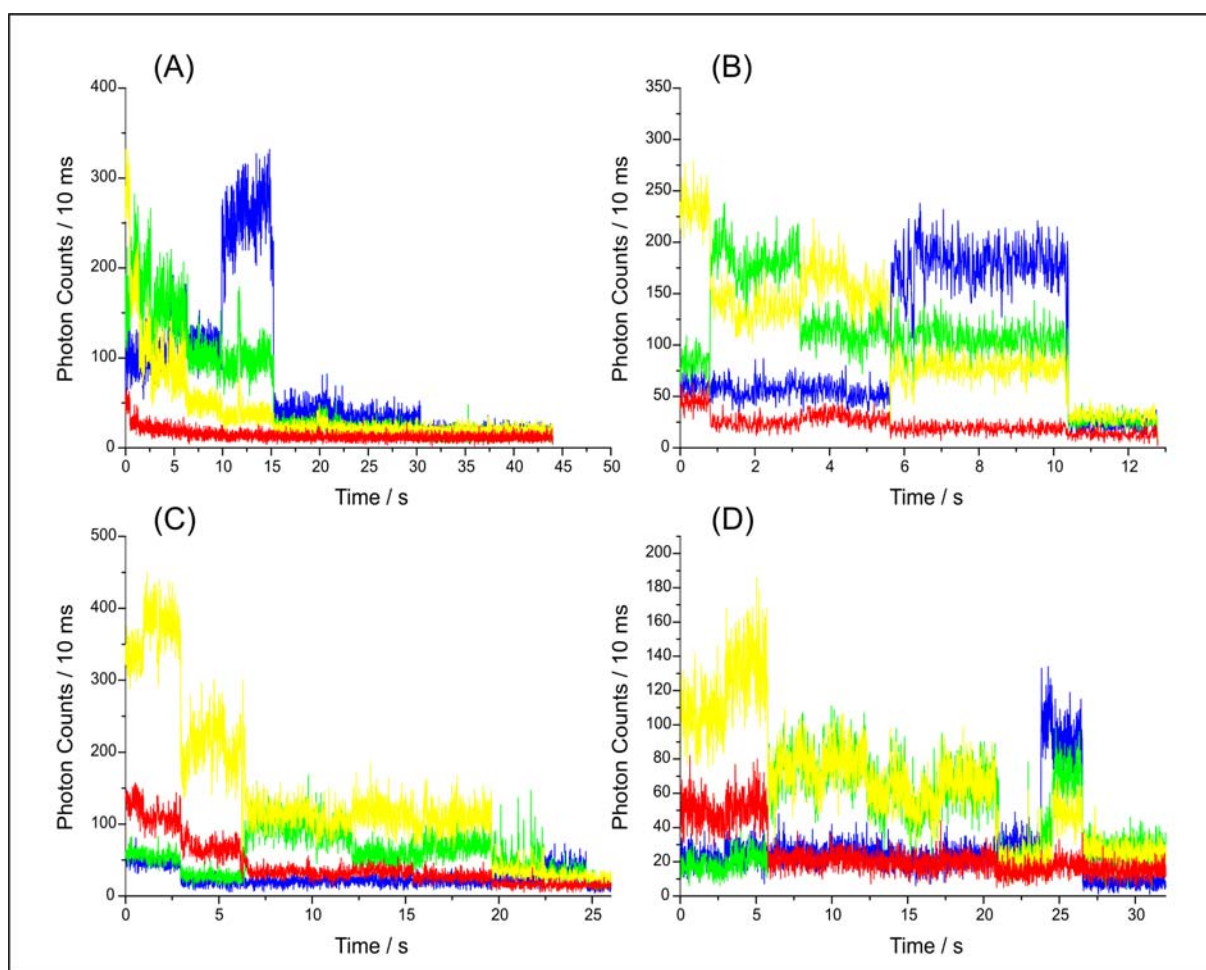


**Figure Figure 4-13: Single-molecule fluorescence trajectories of a three-dye FRET-pair RhG-(N)<sub>10</sub>-TMR-(N)<sub>10</sub>-ATTO590 in (A) and (B) and a four-dye FRET-pair RhG-(N)<sub>10</sub>-TMR-(N)<sub>10</sub>-ATTO590-(N)<sub>10</sub>-ATTO647 in (C) and (D). Trajectories are recorded in PBS/MEA and recorded on four spectrally-separated detectors to better reflect single steps of energy transfer.**

added, denoted “red” and recording photons in a spectral region from 680 to 738 nm. All trajectories exhibit long observation times, showing the applicability of stabilizing rhodamine-like fluorophores in reductive environment. However, three and four fluorophores already present complicated multichromophoric compounds and exhibit complex photophysical behaviour, which shall not be discussed any further in this section, but will be subject of an own section later in this work (see 4.2 and 4.3).

At this point, it could be demonstrated that rhodamine and carborhodamine dyes can be stabilized in aqueous solution to a factor of 10, regarding total photon counts. Precisely, this was demonstrated for the fluorophores Rhodamine Green, TMR, ATTO590 and ATTO647. For the carborhodamine dye ATTO647, a complete suppression of fluorescence intermencencies could be realized in the same environment. Furthermore, smFRET-pairs of up to four fluorophores could be shown

to be substantially more stable, allowing for longer observation times. It can be anticipated that these results are assignable to fluorophores with a similar chemical structure, i.e. many other fluorophores belonging to the class of rhodamines or carborhodamines.

Experimental results obtained in this section will be applied for the construction of artificial photonic wire molecules and are subject of the following section of the discussion. A closer look on energy transfer processes, interchromophoric interactions and a more mechanistic description will be given.

## **4.2. Design of a Unidirectional Photonic Wire**

In the present part of this work, efforts and results towards the realization of synthetic photonic wires are presented. The objective was to design artificial model compounds which do transport light energy, similar to electron transport processes in an electric wire. In contrast to conductive nanowires, these compounds should be addressed from a distance and in a non-invasive way, i.e. excitation via light.

The first synthetic molecular photonic wires had been realized in 1994 by LINDSEY and coworkers [Wagner and Lindsey, 1994], based on conjugated porphyrin arrays. Similar to this approach, photonic wires in the frame of this work were designed with an optical input unit which serves as light absorbing molecule and transfers its energy through a number of transfer units, until finally reaching an output unit. This output unit dispenses energy via light or may be connected to another molecular system, serving as energy donor.

In contrast to the synthetically complicated porphyrin approach, a different route was chosen to design molecular photonic wires. Although slightly different in detail, the principal strategy for the design of such artificial light transporting compounds can be summarised in the following outline:

- DNA was used as rigid scaffold along which fluorophores were conjugated using well-developed labelling strategies to obtain well-defined geometries and make possible many variations.
- Commercially available fluorophores are used as light transmitting units, and were chemically conjugated to modified oligonucleotides.
- An energy cascade as driving force for the excited-state energy transfer was applied to ensure unidirectionality.
- The arrangement of fluorophores was realized such that strong electronic interactions promoting fluorescence quenching are prevented.
- The distance of fluorophores was chosen to be appropriate for weak dipole-dipole induced fluorescence resonance energy transfer (FRET).

Because of the unique molecular recognition properties and the scaffold-like structure, double-stranded (ds) DNA constitutes an ideally suited building block on which the construction of nanoscale molecular devices can be based [Vyawahare et al., 2004]. In addition, the use of DNA offers many well-developed labelling and post-labelling strategies to introduce a variety of different fluorophores in a modular conception, i.e. short oligonucleotides carrying the desired fluorophores can be selectively hybridised to a complementary template strand (figure 4-14). The resulting wire is addressed by excitation of the primary donor, which transfers excited-state energy according to FÖRSTER theory by weak dipole-dipole induced chromophore interactions through the transmitter chromophores to the final acceptor. The acceptor releases the transferred energy by emission of a fluorescence photon.

In the following section, two slightly different approaches based on fluorophores conjugated covalently to oligonucleotides and exploiting hybridisation of single-stranded DNA will be discussed. In all model systems, the interchromophoric distance was chosen to be 10 base pairs, which equals a distance of 3.4 nm. This ensures efficient energy transfer by the FRET mechanism and prevents electronic interactions between adjacent chromophores (see (B) in figure 4-14).

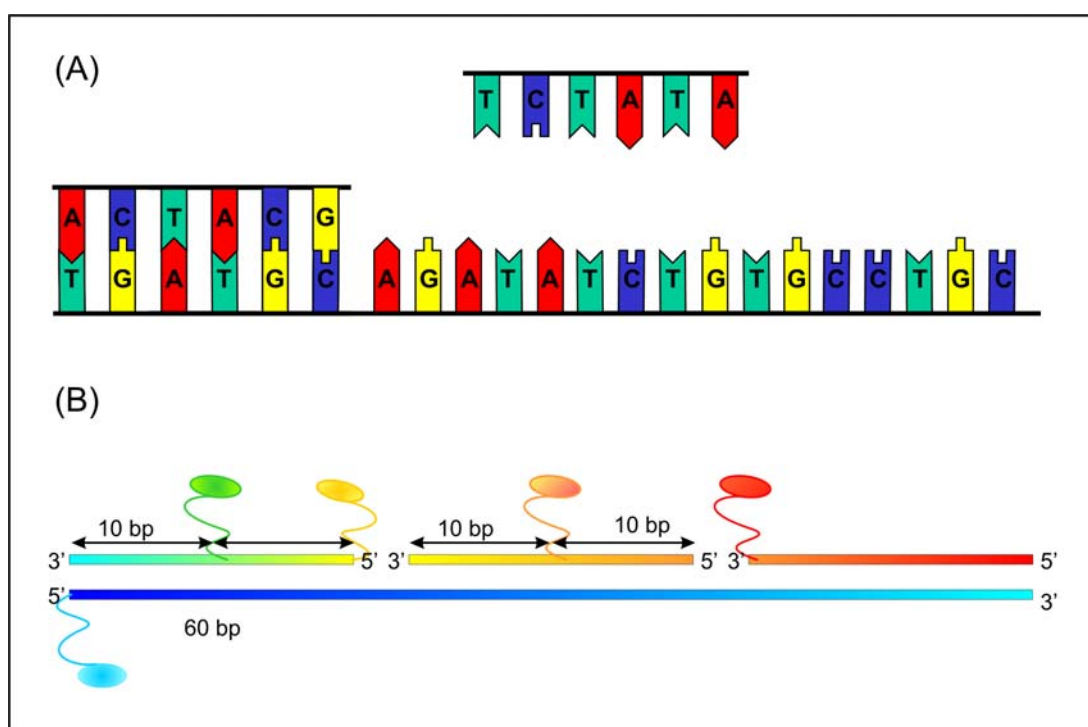


**Figure 4-14: Underlying principle for artificial photonic wires. (A) DNA base pairing, (B) single strand hybridization forming a photonic wire molecule.**

#### 4.2.1. CONFIGURATION OF PHOTONIC WIRES BASED ON 60BP DNA

The most widely used approach to realize unidirectional photonic wires based on multi-step fluorescence resonance energy transfer was realized with four single-stranded DNA fragments of various lengths (60 bases and 20 bases). The DNA sequence and the building principle is depicted in figure 4-15.

Amino-modified single-strand oligonucleotides were conjugated to a number of fluorophores according to the protocol presented in the experimental section (see 3.3.1). Purification by gel filtration and HPLC ensured samples only containing the dye labelled oligonucleotides. Concentrations of samples were measured by steady-state absorption spectroscopy. Both absorption of DNA (at 260 nm) and fluorophore were taken into account for determination of concentration. Appropriate fractions of all four single stranded oligonucleotides were mixed in PBS and hybridised, yielding 60 bp double-stranded DNA with up to five fluorophores at well-defined positions and distances.

To ensure highly efficient fluorescence resonance energy transfer without quenching electronic interactions, an inter-chromophoric distance of 10 bp corresponding to 3.4 nm was used [Dietrich et al., 2002]. The overall spatial range covered by those photonic wires reached 13.6 nm at its maximum. The spectral range comprised more than 270 nm of the visible spectrum, starting from 488 nm to 764 nm in the case of a

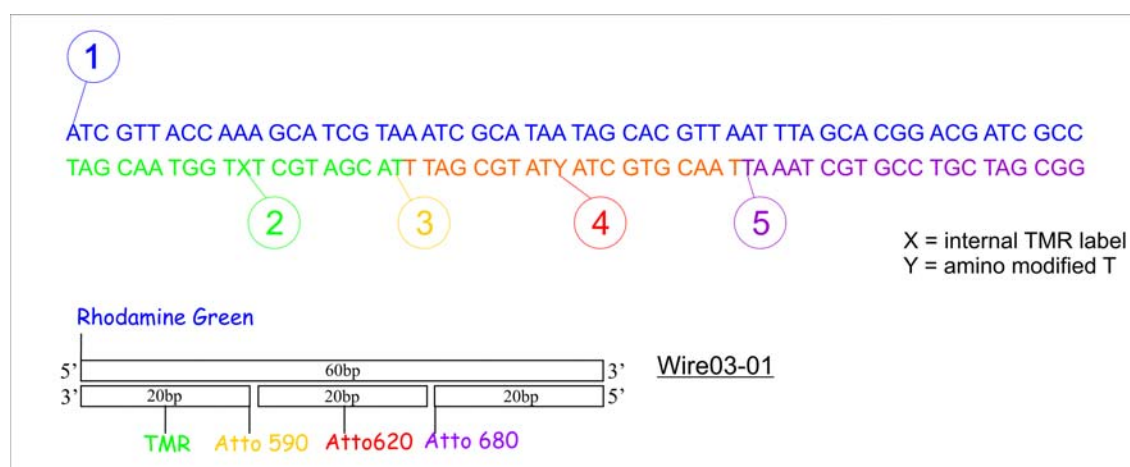


**Figure 4-15: Nucleotide sequence of four single DNA strands used in the 60 bp approach for synthetic photonic wires, containing up to five fluorophores. Exemplary configuration is shown below for Wire03-01.**

far-red emitting final acceptor. As calculated from the spectroscopic characteristics of singly labelled oligonucleotides, each FRET step should occur with more than 95% efficiency, assuming free rotation of the chromophores ( $\kappa^2 = 2/3$ ). For the exemplary compound Wire03-01 (see figure 4-13), values obtained for single energy transfer efficiencies are presented in table 4-9.

	$\lambda_{\text{abs}}/\text{nm}$	$\lambda_{\text{em}}/\text{nm}$	$\varepsilon/\text{l mol}^{-1} \text{ cm}^{-1}$ ( $\times 10^5$ )	$\Phi_f$	$R_0/\text{\AA}$	$E_{\text{FRET}}$
<i>RhG</i>	<b>508</b>	<b>534</b>	<b>0.74</b>	<b>0.9</b>	<b>65.0</b>	<b>0.98</b>
<i>TMR</i>	<b>560</b>	<b>582</b>	<b>0.95</b>	<b>0.9</b>	<b>71.7</b>	<b>0.99</b>
<i>ATTO590</i>	<b>603</b>	<b>625</b>	<b>1.20</b>	<b>0.8</b>	<b>72.3</b>	<b>0.99</b>
<i>ATTO620</i>	<b>622</b>	<b>638</b>	<b>1.20</b>	<b>0.5</b>	<b>74.5</b>	<b>0.99</b>
<i>ATTO680</i>	<b>689</b>	<b>703</b>	<b>1.25</b>	<b>0.3</b>		

**Table 4-9: Spectroscopic properties, FÖRSTER radii and energy transfer efficiencies for fluorophores bound to DNA and contributing to the photonic wire Wire03-01.**

Assuming an inter-chromophoric distance of 3.4 nm and neglecting the length of chemical linkers to fluorophores, an overall transfer efficiency of 95% is calculated for a perfectly aligned wire with the configuration of Rhodamine Green, TMR, ATTO590, ATTO620 and ATTO680.

Table 4-10 gives an overview of photonic wires which have been synthesized using a 60 bases double-stranded DNA as rigid scaffold. Fluorophores attached to corresponding single strands are listed, together with the number of energy transfer steps,  $N_{\text{ET}}$ , and the overall energy transfer efficiencies derived from steady-state ensemble spectroscopy.

Name	Fluorophores	$N_{ET}$	Efficiency <sup>(1)</sup>
Wire03-01	RhG, TMR, ATTO590, ATTO620, ATTO680	4	0.15-0.19
Wire03-02	RhG, TMR, ATTO590, LCR, ATTO680	4	0.15-0.21
Wire03-03	RhG, TMR, ATTO590, LCR, Cy5.5	4	0.13-0.18
Wire04-01 <sup>(2)</sup>	RhG	0	-
Wire04-02	RhG, TMR	1	0.37-0.59
Wire04-03	RhG, TMR, ATTO590	2	0.35
Wire04-04	RhG, TMR, ATTO590, LCR	3	0.17
Wire04-05	RhG, TMR, ATTO590, LCR, ATTO680	4	0.12
Wire04-06 <sup>(3)</sup>	RhG, TMR, ATTO590, LCR, ATTO680	4	0.14
Wire04-07	RhG, TMR, Cy3.5, LCR, ATTO680	4	0.05
Wire04-08	RhG, TMR, ATTO590, LCR, Cy5.5	4	0.14
Wire04-09	RhG, TMR, ATTO590, ATTO647	3	0.37
Wire04-09B <sup>(4)</sup>	RhG, TMR, ATTO590, ATTO647	3	0.34
Wire04-09C	RhG, TMR, ATTO590, ATTO647, ATTO680	4	0.16
Wire04-10	RhG, TMR, ATTO590, ATTO647, Cy5.5	4	0.11
Wire04-11	RhG, TMR, ATTO590, ATTO647, ATTO725	4	<sup>(5)</sup>
Wire04-12	RhG, TMR, ATTO590, ATTO647, ATTO740	4	<sup>(5)</sup>

**Table 4-10: Summary of photonic wire constructs synthesized using the 60bp DNA approach,  $N_{ET}$  represents the number of energy transfer steps. RhG = Rhodamine Green, TMR = Tetramethylrhodamine, LCR = LightCycler Red. <sup>(1)</sup> Energy transfer efficiency from input to output unit was determined from steady state emission or excitation spectra; if more than one method was used, a range of values is given. <sup>(2)</sup> Photonic wires numbered 04-xx exhibit a biotin linker at the 3' end of the sense strand, <sup>(3)</sup> equals Wire04-06 with different concentration of sense strand, <sup>(4)</sup> slightly different concentrations compared to Wire04-09, for hybridisation studies with varying temperature only, <sup>(5)</sup> these wires were only constructed at the single-molecule level, no ensemble spectra and energy transfer efficiency are available.**

Energy transfer efficiencies listed in table 4-10 differ substantially from theoretically expected values. Photonic wires containing five fluorophores exhibit energy transfer efficiencies between 13 and 21%, the most efficiently working compound is Wire03-02 reaching 15 to 21%. It can be anticipated that because of the huge size and complexity of the system, unfavourable conformational orientations of the chromophores, insufficient hybridisation, and/or additional quenching pathways including electron-transfer reactions with DNA nucleotides [Heinlein et al., 2003] will generate an inhomogeneous broadening of the transfer efficiencies. Nevertheless, ensemble spectroscopy can give a first estimation of the suitability of a construct. This is demonstrated by a comparison of energy transfer efficiencies in four dye photonic wires Wire04-04 (17%) and Wire04-09 (37%) (table 4-10).

Before going more into mechanistic details of artificial photonic wires by applying single-molecule spectroscopy, different methods suitable to derive energy transfer efficiencies in multi-chromophoric compounds are the subject of the next paragraph, including steady-state and time-resolved ensemble spectroscopic methods. The following considerations only include energy transfer steps between adjacent fluorophores, the interactions between fluorophores spaced by more than 10 bp is neglected.

#### **4.2.2. ESTIMATING ENERGY TRANSFER EFFICIENCIES IN PHOTONIC WIRES FROM ENSEMBLE STEADY-STATE MEASUREMENTS**

The quality of energy transfer through an artificial photonic wire is characterized by its overall energy transfer efficiency. Although this is theoretically easy to determine from ensemble spectroscopic data for a homogeneous sample exhibiting FRET, a number of complications occur in photonic wires designed in the described way:

- Hybridisation, although being a very selective and efficient process, can be difficult if more fragments are involved due to unfavourable secondary structure, e.g. kinks, or dye-nucleobase interactions [Waggoner and Randolph, 1997].

- Exact concentrations of single stranded oligonucleotides labelled with fluorophores are difficult to obtain, since extinction coefficients from fluorophores may vary substantially, a result of an altered electronic environment [Haugland, 1989; Clegg et al., 1992b; Han, 2005].

As a result, energy transfer efficiencies from ensemble spectroscopic data essentially are approximated values, and strongly depend on the heterogeneity of the sample and the number of energy transfer steps.

Methods to obtain reliable data for energy transfer efficiencies are well-elaborated for simple FRET-pairs, and include decrease of donor lifetime or quantum yield, normalized fluorescence emission spectra or anisotropy [Clegg 1992]. Unfortunately, these methods become extremely uncertain if more than two fluorophores are participating or larger deviations in concentrations appear. Most work on ensemble multistep FRET therefore exploited variations in donor emission to determine FRET efficiencies [Ohya et al., 2003]. Other works leave out the calculation of energy transfer efficiencies and focus on changes in fractional intensities to derive proximity data [Clamme and Deniz, 2004]. Especially for three-colour FRET experiments, a number of sophisticated models were worked out, but model compounds usually are constructed from one or two components [Liu and Lu, 2002; Watrob et al., 2003]. The great advantage of single-molecule multi-FRET experiments lies in the observation of only one multichromophoric system, simplifying data analysis enormously [Hohng et al., 2004].

To calculate energy transfer efficiencies for photonic wire molecules designed in this work, a combination of several techniques was used. Especially complex compounds with more than three fluorophores did not allow the use of time-resolved data, and a combination of steady-state spectroscopic methods revealed a rough approximation for energy transfer efficiencies.

- Absorption spectra can be expressed as linear combination of contributing single fluorophore spectra. This allows the estimation of the overall stoichiometry of the samples. Possible pipetting errors can be revealed yielding unhybridized DNA. Uncertainty remains due to variable extinction coefficients.

- A linear combination of emission spectra, normalized to the quantum yield of each fluorophore, gives a direct estimation of energy transfer efficiencies for each step (very similar to the method of sensitised emission [Clegg, 1992]).
- A comparison of fluorescence photons obtained via energy transfer steps and direct excitation of the final emitting fluorophore are a measure for the overall energy transfer efficiency. (This method is closely related to comparing a measured transfer efficiency to 100% transfer efficiency, [Clegg 1992]).
- Excitation spectra, recorded at the main emission wavelength from the last emitting fluorophore, can be approximated as linear combination of the absorption spectra of contributing fluorophores. A normalization to the extinction coefficients of the fluorophores yields transfer efficiencies for all single steps.

By combining the results obtained in each analysing step, steady-state spectroscopy yields a sufficient approximation of energy transfer efficiencies. An exemplary calculation, using spectroscopic data shown in figure 4-16, will be presented for the system Wire03-01 in the following. These methods were used for the determination of energy transfer efficiencies listed in table 4-10.

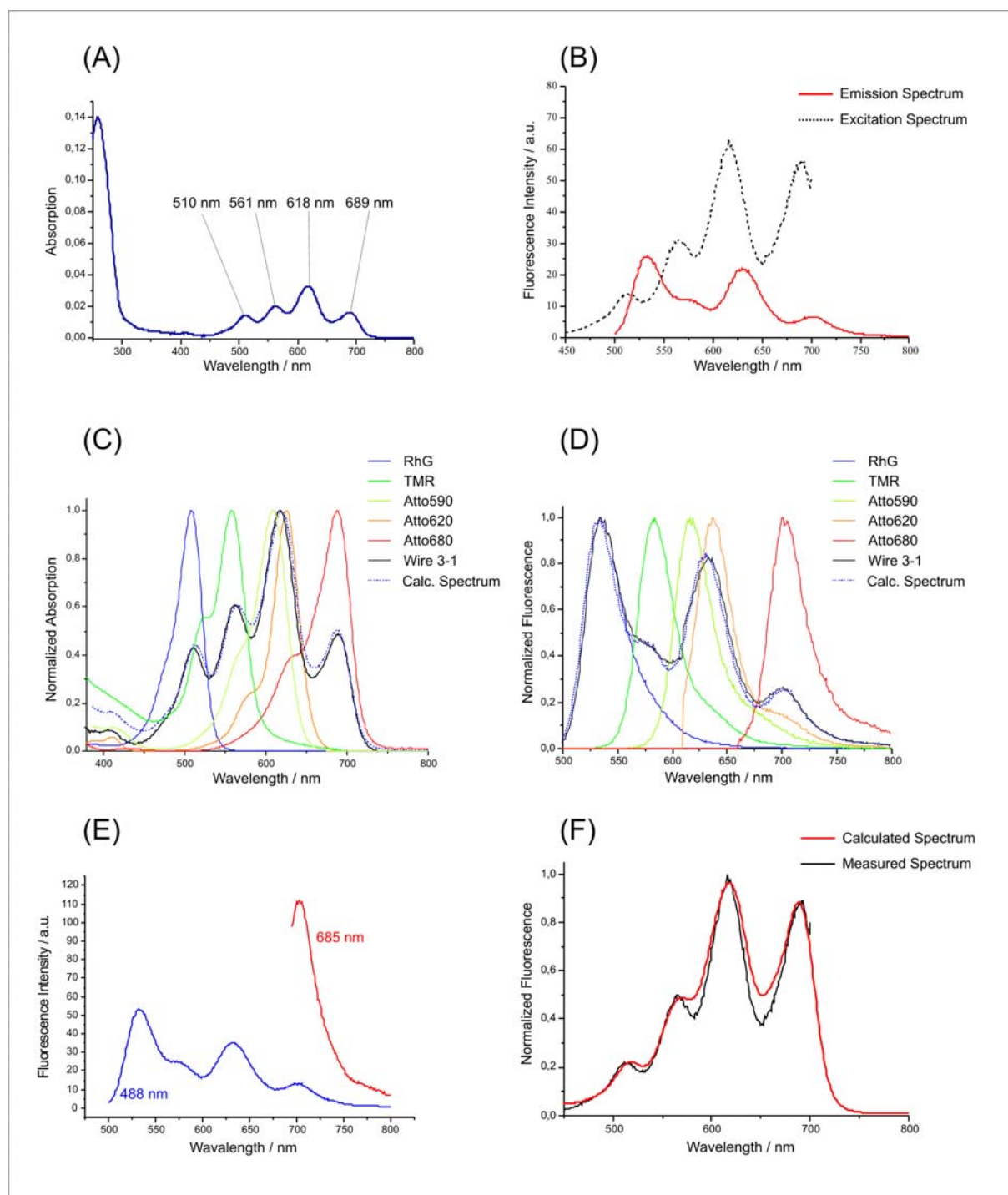


**Figure 4-16: Overview of ensemble-spectroscopic steady-state methods to characterize photonic wire molecules, exemplary for the compound Wire03-01 with 5 fluorophores. (A) Absorption spectrum exhibiting four peaks (two dyes are contributing to the 618 nm absorption peak); (B) emission (488 nm excitation) and excitation spectrum (fluorescence recorded at 720 nm); (C) and (D): the measured overall absorption spectrum and emission spectrum is calculated as linear combination of single fluorophore spectra; (E) emission of the last acceptor excited via energy transfer and directly; (F) excitation spectrum calculated from single fluorophore absorption spectra.**

### Steady-State Absorption Spectra

In a first step, the absorption spectrum of a photonic wire sample,  $A(\lambda)$ , is approximated by single fluorophore absorption spectra,  $a_i(\lambda)$ ,

$$A(\lambda) = \sum_i \alpha_{i,rel} a_i(\lambda) \quad ( 4-2 )$$

Since both absorption wavelength and extinction coefficient slightly change, these values are necessarily approximated. Values obtained for the approximation of the absorption spectrum of Wire03-01 are listed in table 4-11.

	<b>RhG</b>	<b>TMR</b>	<b>ATTO590</b>	<b>ATTO620</b>	<b>ATTO680</b>
$\alpha_{rel}$	0.27	0.35	0.47	0.47	0.50
$\epsilon_{max}$ (l mol <sup>-1</sup> cm <sup>-1</sup> )	74000	95000	120000	120000	125000
$\alpha_{abs}$	0.91	0.92	0.98	0.97	1.00

**Table 4-11: Linear combination of single fluorophore absorption spectra to approximate the absorption spectrum of Wire03-01, normalized to the extinction coefficient.**

In table 4-11,  $\alpha_{rel}$  represents the relative contribution to the overall absorption of the hybridised photonic wire, which was normalized to a maximum value of 1 (see part (C) in figure 4-16). Corrected by the extinction coefficient of each fluorophore,  $\epsilon_{max}$ , an absolute contribution or ratio is obtained,  $\alpha_{abs}$ , which was normalized with respect to the maximum ratio appearing.

Regarding the data presented in table 4-11, a few issues are worth mentioning. First, ratios of fluorophores are not equal. The reason is a combination of uncertainties in concentration determination, insufficient purification steps, and errors made when pipetting single strand volumes for hybridisation. Total differences of  $\sim 10\%$  in concentration are observed. Secondly, both TMR and ATTO590 are conjugated to the same strand, so their relative contribution is expected to be identical. In this case, a slight change in the extinction coefficient can be assumed.

### Steady-State Emission Spectra

In a second step, the overall emission spectrum of a photonic wire,  $F(\lambda)$ , is approximated by a linear combination of single emission spectra of contributing fluorophores bound to DNA,  $f_i(\lambda)$ ,

$$F(\lambda) = \sum_i \alpha_{i,rel} f_i(\lambda) \quad ( 4-3 )$$

This calculation is a variation of the often used method of sensitised emission [Clegg 1992], values obtained for the linear combination of Wire03-01 are listed in table 4-12, fluorescence emission spectra are shown in figure 4-16, (D).

	<b>RhG</b>	<b>TMR</b>	<b>ATTO590</b>	<b>ATTO620</b>	<b>ATTO680</b>
$\alpha_{rel}$	1.00	0.20	0.27	0.60	0.15
$\phi$	0.9	0.9	0.8	0.5	0.3
$\alpha_{abs}$	1.11	0.22	0.34	1.20	0.50
$\alpha_{abs, norm}$	0.33	0.06	0.10	0.36	0.15

**Table 4-12: Linear combination to approximate the emission spectrum of Wire03-01 by relative contributions of single fluorophores,  $\alpha_{rel}$ . Normalized to the quantum yield,  $\phi$ , absolute contributions  $\alpha_{abs}$  are obtained and normalized to the sum of 1,  $\alpha_{abs, norm}$ , now giving a measure of energy transfer at each step.**

Relative contributions to the overall emission spectrum of the sample Wire03-01 must be normalized to the quantum yield of each individual fluorophore to obtain absolute contributions,  $\alpha_{abs}$ . This representation now allows to estimate energy transfer efficiencies by analysing the “distribution” of energy along the multichromophoric sample. The value  $\alpha_{abs}$  for the last emitter, ATTO680, gives a value of 15% for the total energy transfer observed.

The method of approximating multi-step FRET emission spectra is only reliable if the quantum yield of fluorophores in the hybridised compound is comparable to the quantum yield of fluorophores attached to single strand DNA. Excitation of the second fluorophore or skipping of transfer steps are not taken into account, since a possible better accuracy would not compensate greater sources of errors.

Furthermore, the absorption spectrum should exhibit equal contributions of chromophores.

Remarkably, this approximation already reveals a major problem of photonic wire molecules designed from several single stranded DNA molecules exploiting hybridization, showing energy loss at two important positions: the first dye and input unit, and the fourth dye in the cascade.

#### *Direct Excitation of the Last Emitter*

Another method applied to evaluate the overall transfer efficiency is illustrated in part (E) of figure 4-16. The approach is related to the method of comparing the acceptor emission of a sample to a second sample exhibiting 100% FRET [Clegg 1992]. As no sample with 100% FRET is available with the present design, fluorescence emission of the last emitting unit was compared to direct excitation of the fluorophore. For comparability of both values, differences in the excitation probability of a fluorophore must be taken into account, which is realized by normalizing fluorescence intensity to the extinction coefficient.

An exemplary calculation for the sample Wire03-01 (see figure 4-16, (E)) is summarized in table 4-13.

	Excitation via FRET (488 nm)	Direct Excitation (685 nm)
Fluorescence emission at 700 nm (counts)	14	113
Contributing emission from ATTO680 (counts)	8.1	113
Extinction coefficient at excitation wavelength ( $l \text{ mol}^{-1} \text{ cm}^{-1}$ )	42000	119000
Normalized emission (counts)	20.3	100

**Table 4-13: Calculation of energy transfer by comparing fluorescence emission along the FRET-system and direct excitation of the last emitter. Fluorescence emission is corrected for preceding fluorophores in Wire03-01 and for the extinction coefficient of the excitation wavelength; finally, the value for direct excitation is set to 100 for more clarity.**

Excitation of Wire03-01 at 488 nm yields a fluorescence emission intensity of the last emitter (measured at 700 nm) of 14 counts via energy transfer and 113 counts via direct excitation, respectively (685 nm excitation). Fluorescence emission of ATTO680 derived from FRET-excitation has to be corrected, i.e. the overlap with preceding fluorophores has to be ruled out. In a final step, extinction coefficients at the excitation wavelength have to be included, yielding a final value of 21% for energy transfer in Wire03-01.

This approach is very sensitive to an excess of concentration of the final dye which is not involved in the formation of double strand DNA, e.g. due to concentration errors or incomplete hybridisation.

### *Steady-State Excitation Spectra*

The last method makes use of the excitation spectrum of a photonic wire sample, recorded at the emission wavelength of the last emitting dye in the energy transfer cascade. This method is not reliable if an excess of the last fluorophore is present. The excitation spectrum is approximated by a linear combination of single dye absorption spectra, yielding relative contributions of participating fluorophores which contribute to the emission of the last fluorophore, see (F) in figure 4-16. Exemplary calculations for Wire03-01 are listed table in 4-14. Note that a normalization to quantum yields is not necessary, since only one emission wavelength which originates mostly from the last emitter is observed.

	<b>RhG</b>	<b>TMR</b>	<b>ATTO590</b>	<b>ATTO620</b>	<b>ATTO680</b>
$\alpha_{rel}$	0.10	0.20	0.55	0.23	0.88
$\epsilon_{max}$ (l mol <sup>-1</sup> cm <sup>-1</sup> )	74000	95000	120000	120000	125000
$\alpha_{abs}$	0.19	0.30	0.65	0.27	1.00

**Table 4-14: Energy transfer efficiency derived from linear combination of excitation spectrum. Relative contributions  $\alpha_{rel}$  are normalized to the extinction coefficient, yielding absolute contributions,  $\alpha_{abs}$ .**

From the relative contributions of fluorophores to the recorded excitation spectra of Wire03-01, absolute values can be obtained by normalizing to the extinction coefficients of the dyes. These absolute values  $\alpha_{abs}$  are then normalized to the value of 1 for the final fluorophore, ATTO680. As a result, the excitation efficiency of ATTO680 along the energy transfer cascade is 19% with respect to the first fluorophore RhG.

Three different models of calculating energy transfer efficiencies were demonstrated for the sample Wire03-01 and yielded values between 15% and 21% (and a mean value of 18%). The combination of steady-state spectroscopic techniques allows to a certain extent to characterize the quality of a sample as artificial photonic wire, but implies a number of difficulties. The number of five spectrally close fluorophores prevents to account for unequal stoichiometry of contributing oligonucleotides, and subpopulations cannot be identified. At this step, it becomes clear that more sensitised methods must be applied, which allow to watch single photonic wires at their working level, i.e. the single-molecule level.

### 4.2.3. TIME-RESOLVED ENSEMBLE SPECTROSCOPY OF PHOTONIC WIRES

Besides ensemble spectroscopic data derived from steady-state measurements, time-resolved data can be consulted to determine energy transfer efficiencies [Clegg, 1992]. This is particularly feasible in “classic” FRET-pairs, constituted of two fluorophores, although often less precise due to a complex environment of fluorophores attached to DNA which may lead to deactivation processes influencing the fluorescence lifetime [Dietrich et al., 2002]. Nevertheless, subpopulations with different kinetic parameters can be distinguished and quantified, which allows a more detailed description beyond the possibilities of steady-state spectra.

As an example for determination of energy transfer efficiency based on time-resolved measurements, the sample denoted Wire04-02 is discussed in the following. It consists of only two fluorophores with a distance of 10 base pairs or 3.4 nm, Rhodamine Green and TMR, respectively. The free dyes exhibit a fluorescence

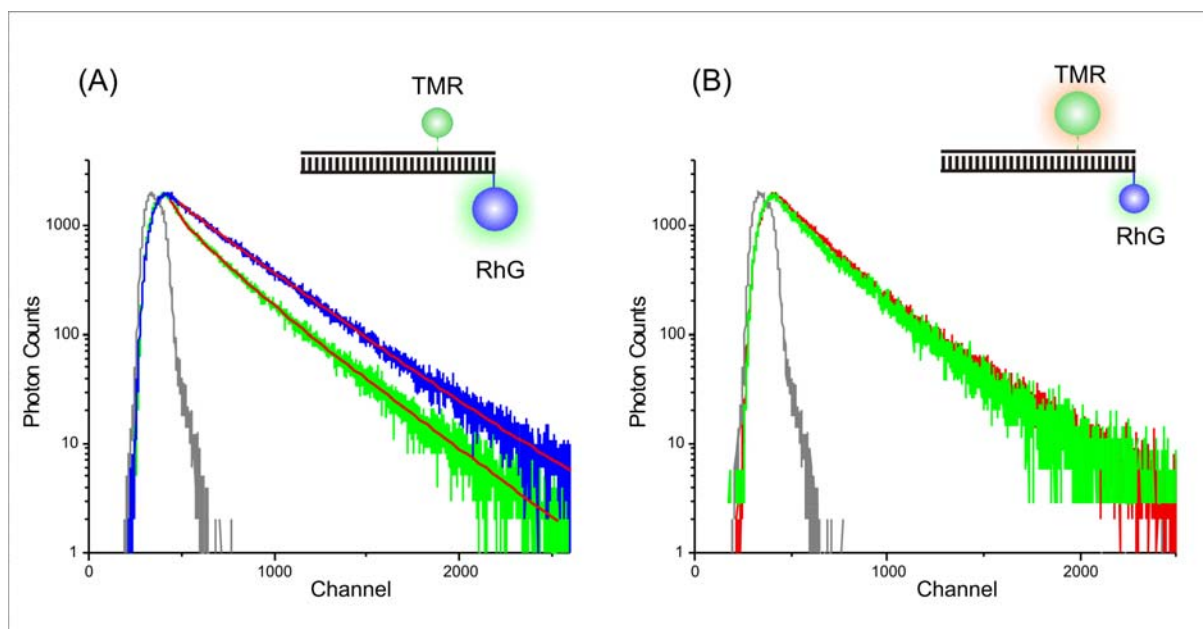


**Figure 4-17:** Time-resolved fluorescence measurements of the FRET-pair RhG-TMR, spaced by 10 base pairs of dsDNA (excitation at 495 nm, 2000 counts in maximum channel, time resolution 0.012 ns/channel). (A): donor emission (green) compared to free donor (blue) recorded at 535 nm, lamp profile (grey); (B) Acceptor emission (red) and free acceptor (green) recorded at 585 nm.

lifetime of 3.7 ns for RhG and 2.2 ns for TMR, respectively. Measurements were performed at a concentration of  $\sim 10^{-6}$  M in PBS using a time-resolved spectrometer with an LED as excitation source, emitting at 495 nm. Fluorescence emission from the donor fluorophore was recorded at 535 nm, acceptor fluorescence at 585 nm. For a better comparability, fluorescence decays of both donor and acceptor only, both conjugated to the same double-stranded DNA, were measured as well. Fluorescence decays and the lamp profile are shown in figure 4-17. From a first view, the decay of the donor fluorophore shows a short component with respect to the free fluorophore, which results from a fast deactivation of the excited state by energy transfer. This is predominantly the case for short times of the decay. Going to longer times, both decays appear parallel and exhibit similar exponential kinetics, which indicates a second subpopulation in the FRET-pair sample of Wire04-02 that does not exhibit energy transfer. This can be confirmed by the results obtained after deconvolution and fit procedures, listed in table 4-15.

	$\tau_1 / \text{ns}$	$A_1$	$\tau_2 / \text{ns}$	$A_2$	$\chi^2$
<i>Rhodamine Green</i>	4.20	1.00	-	-	1.154
<i>Rhodamine Green (donor)</i>	0.70	0.23	3.66	0.77	1.084

**Table 4-15: Fluorescence kinetics from Rhodamine Green bound to dsDNA in the presence and absence of an acceptor molecule.**

The results from the fit procedure for Rhodamine Green in the presence of an acceptor fluorophore confirms the first impression: two subpopulations can be distinguished. A first fraction shows high efficient FRET with a transfer efficiency of  $E = 0.83$  and an amplitude of  $A = 0.23$ . A second fraction of 77% exhibits a fluorescence lifetime which is comparable to the free dye, but still a difference of 0.54 ns is observed. If calculating a FRET-efficiency, a value of  $E = 0.13$  is obtained. At this point, it is difficult to further characterize this second subpopulation. A more detailed picture of Rhodamine Green as donor fluorophore attached to DNA will be given from single-molecule results later in this work.

The decays in the acceptor channel are more difficult to interpret. Results from the fit procedures are listed in table 4-16.

	$\tau_1 / \text{ns}$	$A_1$	$\tau_2 / \text{ns}$	$A_2$	$\chi^2$
<i>TMR</i>	3.45	0.85	0.69	0.15	1.126
<i>TMR (acceptor)</i>	2.25	0.48	4.39	0.52	1.092

**Table 4-16: Fluorescence kinetics calculated for TMR bound to DNA and as the acceptor in Wire04-02.**

Without the presence of a donor fluorophore, TMR exhibits two fluorescence lifetimes of 3.45 ns (85%) and 0.69 ns (15%). This behaviour can be explained by efficient dynamic quenching of fluorescence by a neighbouring guanosine residue [Eggeling et al., 1998b]. If a donor fluorophore is present, one would expect a broadened fluorescence decay of the acceptor around the maximum, which is slightly shifted with respect to the decay of the acceptor fluorophore without the presence of a donor. The reason for the appearance of a so-called rise time lies in the “excitation profile” for the acceptor: unlike the donor whose fluorescence decay is convoluted with the lamp profile, the decay of the acceptor is additionally convoluted with the fluorescence decay of the donor. In mathematical analysis by deconvolution and multi-exponential fitting, this usually yields a short component with a negative amplitude. The absolute value of this negative amplitude determines the fraction of acceptor molecules which is excited through energy transfer, and the rise time itself allows to determine energy transfer efficiencies, complementary to the procedure applied for the donor fluorophore. Regarding fluorescence decays in figure 4-17, the rise time can only be anticipated from the shape of the acceptor decay, but cannot be resolved mathematically. The values obtained suggest many contributions to fluorescence at 585 nm and do not allow an exact interpretation. Direct excitation of the acceptor (~20 % at 495 nm for TMR) and remaining fluorescence of the donor (~18% for Rhodamine Green) generally make the determination of energy transfer efficiencies very difficult, which explains the more common use of donor fluorescence decays.

It is now interesting to compare the results obtained from time-resolved ensemble measurements to steady-state measurements performed under equal conditions for the same sample. Steady-state absorption, emission and excitation spectra are depicted in figure 4-18.

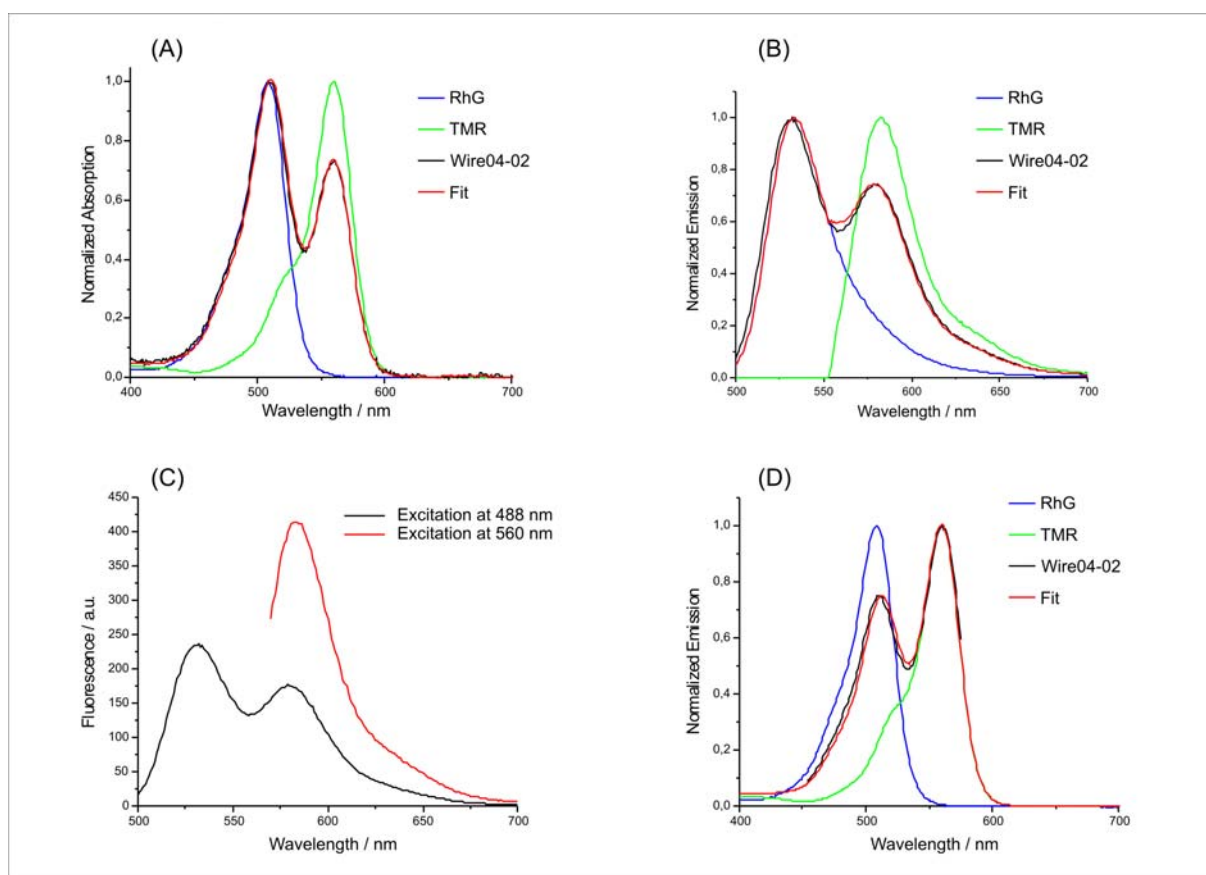


**Figure 4-18: Steady-spectra of the FRET-pair RhG-TMR (Wire04-02): (A) absorption spectra, (B) emission spectra, (C) excitation by two wavelengths (488 nm and 560 nm), (D) excitation spectra.**

First, the absorption spectrum of the compound Wire 04-02 is approximated by linear combination of single fluorophore spectra. Values obtained are listed in table 4-17.

	RhG	TMR
$\alpha_{\text{rel}}$	0.84	0.73
$\epsilon_{\text{max}} (\text{l mol}^{-1} \text{cm}^{-1})$	74000	95000
$\alpha_{\text{abs}}$	1.00	0.74

**Table 4-17: Linear combination of the absorption spectrum of Wire04-02.**

The linear combination of table 4-17 reveals an excess of 26% for Rhodamine Green in Wire04-02. Using previously presented approaches to calculate the energy

transfer efficiencies, values obtained from different emission spectra are summarized in table 4-18. Concentration errors were taken into account.

	$E_T$
<i>Emission spectra</i>	0.46
<i>Direct excitation of acceptor</i>	0.59
<i>Excitation Spectra</i>	0.37

**Table 4-18: Energy transfer efficiency calculated for Wire04-02 applying different methods.**

All three methods used for calculation of energy transfer efficiencies yield varying results, and a mean value of 47% can be given. To compare this value with the result from time-resolved spectroscopy, a surplus of 26% of RhG must be included (the method of time-resolved spectroscopy is more sensitive to a higher donor concentration than the method of excitation spectra or direct excitation of acceptor). By this, the energy transfer efficiency is reduced to 35%, whereas time-resolved measurements yield 19% (if only the first population with very efficient FRET is taken into account) or 29% (with both distributions) as a mean value, respectively. As a result, it can be stated that absolute values for transfer efficiencies are quite different. This ambiguity between time-resolved and steady-state spectroscopy has already been observed previously [Dietrich et al., 2002].

### **Time-Resolved Emission Spectroscopy of Photonic Wires**

As an extension to mere time-resolved measurements of fluorescence kinetics at fixed wavelengths, an impression of the complexity of energy transfer along a photonic wire with five fluorophores can be obtained from spectrally resolved fluorescence decays. This was realized by excitation at 495 nm and recording fluorescence decays in steps of 10 nm, yielding a time-resolved emission spectrum (TRES). In part (A) of figure 4-19, a two-dimensional projection of a TRES spectrum from Wire03-01 ranging from 520 nm to 740 nm detection wavelengths is depicted, and a number of spectroscopic properties can be read out immediately from such presentations. First, short fluorescence lifetimes are observed in the donor region (around 550 nm), whereas in the acceptor region (> 630 nm), fluorescence lifetimes

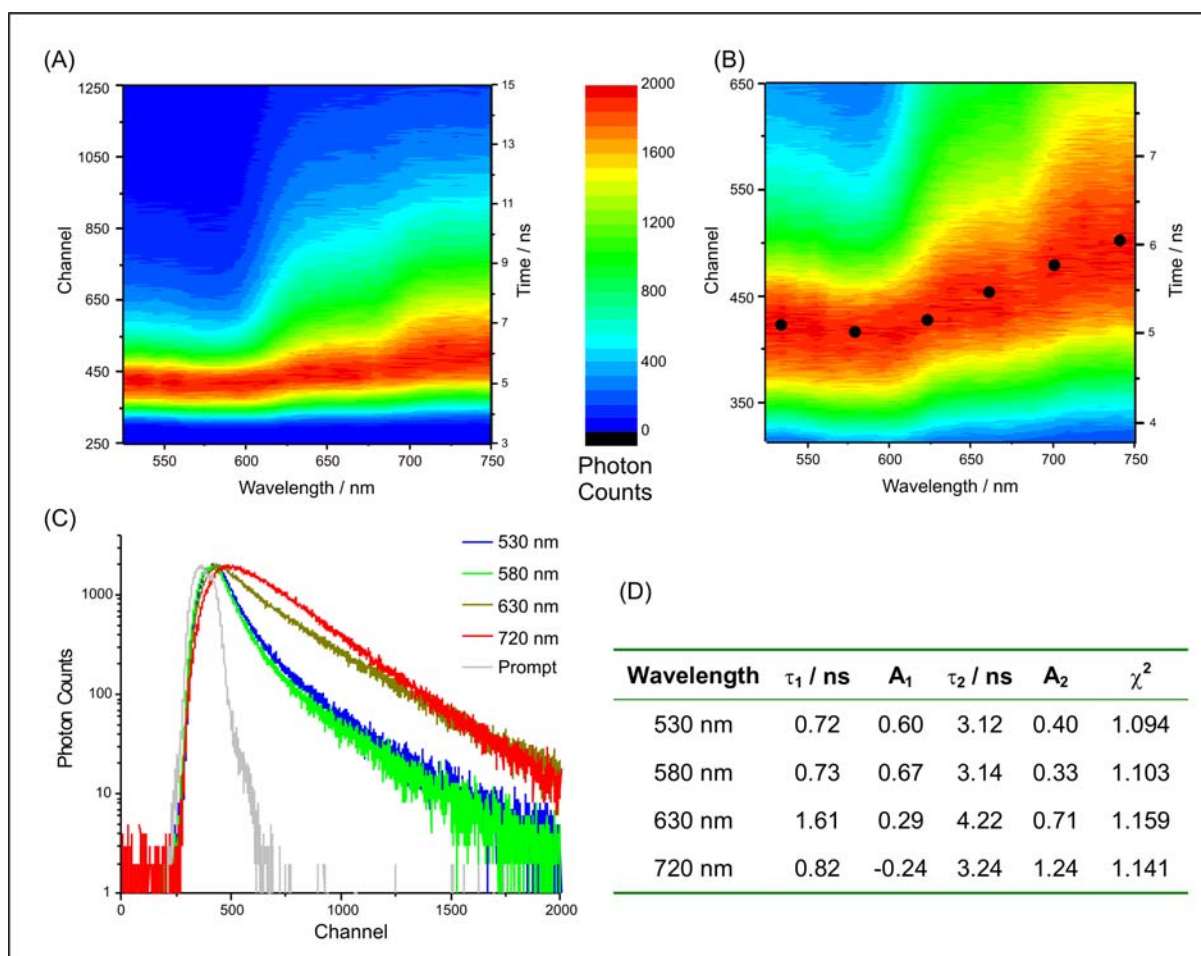


**Figure 4-19: (A) Time-resolved emission spectrum of Wire03-01, recorded in 10 nm steps from 520 nm to 740 nm (2000 maximum counts, 495 nm excitation, channel resolution 0.012 ns). (B) Magnification shows a shift of the area of maximum photon counts towards longer time channels of 0.84 ns at its maximum. (C) Fluorescence decays of the four most important emission wavelengths of Wire03-01, (D) calculated fluorescence kinetics after deconvolution and biexponential fitting.**

are considerably longer. A second issue which is emphasized by black circles in part (B) of figure 4-19 is the broadening and shifting of the fluorescence decay around its maximum. With a channel length of 12 ps, a shift of 70 channels or 0.84 ns is observed. Both shifting and broadening are due to rise times that appear in each step of energy transfer. In part (C), four selected decays together with the lamp signal show the behaviour of both broadening and shifting for the most important emission wavelengths of the sample, Wire03-01.

Deconvolution and fit procedures (see part (D), figure 4-19) yield strongly quenched subpopulations at shorter wavelengths, whereas at longer emission wavelengths, a rise time with a contribution of 24% appears.

Interestingly, shortest times and largest amplitudes are not observed around the emission wavelength of the first fluorophore, but at  $\sim 590$  nm. This may be explained by a fraction of donor fluorophores which fluoresces without any energy transfer process, comparably to previously presented results for the FRET-pair RhG-TMR. On the other hand FRET from TMR to ATTO590 is very efficient and quantitative.

In Figure 4-20, fluorescence emission spectra and time-resolved spectra of two compounds denoted Wire04-09 and Wire04-10 are depicted. Both are build up from rhodamine dyes (RhG, TMR, ATTO590) and a carborhodamine dye on position 4 (ATTO647). Additionally, Wire04-10 has a dye at position 5, the carbocyanine dye Cy5.5 which exhibits a fluorescence lifetime of  $\sim 1.0$  ns. Spectra are recorded from 530 nm to 690 nm and 720 nm, respectively. In the case of Wire04-09, a broader “shoulder” appears around 640 nm. This “shoulder” is depopulated by energy transfer towards Cy5.5 in Wire04-10. Due to a significantly shorter lifetime, the broadening becomes smaller and demonstrates the presence of a subpopulation which exhibits energy transfer to the last fluorophore.

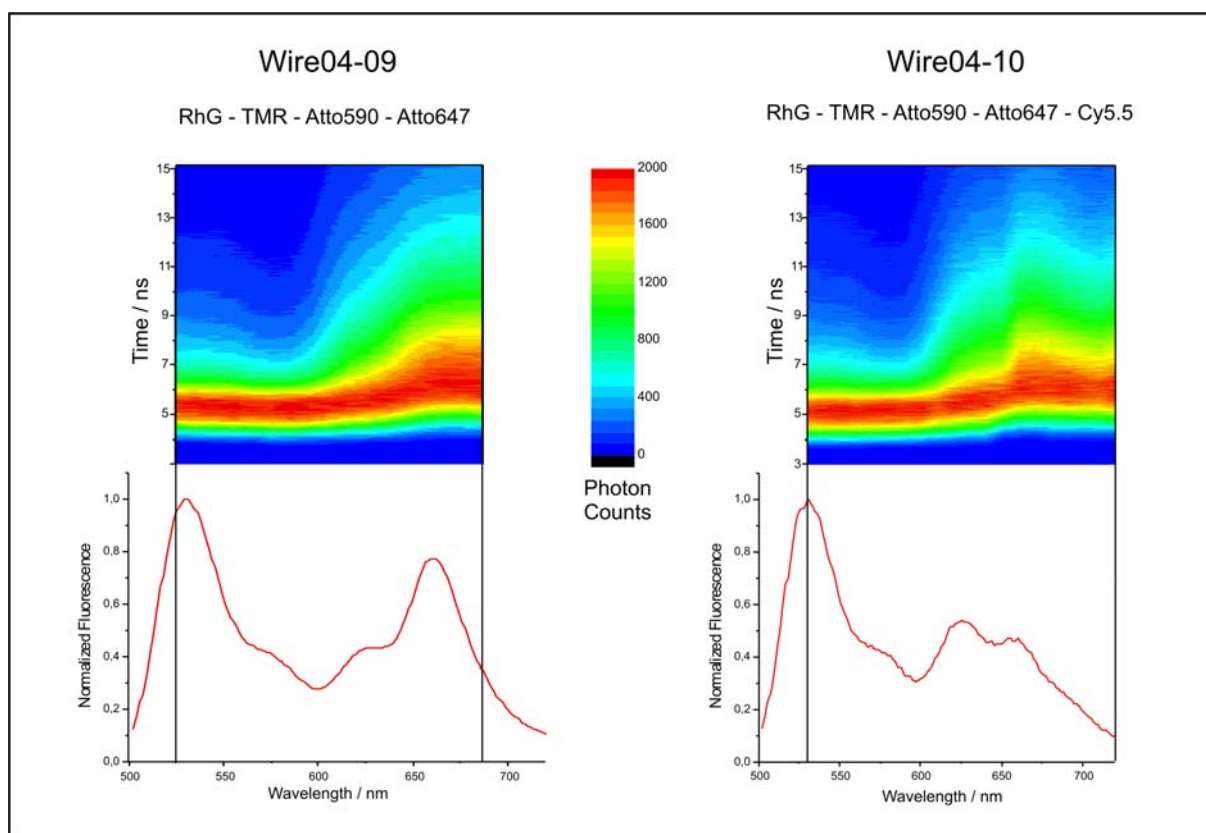


**Figure 4-20: Ensemble and time-resolved emission spectra of photonic wires Wire04-09 (530 to 690 nm) and Wire04-10 (530 to 720 nm). 495 nm excitation, 2000 maximum counts, 0.012 ns / channel.**

Compared to Wire03-01 (figure 4-19), a shift of fluorescence decays of 1.07 ns is observed for Wire04-09 (figure 4-20). This underlines a higher efficiency in energy transfer which was already calculated from steady-state ensemble spectra (energy transfer efficiency is determined to be 37%, see table 4-10). In Wire04-10, a shift of 0.70 ns is observed at 720 nm (mainly fluorescence emission from Cy5.5), together with 0.97 ns at 670 nm (maximum emission wavelength of the fluorophore ATTO647). This observation is in good agreement with steady-state spectroscopy, where Wire04-10 only yields 11% of energy transfer efficiency (in other words, only ~30% of energy transfer from ATTO647 to Cy5.5 is observed). This observation is in agreement with the emission spectrum of Wire04-10 (figure 4-20), which exhibits a weak contribution from the last chromophore (Cy5.5), but still considerable contribution from the fourth dye (ATTO647).

Both Wire04-09 and Wire04-10 will further be characterized in single-molecule experiments in aqueous environment.

### **4.3. Studying Photonic Wires with Single-Molecule Spectroscopy**

It is the complexity of the systems - independent of the energy-transfer mechanism employed - which determines the need for new analytical techniques for the characterisation of bottom-up nanotechnological devices, such as photonic wires. Single-molecule fluorescence spectroscopy (SMFS) is a technique that provides detailed information required for the analysis of static heterogeneity. In addition, SMFS also enables to probe the quality of the device.

Molecular photonic wires have to operate at the single-molecule level and, hence, they have to be characterised at this individual level as well. This was realized by using two principal techniques of immobilization. At first, fluorescence imaging and traces of individual photonic wires were derived from molecules adsorbed on a dried glass substrate. The second technique made use of biotin-streptavidin interaction and allowed immobilization in liquid environment, which is of particular interest if the chemical properties of the surroundings are object of change.

### 4.3.1. SPECTRALLY RESOLVING SINGLE PHOTONS ON FOUR DETECTOR CHANNELS

Spectral information of photons emitted from photonic wire samples is detected with four APDs as detector channels. A set of dichroic beamsplitters and filters hereby selects a spectral region. At the single-molecule level, it is possible to assign a photon to a certain emitter, by exploring its spectral characteristics.

To get an idea of the origin of a photon, i.e. to assign probabilities which dye contributed a particular detected photon, two approaches to obtain the spectral distribution of a fluorophore onto the four detectors were used. At first, solutions of all fluorophores bound to DNA were excited with 488 nm and fluorescence was collected independently. To excite longer wavelength absorbing dyes with the excitation source, higher concentrations were used to compensate a lower absorption probability (it is assumed that the fluorescence emission of these fluorophores does not alter with the excitation wavelength). In general, concentrations between  $10^{-8}$  M and  $10^{-6}$  M were used. This minimizes contributions from Raman scattering around 570 nm, originating from symmetric and asymmetric vibrations of water molecules. Fluorescence emission of the five chromophores from Wire03-02 broken down into detector channels are presented in table 4-19. Detector channels are denoted according to their approximated spectral detection area, i.e. blue, green, yellow and red.

	Blue	Green	Yellow	Red
<i>RhG</i>	0.58	0.37	0.05	0.01
<i>TMR</i>	0.02	0.72	0.22	0.03
<i>ATTO590</i>	0.01	0.33	0.54	0.12
<i>LCR</i>	0.06	0.14	0.61	0.19
<i>ATTO680</i>	0.02	0.08	0.08	0.82

**Table 4-19: Measured relative spectral distribution from five fluorophores constituting Wire03-02 onto four detector channels.**

In a second approach, the fluorescence emission spectra of each fluorophore was multiplied with the transmission curves of the detectors (see section 3.1 and figure 3-5, 3-6). Spectrally separated detection patterns for the fluorophores discussed in this section are depicted in figure 4-21.

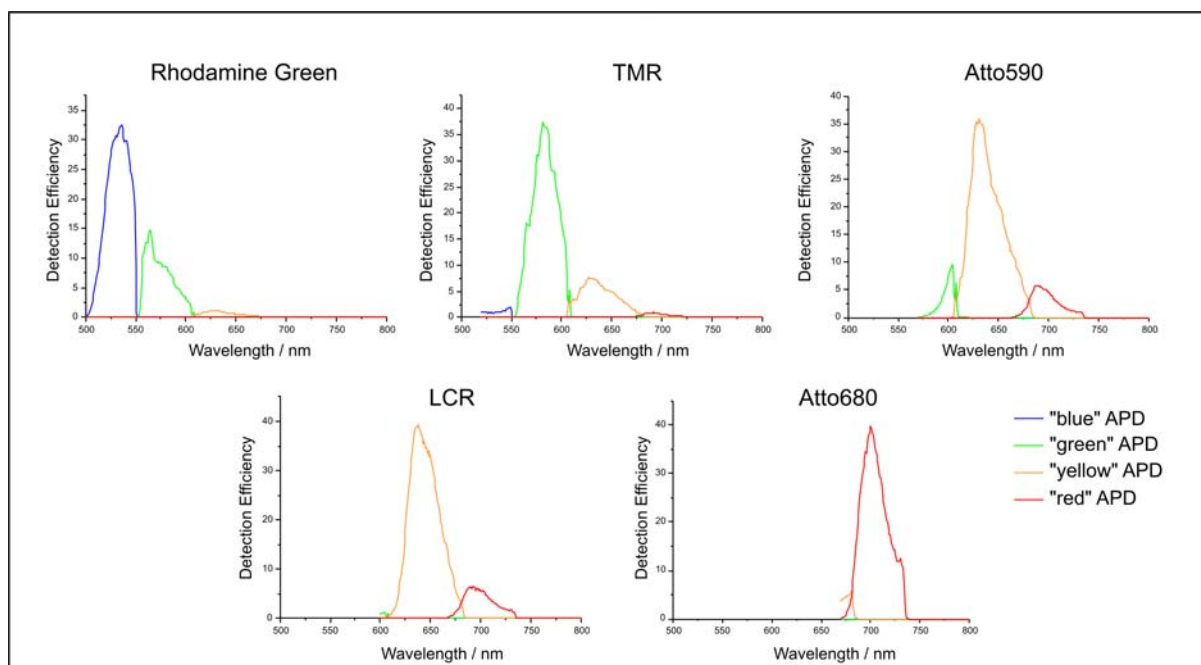


**Figure 4-21: Calculated distributions of fluorescence spectra on the four detector channels from five fluorophores constituting the sample Wire03-02, i.e. Rhodamine Green, TMR, ATTO590, LCR and ATTO680.**

After integration and normalization of the calculated patterns, theoretical spectral distributions are derived. Values are listed in table 4-20.

	Blue	Green	Yellow	Red
<i>RhG</i>	0.68	0.28	0.03	0.00
<i>TMR</i>	0.02	0.75	0.21	0.02
<i>ATTO590</i>	0.00	0.07	0.82	0.11
<i>LCR</i>	0.00	0.01	0.86	0.14
<i>ATTO680</i>	0.00	0.00	0.05	0.95

**Table 4-20: Relative spectral distribution (calculated) from five fluorophores constituting Wire03-02 onto four detector channels.**

Differences between the measured and calculated spectral distributions do appear, if tables 4-19 and 4-20 are compared. This should be viewed from the point that measured values are obtained using a configured set-up, whereas calculated values were obtained from individual absorption and emission spectra of set-up components, e.g. filters and dichroic beamsplitters, together with the quantum efficiency of an APD. Sources of error that are to be mentioned are the polarization dependence of transmission properties from dichroic beamsplitters, small deviations from a perfect geometrical arrangement of all four detectors or possible optical aberrations along the detection pathway.

In the following sections, all spectral considerations used in the interpretation of single-molecule data are based on the measured distributions of fluorescence.

#### 4.3.2. PHOTONIC WIRES ADSORBED ON DRY GLASS SUBSTRATE

First single-molecule measurements of photonic wire compounds were realized at a glass-air surface [Heilemann et al., 2004]. Sample molecules were randomly adsorbed on a dried glass surface and scanned. To provide intensity scan images with more information, the spectral characteristics of emitted photons is displayed in scan images as false colour code. This is realized by assigning a colour bit, i.e. blue, green, yellow or red, to a certain x,y-position and calculate a colour value by weighting the intensity of each channel. As a result, a false colour byte is obtained and allows for a first impression from which unit of a photonic wire a photon originates. Since four detector channels are used, the representation as false colour image is ambiguous. In its classical use, false colour information is created using red, green and blue (RGB) colour bits, resulting in the combination of colours yellow, magenta and cyan (see figure 4-22). If yellow is used as fourth colour and independently, additional combination colours do appear. Nevertheless, this method is applied for a first visualization of the spectral distribution of fluorescence data, and exact evaluation requires a

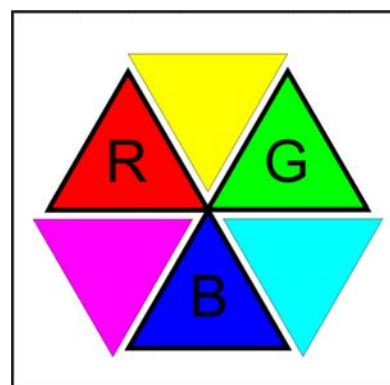


**Figure 4-22: RGB scheme to produce false colours. A mixture of red, green and blue yields white.**

closer look.

An exemplary scan image is shown in figure 4-23. The magnification of two individual spots gives a nice impression of the usefulness of false colour images in multichromophoric systems, revealing photophysical reactions of photonic wire molecules which occur on a millisecond timescale.

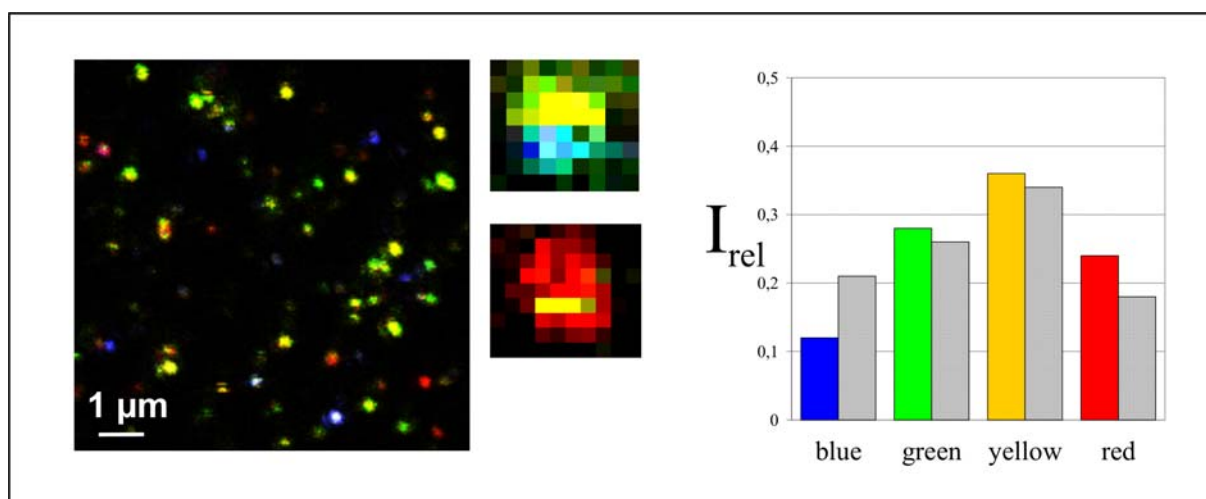


**Figure 4-23:** 10x10 μm scan image of Wire03-02, represented as false colour image (2 ms integration time, 10 – 100 counts / 2 ms). The sample is composed of the fluorophores Rhodamine Green, TMR, ATTO590, LightCycler Red, ATTO680. Two magnified spots show spectral dynamics. The histogram on the right side compares the theoretical spectral distribution of the sample derived from ensemble spectroscopy (grey columns) to single molecule data, derived from about 200 photonic wire spots.

As indicated in figure 4-23, the majority of fluorescence spots is dominated by the emission of one of the five chromophores. Besides unfavourable conformations and competing quenching pathways, premature photobleaching of chromophores can as well substantially control the observed EET pathways and efficiencies. On the other hand, about 10% of all photonic wires show predominately emission on the red channel, that is, highly efficient (up to 90%) multistep EET across 13.6 nm. Single spots are often heterogeneous due to photobleaching or due to reversible photophysical and chemical reactions.

To better characterise spectral properties of fluorescence emission and compare single-molecule results to ensemble measurements, ~200 fluorescence spots were chosen and histogrammed according to their individual spectral pattern (see figure 4-23, coloured bars in histogram). In a second step, an ensemble fluorescence emission spectrum of a  $10^{-7}$  M solution of the photonic wire was taken to derive the

spectral ensemble pattern on four detectors (grey bars in histogram). With the exception of the blue channel, the histogram corresponds well to the ensemble fluorescence spectrum of the photonic wire.

The deviation found for the blue channel is a result of the lower photostability and a second red-shifted emissive state of the first donor RhG when immobilized on dry glass surface. About 60-70% of the RhG molecules show this red-shifted state before complete photodestruction. These observations for RhG are summarized in figure 4-24. Part (A) shows the normalized absorption and fluorescence emission spectrum of

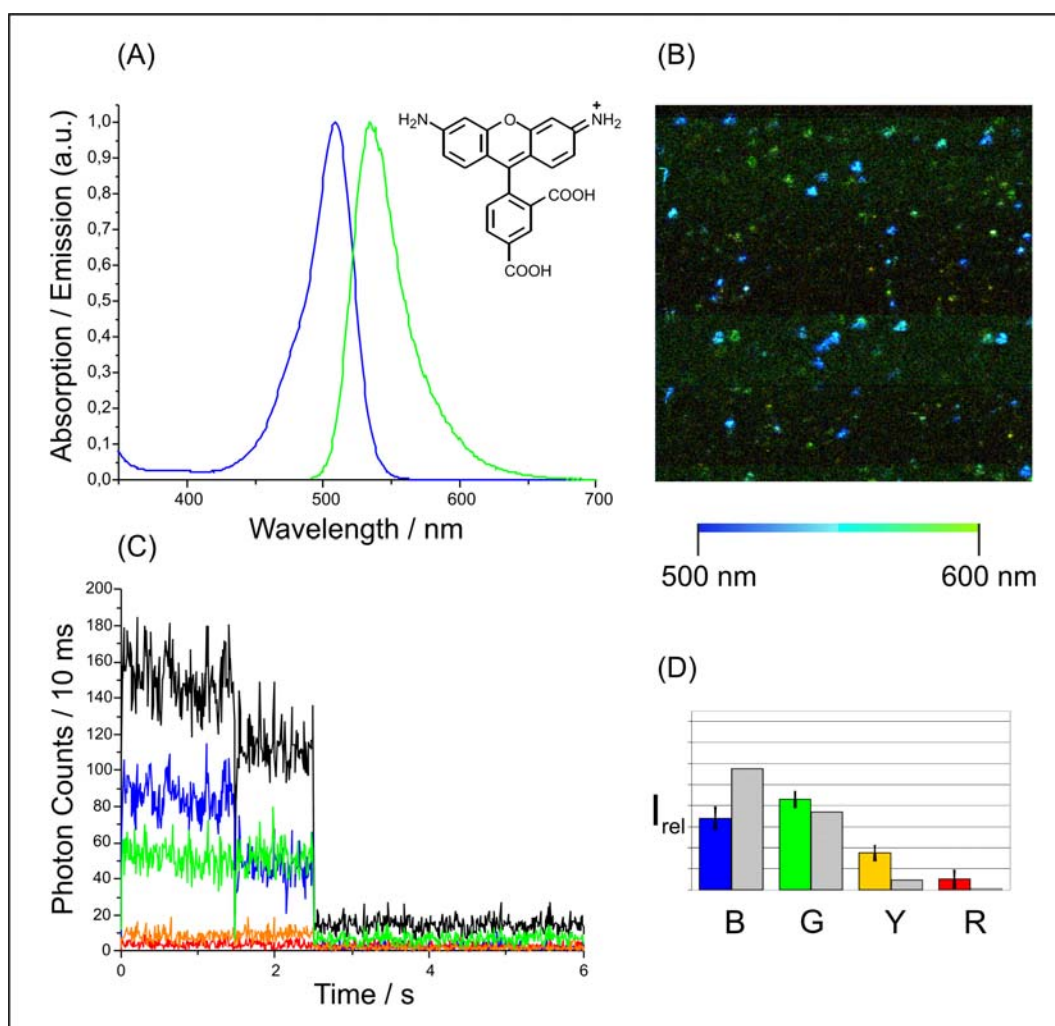


**Figure 4-24:** (A) Ensemble absorption and emission spectra of RhG labelled oligonucleotides, (B) False colour fluorescence intensity image ( $20 \times 20 \mu\text{m}^2$ ) of RhG labelled oligonucleotides adsorbed on dry glass surface (488 nm excitation, 50 nm/pixel, 2 ms integration time, 5-60 counts/2 ms). (C) Fluorescence intensity trajectory of an individual RhG labelled oligonucleotide measured on the four spectrally separated APDs ( $3 \text{ kW/cm}^2$  average excitation intensity at 488 nm). (D) Spectral distribution histogram of individual RhG fluorescence spots (coloured bars) compared to ensemble pattern (grey bars).

a  $10^{-6}$  M solution of RhG in PBS, exhibiting a maximum at 509 nm and 534 nm, respectively. However, if absorbed onto a glass surface, an important fraction shows red-shifted emission, demonstrated in the false colour scan image ( $15 \times 15 \mu\text{m}^2$ ) in figure 4-24, (B). An exemplary fluorescence trajectory affirms this observation ((C), figure 4-24): while the spectral pattern of emission during the first  $\sim 1.5$  s matches the ensemble emission spectrum, a spectral shift towards longer emission wavelengths is observed before photobleaching at  $\sim 2.5$  s. To quantify this observation and compare the spectral behaviour of RhG in ensemble and single-molecule measurements performed on dry glass, a similar spectral pattern as in figure 4-23 was elaborated, shown in figure 4-24 (D). The histogram reflects the tendency of red-shifted fluorescence observed for single RhG molecules adsorbed randomly on dried glass in a nice way. Interestingly, this behaviour was not observed for single RhG molecules immobilized under aqueous conditions (see 4.3.3).

Better insight into dynamic behaviour can be obtained from fluorescence trajectories of individual photonic wires. The subpopulation of wires that initially emits predominately on the red channel exhibits up to five successive photobleaching events. Sequential photobleaching accompanied by a shift in the emission spectrum from the red back toward the blue confirms that the energy is transferred stepwise among the chromophores, that is, subsequent unidirectional four-step EET [Heilemann et al., 2004]. An exemplary fluorescence trajectory exhibiting all five steps is depicted in figure 4-25. The spectral information provided by fluorescence photons is integrated for each emission step (see histograms in figure 4-25, coloured bars) and compared to the single fluorophore's spectral signature derived previously (see section 4.3.1; grey bars in histograms).

According to these patterns, five regions with different spectral characteristics can be retrieved from the four different fluorescence intensity trajectories (figure 4-25). The first 0.4 s of the trajectory (part 1) are dominated by the emission of the far-red chromophore ATTO680. Here, the transfer efficiency reaches a value of  $\sim 90\%$ . After photobleaching of the final acceptor, the fluorescence emission is dominated by LCR (part 2) followed by ATTO590 (part 3), TMR (part 4), and finally Rhodamine Green (part 5). Overall, five subsequent photobleaching events can be uncovered. Comparison of the intensity patterns measured (colour columns) to the ones expected for the different chromophores (grey columns) demonstrates that the fluorescence emission is dominated by one chromophore at all times. Small

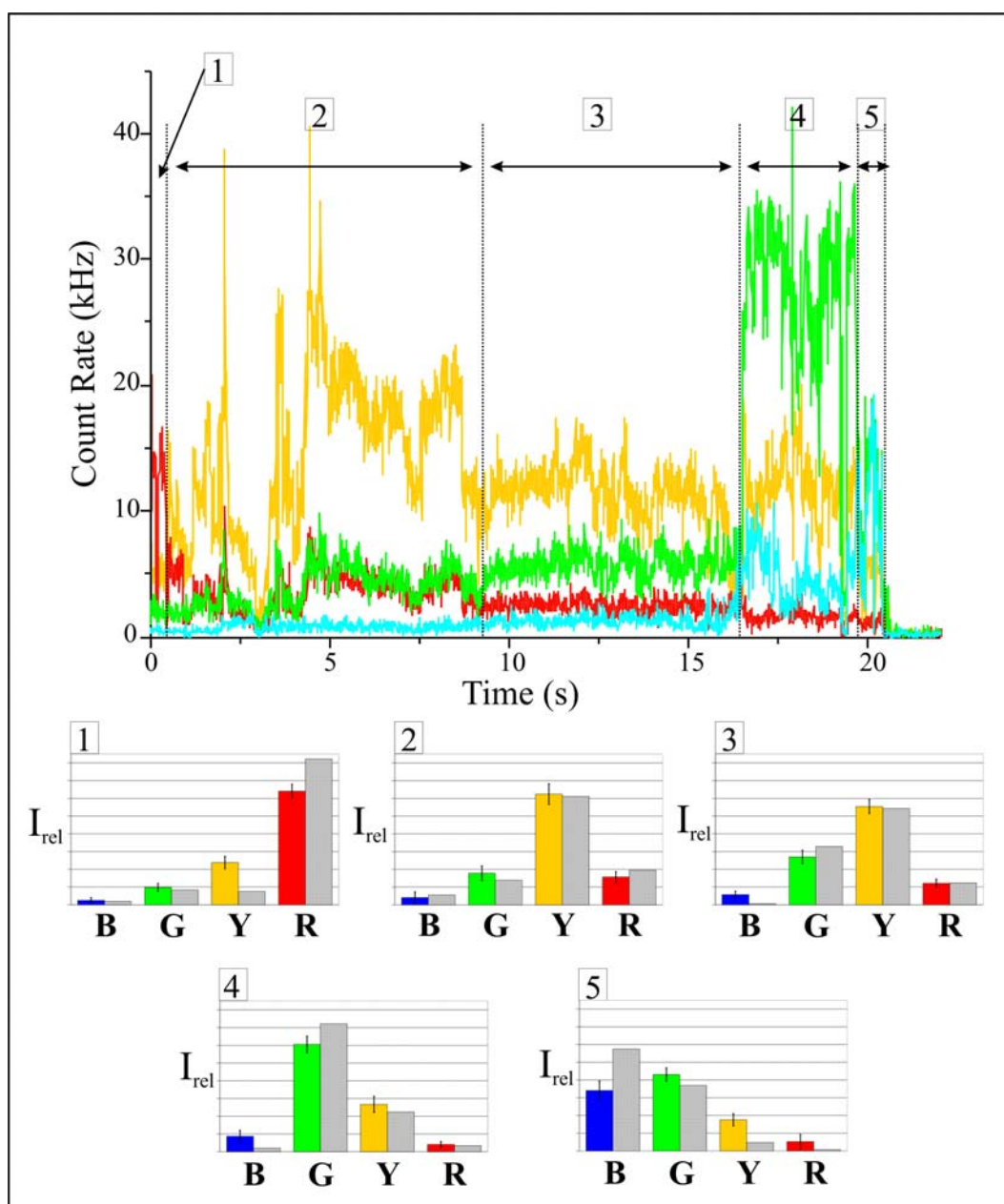


**Figure 4-25:** Fluorescence intensity trajectory of an individual photonic wire measured on the four spectrally separated APDs ( $3 \text{ kW/cm}^2$  average excitation intensity at 488 nm). Five different emission patterns can be observed indicating that subsequent photobleaching of the chromophores starting with ATTO680 (part 1) occurred. In the lower part, intensity patterns (colour columns) measured for the five different parts are compared to those measured for singly labelled oligonucleotides (grey columns).

deviations, e.g., those observed for part 1 in figure 4-25, indicate less efficient energy transfer between some chromophores, i.e., a leakage of the wire, possibly induced by unfavourable orientations of some fluorophores.

Many trajectories, however, exhibit a more complex photophysical behaviour and do not show five successive photobleaching events. The trajectory of the photonic wire

shown in figure 4-26 (A), for example, initially exhibits efficient EET to the final acceptor ATTO680 with an efficiency of  $\sim 70\%$ . Further on, the trajectory is characterised by collective off-states of the whole wire and fluctuations in EET efficiency along the wire. Collective off-states have frequently been observed in multi-chromophoric systems and are ascribed to quenching of the fluorescence by nonfluorescent traps such as, for example, triplet states or radical ions.[Yu et al., 2000; Tinnefeld et al., 2003; Hofkens et al., 2000; Vosch et al., 2003].

It is interesting to note that the collective off-states, which are most likely caused by traps located on the final acceptor ATTO680, exhibit a higher quenching efficiency for the other fluorophores than for the active ATTO680. In addition, the fluorescence of the wire does not cease by successive bleaching events but some bleaching steps are lacking (e.g., the part dominated by TMR emission at about 5.8 s is missing, figure 4-26 (A)).

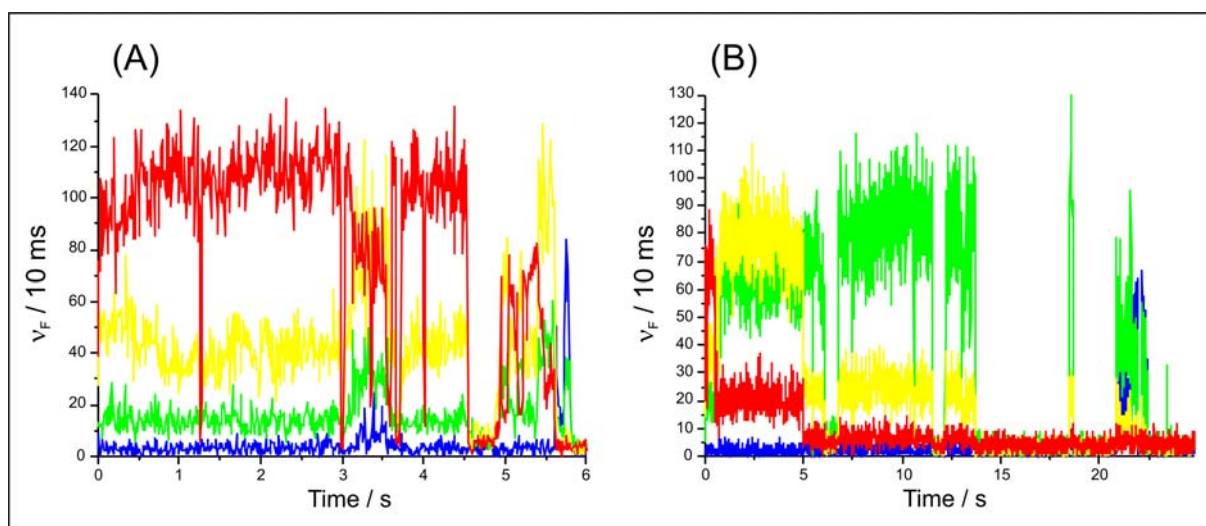


**Figure 4-26: Fluorescence trajectories (fluorescence photons,  $v_F$ , in 10 ms versus time in seconds) of two photonic wire. Photophysical dynamics beyond bleaching of the chromophores are evident.**

As another example, the fluorescence trajectory (B) in figure 4-26 starts with emission from ATTO680, but misses the next step and directly shows a spectral pattern which resembles a mixed signature from ATTO590 and TMR. After a long “off”-period, fluorescence from TMR is recovered and finally followed by Rhodamine Green.

The complex behaviour of the photonic wires is not necessarily surprising as the photophysics and photochemistry of the wire do not have to represent the sum of the behaviour of the individual chromophores; for example, EET in the weak coulombic regime is not restricted to the nonradiative transfer of energy from a donor in the excited state to a ground-state acceptor. Transfer processes that are allowed within the FÖRSTER formalism are those for which there are no changes in electron spin in the acceptor transition. Hence, the transfer of excitation energy from a chromophore residing in the first excited singlet state to another chromophore residing either in the triplet or in an excited singlet state are possible and competitive energy-transfer pathways, which have far-reaching impact on the photophysics and photochemistry of multichromophoric systems, such as enhanced intersystem crossing and reduced photostability [Hofkens et al., 2003; Tinnefeld et al., 2004].

#### **4.3.3. PHOTONIC WIRES IMMOBILIZED IN AQUEOUS SOLUTION**

An improved approach to try to control the enormous inhomogeneous broadening observed in single-molecule measurements of artificial photonic wire molecules was realized by immobilization photonic wires onto a coated glass surface under aqueous conditions (see 3.3.2). Samples that are denoted Wire04-xx were equipped with a biotin linker and allowed binding onto a streptavidin coated surface under aqueous conditions. Photonic wires were predominantly constructed using rhodamines (Rhodamine Green, TMR, ATTO590) and carborhodamines (ATTO647) in reductive environment by adding around 100  $\mu\text{l}$  of 1 M solution of MEA. As discussed previously, this treatment reduces “off”-times and enhances photostability of this class of fluorophores and allows longer observation times. Since long-wavelength fluorophores with rhodamine-like structure are not available for conjugation chemistry, final acceptor dyes were carbocyanines (Cy5.5), oxazines (ATTO680) or carbopyronines (ATTO725, ATTO740). Scan images from six different photonic wires are portrayed in figure 4-27.

The left image in the upper row of figure 4-27 shows a  $8 \times 8 \mu\text{m}^2$  false colour scan from Wire04-01, which only contains one fluorophore, Rhodamine Green. The whole image demonstrate a higher homogeneity than observed on glass (see 4.3.2), which is explained by a very similar environment for each fluorophore. It can be noted that

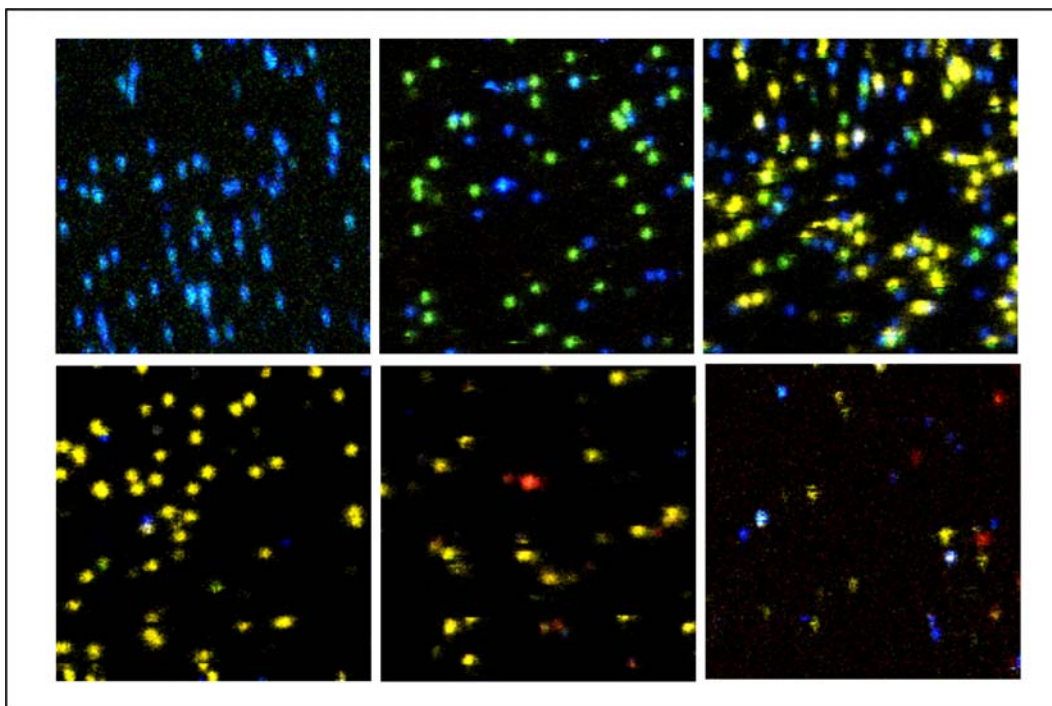


**Figure 4-27: 8  $\mu\text{m}$  x 8  $\mu\text{m}$  false colour scan images of photonic wire compounds immobilized in PBS buffer with MEA added (excitation wavelength 488 nm, integration time 2 ms/pixel, intensity 20 – 200 counts/2 ms). Upper row: Wire 04-01, Wire04-02, Wire04-03, lower row: Wire04-09, Wire04-10, Wire04-11.**

no spectral shifts of fluorescence are observed, as previously discussed when the fluorophore is adsorbed on dry glass. The second image and the third image in figure 4-27 represent false colour scan images of Wire04-02 and Wire04-03, respectively. The false colour information allows in both images to distinguish between the final emitting fluorophore, which is either RhG, TMR or ATTO590. In the lower row, scan images of the samples Wire04-09, Wire04-10 and Wire04-11 are shown.

Due to the higher homogeneity observed in aqueous solution, fluorescence emission of single photonic wires is analysed by fractional intensity distributions. The spectral information which is encoded in the false colour images can be extracted by calculating the fractional intensity for each pixel which is above a certain threshold and belongs to a PSF of a molecule. The fractional intensity for different spectral signatures is hereby expressed as

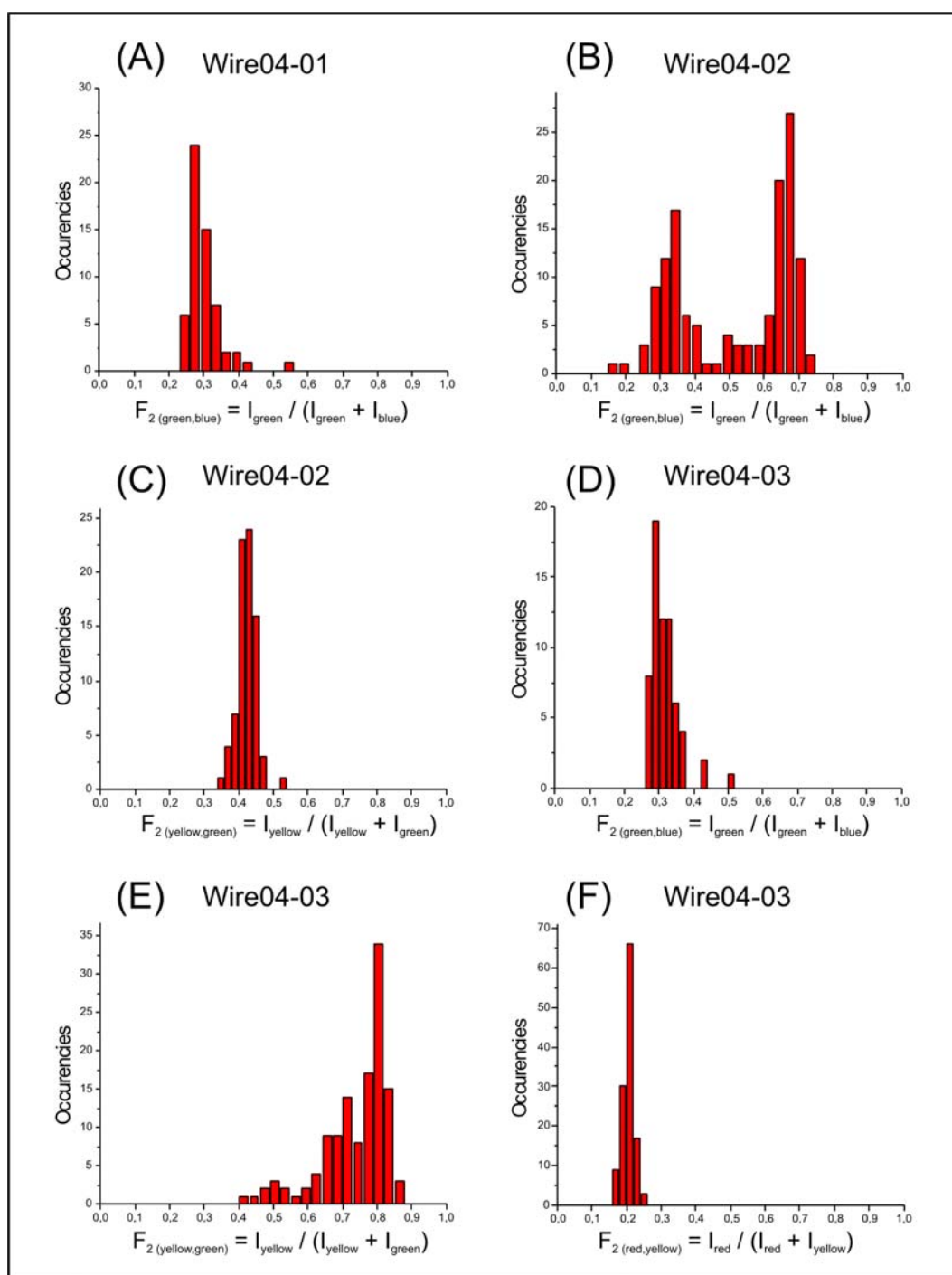
$$F_{2(\text{green,blue})} = \frac{I_{\text{green}}}{I_{\text{green}} + I_{\text{blue}}} \quad ( 4-4 )$$

$$F_{2(\text{yellow,green})} = \frac{I_{\text{yellow}}}{I_{\text{yellow}} + I_{\text{green}}} \quad ( 4-5 )$$

$$F_{2(\text{red,yellow})} = \frac{I_{\text{red}}}{I_{\text{red}} + I_{\text{yellow}}} \quad ( 4-6 )$$

If we assume that a fluorophore predominantly emits on two detector channels, each fluorophore gets a signature by at least one of these values which allows to discriminate between different emitters.

Histograms for fractional intensities obtained for Wire04-01 , Wire 04-02 and Wire04-03 are depicted in figure 4-28 and were calculated from 100-300 individual fluorescence spots each. To derive characteristic values for each fluorophore, the mean value of the distribution was determined. Any symmetric fit function, e.g. Gaussian or Lorentzian functions, is not suitable, since the definition of fractional intensities is naturally asymmetric. For Wire04-01 (image (A) in figure 4-28), a small spectral pattern for Rhodamine Green as single emitter in this construct is observed, characterized by a mean value of  $F_{2(\text{green, blue})} = 0.30$ . In the case of Wire04-02, which is constituted of two fluorophores, Rhodamine Green and TMR, the same signature is observed for the donor dye, and the acceptor shows a well separate distribution with a mean value of  $F_{2(\text{green, blue})} = 0.67$  (image (B) in figure 4-28). Additionally, the fractional intensity of the yellow and green channel yields a value of  $F_{2(\text{yellow, green})} = 0.42$  (image C). Adding one more fluorophore for Wire04-03, the fractional intensity exhibits the previously determined value for Rhodamine Green on the green and blue channel (image D), but shows a broader distribution for  $F_{2(\text{yellow, green})}$ , which is a combination of ATTO590 and TMR (image E). The last emitter of this compound can be identified in the histogram of  $F_{2(\text{red, yellow})}$  with a mean value of 0.21. Altogether, fractional intensities calculated from intensities of two neighbouring spectral channels allow to assign the principal emitting unit to a fluorophore of a photonic wire. Furthermore, the histograms exhibit a certain homogeneity and a poor influence of photophysical processes, as compared to scan images derived from wires adsorbed on dry glass substrate.



**4-28: Fractional intensities for different detector channels calculated for Wire 04-01 (A), Wire04-02 (B and C) and Wire 04-03 (D-E). Spectral distributions allow to discriminate the emitting species in a photonic wire.**

Fractional intensity analysis discussed above for the fluorophores RhG, TMR and ATTO590 was extended to two more fluorophores, ATTO647 and Cy5.5. Mean values of distributions are summarized in table 4-21.

	$F_2$ (green, blue)	$F_2$ (yellow, green)	$F_2$ (red, yellow)
<i>RhG</i>	0.30	-	-
<i>TMR</i>	0.67	0.42	-
<i>ATTO590</i>	-	0.65	0.21
<i>ATTO647</i>	-	0.81	0.33
<i>Cy5.5</i>	-	-	0.61

**Table 4-21: Fractional intensities derived from different combinations of detector channels characterize five fluorophores contributing to Wire04-10 in aqueous solution.**

This method allows to differentiate between spectral emission patterns of single photonic wire samples observed under aqueous conditions. Nevertheless, a few comments are necessary for a better understanding. First, a contribution of TMR onto the blue detector channel cannot be understood from the emission spectrum of TMR, but is a measure of lower FRET efficiency frequently detected in the FRET-pair RhG-TMR. This issue was discussed in section 4.1.6 with fractional intensities determined from fluorescence trajectories of single FRET-pairs. It was found that a value of  $F_2$  (green, blue) = 0.70 equals an energy transfer efficiency of ~80%, which is affirmed by the spot statistic which is based on data analysis in table 4-21. Similarly, emission from the last fluorophore Cy5.5 is expected to occur on the “red” detector channel only. Contrary to this assumption, a value of  $F_2$  (red, yellow) = 0.61 was observed. This fact suggests less efficient energy transfer from the fourth dye to the fifth dye, ATTO647 to Cy5.5. It is to mention that quantum efficiencies are the main reason for this observation, which differ in both fluorophores, with values of 0.65 and 0.28 respectively. Nevertheless, the last energy transfer step exhibits a lower transfer efficiency, but reliable values can not be obtained by this method and will be derived from time-resolved single-molecule trajectories later.

#### 4.3.4. BUILDING-UP SINGLE PHOTONIC WIRE MOLECULES ON A SURFACE

In the last section, the positive effect of changing measurement conditions on single-molecule experiments was demonstrated. Inhomogeneous broadening of fluorescence properties are reduced dramatically by measuring in aqueous solution. A further step towards increased homogeneity and long observation times was made by working with rhodamine dyes in reductive environment. A glaring example can be found if single-molecule experiments with RhG performed on dried glass (section 4.3.2) and in aqueous solution (section 4.3.3) are compared.

Besides reducing inhomogeneous broadening of single fluorophores, it is desirable to have a strategy for a selective construction of multichromophoric molecules, with reduced chemical heterogeneity. Still, hybridisation of single strands at the ensemble level yields many subpopulations, as can be seen in the scan images shown in figure 4-27. There are several reasons that can be thought of, starting with concentration errors, difficulties in hybridising such a complex system out of chemically modified oligonucleotides, or a chemical equilibrium between different species. To circumvent these chemical heterogeneities, a method of “forced hybridisation” directly at the single-molecule level was elaborated.

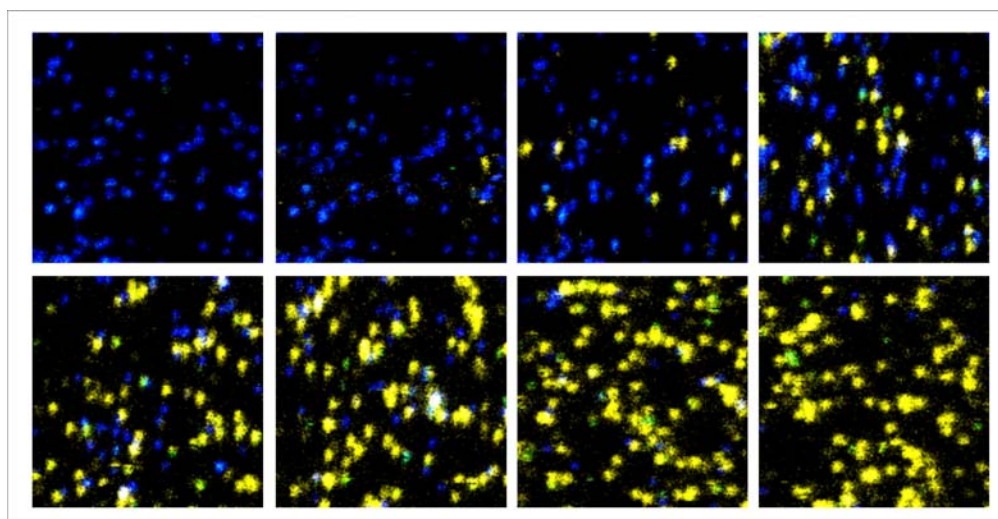


**Figure 4-29: Sequence of scan images ( $8 \times 8 \mu\text{m}^2$ ,  $2 \text{ kW/cm}^2$ ,  $50 \text{ nm}$  pixelsize and  $2 \text{ ms/pixel}$  integration time) of a surface with Rhodamine Green labelled to ss60bp DNA in PBS/MEA. After the first scan image, a  $10^{-8} \text{ M}$  solution of a complementary ss20bp DNA labelled with TMR and ATTO590 was added. Fluorescence was recorded on three detector channels.**

In single-molecule hybridisation experiments, a streptavidin coated surface was treated with a solution of single-stranded DNA labelled with Rhodamine Green at its 5'-end and carrying a biotin anchor at its 3'-end. In a next step, the solution was washed off and replaced by a second solution, containing the first antisense sequence of 20bp length with a concentration of  $\sim 10^{-8}$  M, labelled with both TMR and ATTO590. By constantly scanning the surface with relatively low excitation power (which prevents photobleaching of Rhodamine Green dyes), the first binding events occurred after a few minutes, distinguishable by the appearance of energy transfer. Since both fluorophores TMR and ATTO590 are attached to the same oligonucleotide, fluorescence emission is mainly observed from ATTO590, i.e. detected on the "yellow" detector. A sequence of eight scan  $8 \times 8 \mu\text{m}^2$  scan images visualises this process in figure 4-29.

The scan images shown in figure 4-29 were taken every two minutes and show a considerable process of hybridisation of the antisense oligonucleotide to the single stranded DNA previously attached to the surface. This process is driven by the diffusion of the antisense oligonucleotide. Already in the third image, 10 molecules out of  $\sim 60$  molecules exhibit photon emission in the "yellow" detector, a tendency which continues in the following images until nearly all surface-bound oligonucleotides are hybridised. Eventually, emission is detected on the "blue" channel, but most molecules exhibit efficient energy transfer from the first chromophore RhG via TMR to ATTO590. As previously mentioned, hybridisation at the single-molecule in the way it was demonstrated is a forced process. This can be visualized by a few numbers. If we assume a typical single-molecule density of one molecule per square micrometer and observe a volume cube of  $10 \times 10 \times 10 \mu\text{m}^3$ , this cube contains 100 molecules immobilized at the surface. In the total volume of the cube (which equals  $10^{-12}$  l), we will find  $\sim 6000$  molecules from the antisense oligonucleotide. These oligonucleotides in the solution need 10 to 100 ms to diffuse randomly through the volume of the cube. If an appropriate binding site is in range, the very efficient process of hybridisation can occur, but contrary to equal concentrations in ensemble hybridisation, a possible interaction between oligonucleotides can occur many times until appropriate conditions lead to final hybridisation.

Furthermore, hybridisation of four and five chromophores was demonstrated. Adding the second single stranded oligonucleotide labelled with ATTO647 showed a similar

hybridisation efficiency, as shown in figure 4-30 (C). To better distinguish the spectrally near emitting fluorophores ATTO590 (see scan image (A) in figure 4-30)

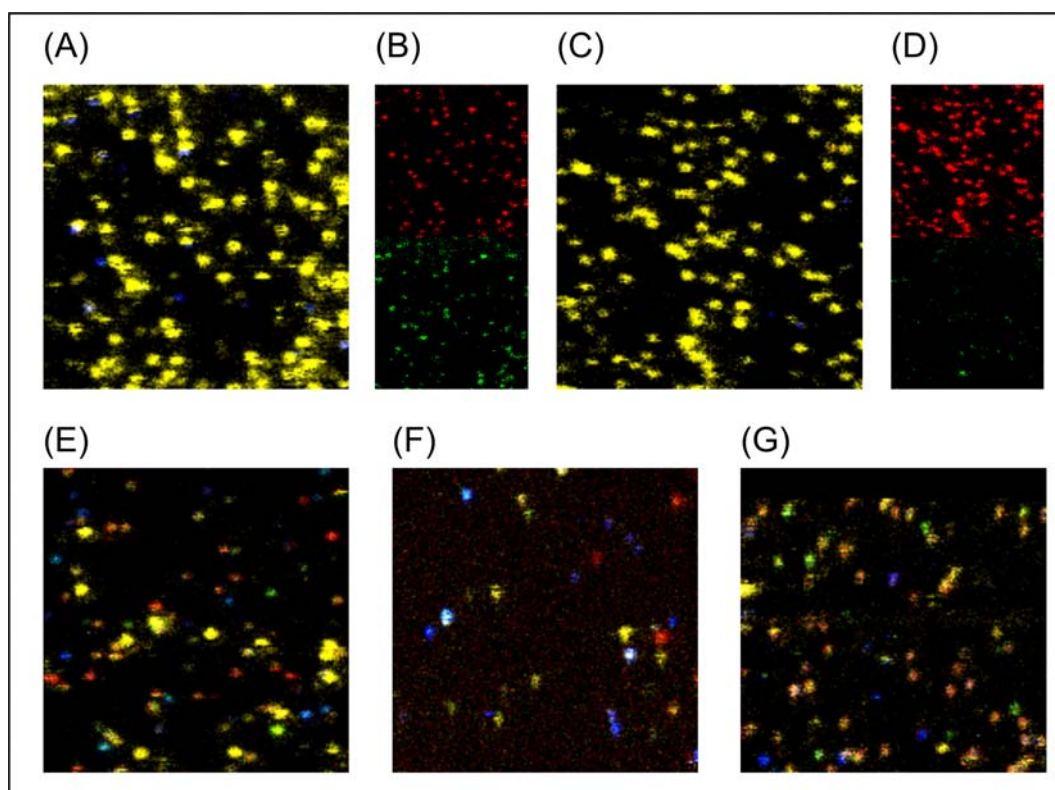


**Figure 4-30: 8x8  $\mu\text{m}^2$  scan images of surface-hybridized photonic wires. Samples Wire04-03 (A) together with spectrally-resolved emission on “red” and “green” channel (B), Wire04-09 (C) with spectrally-resolved emission in (D). Five-dyes containing photonic wires shown are Wire04-10 (E), Wire04-11 (F) and Wire04-9C (G).**

and ATTO647, the spectrally separated images of the “red” and the “green” channel are presented for each scan image (see (B) and (D) in figure 4-30), showing a higher contribution on the “red” channel for ATTO647. Less efficiency is observed for the third antisense oligonucleotide, in dependence of the fluorophore used. Scan images of Wire04-10 (scan image (E) in figure 4-35, Cy5.5 as final emitter), Wire04-11 ((F), ATTO725 as final emitter) and Wire04-9C ((G), ATTO680) demonstrate this observation for different fluorophores. In the case of Wire04-11, the reduced density of “red” spots (e.g. with respect to Wire 04-10) is explained by a poor photostability of far-red emitting fluorophores ATTO725 (a similar observation was made for ATTO740). A relatively high intensity of red-emitting species in the scan image of Wire04-9C was achieved by incubating a surface with a higher-concentrated solution ( $10^{-7}$  M) over night. At this point, one must consider the influence of fluorophores on

DNA-hybridisation: one of the conspicuous effects of multiple labelling of DNA oligonucleotides is the degree to which it lowers the melting temperature,  $T_m$ . The source of this destabilization was demonstrated to arise from dye–dye and dye–nucleotide interactions [Waggoner and Randolph, 1997] (dye-dye interactions were observed for cyanine dyes in distances of 6 nucleobases and can be neglected for photonic wires in this work).

In this passage, it could be demonstrated that online DNA-hybridisation of short oligonucleotide sequences can be exploited for the construction of photonic wires with up to five fluorophores at the single-molecule level. A higher chemical homogeneity can be achieved, and a hindered hybridisation step of the third antisense oligonucleotide is observed.

#### **4.3.5. TIME-RESOLVED SINGLE-MOLECULE SPECTROSCOPY OF PHOTONIC WIRES**

The mere detection of spectrally-resolved fluorescence of multichromophoric photonic wire samples relies on spectral changes observed, which consecutively are assigned to a change of the emitting unit in a photonic wire. In many cases, this observation is valid, but some scenarios can not be resolved. There can be, on the one hand, spectral jumps of one chromophore, but also inefficient energy transfer and fluorescence of two fluorophores simultaneously, which could exhibit a similar spectral signature as a single fluorophore in the energy cascade. To resolve these phenomena and contribute to a further characterization of these complex samples, time-resolved experiments at the single-molecule were realized. Set-ups used for experiments are described in chapter 3.1.1. Experiments at 476 nm excitation were performed on dried glass, whereas experiments at 488 nm were performed in aqueous solution (for surface preparation, see 3.3.2).

#### **Time-Resolved Single-Molecule Experiments of Photonic Wires Adsorbed on Dry Glass Substrates**

For investigation on dried glass substrate, Wire04-06 was chosen, constituted of the chromophores Rhodamine Green, TMR, ATTO590, LCR and ATTO680 (for

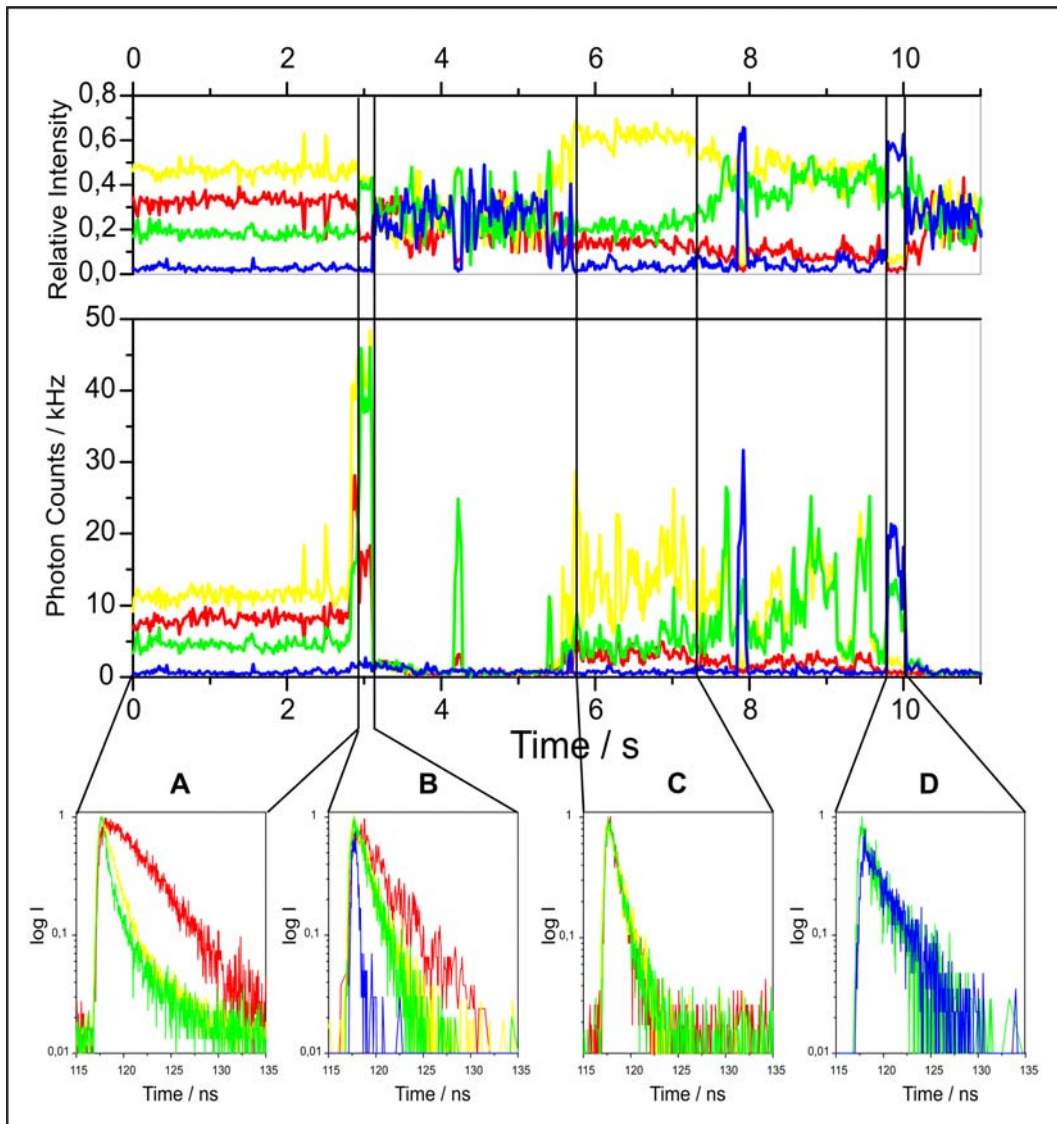


**Figure 4-31: Fluorescence trajectory with relative intensities recorded from a single photonic wire (Wire04-06). Fluorescence decays for four different parts of the trajectory, A-D, are shown below.**

fluorescence properties see table 4-9; ATTO620 was replaced by LCR, but exhibits spectrally similar properties).

An exemplary fluorescence trajectory of this photonic wire sample which was chosen because of additional information not available in previous experiments is shown in figure 4-31. For more clarity, relative intensities of each detector channel are added above the trajectory in figure 4-31, i.e. the fluorescence detected on each channel normalized to the overall emission. This approach is a little different to fractional intensities used so far (see 4.3.3), but offers an easier way to determine fluorescence changes (this method is often used under the name of “proximity values” [Clamme and Deniz, 2004]). The practical importance can be seen after ~3 s in the trajectory,

where a sudden increase in fluorescence is observed, but no spectral change is observed in relative spectral intensities. The fluorescence trajectory was further separated into four sections (according to regions which do exhibit different spectral signatures), named A to D, and fluorescence decays recorded at the different detector channels are shown in figure 4-31. Fluorescence lifetimes obtained from decays are listed in table 4-22.

	“blue”	“green”	“yellow”	“red”
A	-	4.0 ns/1.1 ns	4.0 ns/1.1 ns	4.0 ns
B	< 0.3 ns	1.4 ns	3.2 ns/1.5 ns	3.2 ns
C	-	1.0 ns	1.1 ns	1.0 ns
D	2.8 ns	2.9 ns	-	-

**Table 4-22: Spectrally-resolved fluorescence lifetimes from the trajectory in figure 4-31.**

The mere look on the spectral pattern of fluorescence intensity in the first section (A) suggests a predominant emission from the fourth dye, LCR (see spectral pattern in section 4.3.1). Fluorescence lifetime implies another interpretation: a well pronounced rise time is observed on the “red” detector, and fluorescence on both “green” and “yellow” channel are strongly quenched (1.1 ns), but still exhibit a component of 4.0 ns, which is the lifetime of both ATTO590 and LCR. In the next short period (B), relative intensities change, and the spectral pattern with equal intensity on the “green” and “yellow” channel could suggest emission of both ATTO590 and TMR. Again, fluorescence lifetime draws a different picture: a lifetime of 1.4 ns and 1.5 ns observed for decays of the “green” and “yellow” detectors suggest an efficient energy transfer from ATTO590 towards the last emitter, ATTO680. Emission of LCR can be excluded, since a much more pronounced contribution of 3.2 ns should be observed on the “yellow” detector. Part (C) shows the typical intensity pattern observed for ATTO590 on dry glass, and lifetime measurements supply the additional information of a quenched state of this fluorophore. This could be either due to an absorbing and nonfluorescent fluorophore, e.g. ATTO680, or due to quenching by guanosine residues neighbouring

the dye. The last part (D) shows the emission pattern of green-shifted Rhodamine Green (see 4.3.2), accompanied by a weak quenching.

Beyond the previous discussion of fluorescence lifetimes observed on different detector channels, a distributional analysis applying a deconvolution procedure and using multiexponential fits was made, using custom-made software (LabView, National Instruments, USA)). The method is very similar to the one described for time-resolved ensemble-spectroscopy (see section 3.3.2), and uses the IRF of each separate detector (see 3.1.2). Finally, energy transfer efficiencies for each of the four steps along the photonic wire can be calculated, and results for parts A-D in figure 4-31 are summarized in table 4-23.

	$E_1$	$E_2$	$E_3$	$E_4$
A	0.99	0.99	0.74	0.43
B	0.99	0.99	0.19	0.83
C	0.99	0.99	0	0
D	0	-	-	-

**Table 4-23: Energy transfer efficiencies for each of the four transfer steps of different parts of the fluorescence trajectory in figure 4-31.**

Values listed in table 4-23 complete the picture drawn in a first description: in part (A) of the trajectory, the first two steps exhibit highest energy transfer efficiencies, whereas values decrease for the third and fourth step. In (B), no efficient transfer towards LCR is observed, whereas still strong energy transfer towards ATTO680 occurs (at this point, it can be assumed that LCR is photobleached, and that the fourth rate describes the energy transfer from the third dye to the last one). Part (C) shows emission of ATTO590 predominantly, although a strong quenching is observed, and part (D) shows no contribution to any energy transfer rate, i.e. Rhodamine Green is finally the single emitter.

To verify lifetime calculations and interpretations made above, the relative contributions of each fluorophore can be summed up to obtain a spectral pattern, which again can be compared to the spectral intensity pattern observed in the trajectory (see table 4-24).

	“blue”	“green”	“yellow”	“red”
A	0.02/0.06	0.18/0.18	0.47/0.41	0.32/0.36
B	0.02/0.02	0.40/0.29	0.42/0.46	0.16/0.23
C	0.03 / 0.04	0.22/0.32	0.61/0.51	0.13/0.13
D	0.55/0.58	0.36/0.37	0.07/0.05	0.02/0.01

**Table 4-24: Relative intensities for each detector for parts A-D of the fluorescence trajectory in figure 4-31, observed/calculated values.**

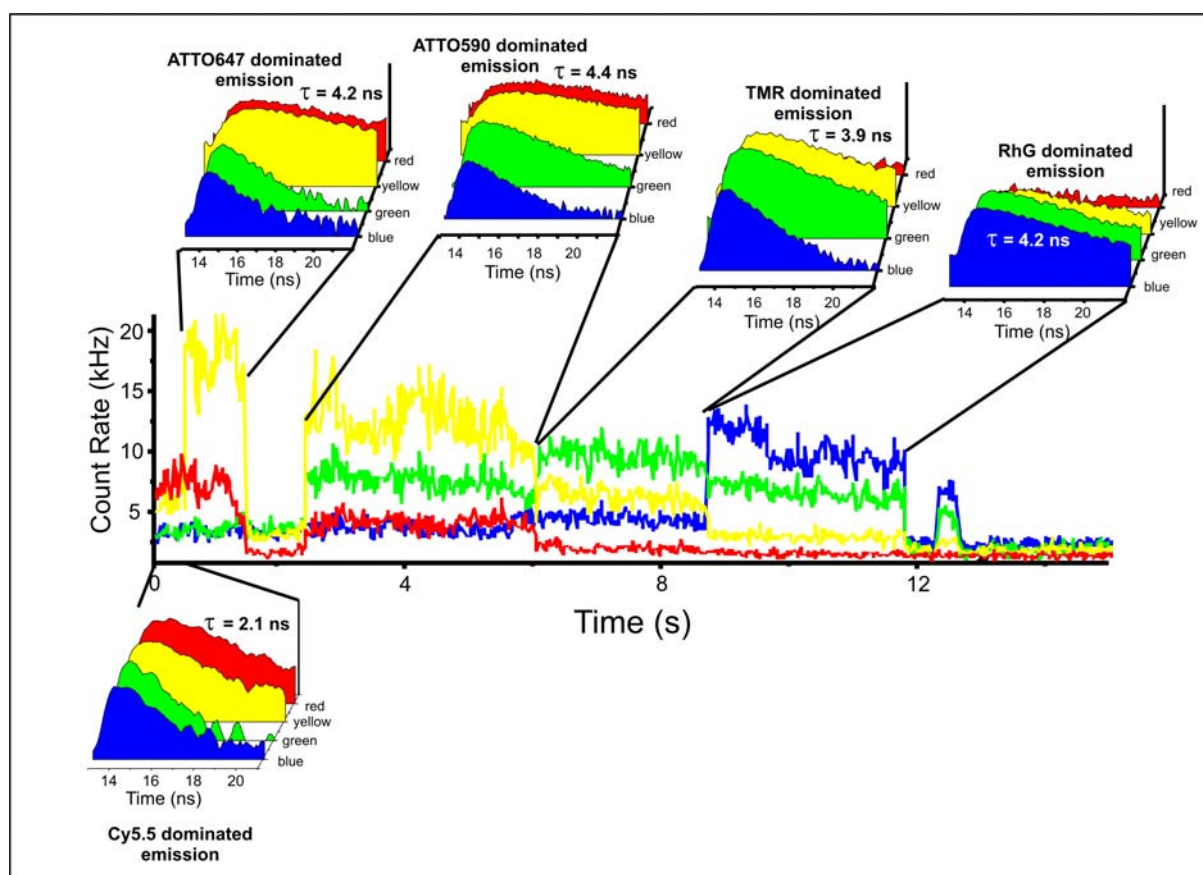
Values in table 4-24 represent one linear combination of single fluorophores which was obtained by pure lifetime analysis. A good accordance to measured intensities can be stated from these results.

The important information obtained in this section can be summarized as follows: a constant spectral pattern of a single photonic wire observed cannot necessarily be explained by only one linear combination of spectral patterns from single fluorophores. Insufficient energy transfer steps cannot be resolved, and a “leak” in the chain of transmitting units (as observed for LCR in the previous discussion) may lead to false interpretations. Time-resolved analysis can unravel fluorescence data and contribute to an improved understanding of the functionality of such complex optical devices.

### **Time-Resolved Single-Molecule Experiments of Photonic Wires Immobilized in Solution**

Similar experiments were performed with photonic wire samples immobilized in solution (see 4.3.3) using a mode-locked titan sapphire laser, operating at 488 nm with a repetition rate of 80.77 MHz (see 3.1; the identical set of filters and beamsplitters was used as for continuous wave excitation, see 4.3.1).

A fluorescence trajectory of Wire04-10 is presented in figure 4-32. The sample is constituted of the chromophores Rhodamine Green, TMR, ATTO590, ATTO647 and Cy5.5, which allows a better identification of the last fluorophore by fluorescence lifetime (a value of ~1 ns is observed for the free dye, whereas bound to DNA, the



4-32: Fluorescence trajectory of a single Wire04-10. The trajectory exhibits a signature of sequential photobleaching from the last acceptor Cy5.5 over ATTO647, ATTO590, TMR and finally Rhodamine Green. Decays for five representative regions are shown and confirm the interpretation derived from spectral signatures of fluorescent dyes.

fluorescence lifetime increases to  $\sim 1.5$  ns). For stability reasons, single-molecule measurements were performed in PBS/MEA (see 4.1.2-4.1.5; rhodamine derivatives and carborhodamines yield higher photon counts, and carbocyanine dyes are not affected in their fluorescence properties if observed in reductive environment).

The fluorescence trajectory represents an example for a rarely observed (and also not expected event) of sequential photobleaching of a photonic wire: five well-distinguishable levels of emission can be discriminated already by a mere look on the spectral characteristics of emission. The first 1.1 s of the trajectory show emission on the red channel. This observation is supported by a significant rise time appearing on the “red” channel, together with a fluorescence lifetime of 2.1 ns. A slightly longer lifetime of 2.3 ns is observed on the “yellow” channel, indicating that this step only transfers a part of the energy. Both “blue” and “green” channel are characterized by strong quenching caused by energy transfer, exhibiting a lifetime of  $\sim 1.2$  ns. In the

second step, fluorescence emission is dominated by ATTO647 (4.2 ns for both “yellow” and “red”). Due to a higher quantum yield of ATTO647 (~0.65) compared to the previous emitter Cy5.5 (0.28), an increase in total intensity is observed. Between ~2 s and ~3 s, a collective “off” period is observed on the “yellow” and “green” channel, but still photons are detected on the “blue” and “green” detector (1.3 ns). Therefore, a fluorescent trap of either ATTO647 or ATTO590 can be postulated, still absorbing but not exhibiting fluorescence anymore. Fluorescence is recovered at ~3 s with the spectral and temporal signature of ATTO590, followed at ~6 s by TMR and at ~9 s by Rhodamine Green. Interestingly, fluorescence emission is still observed after ~13 s for Rhodamine Green with a similar fluorescence lifetime of ~4 ns. A summary of fluorescence lifetimes of various parts of the trajectory in figure 4-32 is given in table 4-25.

<i>Time / s</i>	“blue”	“green”	“yellow”	“red”
<i>0.00-1.05</i>	1.4 ns	1.2 ns	2.3 ns	2.1 ns
<i>1.05-2.10</i>	1.3 ns	1.3 ns	4.2 ns	4.2 ns
<i>2.10-3.00</i>	1.3 ns	1.3 ns	-	-
<i>3.00-6.50</i>	1.5 ns	2.3 ns	4.4 ns	4.2 ns
<i>6.50-9.00</i>	1.8 ns	3.9 ns	4.1 ns	-
<i>9.00-12.25</i>	4.2 ns	3.4 ns	-	-
<i>12.25-end</i>	4.0 ns	3.8 ns		

**Table 4-25: Fluorescence lifetimes for each detector channel determined from the fluorescence trajectory in figure 4-32.**

Due to a broader instrument response function exhibiting a “tail” (see section 3.1.1), the method of deconvolution could not be used. Mathematical fits did not lead to a satisfactory convergence, and energy transfer efficiencies could not be determined in a similar way. Nevertheless, the information won at this point is the occurrence of collective “off” states, whereas still quenched emission from the first (and eventually second?) fluorophore is observed. Energy transfer efficiencies with a carbocyanine dye as last emitter of a photonic wire make it possible to determine energy transfer efficiencies easier due to a shorter lifetime. This is especially important for the last

energy transfer step, which has proven to be the weakest in many experiments (compare to paragraph 4.3.2, 4.3.3, and the beginning of this section). In the exemplary trajectory of figure 4-32, the transfer efficiency of the last step can be estimated by the change in lifetime of ATTO647, serving as the donor for Cy5.5, and yields a value of  $E_4 = 1 - (2.3 \text{ ns}/4.2 \text{ ns}) = 0.45$ . Furthermore, more than one intensity level (but equal spectral patterns) are observed for Rhodamine Green, which merit a more detailed analysis of this fluorophore by an extended technique in the following section.

#### **4.3.6. POLARIZED EXCITATION OF THE INPUT UNIT RHODAMINE GREEN**

If we think about the structural organization of a photonic wire sample, many possible configurations and conformations might be possible. These are of great importance for the energy transfer method chosen for the design of these compounds in this work, i.e FRET, since the absolute orientation and the mobility of a fluorophore has a major influence on transfer efficiencies (see 2.1.2). The ideal case of  $\kappa^2 = 2/3$  for randomly orientated and diffusing molecules might therefore be an assumption which fails in some cases.

To elucidate the structural mobility of Rhodamine Green, the polarization of the 488 nm excitation light source (TiSaph, see 3.1 and 3.1.1) was modulated regularly using an electrooptical modulator (EOM, Linos, USA). Photon absorption occurs preferentially if the orientation of the electric field vector of light is parallel to the absorption dipole moment of the chromophoric unit of a fluorophore (see 1.1.1). If a fluorophore is freely rotating, no modulation should be observed, whereas a immobile fluorophore should show modulation in fluorescence. Experiments were carried out with Rhodamine Green bound to DNA and immobilized in water (see 4.1.5). Excitation light modulation was done with a frequency of 20 Hz. Fluorescence trajectories from single Rhodamine Green molecules are shown in figure 4-33.

In part (A) of figure 4-33, a fluorescence trajectory with two steps in intensity is shown, recorded from one single fluorophore. A magnified view at the transition between both intensity levels portrays the rotational mobility. In both parts of the trajectory, fluorescence emission follows the modulation of the polarization, which indicates hindered rotation of the molecule. Two different fluorescence lifetimes are

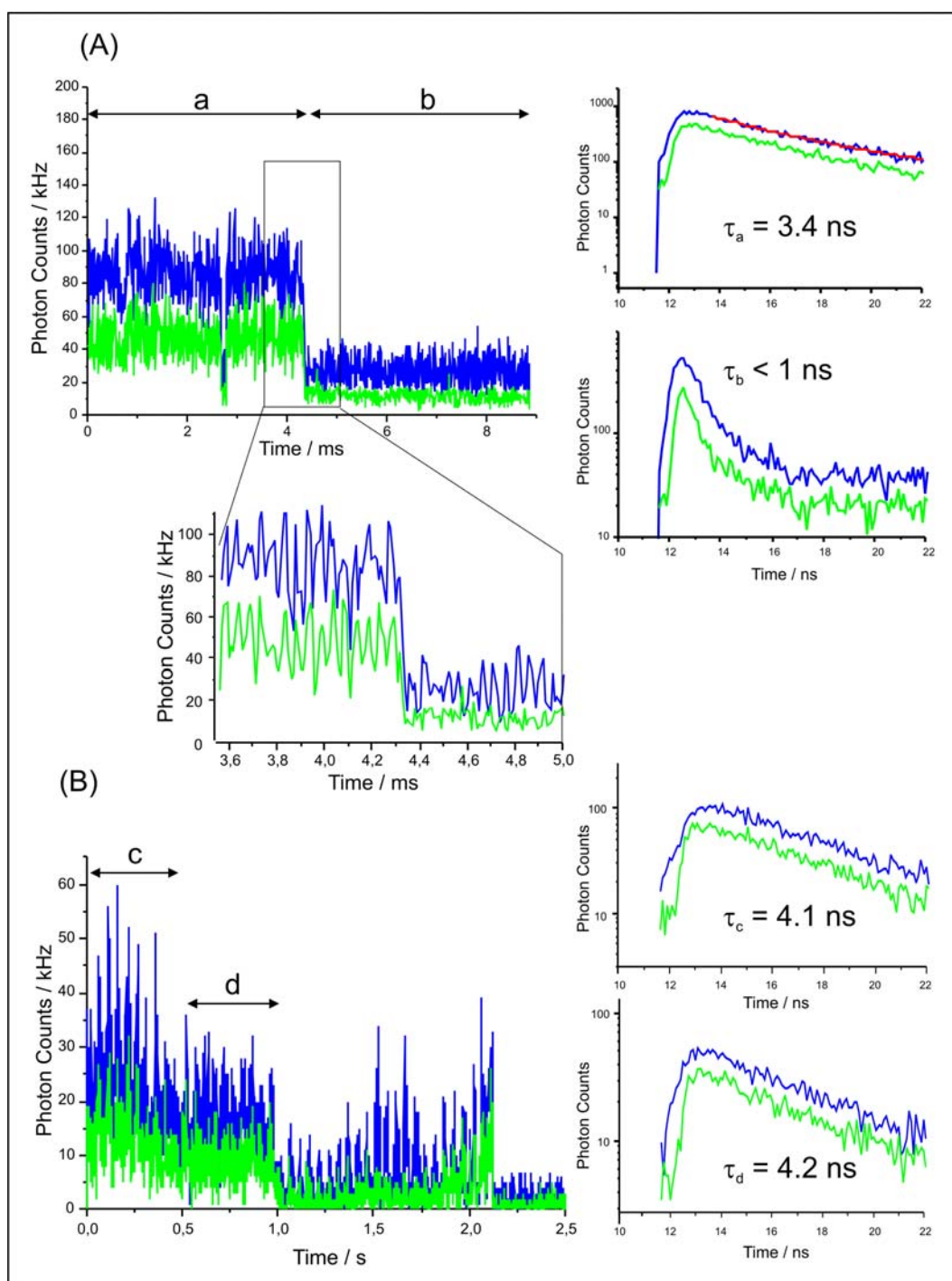


**Figure 4-33: Single-molecule trajectories of two Rhodamine Green molecules derived by modulation of the polarization of the excitation light. Both molecules exhibit different degrees of rotational mobility. Fluorescence decays of assigned parts a-d of the trajectories are shown for each fluorophore.**

observed, i.e. 3.4 ns in the part a (0 – 4.2 s) and a strongly-quenched lifetime of below 1 ns in part b (which cannot be resolved further due to pronounced broadening of the IRF, see 3.1.1 and 4.3.5).

Different to the first trajectory, the second one shown in part (B) of figure 4-33 shows many levels of rotational mobility in one single fluorophore: during the first 0.5 s of observation time, the fluorophore exhibits fluctuations in fluorescence intensity according to the modulation frequency of the excitation light. This is followed by a period of 0.5 s which exhibits nearly no modulation, indicating a freely rotating dye. Fluorescence lifetime in both cases is very similar, values of 4.1 ns (part c) and 4.2 ns (part d) are determined. From a time of 1 s on, an even stronger modulation of fluorescence is observed until the fluorophore goes into a state with substantially lowered quantum yield of fluorescence (~2.1 s).

A similar observation of changing fluorescence lifetimes and quantum yields was made for the dye TMR [Eggeling et al., 1998b]. Accordingly, three different states for Rhodamine Green bound to DNA can be postulated, which are:

- (1) A freely-rotating fluorophore (no modulation, lifetime of 4.2 ns)
- (2) Hindered rotation and high quantum yield (modulation of fluorescence, but similar lifetime of ~4 ns)
- (3) Hindered rotation and strongly quenched intensity (modulation of fluorescence and quenched lifetime down to ~1 ns)

States with hindered rotation can be attributed to interactions of the fluorophore with nucleobases (state (2)) and possible quenching reactions, e.g. with the guanosine residue at position 4 (state (3), compare to figure 4-14 in section 4.2.1 for the DNA sequence of the single-stranded 60bp oligonucleotide).

These different structural configurations observed for Rhodamine Green complicate the understanding of the working principle of photonic wires. The orientation of a fluorophore which is part of an energy transfer cascade is crucial for transfer efficiencies, and certainly the assumption of freely rotating fluorophores cannot be held. On the other hand, single-molecule experiments can refine the understanding from steady-state experiments (section 4.2.2 and 4.2.3) and explain lower energy transfer efficiencies observed for the first step in photonic wires.

#### **4.4. Carbocyanine Dyes as Optical Single-Molecule Switch**

Single-molecule fluorescence experiments have revealed several expected and unexpected photophysical phenomena of the carbocyanine dye Cy5 such as *cis-trans* isomerisation, “off”-states additional to triplet formation, and complex photobleaching pathways including nonfluorescent intermediates that still absorb light in the visible range [Widengren and Schwille, 2000; Ha et al., 1999; Tinnefeld et al., 2003; Ha and Xu, 2003]. Beyond the characterisation of fluorescence intermittencies observed for Cy5 which were presented earlier (see section 4.1.2), the photophysical characteristics of this fluorophore represent a pivot point for extended studies. At least three intermediate states towards photobleaching were discovered [Ha and Xu, 2003], and it was one focus of this work to further investigate the complex photodestruction pathway and to influence it by optical means. Transitions into such intermediate states offer a possibility to use conventional fluorophores as single molecule switches, presumed that the transition is reversible.

In general, controlled on/off switching of the fluorescence of a single chromophore at room temperature affords the introduction of a controllable and highly efficient competing quenching pathway that prevents emission from the excited singlet state of the chromophore via, for example, excitation energy transfer or photoinduced electron transfer. Switching might be accomplished by light-induced deactivation of the quencher or changes in the chromophore/quencher interaction geometry [Liang et al., 2003]. More recently, the first room temperature single-molecule photoswitch based on optical switching of the transfer efficiency in a FRET-pair was published [Irie et al., 2002; Fukaminato et al., 2004]. In a two-colour experiment, it was demonstrated that a donor chromophore (bis(phenylethynyl)anthracene) connected to a switchable quenching unit (a diarylethene derivative) could be switched on and off by 488- and 325-nm light, respectively. UV light was used to activate the quencher (energy transfer acceptor), while 488-nm light was used for deactivation of the quenching unit and probing of the fluorescence of the donor chromophore. The use of identical wavelengths (488 nm) for probing and switching was possible because the deactivation (isomerisation) is about 1000 times less efficient than the

activation of the quenching unit. Thus, probing and isomerisation can be controlled by changing the excitation light intensity.

#### 4.4.1. SWITCHING OF SINGLE CY5 MOLECULES IMMOBILIZED IN SOLUTION

To probe intermediate states of individual Cy5 molecules, oxygen has to be removed efficiently, since irreversible photooxidation would be the consequence. As presented in section 4.1.2, the observation time of an individual carbocyanine prior to photodestruction is relatively short and makes further studies of intermediate states impossible. To eventually change the chemical environment and reduce inhomogeneous broadening, carbocyanine derivatives Cy5 or Alexa 647 (Molecular Probes, USA) were thus coupled covalently to double-stranded biotinylated DNA and immobilized on surface under aqueous conditions. A dual-laser set-up with two excitation wavelengths was used for two-colour excitation of single molecules, i.e. 488 nm and 632.8 nm supplied by an argon ion laser and a helium-neon laser, respectively (see 3.1.3). Fluorescence light was split onto two detectors using a dichroic beamsplitter (680DRLP) and two bandpass filters (675DF50, 700DF75).

A series of scan images recorded from individual Cy5-molecules in PBS with 100 mM MEA is shown in figure 4-34.

First, a fluorescence image was recorded exciting the sample at 633 nm to verify the presence of single immobilized labeled dsDNA molecules (figure 4-34, A). Depending on the excitation intensity, most molecules were found in a nonfluorescent state after

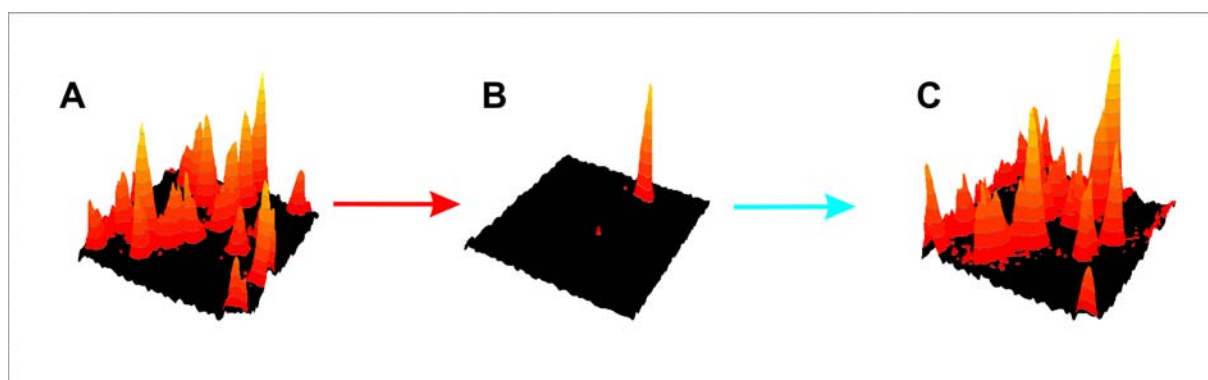


**Figure 4-34: Series of fluorescence scan images demonstrating the principle of optical switching of Cy5-molecules. Image A was recorded at 633 nm and led to an important reduction of fluorescent molecules B. After scanning the same surface with 488 nm, fluorescence of most molecules is recovered, demonstrated in the scan image C.**

the first image scan (figure 4-34, B). After the same area was scanned with 488-nm laser light under otherwise identical conditions, the fluorescent state was recovered, as shown in figure 4-34, C.

Selection of a single Cy5 molecule in an image scan and monitoring its fluorescence with time under alternating or simultaneous 488- and 633-nm excitation enables the investigation of the switching behaviour in more detail. Figure 4-35 A shows a fluorescence intensity trajectory of a single Cy5 labelled dsDNA molecule continuously excited at 633 nm. After about 500 ms, the fluorescence ceased and did not recover for 5 s of 633-nm laser irradiation. The bright state could, however, be reproducibly recovered within a few hundred milliseconds by simultaneous irradiation at 488 nm (after 5 s in the trajectory of figure 4-35, A). Subsequently, driven by simultaneous irradiation at 488 and 633 nm, the molecule switches between a

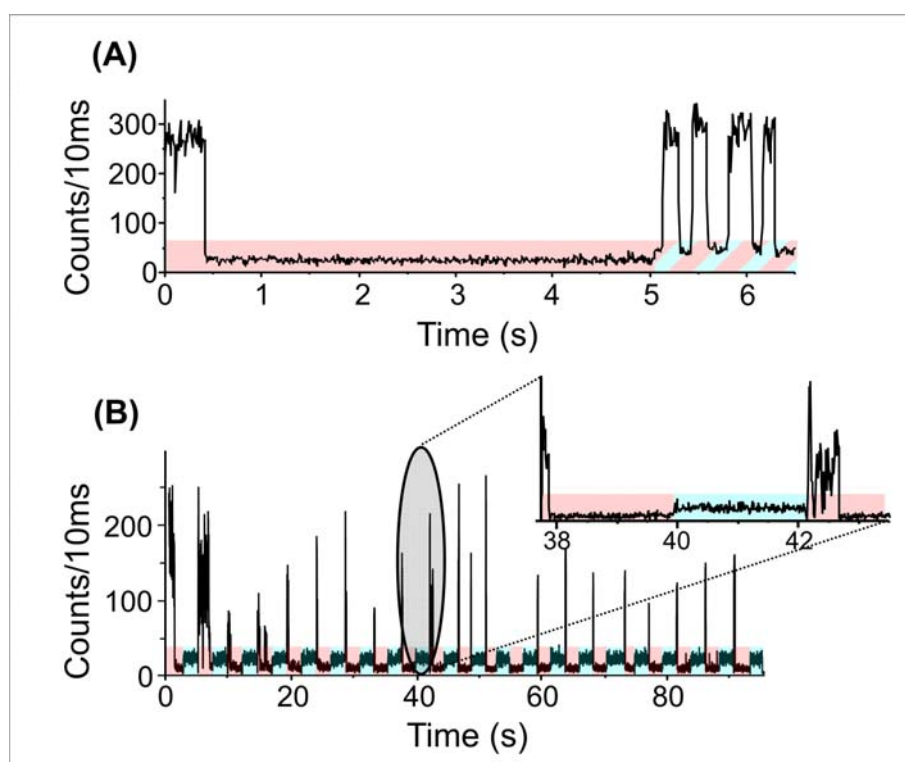


**Figure 4-35:** (A) Fluorescence trajectory of a single Cy5-labeled dsDNA molecule in deaerated PBS, pH 7.4. During the first 5 s, the sample was irradiated at 633 nm with an excitation intensity of 14 kW/cm<sup>2</sup>. After ~500 ms, the fluorescence of the molecule disappeared and did not recover. At 5 s, the molecule was irradiated simultaneously at 488 nm with equal intensity (14 kW/cm<sup>2</sup>). Subsequently, the fluorescence recovered and ceased in an alternating fashion. (B) Reversible optical switching of a single Cy5 molecule. The molecule was irradiated at 633 nm until fluorescence ceased (generally within 1 to 2 s) and then recovered by irradiation at 488 nm for 2.5 s. The underlaid colour indicates the excitation wavelength (blue: 488 nm, red: 633 nm).

fluorescent and nonfluorescent state on a time scale of a few hundred milliseconds.

To demonstrate the applicability of single Cy5 molecules as controllable and reversible optical switches, a single Cy5-labeled dsDNA molecule was irradiated at 633 nm until fluorescence ceased (generally within 1 to 2 s) and then recovered by irradiation at 488 nm for 2.5 s (trajectory (B) in figure 4-35). Out of 21 on/off cycles shown, the fluorescent state of Cy5 could be recovered 20 times upon irradiation at 488 nm with an excitation intensity of 14 kW/cm<sup>2</sup>. Switching failed only once either because irradiation at 488 nm was not sufficient to recover the emissive state or because the time the molecule spent in the fluorescent state was too short to detect a sufficient number of fluorescence photons for an unequivocal discrimination against background signal.

#### **4.4.2. MECHANISTIC STUDIES ON CY5-PHOTOSWITCH**

The efficiency of Cy5 as a photoswitch strongly depends on the buffer conditions used: For best performance, oxygen has to be removed rigorously and a triplet quencher such as MEA has to be added. The need for a triplet quencher also indicates that the triplet state is not involved in the formation of the nonfluorescent switchable state. Under such conditions, more than 100 switching cycles could be achieved for single Cy5 molecules with a reliability of >90%. While the efficiency of switching strongly depends on switching conditions (i.e., oxygen, MEA, and irradiation wavelength), it does not require double-stranded DNA. Both biotinylated Cy5 and Cy5-labeled single-stranded DNA immobilized on BSA/ biotin-streptavidin coated glass substrates could be switched as well with comparable efficiency irradiating either at 488 or at 532 nm. Under dry conditions in the presence of oxygen, however (e.g., adsorbed on bare glass surface), the fluorescent state could not be recovered. Furthermore, switching could also be observed for immobilized Alexa647, a structural related dye which implies that the underlying mechanism constitutes a general feature of certain carbocyanine dyes.

To investigate the nature of the switchable state and the switching mechanism, the photophysics of Cy5 under 633-nm irradiation was compared to the photophysics of Cy5 simultaneously using 633 and 488 nm irradiation. In agreement with Widengren and Schwille and previously presented results for Cy5, autocorrelation of

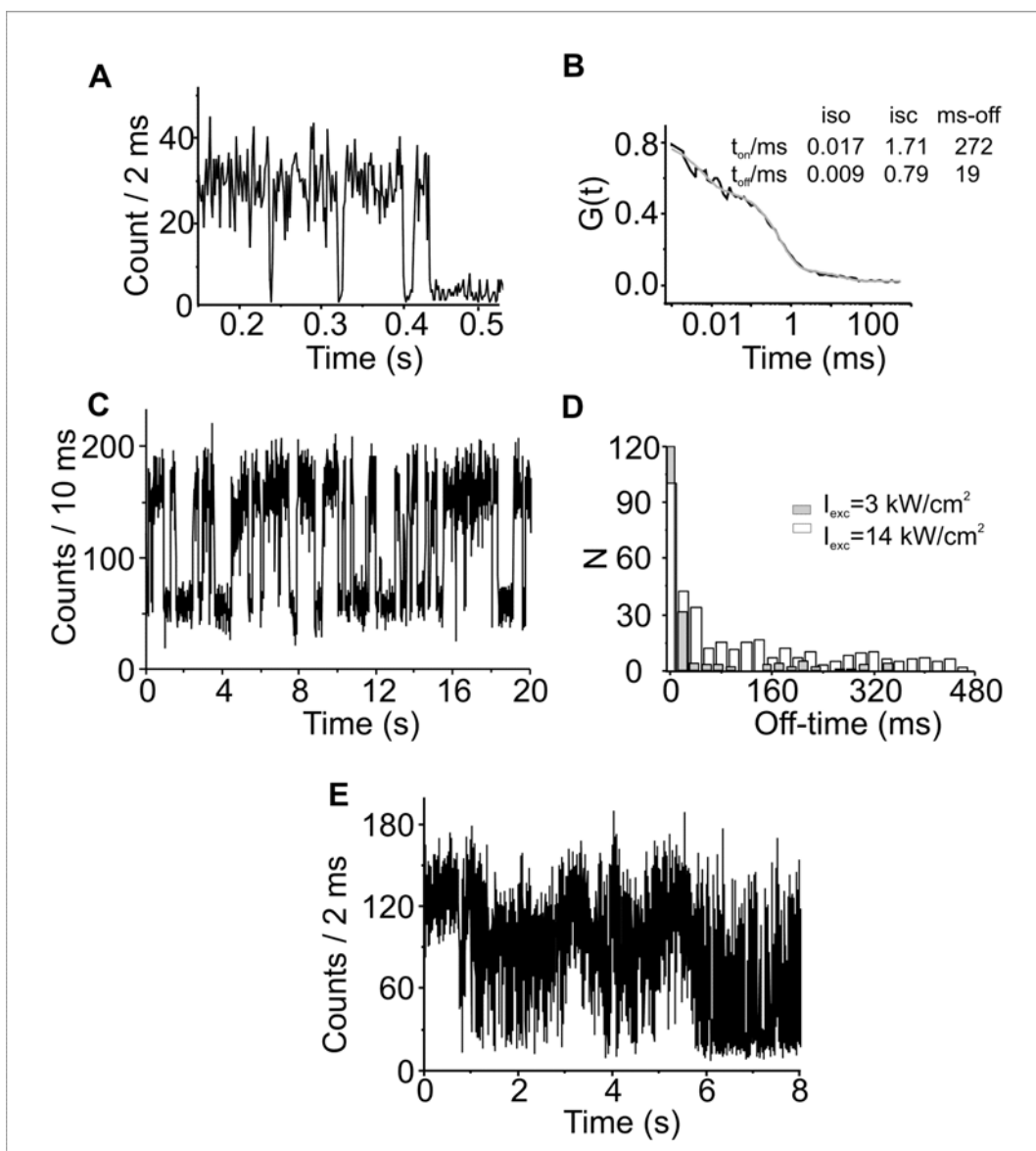


**Figure 4-36:** (A) Fluorescence intensity trajectories of single immobilized Cy5-labeled DNA molecules show additional off states with durations of several milliseconds (oxygen-free PBS without triplet quencher, excitation intensity of 3 kW/cm<sup>2</sup> at 633 nm). (B) Autocorrelation of an intensity trajectory recorded in the absence of a triplet quencher shows “off” states with three distinct time scales: cis-trans isomerisation (iso), triplet states (isc) at reduced oxygen concentration, and an additional off state in the millisecond range. Additionally, a three-exponential fit plus “on” and “off” times for three independent processes is given. (C) Trajectory of a single Cy5-labeled DNA molecule under simultaneous 488- and 633-nm excitation (each with 3 kW/cm<sup>2</sup>), 100 mM of the triplet quencher MEA was added. (D) Off-times histogram of Cy5 trajectories as in (C). (E) In the absence of a triplet quencher and oxygen, Cy5 exhibits dynamic changes in fluorescence intensity and blinking parameters (excitation at 633 nm with 14 kW/cm<sup>2</sup>).

fluorescence intensity trajectories of immobilized Cy5 molecules revealed two components, which can be ascribed to intersystem crossing and *cis-trans*

isomerization [Widengren and Schwille, 2000] In these experiments, oxygen was removed while no triplet quencher was added to separate the time scale of triplet blinking and *cis-trans* isomerisation. Additionally, another off state in the lower millisecond time range (2-20 ms) is visible in the fluorescence intensity trajectory (figure 4-36, A) as well as in the autocorrelation function of immobilized molecules (figure 4-36, B). In the presence of triplet quencher (100 mM MEA) and oxygen scavenger, simultaneous irradiation at 488 and 633 nm produces similar intensity fluctuations and an additional “off” state with a duration of about 200 ms (figure 4-36, C). The additional “off” state in the higher millisecond time scale only appears with simultaneous 488-nm excitation. As a consequence, this long “off” state can be assigned to the photoswitched state. As these rare long “off” times are not well amenable to autocorrelation analysis, “off”-time histograms (figure 4-36, D) were used for closer analysis. The first bins in the histogram of figure 4-36 (D) represent predominantly the shorter millisecond off state. Longer off states show a broad distribution on time scales of up to several seconds. In contrast to the “on” state, which shows a simple power dependence (i.e., independent of 633-nm excitation power), on average 5000 photons could be detected during each “on” time), and the long “off” times show a weak 488-nm excitation power dependence (figure 4-36, D), indicating the presence of an additional intermediate that might be formed thermally. However, the broad distribution of “off” states and also significant differences in the time scale of this “off” state from molecule to molecule suggest that the local environment of the chromophore could play an important role. Although the molecules are immobilized in a way that surface interactions are minimized, temporary interactions of the chromophore with the DNA and proteins used for immobilization cannot be excluded. Evidence that changes in the local environment influence the photophysics of single Cy5 molecules comes from the observation of triplet blinking fluctuations (figure 4-36, E). In the absence of triplet quencher, the observed changes in blinking pattern account for variations in intersystem crossing yield and triplet lifetime, which are caused by varying local oxygen concentration, different interaction geometries with DNA or protein, or other influences of the macromolecules on the chromophore [Köhn et al., 2001].

To further characterise the photophysical properties of the reversible switchable state and to evaluate the implications of photoswitching for common single-molecule FRET experiments, TMR as an energy transfer donor was attached, together with Cy5 to

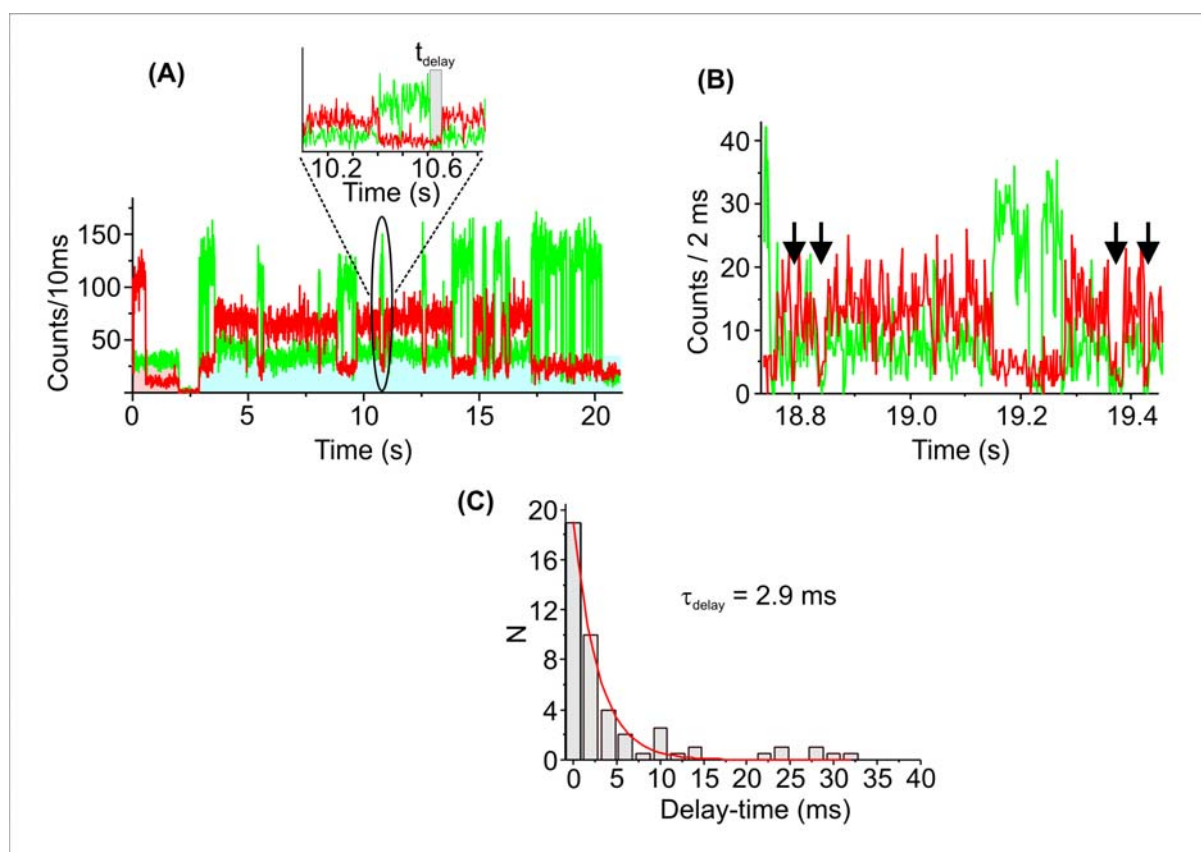


**Figure 4:37: (A,B) Fluorescence trajectories of donor-acceptor (TMR-(N)<sub>10</sub>-Cy5)-labelled dsDNA in PBS/MEA. (A) After preparation of Cy5 in its nonemissive state (irradiation at 633 nm for 2 s), the molecule was excited at 514 (14 kW/cm<sup>2</sup>) starting at 3 s to probe donor emission. Appearance of the donor emission demonstrates that the nonfluorescent state does not quench donor emission. After a few hundred milliseconds, the fluorescent state of the acceptor recovers, thus quenching the donor emission via resonance energy transfer. As expected from the other experiments, Cy5 undergoes several additional transitions to nonfluorescent states during the experiment. The underlayered colour indicates the excitation wavelength (light blue: 514 nm, red: 633 nm). The expanded view of a switching event uncovers the presence of an additional nonfluorescent state of Cy5, which efficiently quenches the donor emission (indicated by  $\tau_{\text{delay}}$ ). (B) The arrows indicate Cy5 off states in the lower millisecond time scale that quench TMR more efficiently than the fluorescent state. (C) Lifetime histogram of  $\tau_{\text{delay}}$ .**

dsDNA. For a separation of  $\sim 3.4$  nm (10 base pairs), strong coupling of donor and acceptor or the formation of ground-state complexes is prevented, and the donor transfers its excited-state energy via nonradiative dipole-dipole interaction efficiently to the acceptor Cy5. Therefore, the donor fluorescence can be advantageously used to report on the photophysical states of the acceptor Cy5. Figure 4-37 (A) shows a fluorescence trajectory recorded from a single double-labelled DNA molecule recorded in standard buffer. During the first few seconds of the experiment, Cy5 was

“prepared” in its nonfluorescent state by 633-nm excitation. Upon changing the excitation wavelength from 633 to 514 nm after  $\sim 3$  s, the donor fluorophore TMR shows strong emission, demonstrating that the absorption of the nonfluorescent state of Cy5 is not in resonance with TMR emission (i.e., it does not absorb in the spectral range of the donor emission between 570 and 650 nm). Hence, no energy transfer occurs. A few hundred milliseconds later, however, the fluorescent state is recovered by 514-nm excitation and energy transfer takes place with high efficiency until Cy5 enters again the nonfluorescent state. Subsequently, Cy5 switches between the nonfluorescent and fluorescent states. Closer examination of the switching events shown in figure 4-37 (A) reveals that TMR is nonfluorescent about to the recovery of the fluorescent Cy5 state. Although this off state, which is denoted  $\tau_{\text{delay}}$ , covers the same time scale as frequent donor blinking (see Figures 4-36 (B) and 4-37 (A)), statistical analysis suggests that the probability of Cy5 recovery is much higher when TMR is not emitting. Thus, one can assume that  $\tau_{\text{delay}}$  is due to quenching by the nearby Cy5 residing in an additional “off” state. The distribution of  $\tau_{\text{delay}}$  is exponential with a decay time of 2.9 ms (figure 4-37 (C)). Because of the 3.4-nm separation, quenching of TMR by Cy5 in this nonfluorescent state occurs most likely via resonance energy transfer. This implies that the absorption of the state is in resonance with the emission of the donor. Furthermore, the efficiency of energy transfer from TMR to Cy5 in the quenching state appears to be more efficient than the standard energy transfer from TMR to Cy5 in its fluorescent state (see donor intensity in figure 4-37 (B) or in the expanded view of figure 4-37 (A)). Therefore, we conclude that the short-lived nonfluorescent state of Cy5 exhibits a slightly higher absorption cross section at shorter wavelengths. It is also possible that this off state is related to the millisecond off state of Cy5 discussed above (figure 4-36 (A)). As shown in figure 4-37 (B), this off state is also capable of completely quenching the donor emission. The fact that it exhibits a similar lifetime and similar acceptor properties could mean that these two off states represent the same intermediate.

Overall, this study indicates that there are several nonfluorescent states involved in the switching cycle. The oxygen and triplet dependence of the switching performance propose that the triplet state is not involved in the formation of the switchable states but, rather, competes with it. After formation of the first photoswitched product there seems to be a cascade of events to restore the fluorescent state. “Off” times together with FRET trajectories suggest one photoactive intermediate and two further

intermediates, one with a duration in the 200-ms range and another with a lifetime of a few milliseconds. The 200-ms state does not function as FRET acceptor, whereas the state with a lifetime of a few milliseconds is able to absorb the donor energy more efficient than fluorescent Cy5. Furthermore, this short-lived nonfluorescent state exhibits similar properties as an off state also found for Cy5 using 633-nm excitation only and might therefore represent the same state.

One known state of Cy5 that likely exhibits an  $R_0$  value larger than that in Cy5 in the fluorescent state is the *cis*-conformation of Cy5 [Widengren and Schwille, 2000; Tinnefeld et al., 2003]. Back-isomerization from the nonfluorescent *cis* to the fluorescent *trans* conformation also occurs photoinduced. Because of the low rates for thermal relaxation of the photoinduced *cis* state, photostationary equilibrium is established between the two isomeric forms already at low excitation intensities. That is, under laser irradiation a single Cy5 molecule stays in its nonfluorescent *cis* state about 50% of the time. *trans-cis* and back-isomerization generally occur on the microsecond time scale for Cy5 in solution (figure 4-36 (B)). On the other hand, it can be anticipated that Cy5 molecules in free solution behave different from those attached to biomolecules and immobilized onto solid supports. If Cy5 is attached to DNA or proteins the conformational flexibility of the linker used enables occasional sticking of the dye on the DNA or protein [Eggeling et al., 1998b]. The steady-state fluorescence anisotropy of Cy5 attached to dsDNA was determined to be  $r = 0.24$  in ensemble measurements (i.e., it cannot be regarded as free rotor). Thus, the *cis* state could be stabilized for micro- to milliseconds. Accordingly, the off state with a duration of a few milliseconds that functions as an efficient FRET acceptor could be associated with a stabilized *cis*-Cy5 adsorbed to surrounding macromolecules. The duration of the off state would consequently represent the time of the sticking event. Even though the triplet state is not involved in the formation of the nonfluorescent state(s), it can still play a role in the restoration of the fluorescent state. For example, intersystem crossing of the nonfluorescent state into the triplet state and subsequent conversion to the triplet state of fluorescent Cy5 followed by intersystem crossing to the singlet ground state might also contribute to the switching mechanism.

#### 4.4.3. OPTICAL SWITCHING OF CYANINE DYES IN ENSEMBLE EXPERIMENTS

In addition, optical switching does not require single-molecule conditions, that is, high excitation intensity. The fluorescent state can be reproducibly but only partly restored as well from an ensemble of molecules irradiating, for example, a  $10^{-6}$  M aqueous Cy5 solution first at 647 nm and then, to restore the fluorescent state, at either 337, 488, or 532 nm (figure 4-38).

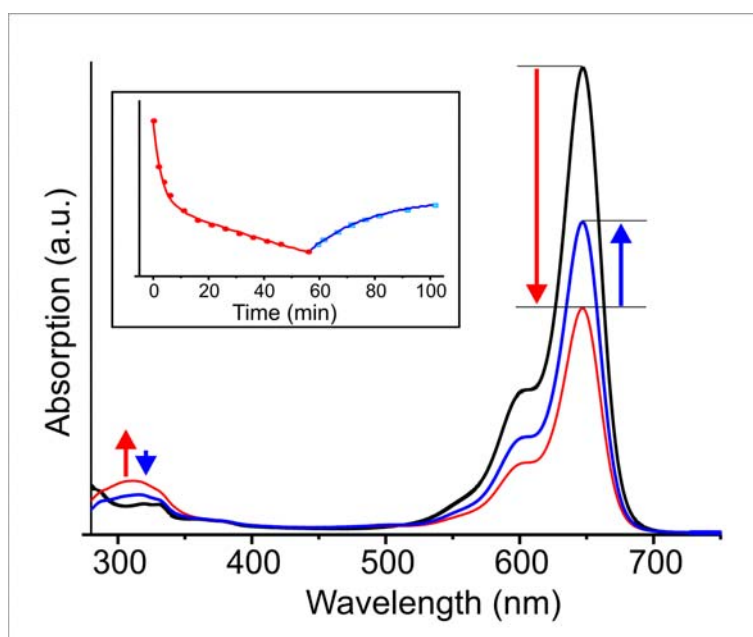


**Figure 4-38:** Ensemble switching experiment of an argon-bubbled  $10^{-6}$  M aqueous Cy5 solution (PBS, pH 7.4, containing 100 mM MEA). The original Cy5 absorption spectrum is shown in black. After being bleached for 30 min at 647-nm (300 mW) irradiation by a defocused laser beam, the absorption decreased by  $\sim 50\%$  at 650 nm (red). About 40% of the absorption could be restored upon irradiation at 488 nm (300 mW) for 30 min (blue). The inset shows the temporal evolution of bleaching and absorption restoration. While the bleaching curve has to be fitted with a two-exponential model with decay times of  $\tau_1 = 3.1$  min (32%) and  $\tau_2 = 162$  min (68%), absorption recovery is well-described by a single exponential with  $\tau = 23$  min.

Most notably in the ensemble experiment, the extinction of the reversible off state shows an increased absorption around 310 nm. Although no substantial increase in extinction is observed in the range of  $\sim 450$ -532 nm, it is advantageous to use this wavelength range for switching as the fluorescent subpopulation of Cy 5 is not

excited significantly. A small band appearing at ~500 nm after continuous bleaching is not related to the photoswitched product as the band does not vanish when Cy5 is switched on again. It is also interesting to note that switching is more efficient at the level of single molecules than at the ensemble level. In ensemble experiments on average only about 40% of the molecules can be switched on independent of the irradiation wavelength. The different switching efficiency observed at the single-molecule and ensemble levels might be caused by the different experimental conditions such as different oxygen-removing efficiencies, different excitation intensities, and/or different local environment on a surface and in solution.

## 5. Conclusion and Outlook

In this work, an DNA based unidirectional photonic wire and a molecular photoswitch were realized. Both nanooptical devices can be selectively addressed by light, which circumvents the connection problem to macroscopic objects. The working principle and performance of the two molecular elements was investigated by steady-state optical methods, time-resolved ensemble spectroscopy and single-molecule fluorescence techniques. In particular, experiments carried out at the single-molecule level revealed information about important details of the working principle. For individual photonic wire molecules, energy leaks were identified, the influence of rotational mobility was investigated and collective nonfluorescent states were observed. Photoswitches were realized with single carbocyanine dyes. These fluorophores exhibit a number of intermediate states which strongly depend on environmental conditions. Two-colour experiments showed efficient and reversible transitions from the fluorescent state to a dark state. Single-molecule FRET-experiments with a well-suited donor fluorophore probing the dark state of a carbocyanine yielded further kinetic information on intermediate states and helped to elucidate their absorption properties.

It is the intent of the following section to draw a picture of the working principle of photonic wires and optical switches, as it is derived from the present work. Pivot points for further studies are discussed which would lead to a more precise description of the working principle. Finally, possible applications of these nanooptical devices are introduced.

### 5.1. DNA Based Photonic Wires

First studies on photonic wires were published in 1994 and used the porphyrin-approach [Wagner and Lindsey, 1994]. A boron-dipyrromethene dye provided an input unit at one end, a linear array of three zinc porphyrins were employed as signal transmission elements, and a free base porphyrin provided an optical output unit at the other end. Total energy transfer efficiencies of up to ~70% were observed in these molecular constructs with a total length of ~9 nm.

In this work, a stepwise design of a molecular photonic wire using DNA as rigid scaffold and conventional fluorophores as energy-transferring units was presented. The advantage of the approach lies in a simplified synthesis strategy based on DNA as rigid scaffold, and the large variety of fluorophores available for conjugation to DNA. Sequential hybridisation enabled the construction of multi-dye labelled photonic wires with appropriate distances for energy transfer in the FRET regime.

To outline the working principle of the photophysical and structural properties of such multistep energy transfer systems, a number of different techniques were used. Among steady-state and time-resolved ensemble experiments, single-molecule experiments especially contributed to a refined understanding of synthetic photonic wires. A pictorial view of an exemplary photonic wire emphasizing several working points critical for the development and further improvement of the performance of such devices is presented in figure 5-1.

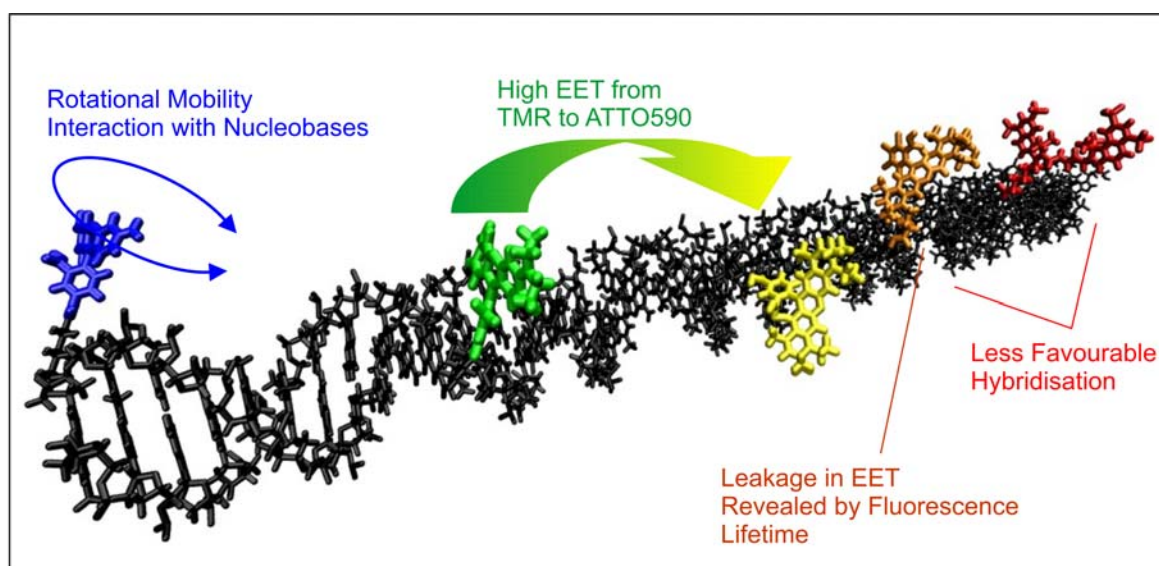


Figure 5-1: Model construct of a photonic wire. Focus was set on the rotational mobility of fluorophores, energy transfer efficiencies in single steps, search for leakages by time-resolved measurements and evaluation of hybridisation steps.

### Rhodamine Green as Input Unit

Rhodamine Green was chosen as input unit for all photonic wire samples synthesized in this work. As a rhodamine derivative, the fluorophore exhibits a high number of emitted photons in a reductive environment (see 4.1.5) and shows improved stability compared to other short-wavelength absorbing fluorophores.

Steady-state and single-molecule fluorescence experiments of this input unit were one main focus of this work, since an efficient and funnel-like “collection” of light is crucial for the following processes of energy transfer along the multichromophoric chain.

First, steady-state measurements probed the efficiency of energy transfer exciting Rhodamine Green in the presence of an acceptor dye, TMR. These experiments only exhibited poor energy transfer efficiency with a mean value of 0.47 (see 4.2.3), which is low when compared to the theoretically expected efficiency of 0.99. Time-resolved spectroscopy revealed two populations with different FRET efficiencies: one with very high FRET efficiency (0.83 for 23% of the molecules) and a second with a very low efficiency (0.13 for 77% of the molecules). The second subpopulation was determined from a fluorescence lifetime of 3.66 ns which is significantly different from the value observed for Rhodamine Green only (but bound to dsDNA), i.e. 4.20 ns. Remarkably, a similar observation was made for Rhodamine Green and Cy5 in direct proximity: ensemble studies revealed a proximity value of 0.44, whereas single-molecule experiments revealed two equal distributions, one at zero and another at 0.95 [White et al., 2004].

An explanation for the heterogeneity observed for the FRET-pair Rhodamine Green/TMR can be given by a closer look at the underlying energy transfer mechanism. Here, the orientation of fluorophores is a crucial factor, which leads to the interpretation that one subpopulation might be unfavourable for energy transfer. Orientation effects are taken into account by the  $\kappa^2$  factor, for which a value of 2/3 is assumed in the case of freely-rotating molecules. In many cases, this assumption is not totally correct, and theoretical work on orientation probabilities showed a pronounced contribution at values around zero for the  $\kappa^2$  factor, which might explain poor transfer efficiencies [Dale and Eisinger, 1979]. On the other hand, single-molecule studies on the rhodamine derivative TMR bound to DNA revealed three subpopulations with different fluorescence lifetime and quantum yield, the result of an interaction with nucleobases [Eggeling et al., 1998b]. This observation might hint at a similar behaviour of Rhodamine Green and could explain a subpopulation which does not show energy transfer (or only weak energy transfer). To evaluate this assumption, experiments with modulated polarization of a pulsed excitation light source were performed, in order to characterize the mobility of the fluorophore

simultaneously with its fluorescence lifetime (see 4.3.6). It can be assumed that a 60 base pair double-stranded DNA does not rotate on the timescale chosen for modulation (20 Hz), and hence all rotation is attributed to the fluorophore itself. Structurally different states were observed for one molecule, exhibiting distinct mobility and fluorescence lifetimes. In many cases, however, hindered rotation was observed, and interactions with nucleobases may therefore lead to conformations unfavourable for efficient energy transfer (similar to TMR).

An extension to experiments with modulated polarization of excitation light could be polarized detection. This would allow the detection of the polarization of fluorescence emission of each fluorophore in the multichromophoric chain, and would yield additional information on the working principle of photonic wires. To maintain the spectral resolution of the present set-up, four additional detectors are necessary, together with polarizing beamsplitters for each detector channel. Such an extension of the set-up would require a change in the geometry of the detection path and is probably difficult to realize with the present 2f-scheme. More flexibility for extension is envisable if the detection path is designed for parallel light which is finally focussed onto each detector separately.

On the other hand, no such subpopulations were observed when hybridisation was carried out directly on surfaces. A nearly perfect homogeneity of smFRET-efficiencies could be realized. This observation is contrary to assumptions made above, but would better correspond to a general heterogeneity in hybridisation at the ensemble level.

### **Energy Transfer Efficiencies and Hybridisation**

The method for the design of molecular photonic wires which was chosen in the present work makes use of the efficient process of DNA hybridisation of up to four single-stranded oligonucleotides. As a result, up to five fluorophores constitute an energy-transferring chain (see 4.2.1). It was shown that “classical” hybridisation of single-stranded DNA yields many products besides the desired construct. This large heterogeneity is also observed in single-molecule experiments, both on dry glass substrates and immobilized in aqueous environment. Among a number of reasons that can be given are uncertainties in chemical stoichiometry and possible

unfavourable conformations of oligonucleotides which represent a barrier for efficient hybridisation.

A strategy to rule out these heterogeneities was presented in this work (see 4.3.4). Sequential hybridisation of oligonucleotides to a template single strand bound to a surface yielded ~90% of desired constructs. The hypothesis of structural hindrance at the last hybridisation step was verified by longer incubation times and higher concentration.

The big advantage of sequential hybridisation lies in the fact that energy transfer efficiencies of photonic wires can be estimated stepwise at the single-molecule level. As expected, single photonic wires show much better values than determined from ensemble experiments. Constructs with three and four fluorophores yielded up to ~90% of transfer efficiencies, and ~70% were observed for five fluorophores.

### **Future Experimental Research on Photonic Wires**

Single-molecule techniques have proven their applicability to aid investigation of the working principle of complex energy transfer constructs as photonic wires. Important characteristics of such complexes were unravelled, e.g. interaction of fluorophores with the scaffold DNA, inefficient energy transfer steps, leakages along the energy transfer chain and unfavourable hybridisation deficiencies.

An improved understanding of these molecular complexes can be obtained by extending the present set-up at several points. First, alternating-laser excitation (ALEX) offers the possibility to access structural and interaction information at the same time [Kapanidis et al., 2004 and 2005]. Experiments on single-molecule FRET constructs allowed further discrimination of FRET-species by introducing a stoichiometry factor. In the case of photonic wires, fast alternation between two (or possibly more) excitation laser wavelengths on a  $\mu\text{s}$  timescale could probe the state of different fluorophores along the energy transfer chain. This would present an easier approach to identify leakages on the one hand, but also to determine stepwise energy transfer efficiencies on the other hand. If multiple laser excitation is envisaged, a well-balanced combination of dichroic beamsplitters and bandpass filters must be used.

A slightly different approach for studies on photonic wires includes the use of spectrographs and CCD-cameras. With the high fluorescence intensity observed for some constructs, it may be envisaged to collect spectra of photonic wires. This represents a well-suited method to obtain information about the contributions from individual fluorophores along the chain. A high quantum yield is required for suitable CCD devices, and a sufficient number of photons must be emitted by the molecular constructs.

From the synthetic point of view, DNA represents an ideal scaffold to design optical devices as multistep energy transfer constructs. In combination with post-labelling strategies, advanced purification methods and hybridisation, well-defined geometries can be realized. To work unidirectional, an energy cascade from high energy at the input unit to lower energies along the chain of fluorophores was designed. Overall, a spatial range of 13.6 nm over a wavelength range of ~250 nm was realized. To extend both parameters and still work with optimal distances between fluorophores for FRET, more fluorescent dyes could be introduced. Since the spectral bandwidth for fluorophores is limited to avoid possible two-photon or  $S_0$ - $S_2$  excitations, an increasing number of fluorophores results in shorter distance between absorption and emission spectra. As a result, the analysis of energy transfer steps gets more difficult and ambiguous. One possible solution at this point could be the casual application of homo-FRET steps along the chain, i.e. energy transfer between two identical fluorophores.

Finally, a desirable extension of photonic wires would be a switching element for energy transfer. This could be realized by a combination with a molecule which can be addressed by chemical or electrical influences or light. Hereby, the molecule undergoes a reversible transition from a non-absorbing state to an absorbing state with negligible fluorescence quantum yield. Concerning the mechanism for switching, chemical methods would require a flow chamber and suffer from slow reaction times. Light-induced switching requires photoinduced reactions (e.g. cyclization) which can be excited exclusively, i.e. without exciting any chromophoric unit along a photonic wire. The generation of an electric field usually affects larger volumes and does not allow exclusive switching of one single photonic wire.

## 5.2. Single-Molecule Photoswitch: A Mechanistic View

The first experiments in preparing a reversible dark-state of a single fluorescent molecule were carried out in 1992 [Basché and Moerner, 1992]. At the cryogenic temperature of liquid helium, they demonstrated the process of “spectral hole-burning” at a single perylene molecule embedded in a host crystal of polyethylene.

At room temperature, the first molecule which exhibited reversible activation of a dark state was derived directly from nature, i.e. the chromophoric unit of the green fluorescent protein (GFP) of *aequorea victoria* [Dickson et al., 1997]. The chromophoric unit is spontaneously formed by three amino acids, i.e. glycine, tyrosine and threonine (or serine), totally shielded from the surrounding environment by a cylindrical barrel of the protein backbone. Responsible for the observation of fluorescence switching is a reversible proton exchange at the chromophoric unit of the protein.

Many approaches of switching single molecules were done by exploiting photoinduced chemical reactions, e.g. cyclization-reactions of an arrangement of  $\pi$ -electrons forming or breaking bonds [Chibisov and Görner, 1997 and 1997b]. At the single-molecule level, Irie and coworkers used such a light-induced cyclization reaction to create an internal quenching unit which absorbs fluorescence light via FRET and hereby “turns” fluorescence off [Irie et al., 2002]. The reaction is reversible, and the donor molecule exhibits fluorescence again after a few seconds.

This work represents the first successful single-molecule photoswitch at room temperature using a commercially-available fluorophore [Heilemann et al., 2005]. Fluorescence of carbocyanine derivatives was reproducibly restored by applying two distinct laser wavelengths. First, laser light excitation at 633 nm probed fluorescence and prepared a dark-state. In a second step, excitation at 488 nm restored the fluorescent state. A mechanistic description of this process was given in the experimental part of this work (see 4.4). The reversible dark-state is only observed in the absence of oxygen and requires the presence of a thiol-reagent at higher concentration. This leads to the interpretation that competing reactions leading to

photobleaching are more likely for carbocyanines and have to be excluded imperatively. Furthermore, the presence of thiol-containing reagents is required: acting as triplet-quenchers for carbocyanine derivatives, they must - in a more general description - be regarded as potential electron-donors.

Experiments with other fluorophores demonstrated the importance of the redox properties of the environment on the formation of dark-states (see 4.1.2-4.1.5). It was demonstrated that fluorescence intermittencies (i) can be suppressed in reductive environment for carborhodamine derivatives (see 4.1.4) or (ii) can be generated in a similar environment for oxazine derivatives (see 4.1.3). Yet, a direct proof of this theory by detecting a radical anion or cation species could not be furnished. In context with fluorescence switching of carbocyanine dyes, an intermediate radical ion state which plays a key role in this process may be expected. This would be in agreement with other observations made for carbocyanine dyes and very recently published: in the presence of the short-wavelength absorbing fluorophore Cy3, the fluorescence of the reporter fluorophore Cy5 could be turned “on” and “off”, requiring very short distances below 3 nm [Bates et al., 2005]. It can be assumed that Cy3 acts as an electron-donor and provides the electron to neutralize a radical cation state of Cy5, explaining both the pre-requisite of very short distances and an exponentially-shaped distance dependence. In agreement with the experimental conditions determined in this work (see 4.1.2), experiments were carried out in the absence of oxygen. Contrarily, the presence of potassium iodide was required, which is known to enhance the triplet formation by the heavy-atom effect [Kasha, 1952]. This should be viewed with similar caution as the effect of thiol-reagents: triplet-depopulating properties and redox-properties cannot be separated and depend on the molecular species under investigation. Iodine promotes triplet transitions and provides electrons as reductive agents, together with fluorescence quenching at higher concentration. As a consequence, the role of the triplet state may be smaller than assumed from the first results, and a radical state is more probable. Other work published recently shows that the fluorescent state of the structurally closely related carbocyanine Alexa647 [Buschmann et al., 2003] could be manipulated by generation of an electric field [White et al., 2004]. Together with a donor fluorophore, the carbocyanine dye was attached to 40bp double-stranded DNA in direct proximity and at a distance of 40 base pairs, i.e. out of range for the observation of FRET. A solution of this labelled DNA was measured at the output of a nanopipette with two-colour excitation and

controllable electric field. The resulting FRET-efficiency showed a pronounced dependency on the magnitude of the electric field, and a nonfluorescent state of Alexa647 was observed at a negative potential below  $-0.2$  V. The process was only observed at the high electric field generated at the output tip of the nanopipette and was highly reversible.

Published data from three different groups with a similar arrangement of fluorophores and reversible switching of the fluorescent state are summarized in figure 5-2: part (A) shows a carbocyanine dye under two-laser excitation and typical experimental conditions as presented in this work. Molecules switching “on” from a dark state are observed, as well as fluorescence trajectories exhibit fluctuations between dark states and the fluorescent states. In (B), the approach by Zhuang and coworkers is depicted, requiring a neighbouring fluorophore and exhibiting a short-scaled distance dependence, which exhibits similarities to electron transfer processes. In (C), switching of fluorescence by the generation of an electric field is demonstrated, as published by Klenerman and coworkers. The most evident similarity of all three approaches is the need for an electron donor or an electric field. Photooxidation by oxygen and triplet state formation are competing processes and can be neglected.

Nevertheless, the question of the molecular mechanism causing fluorescence switching in carbocyanines remains. The dark-state created upon irradiation at 633 nm was probed for its absorption properties using smFRET. It could be demonstrated that more than one intermediate state is involved, one in resonance with a donor emission, and a second essentially nonabsorbing one. Further, fluorescence “off”-states of Cy5 with increased efficiency of donor quenching compared to FRET were observed. As a consequence, one can assume the presence of different species which exhibit structural changes in the basic chromophoric unit, i.e. in the number of conjugated  $\pi$ -electrons.

Experiments carried out at the ensemble level did not show any significant contribution to the absorption spectrum after preparing the dark state. Reflecting that extinction coefficients for most organic compounds are quite low (as they represent the probability of an absorption process) compared to a value of  $\sim 2.5 \cdot 10^5 \text{ M}^{-1} \text{ cm}^{-1}$  for the maximum absorption wavelength of Cy5, the absorption of the dark states involved may be below the detection limit of absorption spectroscopy and cannot be discriminated from background absorption.

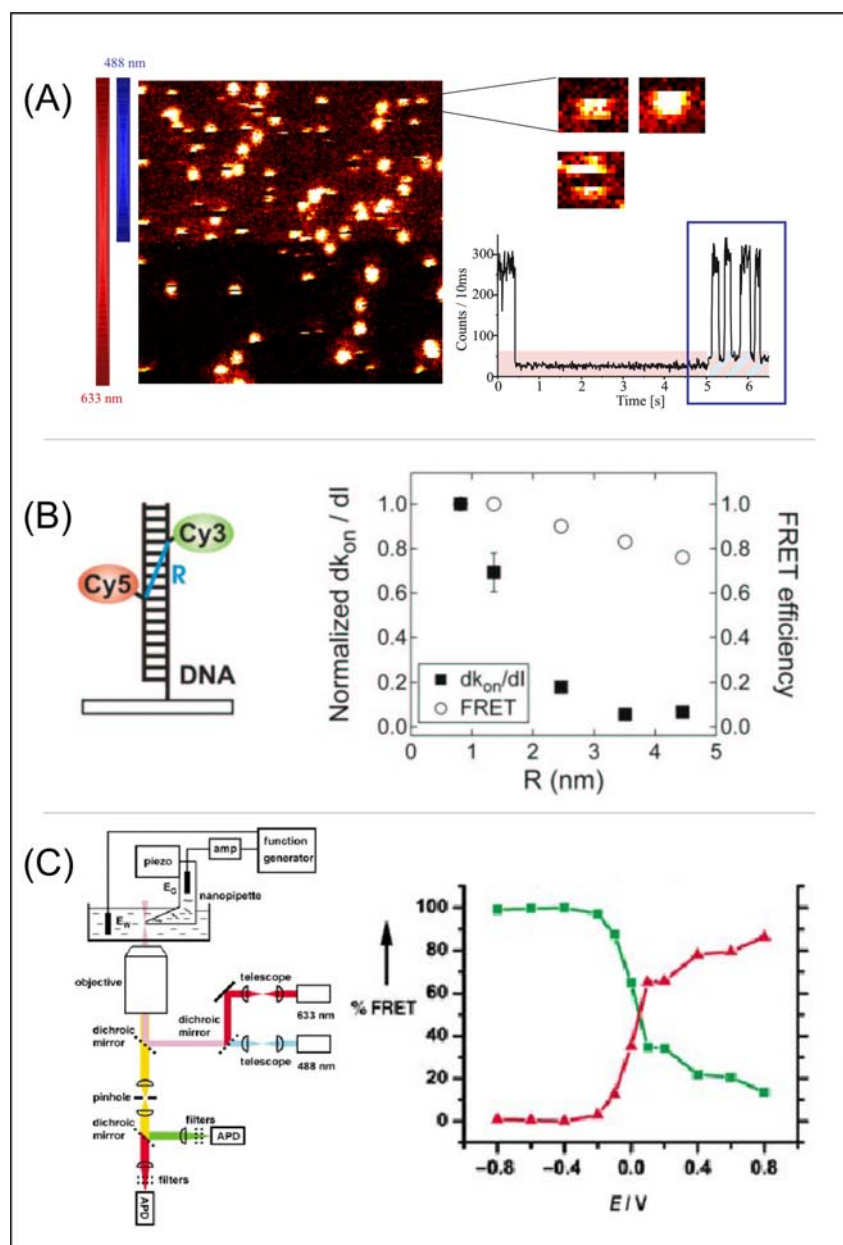


**Figure 5-2:** Three recently published methods for reversible switching of fluorescence from carbocyanine dyes. (A) Fluorescence switching of Cy5 presented in this work (see 4.4), (B) optical switching of Cy5 in the proximity of a donor fluorophore exhibits distance dependency than FRET and was used as short-range spectroscopic ruler, (C) an electric field at the tip of a nanopipette is used to manipulate the FRET efficiency between a nearby donor and carbocyanine acceptor molecule (red: acceptor emission, green: donor emission), generating a dark state of the carbocyanine at negative potential.

Since thermal stability of the dark states which are involved in fluorescence switching is observed for at least a few hours at room temperature, other methods to characterize newly formed species might be used. The most difficult barrier imaginable for most methods is the low concentration. Typical working conditions are solutions of  $10^{-6}$  M of the dye in PBS ( $\sim 10^{-3}$  mg/ml), which excludes structural methods such as nuclear magnetic resonance (NMR) spectroscopy or UV/VIS/IR-spectroscopy. Mass spectroscopic methods are critical because of possibly “extreme” conditions at the injection step and low concentrations, too. Although exhibiting high-pressure or current, HPLC or capillary electrophoresis (CE) could be used for separating compounds, but lacks a detection method that could be applied for dark state intermediates. Single-paired electrons can be observed by electron-

spin resonance, but again concentrations of about 10- to 100fold higher are required. In summary, the fact of low concentration *and* short-time thermal stability together with poor detection possibilities makes a further characterization very difficult.

It seems more promising to think about single-molecule techniques which could probe intermediate dark states. Different redox-properties as well as radical-stabilizing reagents could be envisaged. Single-molecule FRET constructs with different distances, excitation sources and excitation modulation or polarization detection could reveal further information.

Experimental conditions chosen in this work for switching experiments on carbocyanines required oxygen-free environment and the presence of a thiol-moiety as reducing agent. These conditions are frequently used in smFRET-assays for biological applications, since the increased stability of the fluorophores dramatically extends the observation time [Ha et al., 2002]. It is interesting to note that the observation of reversible dark state formation of carbocyanine dyes was reported previously in such smFRET experiments [Blanchard et al., 2004], and were attributed to photophysical phenomena. It is therefore intuitively easy to understand that smFRET-experiments have to be interpreted carefully if carbocyanine dyes are involved. Besides a large spectrum of photophysical reactions, the observation of reversible photoactivation of a fluorescent dark state for carbocyanine dyes represents a further complication which must be taken into account.

Besides further investigation of the switching mechanism observed for carbocyanine dyes, one might think of potentially interesting applications of this method. Optical data storage can, of course, be envisaged, supported by the observed reversibility and high rate of reproducibility. If one molecule is used to store one bit, data storage is only limited by the addressability of this molecule: if a focussed laser is used, the shape of the excitation profile limits the surface density to  $\sim 4$  molecule/ $\mu\text{m}^2$  (or a spacing of at least  $0.5 \mu\text{m}$  between adjacent molecules) to avoid excitation of more than one molecule. This would yield a storage capacity of  $4 \times 10^8$  bits/ $\text{cm}^2$ , i.e. 48 Megabyte. If a better addressability by confined excitation profiles is realized, an even higher density of data storage can be realized. To finally get closer to such applications, experimental conditions have to be modified. Research effort could be focussed on suited polymer materials which do not incorporate molecular oxygen, such as polyvinylalcohol (PVA) or others. Chemical modification of the polymer could

focus on elaborating a similar microenvironment for the fluorophores and make photoswitching possible for incorporated molecules. These approaches could lead to a convenient data storage material with easy handling.

Another application possible is the selective activation of a fluorophore in living cells. Fluorescence recovery after photobleaching and optical highlighting of fluorescent proteins can provide insights into the diffusive or directed movement of proteins and track rapid protein behaviour [Lippincott-Schwartz, 2001; Ando et al., 2004]. Similar to fusion proteins used so far, conventional fluorophores may be envisaged for this purpose as well. The photoactivation process of carbocyanines derivatives presented in this work can offer an alternative method for selective highlighting biomolecules in cells which cannot be tagged with a fluorescent protein.

## 6. References

- A. P. Alivisatos. The use of nanocrystals in biological detection. *Nature Biotechnol.*, **2004**, 22, 47-52.
- W. P. Ambrose, P. M. Goodwin, J. H. Jett, A. Van Orden, J. H. Werner, R. A. Keller. Single Molecule Fluorescence Spectroscopy at Ambient Temperature. *Chem. Rev.*, **1999**, 99, 2929-2956.
- R. Ando, H. Mizuno, A. Miyawaki. Regulated Fast Nucleocytoplasmic Shuttling Observed by Reversible Protein Highlighting. *Science*, **2004**, 306, 1370-1373.
- J. Anzai, T. Hoshi, T. Osa. Controlled deposition of glucose oxidase on platinum electrode based on a avidin/biotin system for the regulation of output current of glucose sensors. *Anal. Chem.*, **1995**, 15, 770-774.
- P. W. Atkins. *Physikalische Chemie*. VCH Weinheim, **1995**.
- R. M. Badger, A. C. Wright, R. F. Whitlock. Absolute Intensities of the Discrete and Continuous Absorption Bands of Oxygen Gas at 1.26 and 1.065  $\mu\text{m}$  and the Radiative Lifetime of the  $^1\Delta_g$  state of Oxygen. *J. Chem. Phys.*, **1965**, 43, 4345-4350.
- G. S. Baird, D. A. Zacharias, R. Y. Tsien. Biochemistry, mutagenesis, and oligomerisation of DsRed, a red fluorescent protein from coral. *PNAS*, **2000**, 97, 11984-11989.
- T. Basché, W. E. Moerner. Optical modification of a single impurity molecule in a solid. *Nature*, **1992**, 355, 335-337.
- M. Bates, T. R. Blosser, X. Zhuang. Short-range spectroscopic ruler based on single-molecule optical switch. *Phys. Rev. Lett.*, **2005**, 94, 10801-10804.
- J. Bernard, L. Fleury, H. Talon, M. Orrit. Photon Bunching in the Fluorescence From Single Molecules – a Probe for Intersystem Crossing. *J. Chem. Phys.*, **1993**, 98, 850.
- R. A. Bissell, E. Cordova, A. E. Kaiser, J. F. Stoddart. A chemically and electrochemically switchable molecular shuttle. *Nature*, **1994**, 369, 133-137.

- 
- S. C. Blanchard, R. L. Gonzalez Jr., H. D. Kim, S. Chu, J. D. Puglisi. tRNA selection and kinetic proofreading in translation. *Nat. Struct. Mol. Biol.*, **2004**, *11*, 1008-1014.
- M. Boehmer, J. Enderlein. Fluorescence spectroscopy of single molecules under ambient conditions: methodology and technology. *ChemPhysChem*, **2003**, *4*, 793-808.
- M. A. Bopp, Y. Jia, L. Li, R. J. Cogdell, R. M. Hochstrasser. Fluorescence and photobleaching dynamics of single light-harvesting complexes. *PNAS*, **1997**, *94*, 10630-10635.
- M. Born, E. Wolf. Principles of Optics, 7<sup>th</sup> edition. *Cambridge University Press*, **2002**.
- V. Buschmann, K. D. Weston, M. Sauer. Spectroscopic Study and Evaluation of Red-Absorbing Fluorescent Dyes. *Bioconjugate Chem.*, **2003**, *14*, 195-204.
- C. Bustamante, J. C. Macosko, G. J. Wuite. Grabbing the cat by the tail: manipulating molecules one by one. *Nat. Rev. Mol. Cell. Biol.*, **2000**, *1*, 130-136.
- F. K. Chan, R. M. Siegel, D. Zacharias, R. Swofford, K. L. Holmes, R. Y. Tsien, M. J. Lenardo. Fluorescence resonance energy transfer analysis of cell surface receptor interactions and signalling using spectral variants of the green fluorescent protein. *Cytometry*, **2001**, *44*, 361-368.
- Y. Chen, A. Periasamy. Characterization of two-photon excitation fluorescence lifetime imaging microscopy for protein localization. *Microscopy Research and Technique*, **2004**, *63*, 72-80.
- A. K. Chibisov, H. Görner. Photoprocesses in Spiropyran-Derived Merocyanines. *J. Phys. Chem. A*, **1997**, *101*, 4305-4312.
- A. K. Chibisov, H. Görner. Singlet versus triplet photoprocesses in indodicarbocyanine dyes and spiropyran-derived merocyanines. *J. Photochem. Photobiol.*, **1997b**, *105* 261-267.
- G. Chirico, F. Cannone, A. Diaspro, S. Bologna, V. Pellegrini, R. Nifosi, F. Beltram. Multiphoton switching dynamics of single green fluorescent proteins. *Phys. Rev. E*, **2004**, *70*, 030901.
- T. Christ, F. Kulzer, P. Bordat, T. Basché. Watching the Photooxidation of a Single Molecule. *Ang. Chem. Int. Ed.*, **2001**, *113*, 4323-4326.
-

- 
- D. M. Chudakov, V. V. Verkhusha, D. B. Staroverov, E. A. Souslova, S. Lukyanov, K. A. Lukyanov. Photoswitchable cyan fluorescent protein for protein tracking. *Nature Biotechnology*, **2004**, *11*, 1435-1439.
- J.-P. Clamme, A. A. Deniz. Three-Color Single-Molecule Fluorescence Resonance Energy Transfer. *ChemPhysChem*, **2004**, *5*, 1-4.
- R. M. Clegg. Fluorescence resonance energy transfer and nucleic acids. *Methods in Enzymology*, **1992**, *211*, 353-388.
- R. M. Clegg, A. I. H. Murchie, A. Zechel, C. Carlberg, S. Diekmann, D. M. J. Lilley. Fluorescence Resonance Energy Transfer Analysis of the Structure of the Four-Way DNA Junction. *Biochemistry*, **1992b**, *31*, 4846-4856.
- R. M. Clegg. Fluorescence resonance energy transfer. *Curr. Opin. Biotechnol.*, **1995**, *6*, 103-110.
- E. U. Condon. Nuclear motions associated with electron transitions in diatomic molecules. *Physical Review*, **1928**, *32*, 858-872.
- R. E. Dale, J. Eisinger, W. E. Blumberg. The orientational freedom of molecular probes. The orientation factor in intramolecular energy transfer. *Biophysical Journal*, **1979**, *26*, 161-194.
- A. A. Deniz, M. Dahan, J. R. Grunwell, T. Ha, A. E. Faulhaber, D. S. Chemla, S. Weiss, and P. G. Schultz. Single-pair fluorescence resonance energy transfer on freely diffusing molecules: observation of Förster distance dependence and subpopulations. *PNAS*, **1999**, *96*, 3670-3675.
- D. L. Dexter. A theory of sensitised luminescence in solids. *J. Chem. Phys.*, **1953**, *21*, 836.
- J. Deisenhofer, O. Epp, K. Miki, R. Huber, H. Michel. X-ray structure analysis of a membrane protein complex. Electron density map at 3 Å resolution and a model of the chromophores of the photosynthetic reaction center from *Rhodospseudomonas viridis*. *J. Mol. Biol.*, **1984**, *180*, 385-398.
- R. M. Dickson, A. B. Cubitt, R. Y. Tsien, W. E. Moerner. On/off blinking and switching behaviour of single molecules of green fluorescent protein. *Nature*, **1997**, *388*, 355-358.
-

- 
- A. Dietrich, V. Buschmann, C. Müller, M. Sauer. Fluorescence Resonance Energy Transfer (FRET) and competing processes in donor-acceptor substituted DNA strands: a comparative study of ensemble and single-molecule data. *Rev. Mol. Biotechn.* **2002**, *82*, 211-231.
- M. Diez, B. Zimmermann, M. Börsch, M. König, E. Schweinberger, S. Steigmiller, R. Reuter, S. Felekyan, V. Kudryavtsev, C. A. M. Seidel, P. Gräber. Proton-powered subunit rotation in single membrane-bound  $F_0F_1$ -ATP synthase. *Nature structural & molecular biology*, **2004**, *2*, 135-141.
- Z. J. Donhauser, B. A. Mantoosh, K. F. Kelly, L. A. Bumm, J. D. Monnell, J. J. Stapleton, D.W. Price, A. M. Rawlett, D. L. Allara, J. M. Tour, P. S. Weiss. Conductance switching in single molecules through conformational changes. *Science*, **2001**, *292*, 2303-2307.
- N. Dontha, W. B. Nowall, W. G. Kuhr. Generation of Biotin/Avidin/Enzyme Nanostructures with Maskless Photolithography. *Anal. Chem.*, **1997**, *69*, 2619-2625.
- S. Doose, H. Neuweiler, M. Sauer. A close look at fluorescence quenching of organic dyes by tryptophan. *ChemPhysChem*, **2005**, *accepted*.
- K. H. Drexhage. Structure and Properties of Laser Dyes. *Topics in Applied Physics – Dye Lasers – Springer Verlag Berlin-Heidelberg-New York*, **1973**, 144-179.
- M. Eigen. R. Rigler. Sorting Single Molecules: applications to diagnostics and evolutionary biotechnology. *PNAS*, **1994**, *91*, 5740-5747.
- C. Eggeling, J. Widengren, R. Rigler, C. A. M. Seidel. Photobleaching of Fluorescent Dyes under Conditions Used for Single-Molecule Detection: Evidence of Two-Step Photolysis. *Anal. Chem.*, **1998**, *70*, 2651-2659.
- C. Eggeling, J. R. Fries, L. Brand, R. Günther, C. A. M. Seidel. Monitoring conformational dynamics of a single molecule by selective fluorescence spectroscopy. *PNAS*, **1998b**, *95*, 1556-1561.
- C. Eggeling, A. Volkmer, C. A. M. Seidel. Photobleaching Kinetics of Rhodamine 6G by One- and Two-Photon Induced Confocal Fluorescence Microscopy. *ChemPhysChem*, **2005**, *6*, 791-804.
-

- 
- S. A. Empedocles, R. Neuhauser, M. G. Bawendi. Three-dimensional orientation measurements of symmetric single chromophores using polarization microscopy. *Nature*, **1999**, 399, 126-130.
- J. Enderlein, P. M. Goodwin, A. Van Orden, W. P. Ambrose, R. Erdmann, R. A. Keller. A maximum likelihood estimator to distinguish single molecules by their fluorescence decays. *Chem. Phys. Letters*, **1997**, 270, 464-470.
- J. Enderlein, I. Gregor, D. Patra, J. Fitter. Art and Artefacts of Fluorescence Correlation Spectroscopy. *Curr. Pharm. Biotechnol.*, **2004**, 5, 155-161.
- D. S. English, E. J. Harbron, P. F. Barbara. Probing Photoinduced Intersystem Crossing by Two-Color, Double Resonance Single Molecule Spectroscopy. *J. Phys. Chem. A*, **2000**, 104, 9057-9061.
- T. Förster. Zwischenmolekulare Energiewanderung und Fluoreszenz. *Annalen der Physik*, **1948**, 2, 55-75.
- T. Fukaminato, T. Sasaki, N. Tamai, M. Irie. Digital photoswitching of fluorescence based on the photochromism of diarylethene derivatives at a single-molecule level. *J. Am. Chem. Soc.*, **2004**, 126, 14843-14849.
- T. Funatsu, Y. Harada, M. Tokunaga, K. Saito, T. Yanagida. Imaging of single fluorescent molecules and individual ATP turnovers by single myosin molecules in aqueous solution. *Nature*, **1995**, 374, 555-559.
- E. Füreder-Kitzmüller, J. Hesse, A. Ebner, H. J. Gruber, G. J. Schütz. Non-exponential bleaching of single bioconjugated Cy5 molecules. *Chem. Phys. Lett.*, **2005**, 404, 13-18.
- E. Galperin, V. V. Verkhusha, A. Sorkin. Three-chromophore FRET microscopy to analyze multiprotein interactions in living cells. *Nature Methods*, **2004**, 1, 209-217.
- L. Giordano, T. M. Jovin, M. Irie, E. A. Jares-Erijman. Diheteroarylethenes as thermally stable photoswitchable acceptors in photochromic fluorescence resonance energy transfer (pcFRET). *J. Am. Chem. Soc.*, **2002**, 124, 7481-7489.
- D. I. Gittins, D. Bethell, D. J. Schiffrin, R. J. Nichols. A nanometre-scale electronic switch consisting of a metal cluster and redox-addressable groups. *Nature*, **2000**, 408, 67-69.

- 
- A. N. Glazer. Light guides. Directional energy transfer in a photosynthetic antenna. *J. Biol. Chem.*, **1989**, 264, 1-4.
- P. M. Goodwin, W. P. Ambrose, R. A. Keller. Single-Molecule Detection in Liquids by Laser-Induced Fluorescence. *Acc. Chem. Res.*, **1996**, 29, 607-613.
- T. Ha, T. Enderle, D. F. Ogletree, D. S. Chela, P. R. Selvin, S. Weiss. Probing the Interaction between two Single Molecules: Fluorescence Resonance Energy Transfer between a single donor and a single acceptor. *PNAS*, **1996**, 93, 6264-6268.
- T. Ha, A. Y. Ting, J. Liang, A. A. Deniz, D. S. Chela, P. G. Schultz, S. Weiss. Temporal fluctuations of fluorescence resonance energy transfer between two dyes conjugated to a single protein. *Chem. Phys.*, **1999**, 247, 107-118.
- T. Ha. Single-Molecule fluorescence resonance energy transfer. *Methods*, **2001**, 25, 78-86.
- T. Ha, I. Rasnik, W. Cheng, H. P. Babcock, G. H. Gauss, T. M. Lohman, S. Chu. Initiation and re-initiation of DNA unwinding by the *Escherichia coli* Rep helicase. *Nature*, **2002**, 419, 638-641.
- T. Ha and J. Xu. Photodestruction Intermediates Probed by an Adjacent Reporter Molecule. *Phys. Rev. Lett.*, **2003**, 90, 22320021-22320024.
- K.-T. Han, private communication, **2005**.
- R. Harnbury-Brown, R. Q. Twiss. *Nature*, **1956**, 177, 27.
- R. P. Haugland. *Optical Microscopy for Biology*, Wiley-Liss, New-York, **1989**, 147-157.
- E. Haustein, P. Schwille. Ultrasensitive Investigations of biological systems by fluorescence correlation spectroscopy. *Methods*, **2003**, 29, 153-166.
- M. Heilemann, D. P. Herten, R. Heintzmann, C. Cremer, C. Müller, P. Tinnefeld, K. D. Weston, J. Wolfrum, M. Sauer. High-resolution colocalization of single dye molecules by fluorescence lifetime imaging microscopy. *Analytical Chemistry*, **2002**, 74, 3511-3517.
- M. Heilemann, P. Tinnefeld, G. Sanchez-Mosteiro, M. Garcia-Parajó, N. F. van Hulst. Multistep Energy Transfer in Single Molecular Photonic Wires. *J. Am. Chem. Soc.*, **2004**, 126, 6514-6515.
-

- 
- M. Heilemann, E. Margeat, R. Kasper, M. Sauer, P. Tinnefeld. Carbocyanine Dyes as Efficient Reversible Single-Molecule Optical Switch. *J. Am. Chem. Soc.*, **2005**, *127*, 3801-3806.
- D. P. Herten, P. Tinnefeld, M. Sauer. Identification of singly fluorescently labelled mononucleotide molecules in solution by spectrally resolved time-correlated single photon counting. *Appl. Physics B*, **2000**, *71*, 765-771.
- T. Heinlein, J.-P. Knemeyer, O. Piestert, M. Sauer. Photoinduced Electron Transfer between Fluorescent Dyes and Guanosine Residues in DNA-Hairpins. *J. Phys. Chem. B.*, **2003**, *107*, 7957-7964.
- T. Heinlein, A. Biebricher, P. Schlüter, C. Roth, D. P. Herten, J. Wolfrum, M. Heilemann, C. Müller, P. Tinnefeld, M. Sauer. Nanometer-localized fluorescence imaging and counting of single molecules with spectrally-resolved fluorescence lifetime imaging microscopy (SFLIM). *ChemPhysChem*, **2005**, *6*, 949-955.
- T. Hirschfeld. Optical microscopic observation of single small molecules. *Appl. Optics* **1976**, *15*, 2965.
- J. Hofkens, M. Maus, T. Gensch, T. Vosch, M. Cotlet, F. Kohn, A. Herrmann, K. Müllen, F. de Schryver. Probing photophysical processes in individual multichromophoric dendrimers by single-molecule spectroscopy. *J. Am. Chem. Soc.*, **2000**, *122*, 9278-9288.
- J. Hofkens, M. Cotlet, T. Vosch, P. Tinnefeld, K. D. Weston, C. Ego, A. Grimsdale, K. Muellen, D. Beljonne, J. L. Bredas, S. Jordens, G. Schweitzer, M. Sauer, F. C. De Schryver. Revealing competitive Förster-type resonance energy transfer pathways in single bichromophoric molecules. *PNAS*, **2003**, *100*, 13146-13151.
- S. Hohng, C. Joo, T. Ha. Single-molecule three-color FRET. *Biophysical Journal*, **2004**, *87*, 1328-1337.
- S. Hohng, T. Ha. Near-Complete Suppression of Quantum Dot Blinking in Ambient Conditions. *J. Am. Chem. Soc.*, **2004**, *126*, 1324-1325.
- S. Hohng, T. Ha. Single-Molecule Quantum Dot Fluorescence Resonance Energy Transfer. *ChemPhysChem*, **2005**, *6*, 1-5.
- X. Hu, K. Schulten. Model for the light-harvesting complex I (B875) of Rhodospira rubra sphaeroides. *Phys. Today*, **1997**, *50*, 28-34.
-

- 
- Z. Huang, D. Ji, A. Xia, F. Koberling, M. Patting, R. Erdmann. Direct Observation of Delayed Fluorescence from a Remarkable Back-Isomerization in Cy5. *J. Am. Chem. Soc.*, **2005**, ASAP Article.
- T. Huser, M. Yan, L. J. Rothberg. Single chain spectroscopy of conformational dependence of conjugated polymer photophysics. *PNAS*, **2000**, *97*, 11187-11191.
- M. Irie, T. Fukaminato, T. Sasaki, N. Tamai, T. Kawai. A digital fluorescent molecular photoswitch. *Nature*, **2002**, *420*, 759-760.
- E. A. Jares-Erijman, T. M. Jovin. FRET Imaging. *Nat. Biotechnol.*, **2003**, *21*, 1387-1395.
- G. Jung, J. Wiehler, A. Zumbusch. The photophysics of green fluorescent protein: influence of the key amino acids at positions 65, 204, and 222. *Biophys. J.*, **2005**, *88*, 1932-1947.
- A. N. Kapanidis, N. K. Lee, T. A. Laurence, S. Doose, E. Margeat, S. Weiss. Fluorescence-aided molecule sorting : Analysis of structure and interactions by alternating-laser excitation of single molecules. *PNAS*, **2004**, *101*, 8936-8941.
- A. N. Kapanidis, T. A. Laurence, N. K. Lee, E. Margeat, X. Kong, S. Weiss. Alternating-Laser Excitation of Single Molecules. *Acc. Chem. Res.*, **2005**, ASAP publication.
- M. Kasha. *J. Phys. Chem.*, **1952**, *20*, 71.
- B. S. T. Kasibhatla, A. P. Labonte, F. Zahid, R. G. Reifenberger, S. Datta, C. P. Kubiak. Reversibly altering electronic conduction through a single molecule by a chemical binding event. *J. Phys. Chem. B*, **2003**, *107*, 12378-12382.
- J. T. M. Kennis, D. S. Larsen, I. H. M. van Stokkum, M. Vengris, J. J. van Thor, R. van Grondelle. Uncovering the hidden ground state of green fluorescent protein. *PNAS*, **2004**, *101*, 17988-17993.
- C. Kluge, T. Seidel, S. Bolte, S. S. Sharma, M. Hanitzsch, B. Hanitzsch. B. Satiat-Jeunemaitra, J. Ross, M. Sauer, D. Gollack, K. J. Dietz.. Subcellular distribution of the V-ATPase complex in plant cells, and in vivo localisation of the 100 kDa subunit VHA-a within the complex. *BMC Cell Biol.*, **2004**, *5*, 1-18.
- J. P. Knemeyer, N. Marmé, M. Sauer. Probes for Detection of Specific DNA Sequences at the Single-Molecule Level. *Anal. Chem.*, **2000**, *72*, 3717-3724.
-

- 
- F. Köhn, J. Hofkens, U. M. Wiesler, M. Cotlet, M. van der Auweraer, K. Müllen, F. C. DeSchryver. Single-molecule spectroscopy of a dendrimer-based host-guest system. *Chemistry*, **2001**, 7, 4126-4133.
- H. Kuhn. Progress in the chemistry of Organic Natural Products, Vol. 16. *Springer Verlag, Wien*, **1959**, 411ff.
- T. D. Lacoste, X. Michalet, F. Pinaud, D. S. Chemla, A. P. Alivisatos, S. Weiss. Ultrahigh-resolution multicolor colocalization of single fluorescent probes. *PNAS*, **2000**, 97, 9461-9466.
- J. R. Lakowicz, Principles of Fluorescence Spectroscopy, Second Edition. *Plenum Press, New York*, **1999**.
- V. LeTilly, C. A. Royer. Fluorescence anisotropy assays implicate protein-protein interactions regulating trp repressor DNA binding. *Biochemistry*, **1993**, 32, 7753-7758.
- Y. C. Liang, A. S. Dvornikov, P. M. Rentzepis. Nonvolatile read-out molecular memory. *PNAS*, **2003**, 100, 8109-8112.
- J. Lippincott-Schwartz, E. Snapp, A. Kenworthy. Studying protein dynamics in living cells. *Nature Rev. Mol. Cell Biol.*, **2001**, 6, 444-456.
- J. Liu, Y. Lu. FRET study of a trifluorophore-labeled DNAzyme. *JACS*, **2002**, 124, 15208-15216.
- J. J. Macklin, J. K. Trautman, T. D. Harris, L. E. Brus. Imaging and Time-Resolved Spectroscopy of Single Molecules at an Interface. *Science*, **1996**, 272, 255-258.
- N. Marmé, J. P. Knemeyer, M. Sauer, J. Wolfrum. Inter- and Intramolecular Fluorescence Quenching of Organic Dyes by Tryptophan. *Bioconj. Chem.*, **2003**, 14, 1133-1139.
- T. B. McAnaney, W. Zeng, C. F. E. Doe, N. Bhanji, S. Wakelin, D. S. Pearson, P. Abbyad, X. Shi, S. G. Boxer, C. R. Bagshaw. Protonation, photobleaching and photoactivation of yellow fluorescent protein (YFP 10C): a unifying mechanism. *Biochemistry*, **2005**, ASAP article.
- P. B. Merkel, D. R. Kearns. Remarkable Solvents effects on the lifetime of  $^1\Delta_g$  oxygen. *J. Am. Chem. Soc.*, **1972**, 1029-1030.
-

- 
- U. Mets, R. Rigler. Submillisecond Detection of Single Rhodamine Molecules in Water. *J. Fluoresc.*, **1994**, *4*, 259-264.
- X. Michalet, T. D. Lacoste, S. Weiss. Ultrahigh-resolution colocalization of spectrally separable point-like fluorescent probes. *Methods*, **2001**, *25*, 87-102.
- X. Michalet, F. F. Pinaud, L. A. Bentolila, J. M. Tsay, S. Doose, J. J. Li, G. Sundaresan, A. M. Wu, S. S. Gambhir, S. Weiss. Quantum dots for live cells, in vivo imaging and diagnostics. *Science*, **2005**, *307*, 538-544.
- M. Minsky. Microscopy apparatus. US patent 3013467, filed **1957**.
- W. E. Moerner, L. Kador. Optical Detection and spectroscopy of single molecules in a solid. *Phys. Rev. Letters*, **1989**, *62*, 2535-2538.
- W. E. Moerner, M. Orrit. Illuminating Single Molecules in Condensed Matter. *Science*, **1999**, *283*, 1670-1676.
- W. E. Moerner, D. P. Fromm. Methods of single-molecule fluorescence spectroscopy and microscopy. *Rev. Sci. Instrum.*, **2003**, *74*, 3597-3619.
- F. Moresco, G. Meyer, K. H. Rieder, H. Tang, A. Gourdon, C. Joachim. Recording intramolecular mechanics during the manipulation of a large molecule. *Phys. Rev. Lett*, **2001**, *86*, 672-675.
- H. Murakoshi, R. Iino, T. Kobayashi, T. Fujiwara, C. Ohshima, A. Yoshimura, A. Kusumi. Single-molecule imaging analysis of Ras activation in living cells. *PNAS*, **2004**, *101*, 7317-7322.
- H. Neuweiler, A. Schulz, A. Vaiana, J. Smith, S. Kaul, J. Wolfrum, M. Sauer. Peptide-based molecular beacons for the detection of p53-autoantibodies in human sera. *Angew. Chem. Int. Ed.*, **2002**, *114*, 4769-4773.
- H. Neuweiler, M. Sauer. Using Photoinduced Charge Transfer Reactions to Study Conformational Dynamics of Biopolymers at the Single-Molecule Level. *Curr. Pharm. Biotechnology*, **2004**, *5*, 285-298.
- H. Neuweiler and M. Sauer. Exploring life by single-molecule fluorescence spectroscopy: molecular characteristics hidden by ensemble experiments can be revealed by fluorescence. *Anal. Chem.*, **2005**, *77*, 179A-185A.
- S. Nie, R. N. Zare. Optical Detection of Single Molecules. *Annu. Rev. Biophys. Biomol. Struct.*, **1997**, *26*, 567-596.
-

- 
- Y. Ohya, K. Yabuki, M. Hashimoto, A. Nakajima, T. Ouchi. Multistep fluorescence resonance energy transfer in sequential chromophore array constructed on oligo-DNA assemblies. *Bioconjugate Chemistry*, **2003**, *14*, 1057-1066.
- M. Orrit, J. Bernard. Single pentacene molecules detected by fluorescence excitation in a p-terphenyl crystal. *Phys. Rev. Lett.* **1990**, *65*, 2716-2719.
- J. Pawley. Handbook of Biological Confocal Microscopy, 2<sup>nd</sup> ed. *Plenum Press, New York*, **1995**.
- E. J. G. Peterman, S. Brasselet, W. E. Moerner. The Fluorescence Dynamics of Single Molecules of Green Fluorescent Protein. *J. Phys. Chem. A*, **1999**, *103*, 10553-10560.
- O. Piestert, H. Barsch, V. Buschmann, T. Heinlein, J.-P. Knemeyer, K. D. Weston, M. Sauer. A Single-Molecule Sensitive DANN Hairpin System Based on Intramolecular Electron Transfer. *Nano. Lett.*, **2003**, *3*, 979-982.
- J. Psencik, Y.-Z. Ma, J. B. Arellano, J. Hala, T. Gillbro. Excitation energy transfer dynamics and excited-state structure in chlorosomes of *Chlorobium phaeobacteroides*. *Biophys. J.*, **2003**, *84*, 1161-1179.
- J. B. Randolph and A. S. Waggoner. Stability, specificity and fluorescence brightness of multiply-labeled fluorescent DNA probes. *Nucl. Acid Res.*, **1997**, *25*, 2923-2929.
- I. Rasnik, S. A. McKinney, T. Ha. Surfaces and Orientations: Much to FRET about? *Acc. Chem. Res.*, **2005**, *ASAP article*.
- D. Rehm, A. Weller. Kinetik und Mechanismus der Elektronenübertragung bei der Fluoreszenzlöschung in Acetonitril. *Ber. Bunsenges. Physik. Chem.*, **1969**, *73* 834.
- R. Rigler, U. Mets, J. Widengren, and P. Kask. Fluorescence correlation spectroscopy with high count rate and low background - analysis of translational diffusion. *European Biophysics Journal*, **1993**, *22*, 169-175.
- R. Rigler, U. Mets. Diffusion of single molecules through a gaussian laser beam. *SPIE Vol. 21, Laser Spectroscopy of Biomolecules*, **1992**, 239.
-

- 
- M. Sauer. Entwicklung effizienter Fluoreszenzfarbstoffe für den hochempfindlichen Nachweis von Biomolekülen unter Einsatz zeitaufgelöster LIF-Spektroskopie. *Dissertation Univ. Heidelberg*, **1995**.
- M. Sauer. Single-molecule sensitive fluorescence sensors based on intramolecular photoinduced electron transfer. *Angew. Chem. Int. Ed.*, **2003**, *115*, 1790-1793.
- B. Schuler, E. A. Lipman, P. J. Steinbach, M. Kumke, W. A. Eaton. Polyproline and the "spectroscopic ruler" revisited with single-molecule fluorescence. *PNAS*, **2005**, *102*, 2754-2759.
- P. R. Selvin. The renaissance of fluorescence resonance energy transfer. *Nature Structural Biology*, **2000**, *7(9)*, 730-734.
- J. Seth, V. Palaniappan, R. W. Wagner, T. E. Johnson, J. S. Lindsey, D. F. Bocian. Soluble Synthetic Multiporphyrin Arrays. Static Spectroscopic and Electrochemical Probes of Electronic Communication. *J. Am. Chem. Soc.*, **1996**, *118*, 11194-11207.
- E.B. Shera, N.K. Seitzinger, L.M. Davis, R.A. Keller, S.A. Soper. Detection of single fluorescent molecules. *Chem. Phys. Lett.* **1990**, *174*, 553.
- O. Shimomura, F. H. Johnson, Y. Saiga. Extraction, purification and properties of aequorin, a bioluminescent protein from the luminous hydromedusan, *aequorea*. *J. Cell. Comp. Physiol.*, **1962**, *59*, 223-239.
- O. Shimomura. Structure of the chromophore of *Aequorea* green fluorescent protein. *FEBS Lett.*, **1979**, *104*, 220-222.
- A. M. Smith, X. Gao, S. Nie. Quantum-Dot Nanocrystals for In-vivo Molecular and Cellular Imaging. *Photochem. Photobiol.*, **2004**, *80*, 377-385.
- S. Speiser. Photophysics and Mechanisms of Intramolecular Electronic Energy Transfer in Bichromophoric Molecular Systems: Solution and Supersonic Jet Studies. *Chem. Rev.*, **1996**, *96*, 1953-1976.
- D. Stoner-Ma, A. A. Jaye, P. Matousek, M. Towrie, S. R. Meech, P. J. Tonge. Observation of Excited-State Proton Transfer in Green Fluorescent Protein using Ultrafast Vibrational Spectroscopy. *J. Am. Chem. Soc.*, **2005**, *127*, 2864-2865.
- L. Stryer, R. P. Haugland. Energy transfer: a spectroscopic ruler. *PNAS*, **1967**, *58*, 719-726.
-

- 
- P. Tinnefeld, D.-P. Hertel, M. Sauer. Photophysical Dynamics of Single Molecules Studied by Spectrally-Resolved Fluorescence Lifetime Imaging Microscopy (SFLIM). *J. Phys. Chem. A*, **2001**, *105*, 7989-8003.
- P. Tinnefeld, V. Buschmann, K. D. Weston, M. Sauer. Direct Observation of Collective Blinking and Energy Transfer in a Bichromophoric System. *J. Phys. Chem. A*, **2003**, *107*, 323-327.
- P. Tinnefeld, J. Hofkens, D.-P. Hertel, S. Masuo, T. Vosch, M. Cotlet, S. Habuchi, K. Müllen, F. C. De Schryver, M. Sauer. Higher-excited-state photophysical pathways in multichromophoric systems revealed by single-molecule fluorescence spectroscopy. *ChemPhysChem*, **2004**, *5*, 1786-1790.
- P. Tinnefeld, M. Sauer. Branching Out of Single-Molecule Fluorescence Spectroscopy: Challenges for Chemistry and Influence on Biology. *Angew. Chem. Int. Ed.*, **2005**, *44*, 2642-2671.
- M. Tomschik, H. Zheng, K. van Holde, J. Zlatanova, S. H. Leuba. Fast, long-range, reversible conformational fluctuations in nucleosomes revealed by single-pair fluorescence resonance energy transfer. *PNAS*, **2005**, *102*, 3278-3283.
- P. M. Torgerson, M. F. Morales. Application of the Dale-Eisinger analysis to proximity the contractile system. *PNAS*, **1984**, 3723-3727.
- R. Y. Tsien. The green fluorescent protein. *Annu. Rev. Biochemistry*, **1998**, *67*, 509-544.
- N. J. Turro. Modern Molecular Photochemistry. *University Science Books, Pasadena, USA*, **1991**.
- D. A. Vanden Bout, W. T. Yip, D. Hu, D. K. Fu, T. M. Swager, P. F. Barbara. Discrete Intensity Jumps and Intramolecular Electronic Energy Transfer in the Spectroscopy of Single Conjugated Polymer Molecules. *Science*, **1997**, *277*, 1074-1077.
- A. M. van Oijen, M. Ketelaars, J. Köhler, T. J. Aartsma, J. Schmidt. Unraveling the electronic structure of individual photosynthetic pigment-protein complexes. *Science*, **1999**, *285*, 400-402.
- A.M. van Oijen, M. Ketelaars, J. Köhler, T. J. Aartsma, J. Schmidt. Spectroscopy of Individually Light-Harvesting 2 Complexes of *Rhodospseudomonas acidophila*:
-

- 
- Diagonal Disorder, Intercomplex, Heterogeneity, Spectral Diffusion, and Energy Transfer in the B800 Band. *Biophys. J.*, **2000**, *78*, 1570-1577.
- J. A. Veerman, M. F. Garcia-Parajo, L. Kuipers, N. F. van Hulst. Time-Varying Triplet State Lifetimes of Single Molecules. *Phys. Rev. Lett.*, **1999**, *83*, 2155-2158.
- G. Viswath, M. Kasha. Confirmation of the anomalous fluorescence of azulene. *J. Chem. Phys.*, **1956**, *24*, 574-577.
- T. Vosch, M. Cotlet, J. Hofkens, K. Van Biest, M. Lor, K. D. Weston, P. Tinnefeld, M. Sauer, L. Latterini, K. Muellen, F. C. De Schryver. Probing Förster Type Energy Pathways in a First Generation Rigid Dendrimer Bearing Two Perylene Imide Chromophores. *J. Phys. Chem. A*, **2003**, *107*, 6920-6931.
- P. Vukusic, J. R. Sambles. Photonic Structures in Biology. *Nature*, **2003**, *424*, 852-855.
- S. Vyawahare, S. Eyal, K. Mathews, S. R. Quanke. Nanometer-scale Fluorescence Resonance Optical Waveguides. *Nanoletters*, **2004**, *4*, 1035-1039.
- R. W. Wagner, J. S. Lindsey. A Molecular Photonic Wire. *J. Am. Chem. Soc.*, **1994**, *116*, 9759-9760.
- D. Wang, E. Geva. Protein Structure and Dynamics from Single-Molecule Fluorescence Resonance Energy Transfer. *J. Phys. Chem. B*, **2005**, *106*, 1626-1634.
- H. M. Watrob, C. P. Pan, M. D. Barkley. Two-Step FRET as a Structural Tool. *J. Am. Chem. Soc.*, **2003**, *125*, 7336-7343.
- S. Weiss. Fluorescence spectroscopy of single biomolecules. *Science*, **1999**, *283*, 1676-1683.
- S. Weiss. Measuring conformational dynamics of biomolecules by single molecule fluorescence spectroscopy. *Nat. Struct. Biol.*, **2000**, *7*, 724-729.
- K. D. Weston, P. J. Carson, H. Metiu, S. K. Buratto. Room-temperature fluorescence characteristics of single dye molecules adsorbed on a glass surface. *J. Chem. Phys.*, **1998**, *109*, 7474-7485.
- S. S. White, L. Ying, S. Balasubramanian, D. Klenerman. Individual Molecules of Dye-Labeled DNA Act as a Reversible Two-Color Switch upon Application of an Electric Field. *Angew. Chem. International Ed.*, **2004**, *116*, 6052-6056.
-

- 
- J. Widengren, R. Rigler. Mechanisms of photobleaching investigated by fluorescence correlation spectroscopy. *Bioimaging*, **1996**, *4*, 149-157.
- J. Widengren, R. Rigler. Fluorescence correlation spectroscopy as a tool to investigate chemical reactions in solutions and on cell surfaces. *Cell. Mol. Biol.*, **1998**, *44*, 857-879.
- J. Widengren, P. Schwille. Characterization of Photoinduced Isomerization and Back-Isomerization of the Cyanine Dye Cy5 by Fluorescence Correlation Spectroscopy. *Journal of Phys. Chem. B*, **2000**, *104*, 6416-6432.
- M. Wu, P. M. Goodwin, W. P. Ambrose, R. A. Keller. Photochemistry and Fluorescence Emission Dynamics of Single Molecules in Solution: B-Phycoerythrin. *J. Phys. Chem.*, **1996**, *100*, 17406-17409.
- E. Yablonovitch. Photonic crystals: semiconductors of light. *Sci. Am.*, **2001**, *285*, 47-51 and 54-55.
- P. Yan, M. W. Holman, P. Robustelli, A. Chowdhury, F. I. Ishak, D. M. Adams. Molecular Switch Based on a Biologically Important Redox Reaction. *J. Phys. Chem. B*, **2005**, *109*, 130-137.
- M. Yang, D. P. Millar. Fluorescence resonance energy transfer as a probe of DNA structure and function. *Methods Enzymol.*, **1997**, *278*, 417-444.
- A. Yildiz, M. Tomishige, R. D. Vale, P. R. Selvin. Kinesin Walks Hand-Over-Hand. *Science*, **2003**, *303*, 676-678.
- W. T. Yip, D. H. Hu, J. Yu, D. A. Vanden Bout, P. F. Barbara. Classifying the photophysical dynamics of single- and multiple-chromophoric molecules by single molecule spectroscopy. *J. Phys. Chem. A*, **1998**, *102*, 7564-7575.
- J. Yu, D. H. Hu, P. F. Barbara. Unmasking electronic energy transfer of conjugated polymers by suppression of O<sub>2</sub> quenching. *Science*, **2000**, *289*, 1327-1330.
- M. Zhao, L. Jin, B. Chen, Y. Ding, H. Ma, D. Chen. Afterpulsing and its correction in fluorescence correlation spectroscopy experiments. *Appl. Opt. Lett.*, **2003**, *42*, 4031-4036.
- J. Zheng, J. T. Petty, R. M. Dickson. High Quantum Yield Blue Emission from Water-Soluble Au<sub>8</sub> Nanodots. *JACS*, **2003**, *125*, 7780-7781.
-

R. Zondervan, F. Kulzer, S. B. Orlinskii, M. Orrit. Photoblinking of Rhodamine 6G in Poly(vinyl alcohol): Radical Dark State Formed through the Triplet. *J. Phys. Chem. A*, **2003**, *107*, 6770-6776.

## 7. Publication List

Parts of this work were published in international scientific journals.

### 7.1. Publications in Scientific Journals

**Heilemann, M.**; Herten, D.- P.; Heintzmann, R.; Cremer, C.; Mueller, C.; Tinnefeld, P.; Weston, K. D.; Wolfrum, J.; Sauer, M. High-resolution Colocalization of Single Dye Molecules by Fluorescence Lifetime Imaging Microscopy. *Analytical Chemistry*, **2002**, *74*, 3511-3517.

**Heilemann, M.**; Buschmann, V.; Piestert, O.; Tinnefeld, P.; Weston, K. D.; Sauer, M. Development of a molecular photonic wire by means of multiparameter single-molecule spectroscopy. *Proceedings of SPIE-The International Society for Optical Engineering*, **2003**, *4962*, 38-46.

Heinlein, T.; **Heilemann, M.**; Herten, D. P.; Mueller, C.; Tinnefeld, P.; Weston, K. D.; Sauer, M. Spectrally-resolved fluorescence lifetime imaging microscopy (SFLIM) and coincidence analysis: new tools to study the organization of biomolecular machines. *Proceedings of SPIE-The International Society for Optical Engineering*, **2003**, *4962*, 47-57.

**Heilemann, M.**; Tinnefeld, P.; Sánchez-Mosteiro, G.; García-Parajó, M. F.; van Hulst, Niek F.; Sauer, M. Multistep Energy Transfer in Single Molecular Photonic Wires. *J. Am. Chem. Soc.*, **2004**, *126*, 6514-6515. (Highlighted by Chin, G. J. *Science*, **2004**, *304*, 1213).

Tinnefeld, P.; Buschmann, V.; Weston, K. D.; Biebricher, A.; Herten, D. P.; Piestert, O.; Heinlein, T.; **Heilemann, M.**; Sauer, M. How single molecule photophysical studies complement ensemble methods for a better understanding of chromophores and chromophore interactions. *Recent Res. Devel. Physical Chem.*, **2004**, *7*, 1-31.

Herten, D. P.; Biebricher, A.; **Heilemann, M.**; Heinlein, T.; Müller, C.; Schlüter, P.; Tinnefeld, P.; Weston, K. D.; Sauer, M.; Wolfrum, J. Optical single molecule techniques for analytical and biological applications. *Recent Res. Devel. Applied Phys.* **2004**, *7*, 2-24.

**Heilemann, M.**; Margeat, E.; Kasper, R.; Sauer, M.; Tinnefeld, P. Carbocyanine Dyes as Efficient Reversible Single-Molecule Optical Switch. *J. Am. Chem. Soc.*, **2005**, *127*, 3801-3806.

Tinnefeld, P.; **Heilemann, M.**; Sauer, M. Design of Molecular Photonic Wires Based on Multistep Electronic Excitation Transfer. *ChemPhysChem*, **2005**, *6*, 217-222.

Heinlein, T.; Biebricher, A.; Schlüter, P.; Roth, C. M.; Hertel, D.-P.; Wolfrum, J.; **Heilemann, M.**; Müller, C.; Tinnefeld, P.; Sauer, M. High-Resolution Colocalization of Single Molecules within the Resolution Gap of Far-Field Microscopy. *ChemPhysChem*, **2005**, *6*, 949-955.

Sánchez-Mosteiro, G.; van Dijk, E. M. H. P.; Hernando, J.; **Heilemann, M.**; Koberling, F.; Erdmann, R.; Sauer, M.; van Hulst, N. F.; García-Parajó, M. F. Monitoring the extent of ET on individual DNA Based Photonic Nanowires. *manuscript in preparation*.

## **7.2. Conference Presentations**

“Design of a Molecular Photonic Wire based on Multistep Energy Transfer” (Poster)  
8<sup>th</sup> International Workshop on Single Molecule Detection and Ultrasensitive Analysis in Life Sciences (PicoQuant 2002), 22-24 September 2002, Berlin.

“Development of a molecular photonic wire by means of multiparameter single-molecule spectroscopy” (Talk)  
Photonics West 2003, 25-31 January 2003, San Jose, USA.

“Multistep Energy Transfer in Single Molecular Photonic Wires” (Talk)  
10<sup>th</sup> International Workshop on Single Molecule Detection and Ultrasensitive Analysis in Life Sciences (PicoQuant 2004), 22-24 September 2004, Berlin.

## 8. Abbreviations

ADC	Analogue-Digital Converter
APD	Avalanche Photodiode
BME	$\beta$ -Mercaptoethanol
CCD	Charge Coupled Device
CFD	Constant-Fraction Discriminator
DNA	Deoxyribonucleic Acid
DTT	Dithiothreitol
EE(E)T	Electron Exchange (Energy) Transfer
EOM	Electrooptical Modulator
FIFO	First-In-First-Out
FLIM	Fluorescence Lifetime Imaging Microscopy
FRET	Fluorescence Resonance Energy Transfer
FWHM	Full Width Half Maximum
GMP	Guanosine monophosphate
HOMO	Highest Occupied Molecular Orbital
HPLC	High Performance Liquid Chromatography
IRF	Instrument Response Function
LUMO	Lowest Occupied Molecular Orbital
MEA	Mercaptoethylamine
NHS	Succinimidyl Ester
PBS	Phosphate Buffered Saline
PET	Photoinduced Electron Transfer
PMT	Photomultiplier Tube
RhG	Rhodamine Green

*Abbreviations*

---

SFLIM	Spectrally-Resolved Fluorescence Lifetime Imaging Microscopy
SMFS	Single-Molecule Fluorescence Spectroscopy
SOMO	Semi Occupied Molecular Orbital
TAC	Time-to-Amplitude Converter
TCBQ	Tetrachlorobenzoquinone
TCSPC	Time-Correlated Single-Photon Counting
TMR	Tetramethylrhodamine
TRES	Time-Resolved Emission Spectroscopy
TTTR	Time-Tagged Time-Resolved
LED	Light-Emitting Diode

## 9. Acknowledgements

I am grateful to all the people who helped me to realize my dissertation work in the last three years.

I am very thankful to Prof. Markus Sauer for introducing me to the exciting field of single-molecule fluorescence spectroscopy and the possibility to work in projects at the cutting-edge of science.

This work would not have been possible without numerous collaborations, fruitful discussions, and always a helping hand and a great working atmosphere. At this point, I want to thank all the people of the “Applied Laser Physics and Laser Spectroscopy” group in Bielefeld. Just as much, I want to thank all members of the biophysical chemistry group in Heidelberg, I enjoyed the time I spent at the PCI during the first half of this work.

This work would not have been possible without many helping thoughts, discussions and inspiration by Markus Sauer, Philip Tinnefeld, Hannes Neuweiler and Sören Doose, Kjung-Tae Han, Dirk-Peter Herten, and Christian Müller. I am thankful to Jörg Enderlein for helping in theoretical questions. Many thanks to Johan Hofkens, Ken Weston and Andrea Vaiana for fruitful discussions.

I am especially thankful to Gerd Wiebusch for all technical help and for an advanced introduction into optics and lasers, to Stephan Wörmer for IT help and guidance and solving “special” hardware problems, to Reinhild Pätzmann for uncomplicated help in many situations, to Rudolph Böttner for helpful advices, and the whole physics department for a great cooperation.

I am happy that I had the chance to be part of a cooperation with the Optical Techniques group at University of Enschede, Twente, in the project of realizing a photonic wire. Particularly, I am very thankful to Gabriel Sánchez-Mosteiro, Niek van Hulst and Maria García-Parajó.

I am grateful to Felix Koberling and colleagues at PicoQuant GmbH for the possibility to use the MicroTime set-up and the opportunity to realize time-resolved measurements on photonic wires.

For providing custom made analysis software and support in technical problems, I thank Christian M. Roth and Dirk-Peter Herten.

For proofreading of this manuscript, I am grateful to Sören Doose, Hannes Neuweiler, Christian Roth, Philip Tinnefeld and Markus Sauer.

Special thanks to Jude Przyborski who was indispensable for revisions of the manuscript in terms of language questions.

For motivation and support during the last years and always being in reach for my thoughts, I want to thank Susanne Nessler.

There are many friends who never saw a single molecule, but, they were the perfect counterpart to scientific work: Sascha Schneider, Stephan Straub, Patrick Knorr, Judith Pfahler, Jude Przyborski, Martin Wenke, Peter Soba. Thank you all!

My greatest thanks are to my family.